Developing Offshore Floating Wind Turbines: The Tension-Leg-Buoy Design

Utvikling av offshore flytende vindturbiner:
Strekkstag-bøye-konseptet

Philosophiae Doctor (PhD) Thesis

Anders Myhr

Department of Mathematical Sciences and Technology
Faculty of Environmental Science and Technology
Norwegian University of Life Sciences

Ås (2016)

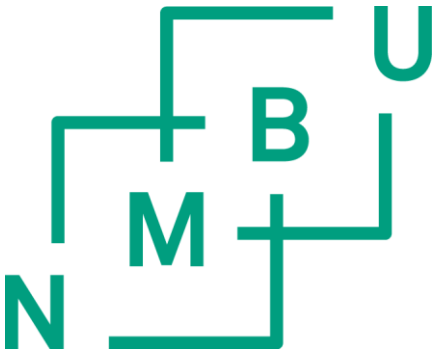

Thesis number 2016:22
ISSN 1894-6402
ISBN 978-82-575-1351-1

APPENDED PUBLICATIONS

Paper 1

Tor Anders Nygaard, Anders Myhr and Karl J. Maus, 2009. "*A Comparison of two Conceptual designs for floating wind turbines*". In Proc. of the European Offshore Wind Conference & Exhibition, Stockholm, Sweden.

Paper 2

Anders Myhr, Karl J. Maus and Tor Anders Nygaard, 2011. "*Experimental and Computational Comparisons of the OC3-HYWIND and Tension-Leg-Buoy (TLB) Floating Wind Turbine Conceptual Designs*". In Proc. of the International Offshore and Polar Engineering Conference, Maui, Hawaii.

Paper 3

Anders Myhr and Tor Anders Nygaard, 2012. "*Load Reductions and Optimizations on Tension-Leg-Buoy Offshore Wind Turbine Platforms*". In Proc. of the International Offshore and Polar Engineering Conference, Rhodes, Greece.

Paper 4

Hanne L. Raadal, Bjørn I. Vold, Anders Myhr and Tor A. Nygaard, 2013. "*GHG emissions and energy performance of offshore wind power*". Elsevier, Renewable Energy Vol. 66, p 314 – 324.

Paper 5

Anders Myhr, Catho Bjerkseter, Anders Ågotnes and Tor A. Nygaard, 2014. "*Levelised Cost of Energy for Offshore Floating Wind Turbines in a Life Cycle Perspective".* Elsevier, Renewable Energy Vol. 66, p 714 – 728.

Paper 6

Anders Myhr and Tor Anders Nygaard, 2014. "*Experimental Results for Tension-Leg-Buoy Offshore Wind Turbine Platforms*". The international Society of Offshore and Polar Engineers (ISOPE), Journal of Ocean and Wind Energy (ISSN 2310-3604). Vol 1. No. 4, November 2014, pp. 217-224.

Paper 7

Anders Myhr and Tor Anders Nygaard, 2015. "*Comparison of Experimental Results and Computations for Tension-Leg-Buoy Offshore Wind Turbines*". The international Society of Offshore and Polar Engineers (ISOPE), Journal of Ocean and Wind Energy (ISSN 2310-3604). Vol 2. No 1. February 2015, pp. 12-21.

ABSTRACT

A 5 MW Tension-Leg-Buoy (TLB) concept has been optimized and developed. The design is based on the MIT Double Taut Leg, initially proposed by Professor Sclavounos of MIT in 2005. Six variants have been tested, in two wave tank tests, to prove the concept and aid validation of 3DFloat, the coupled aero-hydro-servo-elastic tool utilized for the numerical computations. Optimized TLB designs are presented in this thesis for harsh weather sites in the North Sea basin, and a new TLB design (designated TLB B2) for the K13 Deep water site in the Dutch North Sea.

The TLB concept relies on inclined taut synthetic fibre mooring lines and excess buoyancy for stability. Thus, its natural resonance (Eigen) periods must be shorter than wave periods in the high energy part of the wave spectrum, i.e. less than 3.5 seconds. Ensuring that none of the Eigen-periods interfere with the rotor rotational periods then becomes challenging and requires a sophisticated optimization approach. Due to low damping, the structure is prone to resonant behaviour and fatigue becomes important. Fatigue damage is particularly high when the rotor is in idle or parked mode and the aerodynamic damping contribution is low. However, even when accounting for fatigue, the resulting need for primary steel in the construction is low. The TLB B2 design has a draft of 40 m and buoyancy of 2166 tons. The total mass is 1068 tons, of which the floater accounts for only 355 tons. The remaining mass origin from the 350-ton nacelle assembly and the 363 tons of tower structure.

Due to the strong influence of Eigen-periods, the design is sensitive to site conditions, especially water depth and environmental conditions. It is therefore challenging to develop a straightforward strategy to determine its potential at a given site. A specific design approach has therefore been developed and the validity of a two-stage optimization procedure (frequency-domain followed by time-domain optimization) is presented. The approach is verified by Ultimate-, Accidental, and Fatigue Limit state analyses.

The design approach features a cost evaluation in a Levelised Cost of Energy perspective (LCOE) and the concept's performance parameters are compared to those of various floating turbine concepts, bottom-fixed monopiles and jacket structures. In terms of capital expenditure (CAPEX), TLB B2 is the optimal concept for the K13 site, low material and production costs providing a significant advantage. The combined CAPEX of production and mooring is significantly lower than the production cost alone for both jacket and monopile foundations. In terms of LCOE, at about € 107 per MWh over a lifetime of 25 years, the TLB B2 is comparable to monopile foundations in an optimal depth (around 15 m) of water. The relative variation of the concepts' LCOE is assumed to be 7% and 8 %, respectively.

In comparison to previous TLB designs, the TLB B2 design substructure mass is 19 % lower, and the anchor loads are 47 % lower. The mooring loads are comparable to those of typical catenary mooring systems.

The work presented in the thesis shows that TLB designs can potentially provide simple and economically advantageous options for supplying green energy in intermediate water depths of 50 to 100 m and should therefore be pursued further.

FOREWORD

From an engineer's perspective, the world consists of opportunities. Everything is possible. Economic constraints are the limitations. The purpose of my doctoral studies and this thesis was never to *save the world*, nor was it to create the *best* solution to produce renewable energy. In fact, one of the major components of my motivation was that the quality of open discussions presented in the media on such topics was poor.

I have been interested in technical solutions and technological advances since childhood. I therefore often find myself searching for new progress in any field. However, when reviewing and comparing different solutions to a given problem, it often strikes me that the comparison is unfair or has little meaning. A common dominator is a difference in development or marketing strategy. How can you really compare a technology in early in-vitro experimental stages to another that is already implemented at large scale?

Many people have asked me why I started working with wind turbines. I have replied "Why not?" They are large complex machines that still have a lot of potential for improvement. I remember that some argued that wind turbines are large, ugly, noisy and that *we* do not really need nor want them. Personally I don't think *we* need here in Norway either, but *some* countries do. No *one* technology or design is optimal for every site and every country.

I remember the day wind turbines really captured my fascination. A good friend of mine, D. W. Moss, and myself were having a late night at one of the computer labs at the University. We had just finished the week's task for one of our programming courses and were just hitting random technology sites and blogs for something interesting. One of the sites was dedicated to conceptual wind turbines. Truly it illustrated a lot of great work, but it struck us that there was little or no focus on how to construct these machines. That was the starting point of our Master's thesis, "Concept for Installation of Floating Offshore Wind Turbines". It should be duly noted that our initial focus for the Master's degree was construction of land-based buildings, so this was definitely a *jump into the deep end* and we spent the first months merely studying basic aero- and hydro-dynamics.

During our work towards the master's thesis we addressed various floating wind turbine concepts. One of them was the TLB concept Njord. It was the lightest and easiest to handle, assembly-wise. It also looked simple and logical, unlike some of the other concepts we worked with like the SWAY - more like Hywind only slimmer. I remember wondering why the TLB concept had not developed at the same rate.

After completing the master's thesis, I felt quite content with the academic endeavours and started looking for a job in the private sector. However, that feeling faded and I felt there was still work to be done. Thanks to my supervisor Tor Anders Nygaard, a few months later I started on my PhD – eager to unravel the true potential of the TLB concepts.

Early on the question of *what* to compare arose again. That was one of the fundamental issues that had to be solved before we could even start to *show* the concept's potential. This involved addressing complex questions related to economics, emissions, constructability and people's

convictions. Hence, I had to venture into diverse academic fields, as manifested by the appended papers. Accordingly, an objective for this thesis is to present the findings in a format that is relevant not only for academic purposes, but also for other parties who may want to further develop the concept or apply elements of the results to develop new concepts.

The design process is now at a level where the TLB can be compared (at basic design level) to any other concept for a given site in terms of emissions, cost or performance relatively easily and robustly. I hereby lay down my pen, but in anticipation for any next phase that might come for this project.

During the last years, I've had assistance from several master's students who have explored technical solutions, gathered data, built models and assisted experimentally. Anders Spæren, Amund Føyn, Catho Bjerkseter, Anders Ågotnes, Eirik Henanger and Joakim Berg, this would not have been possible without you – thank you.

Special thanks should also go to my family and especially my ray of sunshine, Ellen Øfsdahl, for putting up with and believing in me during this time.

Along the way I've also had the absolute pleasure of being inspired by co-workers and fellow students at Norwegian University of Life Sciences (NMBU). I would like to dedicate a special thank you to my supervisor Tor Anders Nygaard for believing in me and supporting me in this long journey.

Gratitude should also be shown to the personnel at IFREMER wave tank facilities in Brest and SINTEF MARINTEK in Trondheim, where the two wave tank experiments were conducted.

This project was mainly funded through *Oslofjordalliansen* (OFA), a joint support scheme between the NMBU and the academies of Østfold, Buskerud and Vestfold that was initiated to enhance interaction between the institutions and spawn new and challenging cross-disciplinary scientific projects. I also acknowledge support from the Institute of Energy Technology (IFE) and NOWITECH.

Oslo, July 2015

Anders Myhr

NOMENCLATURE

ABBREVIATIONS

1p	The duration of a full rotation of the rotor. With a variable speed generator this will be a range of periods.
3p	The duration of 1/3 of a full rotation of the rotor, corresponding to the number of blades for a three-bladed rotor system. With a variable speed generator this will be a range of periods.
CAPEX	Capital Expenditure
Catenary	A typical slack offshore mooring system used to moor structures in deep water, usually consisting of heavy chains with a large footprint on the seabed.
Constraint	With regards to the optimization, this is used for determining the desired boundaries of the analysis. Typically this is with respect to limits of Eigen-periods or forces.
DECEX	Decommissioning Expenditure
Deep water	Water depths between 200 and 1000 m
DLC	Dynamic load case
DOF	Degree of freedom
EB	Excess buoyancy
Fairlead	The device for connecting the mooring line to the wind turbine
Feathered	When the blades on a wind turbine is pitched to -90 degrees i.e. when the weak axis of the rotor blade is parallel to the wind direction.
Floater	The structural part from 10 m above MSWL and down
FLS	Fatigue limit state
FWT	Floating wind turbine
GHG	Greenhouse Gas
Heave	Vertical direction, corresponding to UZ
H_{max}	The height of the largest wave in a stochastic wave series
H_s	Significant wave height: the mean (trough to crest) height of the highest third of the waves
HSWL	Highest Sea Water Level
Idle	A setting of the power generator at which no power is produced and the blades are in feathered position into the wind, but the turbine brake is not engaged – enabling the rotor to spin freely and slowly.
Intermediate water depths	Water depths between 50 and 200 m
Jacket	Truss-based foundation for offshore wind farms in 5-50 m deep water
J-tube	External guiding tube for the power cable hang off
LSWL	Lowest Sea Water Level
MIT	Massachusetts Institute of Technology
Monopile	Single column foundation embedded in the seabed for offshore wind farms in 5-40 meter depth
MSWL	Mean Sea Water Level

Nacelle	The generator assembly, including the yaw bearing and turbine housing on the top of the wind turbine
NMBU	Norges Miljø- og Biovitenskapelige Universitet (Norwegian University of Life Sciences)
NTM	Normal turbulence model
OC3-Hywind	The ballast stabilized spar buoy design used in the OC3 project (Jonkman, et al., 2009)
OPEX	Operational Expenditure
OWT	Offshore wind turbine
Parked	A setting of the power generator at which no power is produced, the blades are in feathered position into the wind, the turbine brake is engaged and the rotor position is locked
Penalty	With regards to cost functions, a penalty is a term for manipulating the cost contribution of a specific variable to influence to total cost of the design that is used for the evaluation of influence from a given variable in the optimization
Pitch	Rotation about the sway direction
Primary steel	The structural steel in a construction, excluding minor details such as ladders, stairs and brackets
Principal design level	Concept design, establishing (in this context) an accurate estimate of primary steel in the structure.
Rated speed	The wind speed where the turbine reaches maximum power production and the pitch controller starts working. This is also the wind speed that generates the largest thrust force as the blades are pitched fully into the wind.
RNA	Rotor Nacelle Assembly
Roll	Rotation about surge direction
Shallow water	Water less than 50 m deep
Substructure	See floater.
Surge	Horizontal direction, parallel to mooring line 4, corresponding to UX
Sway	Horizontal direction, perpendicular to mooring line 4, corresponding to UY
SWL	Sea Water Level
T	Wave period
TLB	Tension Leg Buoy floating wind turbine
Ton	Metric ton, 1000 kg
Tower	The structural part from 10 m above MSWL and up to nacelle
T_p	Mean peak wave period
ULS	Ultimate limit state
Ultra deep water	Water ≥1000 m deep
Yaw	Rotation about the heave direction

Contents

1 INTRODUCTION

Industrialization in the 19th century generated tremendous increases in wealth, production and standards of living, followed by sociological and attitudinal changes including *everyone* constantly expecting more and better material goods. These changes fostered an ongoing challenge: *an increasing demand for energy*. Railways, highways and power grids were rapidly constructed, but less attention was paid to meeting the increasing demand for resources. One of the main reasons for this was accessibility. Both coal and oil, the main energy resources exploited in the 19th and 20th centuries, were easily available either on top of or in the upper layers of the ground. So, the energy-challenge was largely solved by extracting the readily available non-renewable resources. Consequently, they were also depleted increasingly rapidly.

1.1 The Race for Resources

The challenge involved not only locating and extracting resources, but also doing it efficiently. In early stages coal and oil could be extracted with crude approaches; if you had a shovel you could mine coal and if you had a bucket you could collect oil. However, this rapidly changed, as illustrated by the progression from construction of land-based self-producing wells to wells in water. This was first done in 1891, in only a few meters of water in the Grand Lake St. Mary's in Ohio (Spencer & Camp, 2008). Just half a decade later, the first *inshore* wells were constructed, on piled piers in a few meters of water in the Santa Barbara Channel in California (Graffy, 2010). These were some of the first steps towards modern offshore oil exploitation, with floating rigs and ultra-deep water solutions capable of drilling in some 3000 m of water.

However, in modern times several aspects of the challenge are becoming increasingly problematic: non-renewable resources are still depleting, their collection is becoming increasingly difficult and their use generates large amounts of emissions that are believed to be posing major global climatic threats (IPCC, 2014). This has prompted increasing exploration of renewable energy resources like water, wind, waves and solar power. The idea is far from new; for centuries water and wind have been exploited to produce mechanical energy or propulsion, and solar power has been used to heat water and cook meals. However, modern society demands cheap, high-value energy in electric form for easy consumption anywhere and anytime.

Production of electricity can be a fairly simple process if appropriate resources are available. However, converting energy in many resources to electricity generally raises transport problems, as there are significant distance-related losses. Thus, it is desirable to produce electric energy close to consumers.

Working in the renewable energy industry, one may get the impression that we are in a race to identify and develop the "best" technology to cope with the increasing demands for electric energy, but this is simplistic. In practical terms, most renewable technologies could be applied

almost anywhere because renewable resources, unlike non-renewables, are abundant. However, there are large variations in accessibility and stability, and clearly no *single* technology is likely to be optimal for every site. Thus, it is important to identify the *optimal* technology, or technologies, for specific locations. For instance, hydropower appears to be a good alternative for Norway generally, but certainly not for a country like Denmark, where there is little reservoir capacity and few suitable rivers. So, a key issue is determining rational means for identifying the best options for given sites.

1.2 Follow the Lead – Cost and Availability

An economic evaluation may often be used to assess the value of resources or technology. In such an evaluation of a proposed energy production method, one may compare different possible concepts in terms of production and consumption of resources. As most technologies *could* be applied anywhere, one may even consider several sites as a solution to a local challenge. There are also several factors to evaluate in long-term projects such as power production, as most of the investment occurs early in the service life.

Previously, if a city needed more power, power plants were constructed at suitable locations in the outskirts of the city to avoid the need for an extensive and vulnerable electricity grid. However, transport of renewable energy is not easy without converting it to electricity. Collecting water in trucks and driving it to a power plant simply cannot provide net energy production or any energy at acceptable costs, although this is exactly what we do with coal for instance.

The cost of the fuel is another important variable. For most renewable energy production, the fuel is free and *ever-flowing,* in stark contrast to non-renewable fuels, which must be extracted at high cost. Nevertheless, there are uncertainties of supplies in both cases as renewable sources vary over time and the availability of non-renewable sources experience declines.

Furthermore, not only the availability of resources, but also the availability of land to locate the power-producing facilities may pose challenges. For instance, both wind and solar power plants need substantial areas to produce electricity. There is also the issue of grid connection and transmission lines.

Some of the aspects mentioned can be relatively easily priced, but others are more challenging to price economically - such as carbon footprints, topographical footprints, visual and audible pollution, all of which vary among different concepts and technologies. Further complications lie in accounting for possible technological updates of facilities, given their relatively long life expectancies. For instance, should one account for the possibility that a coal-fired power plant might be supplied with a filter capable of removing all of the pollution after 15 years?

Regardless of such considerations, the key factor for commercial projects seem to be the cost. Ultimately, the total cost or in other words *the cost of the energy* determines if a project will be realised. Taking into account the different factors in play, one can imply that there cannot be one solution that is optimal for every location and use.

The wind resources in the world are vast, amounting to some 1300 PWh annually. Most of this is located onshore in Europe and Russia, as shown in Figure 1. It should be noted that only a fraction

of this could be efficiently harvested, due to limitations related to location and wind stability. The total estimated offshore potential, in sites with steady wind conditions, reasonable water depth (< 200 m) and proximity to shore (< 10 km) is roughly 157 PWh, about half of which is in areas with 50 – 200 m deep water (Lu, et al., 2009). Based on the distribution of wind resources and areas of high energy consumption, Europe is an ideal candidate for exploiting wind power. Fierce competition with area-demanding solar power plants is also restricting the space for onshore wind power, forcing wind power plants offshore.

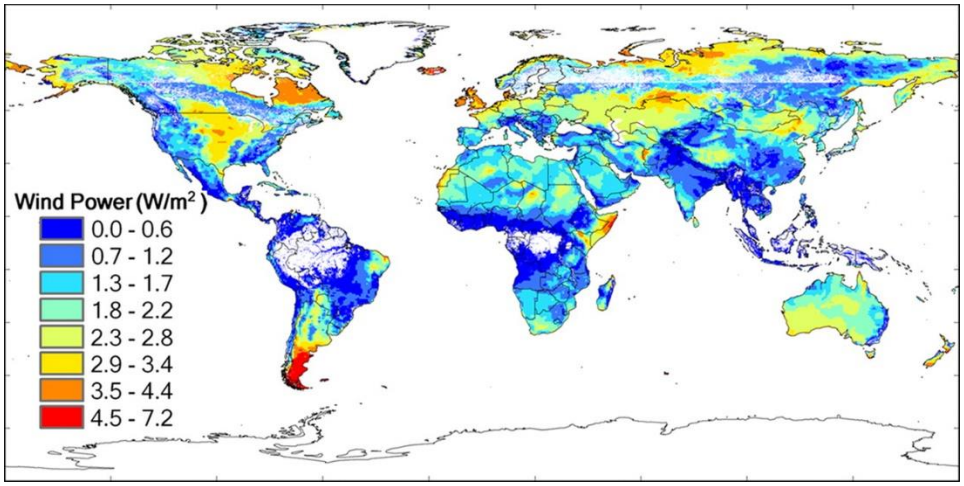

Figure 1: Global wind power potential
(Lu, et al., 2009)

Another country struggling with available land resources is Japan. Fortunately, it has a theoretical wind potential of around 1600 GW, of which around 80 % is in areas with > 50 m deep water (Main(e) International Consulting LLC, 2013). However, Japan's infrastructure also poses problems, especially the physical division of the energy grid into two parts: a 50 Hz grid west of Tokyo, and a 60 Hz grid elsewhere. Expensive physical converters with limited capacity comprise a bottleneck for effective distribution of renewable energy and raises uncertainty regarding investments, but wind power is still considered critical for Japan's energy security (Govindji, et al., 2014).

Australia has some of the world's best wind resources, as its western part is located in the *Roaring 40s*, and wind energy is the country's fastest growing renewable energy source. Although Australia has abundant open land, most of the wind resources are located along the south and south-east shorelines, where most of the people (and thus consumption) are located (ARENA, 2013).

1.3 Problem Outline, Objectives and Scope

Comparing different technologies and concepts for producing energy is challenging. Typically, some of the concepts considered are not fully developed, but they must be compared to existing and developed designs. Development of new technology and new concepts is a continuous process that is both expensive and time-consuming. Hence, detailed verification and design of every

concept for any site is not really feasible. It is therefore crucial to develop concepts within each form of technology that are as robust, generic and or as flexible as possible, and to apply functions in the design process that facilitate adaptation of the technology or concept for different sites, where possible. In this respect wind energy production is currently in an interesting paradigm transition, from *getting it to work* to *making it cheap*.

Production of electricity by wind turbines has been challenging for decades, with respect to cost of energy. In the early 1980s large wind turbine farms were built in the USA as a result of support schemes. They featured relatively small turbines, typically around 50-100 kW, and the maintenance costs were high. Consequently, most of the parks were shut down when the support ended and many people remember wind power as being expensive. Since then, wind power has been growing, in terms of both market share and turbine size. The latter is due to technological improvements and efforts to reduce numbers of turbines and maintenance costs.

Generally, the upper power limit for turbines considered practical to move and assemble on land is 2-3 MW. Thus, to exploit the benefits of larger turbines, sites that facilitate simpler transportation solutions (the sea and large lakes) are required. The size constraints for turbines installed at sea, in water deep enough to accommodate large vessels are much smaller. On the downside, there is less availability of sites in water, and their use increases complexity of both construction and maintenance. Nevertheless, it is commonly assumed that the downsides can largely be countered by technological developments and increases in the size of turbines. Thus, it is not straightforward to determine whether the best location for a wind turbine is on land or in the sea (although one is comparing technologies that are essentially identical, except in the nature of their sites).

To date, turbines in commercial offshore wind farms have been bottom-fixed. Technologically they are roughly limited to water depths of 5 to 50 m, and their foundation costs are assumed exponentially linked to depth.

The foundations, even of shallow water bottom-fixed turbines, have a relatively large mass. A typical monopile, a steel cylinder piled into the seabed, will typically have a mass of more than 500 tons for a 3 – 4 MW turbine. The large amount of material in the foundations incurs correspondingly large costs, related not only to the cost of the material *per se*, but also costs of handling and installation (which can be problematic due to the sheer size of the structure). Overall, this has driven costs of offshore wind power up as the technology has matured, in contrast to common expectations. Of course the size of the foundations is not the sole cause of increasing costs. Fatigue caused by sea loading on the structure, variations in site conditions and maintenance issues have also raised challenges, which sometimes been taken too lightly, and costs.

Nevertheless, this also raises new possibilities. One solution is to use floating concepts. As yet, bottom-fixed turbines have relatively high costs of energy, typically considered about twice those of a *conventional* power mix, but the documentation is poor. Costs of floating concepts are generally believed to be around twice those of bottom-fixed concepts, but this is peculiar, as floating foundations can be lighter and more easily installed, by simply towing them to the site, than bottom-fixed turbines. The belief may be partly due to the fact that developmentally bottom-fixed turbines are about a decade ahead of floating concepts, none of which have been considered

at commercial scale yet. Another likely contributory factor is the current lack of computer tools and design strategies for developing site-optimized designs for floating concepts efficiently and accurately.

During the last few years there have been significant efforts to develop computerized tools capable of coupling the elements required for designing offshore floating wind turbines. Though much work remains to be done in this field, some of the tools are now sufficiently refined for conveniently and efficiently validating designs of good presumed quality. Given this context, the following objectives were set for this thesis:

1. Formulation of an efficient process for developing designs for offshore wind turbines;

2. Development of an optimized design for a floating offshore wind turbine for comparison with other, existing electric energy production systems

Most industrial countries have schemes to support renewable energy production (e.g. taxes on fossil fuels or carbon footprints, and/or investment support for renewable energy production), which are intended to make use of renewable sources more economically viable. Nevertheless, the key factor for ensuring further development of renewable energy is to make it cheap and available. Thus, this thesis focuses on the cost of energy produced by the assessed concepts for comparison.

The Tension-Leg-Buoy is used as the baseline concept, but other concepts are also considered. In order to meet the objectives, it is essential to validate the applicability of analytical tools used for the evaluated concepts. Due to lack of the experimental data from full-scale offshore wind turbine prototypes this is done in the thesis by scaling experiments.

An evaluation of any concept should initially be site-specific, but sensitivity to changes in location should be assessed, in order to estimate the effort required to produce a realistic cost of energy at alternative sites. The optimized design process will account only for a selected number of load cases, i.e. the design will be at a principal level, but it is assumed to inherit a sufficient accuracy to allow reasonable comparison with other concepts on items such as total mass, global responses and survivability.

1.4 Publications

Several publications have been produced during the PhD project that this thesis is based upon. For five of the appended papers, I was the first author and the main contributor during the writing process. Each paper is briefly outlined and my contribution is summarized below.

Paper 1: - Initial Concept Comparisons
This paper explores the possibilities to reduce the steel mass of offshore wind turbines' floating platforms by utilising the TLB concept with mooring lines attached at different elevations in comparison to the OC3-Hywind. My main contribution to this publication was to construct alternative platform designs and to build a model with realistic elastic bodies for the different platform designs based on relevant offshore codes.

Paper 2: - Experiment I
A wave tank test was conducted on conceptual designs for floating wind turbines. I was the project leader for the wave trial and first author of the paper presenting the results. The objectives of the test were to gather practical experience on the performance of the TLB concepts and to perform initial comparisons with 3DFloat.

Paper 3: - Initial Optimization
To further enhance the TLB design, a theoretical optimization study was conducted. Based on experience gained through previous work, another TLB design was suggested in order to address issues regarding high anchor loads. The optimization tool was based on an existing code, so I only had to develop the cost functions and investigate the need for boundary conditions to achieve reasonable solutions. The boundary conditions were adapted to comply with relevant offshore standards. Optimized results for the investigated designs were compared to identify the optimal design from an engineering perspective. This provided valuable input on effects of different parameters on both the shape and cost of a TLB system.

Paper 4: - GHG Concept Comparisons
In order to broaden the scope of an optimal wind turbine platform, a theoretical investigation on greenhouse gas (GHG) emissions related to offshore wind power was conducted. I assessed the mass distribution and consumptions for the various concepts and contributed as the technical advisor. I also contributed significantly to the writing and review process.

Paper 5: - Economical Concept Comparison
The objective of this paper was to compare state of the art floating wind turbines on equal terms in a levelised cost of energy analysis. A comparison with bottom-fixed solutions was also included. Specific aims were to obtain a database for further optimization and identify which concept was most likely to be able to produce energy at the lowest cost. A software tool was developed in collaboration with two master's students. My responsibilities were to lead the project, set up the design of the evaluation system, and provide data for the model. The software tool that was used in the study was a second revision, incorporating input received after the master students' disputations. The paper was written by me and reviewed by my supervisor and the students prior to submission.

Paper 6: - Experiment II

During the first experiment, documented in Paper 2, we gathered valuable experience and know-how regarding the TLB systems, but the data recorded were not of sufficient quality to validate any computer tool. Thus, a second experiment at 1:40 scale was carried out on three different TLB floaters in Brest, France, through the MARINET scheme. I led the building of the models and rig, as well as conduction of the experiment. I was also responsible for processing the results and most of the work on the paper. The experiment provided data for initial validation of the simulation tool and the results will be made publicly available to help other developers to validate their own codes. From the experiment we also gathered valuable information on different TLB concepts for further understanding and knowledge of the systems.

Paper 7: - Simulation Tool Validation
This paper presents an initial validation of the simulation tool. Both regular and irregular load cases are compared and discrepancies are evaluated. This was an important process for identifying limits of the tool and increasing the value of the final optimization presented in this thesis. I performed both the simulations and the data comparisons. The paper was written in close collaboration with my supervisor in order to explore and explain all the effects identified in the results.

1.5 Contributions

This section briefly summarises the main contributions of the work underlying this thesis:

1. It has increased amounts of publicly open experimental data on floating offshore wind turbines for validating simulation tools. The 3DFloat simulation tool has been validated against the data.
2. It has enhanced knowledge of TLB systems, their behaviour and possible design strategies that give an economic advantage. This includes documentation of dynamic effects and the influence of geometrical transitions below the waterline as well as the robustness and predictability of the TLB design.
3. It has provided documentation on the cost of energy for floating offshore wind turbines and a detailed comparison of state-of-the-art concepts. Both pros and cons of the evaluated concepts have been investigated, and different concepts have been shown to be favourable at different depths. Further analysis of cost drivers, with respect to offshore wind power, is also documented, identifying grid, installation and foundations as the most important. The results also show that offshore floating turbines may have economic advantages over bottom-fixed turbines.
4. It has increased knowledge of the total contribution to GHG emissions from offshore wind power in comparison to other alternative ways of generating electric power.
5. It has introduced an efficient optimization scheme, and shown that TLB designs can be optimized efficiently by segregating analysis in the time and frequency domains. In addition, an optimized version of the TLB design has been presented for comparison with other offshore wind turbines or other sources of renewable energy production.

1.6 Research Overview and Relations

Table 1 presents a structured overview of the publications in relation to the focal issues and activities during the PhD project that the thesis is based upon. The steps throughout the process were dictated by the information and experience required to address the consecutive series of focal issues. The papers were both written and submitted in the numbered order.

Table 1: Overview of the goals and activities in the project

Focus	Activity	Publication
Gain knowledge of floating concepts	Comparison of concepts	Paper 1
	Experiments at 1:100 scale	Paper 2
	Initial optimization of TLB	Paper 3
Identify cost drivers and possibilities for floating concepts	GHG comparison	Paper 4
	LCOE comparison	Paper 5
Validation of simulation tool	Experiment at 1:40 scale	Paper 6
	Validation of 3DFloat	Paper 7
Reach an optimized design for offshore floating turbines	Final optimisation and comparison	Thesis

2 BACKGROUND AND MOTIVATION

From experience, one expects costs to decrease when moving from the prototype stage to mass production of an artefact. However, for offshore wind power systems this has not been the case. In fact, the costs have been increasing in recent years. This is probably due to a combination of lack of experience, lack of physical understanding of the complex loads and dynamic responses, and pressure to complete projects in a limited timeframe while offshore standards are still being developed. The safety philosophy has therefore been largely influenced by offshore rules and regulations, without taking into account that wind turbines are typically unmanned, have relatively low costs, and low environmental impact if they fail.

It is commonly accepted that investment costs will be higher for offshore turbines than for onshore turbines. However, due to the higher mean wind speed and lower turbulence offshore, together with the possibility to use larger turbines, their Levelised Cost of Energy (LCOE) may be reduced to a similar level. A complication is that increases in turbine size are accompanied by increases in loads, which drive up costs of bottom-fixed foundations. Findings presented in Paper 5 indicate that bottom-fixed 5 MW turbines may have a higher LCOE than floating concepts even in shallow water, implying that for large turbines floating foundations may be an economical alternative to both onshore wind and bottom-fixed offshore turbines.

2.1 State-of-the-art Floating Concepts

Several floating concepts are currently materializing into full-scale prototypes. Commonly known examples are the WindFloat (Maciel, 2010) and the 2.3 MW Hywind pilot, which has been operating since 2009. The Hywind is currently being taken a step further to a pilot park in the Hywind Scotland project (STATOIL, 2015). Further, several other concepts like the GICON, Ideol, Nautica Windpower's Advanced Floating Turbine and the concrete semi-submersible VolturnUS are emerging. More conceptual designs under development include various Tension-Leg-Buoy (TLB) and Tension-Leg-Platform (TLP) systems, but trials for these concepts have been confined to wave basins to date (Robertson & Jonkman, 2011), (Stewart, et al., 2012) and (Copple & Capanoglu, 2012). Several of the concepts are illustrated in Figure 2.

Currently, technology readiness seems to be a major decision factor regarding the concepts that are being developed into full-scale prototypes. On the upside, this ensures that most of the prototypes going offshore have low risk of structural failure. From a PR-perspective this is probably a good strategy and will presumably increase public acceptance for floating offshore wind turbines – which by any standards are spectacular constructions. However, it may not favor more radical solutions that could lower the LCOE, which will be a requirement for large-scale implementation. It may also reinforce the public perception that offshore wind power is expensive – due to prototype concepts being conservatively designed to provide high structural safety rather than low energy prices.

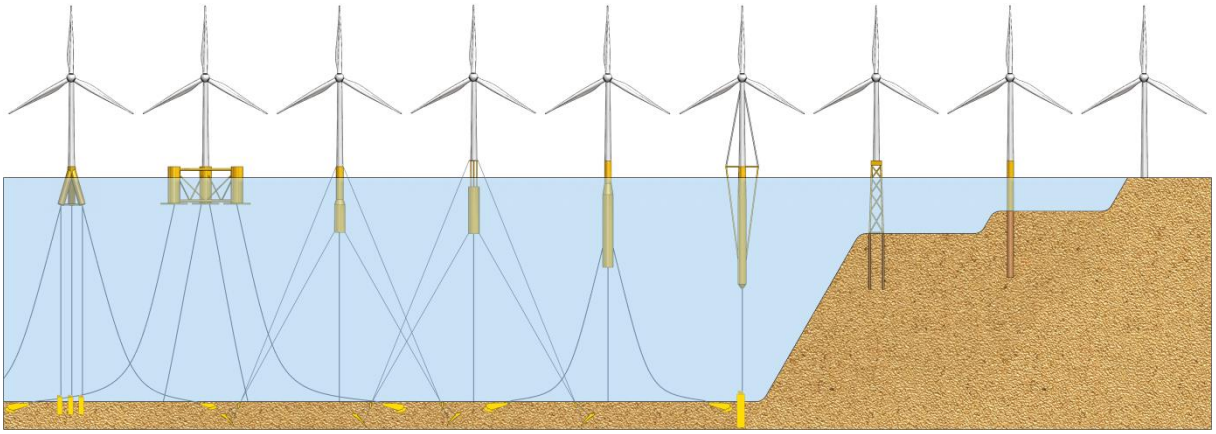

Figure 2: Illustration of, from left to right; TLWT, WindFloat, TLB B, TLB X3, Hywind II, SWAY, Jacket, Monopile concepts, and the onshore reference. The mooring systems are not to scale in the horizontal direction

Assessing technological readiness is a complex matter, and determining optimal means to influence public perceptions may pose even greater challenges. The general experience from offshore operations is that "*It cannot fail*", but although a good ideal, this is an expensive approach.

Traditionally offshore constructions involve processes and goods with high environmental risks and impacts. Thus, it seems reasonable to maintain a high level of technological readiness in order to reduce risk of failure. However, for floating offshore wind turbines this traditional design priority may be less important than economic optimization as they are unmanned and pose low environmental risks and/or impacts if they fail. Following an economic approach one can then start to reduce safety classes and remove expensive redundancy strategies based on expected failure rates for a large volume of turbines. For example, a critical structural failure in a prototype turbine is extremely bad for business if there is only such prototype, but a critical failure in one of 100 turbines in a full park will only cause at most a 1 % loss in net revenues (and possibly much less if it occurs late in service life). Thus, reducing investment costs will be economically advantageous if it does not lead to greater projected losses in revenues at computed failure rates. One of the simplest ways to reduce offshore costs is to reduce redundant safety systems. A typical floating offshore criterion is to always have a redundant stabilizing system. For a *one-off* construction, this may seem wise, but when a large number of constructions is required, a statistical approach can be used to predict failure and the failure rate can be optimized in relation to costs of considered strategies to achieve redundancy.

2.2 The TLB Concept

Tension-Leg-Buoys, or TLBs, are stabilized mooring foundation concepts that rely on excess buoyancy to keep mooring lines taut and thus effectively restrain motion. The mooring lines are fixed at two heights: the bottom of the floater and further up on the tower structure to ensure stability. The first application of the concept was presented in 2005 by Professor Sclavounos of MIT as the MIT Double Taut Leg (Butterfield, et al., 2005) & (Sclavounos, et al., 2010).** The concept has several desirable features, including a slim and simple design, possibility of low draft,

low material consumption, and response characteristics that are closer to those of land-based towers than those of other floating foundation concepts due to the taut mooring lines. On the downside, the technological readiness of TLB concepts has long been regarded as low, in large part because of the relatively high mooring line and anchor loads, as all the loads are transferred more or less directly to the anchors. Thus, key foci in recent years have been to explore ways of reducing the anchor loads and refine the computer models to enable efficient and accurate handling of complex ground conditions and anchor point responses.

An initial concept design for the TLB, code-named Njord, was developed for the comparisons presented in Paper 1. The concept featured a two-bladed down-wind turbine where the height of the upper set of mooring lines could be adjusted – from below the rotor plane up to nacelle level. The upwind line was raised in order to increase stability and reduce the mooring line forces by taking up the forces where they enter the structure. This not only reduces the mooring line loads, but also the moment transferred through the tower. With an active mooring system consisting of mechanical and movable parts, passive stability redundancy was desired, and ensured by a relatively large draft to facilitate stability from buoyancy. A significant effort to simplify the system was also made by investigating different tensioning concepts (Henanger, 2011) and an apparently reasonable system involving use of strand jacks was proposed. Different designs and applications were also investigated, e.g. introducing a prototype through simpler low-risk applications such as floating meteorological masts (MET-masts) (Sclavounos, et al., 2010).

The substructure was completely redesigned before the experiments reported in Paper 2. The design was to be considered proof-of-concept and set for North Sea site conditions, assuming that if it could work under those conditions it should be suitable for any location. The design process involved a simplistic conceptual approach, in accordance with relevant offshore standards. The main focus was on establishing a realistic mass and dimensions. Two versions were developed, designated TLB A and TLB B. TLB A was a version inheriting the redundant stability of Njord with a positive metacentric height and thought to be a solution for full-scale prototype testing. TLB B was a concept aimed at mass-production, with no redundant passive stability system in order to reduce the total cost of constructing a complete wind farm.

The findings presented in Papers 1 and 2 prompted efforts to reduce anchor loads and demonstrate that TLB systems could be viable solutions for producing renewable energy. Thus, TLB B was further optimized (for the site considered in Paper 2), as reported in Paper 3. Extensive work was performed to reduce the mooring loads. Several geometrical variations with space frames and bracings were tested to reduce the wave loading on the structure. For this severe site, a space frame construction reduced the resultant force on the anchors by approximately 10 % compared to TLB B, but at the cost of a ca. 10 % increase in use of materials in the floater. The space frame also increased complexity and was therefore not regarded as a viable option. The proof-of-concept design for the North Sea conditions had a floater steel mass of some 450 tons with mooring line forces peaking at around 17 MN for TLB B with a draft of 50 m.

Figure 3: Artistic illustration of the TLB B conceptual design.

The TLB B proof-of-concept design was also used in the evaluation of GHG emissions associated with selected floating concepts described in Paper 4. Material consumption, particularly steel, proved to be one of the most important parameters for distinguishing the concepts, and TLB systems with a light weight floater proved favourable.

Economic evaluations presented in Paper 5 clearly showed that use of a space frame is not sufficient to reduce the mooring loads sufficiently to influence mooring costs significantly. It provides some reductions in the anchor loads, but anchors are cheap compared to mooring lines so this does not justify the increased cost of fabrication. However, the TLB systems in general proved to be the most cost-effective concepts for intermediate depths, in the range of 50 to ca. 200 m. Prior to the work reported in Paper 5, a large wave tank test was conducted (Spæren, 2013), as documented in Paper 6. The model responses in the wave tank tests matched computer simulations well, as shown in Paper 7.

TLB designs specifically, and offshore wind power systems generally, have two major obstacles to overcome:

1. The observed general assumption is that the mooring loads are high, and no proven anchors or synthetic mooring lines have endured equivalent load cycles over the lifetime of a wind turbine.
2. The LCOE of offshore wind systems must be reduced in order to compete with other sustainable alternative forms of energy production.

The development is now at a level where a new TLB version should be designed for a more realistic site and all the knowledge of costs and performance is incorporated in the same optimization model. Such a version, designated TLB B2, is documented in this thesis.

2.3 Computational Tools

The shift from onshore to offshore bottom-fixed wind turbines increases project complexity through the need to address wave loading and seabed conditions. Arguably, floating structures such as TLPs and TLBs can be treated more like bottom-fixed than freely floating systems. Nevertheless, they are more complex, due to the presence of mooring lines, larger motions and interactions between hydrodynamic forces, flexibility in the structure and the spinning rotor. In addition, detailed hydrodynamic models are needed to account for effects such as diffraction and radiation on large floaters like semisubmersibles. Due to the large number of Load Cases (LCs) needed to check the feasibility of a platform, or during optimizations, the computational tools used need to be both accurate and efficient. As in the appended papers, the modelling presented in this thesis relies on the computational tool 3DFloat and the optimization tool Invalsim. In addition, TurbSim is used to generate the stochastic wind fields for the analyses. These tools are briefly introduced below.

2.3.1 3DFloat

3DFloat is an aero-hydro-servo-elastic analysis simulation software package developed at IFE. The core is a general nonlinear Finite-Element-Method (FEM) based on a co-rotated approach. It is particularly suited for structures that can be modelled with a combination of flexible slender beam elements, rigid bodies, taut or catenary mooring lines, springs and dampers subject to concurrent wave- and wind-loading. Both rigid and flexible rotor models are implemented. The 3DFloat input for two public definitions are available: the NREL 5MW reference rotor (Jonkman, et al., 2009), and DTU 10MW reference rotor (Bak, et al., 2013). 3DFloat can export geometric information and stresses for visualization and animation with Tecplot, ParaView, and Python scripts that come with the 3DFloat package. ParaView is used as an illustrator for this project.

3DFloat has been continuously developed through the course of the PhD project this thesis is based upon. For an updated view of its capabilities readers are suggested to contact Tor Anders Nygaard at IFE directly or see the appended papers. 3DFloat has also been applied in other projects, e.g. to model the OC3-HYWIND floating wind-turbine in the IEA OC3 project (Jonkman, et al., 2010), the bottom-fixed jacket-structure in the IEA OC4 project (Popko, et al., 2014) and the semisubmersible platform in the IEA OC4 project (Robertson, et al., 2014). It is currently being validated against wave tank experimental data for a semisubmersible floater (Azcona, et al., 2010), floater shapes in the IEA OC5 project (Robertson, et al., 2015) and forced motion of an isolated mooring line (Armendáriz, et al., 2011).

2.3.2 Invalsim

Invalsim is a part of an optimization package developed at IFE (Sørheim, 2002), initially as an inverse procedure to optimize heat transfer coefficients in simulation model vs. experiment comparisons. For combination with 3DFloat, it was enhanced with optimization algorithms, such as "Efficient Global Optimization (EGO)", "Genetic Algorithm (GA)", "Bound Optimization BY Quadratic Approximation (BOBYQA)" and "DIviding RECTangles (DIRECT)". The new algorithms in INVALS were briefly evaluated using a benchmark problem from the casting industry. This confirmed the known characteristics of each of the methods. In the optimization problems applied to 3DFloat and offshore wind turbines, the BOBYQA method (Powell, 2009) seems to work well. The BOBYQA approach also proved to be an efficient approach for the work documented in Paper 3 and is therefore used in the optimization presented in this thesis.

General and flexible capabilities allow Invalsim to communicate with other simulation models through text-files or scripts, without the need for linking models. The design variables with limits are specified in the INVALS input, along with tags for identifying the design variables or derived quantities in the simulation model input templates. INVALS generates the 3DFloat input file from a template that is identical to the 3DFloat input file, except for some header information, and formulas identifying how the selected input values are evaluated from the design variables. With the generated input, INVALS runs a script that runs 3DFloat, and subsequently a cost function that parses through the output files of 3DFloat. The cost function is evaluated and exported to a text file that is subsequently read by the optimizer. The constraints are implemented as penalty functions in the cost model.

2.3.3 TurbSim

Stochastic wind fields applied in the optimisation are computed using TurbSim 1.06.00, developed at NREL, USA. The TurbSim stochastic inflow turbulence code was initially developed, according to its manual, to provide a numerical simulation of a full-field flow that contains bursts of coherent turbulence (organized turbulent structures in the flow with well-defined spatial relationships) that reflect the proper spatiotemporal turbulent velocity field relationships seen in instabilities associated with nocturnal boundary layer flows. Its purpose is to enable wind turbine designers to drive design code simulations of advanced turbine designs with simulated inflow turbulence environments that incorporate many of the important fluid dynamic features known to adversely affect turbine aero-elastic response and loading.

TurbSim is based on the SNLWIND and SNwind inflow turbulence simulators, with six available spectral modes (SMOOTH, WF_UPW, WF_07D, WF_14D, IEC Kaimal and von Karman). SMOOTH models flow over flat homogenous terrain, and the WF modes compute turbulent flows upwind in multi-row wind farms with 7 and 14 rotor-diameter row-to-row spacing. In the simulations described here the IEC Kaimal spectrum is applied, in accordance with DNV-OS-J101 section 3.2.4.3.

3 APPROACH

3.1 Description

The approach applied to fulfil the objectives of this thesis builds on the findings in the appended papers. In Paper 3, an approach involving independent optimization in the time and frequency domains was applied. This allowed reduction of the number of design variables included in each of the optimization phases, dramatically reducing the simulation time relative to integrated optimization with all of the load cases required to characterize the system's dynamic responses. Findings in paper 3 also showed that the approach was robust and that changes made in the time domain analysis had little or no effect on the relevant natural resonance (Eigen) periods of the system. They also demonstrated that the simple variant of the TLB solution should be a favourable option for shallow water sites in terms of both costs of energy and GHG emissions.

In order to generate a design that allows comparison with other means of producing electricity, it is convenient to optimize the system for a site that is actually considered for an offshore wind farm, rather than the harshest conditions in the North Sea, as in Paper 3.

The optimization presented here is divided into two steps, following the approach shown to be viable in Paper 3. However, the cost functions are adjusted in accordance with findings reported in Papers 4 and 5. A quantified illustration of the approach is shown in Figure 4. The cost functions are used as a basis for a full LCOE evaluation that should be used for comparison to other wind turbine concepts, both offshore and onshore. A verification step is added to the approach to demonstrate that the optimization approach produces an efficient solution.

The verification involves a simplified procedure based on established rules and regulations from the DNV GL set of offshore standards (OS), recommended practices (RP) and supplementary standards from the International Electrotechnical Commission (IEC), more specifically:

1. DNV-OS-J103 Design of Floating Wind Turbine Structures
2. DNV-OS-J101 Design of Offshore Wind Turbine Structures
3. DNV-OS-E301 Position Mooring
4. DNV-RP-C205 Environmental Conditions and Environmental loads
5. IEC 61400-1 Design Requirements
6. IEC 61400-3 Design Requirements for offshore wind turbines

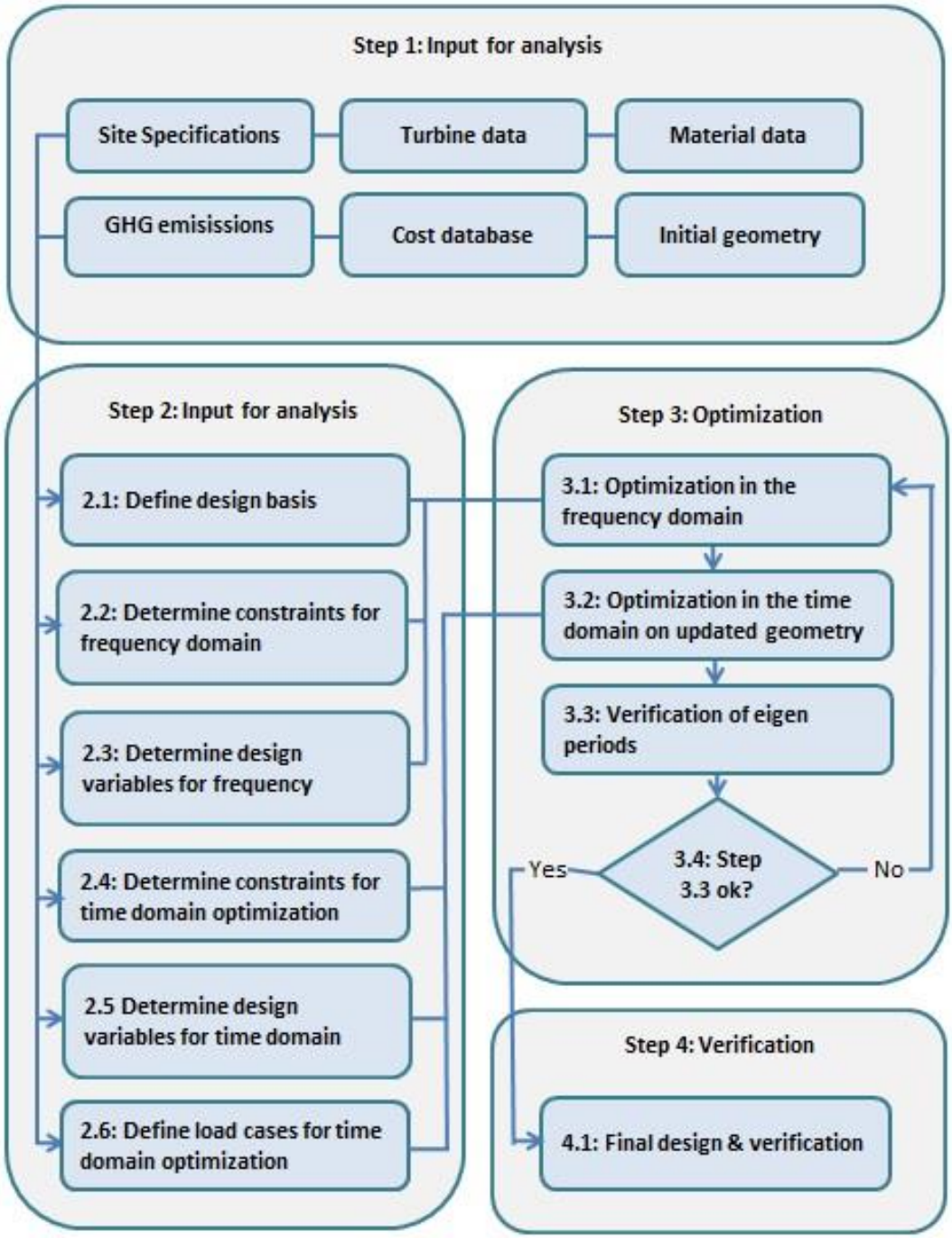

Figure 4: Flow chart for the design- and optimization process

4 OPTIMIZATION SETUP

The approach applied here is similar to that presented in Paper 3, but a more realistic location is used, and there is greater emphasis on maintaining a simple, cheap structure, further reducing the mooring forces and implementing findings from previous work.

4.1 Site – Environmental Conditions

As previously mentioned, previous optimization of the TLB design was carried out in relation to particularly harsh environments that were not suitable for demonstrating the economic potential of TLBs. To increase comparability with other concepts, the K13 Deep Water site in the Dutch North Sea, described in the Upwind Design Basis (Fisher, et al., 2010), is utilized here.

A water density of 1025 kg/m^3 is assumed, the water depth at the K13 site is around 50 m, HSWL is reportedly +3.29 m, and LSWL -2.37 m (Fisher, et al., 2010). The variation in water level is small relative to the total draft of the TLB, which is assumed to be 30-40 m, and thus is ignored at this stage of the design phase.

The directionality of the environmental loads is not taken into account in this thesis, as no park layout has been defined. Therefore the resulting design is assumed to be relatively conservative.

4.1.1 Current

Both the subsurface tidal (U_{ss}) and wind-driven surface currents (U_w) are specified and described by the following individual profiles:

$$U_w(z) = U_w(0)\left(1 + \frac{z}{20}\right) \quad \textbf{Equation 1}$$

$$U_{ss}(z) = U_{ss}(0)\left[\frac{(z+d)}{d}\right]^{\frac{1}{7}} \quad \textbf{Equation 2}$$

Due to preliminary limitations in the 3DFloat code, only one current profile may be applied at a given time. As a conservative approach both the subsurface and surface current are combined in the subsurface power law description. The upwind design basis estimated 0.6 m/s speeds for both subsurface and surface currents, giving a total of 1.2 m/s during extreme events with 50-year recurrence (hereafter designated x-year events, where x is the recurrence period of extreme events). For 1-year and 5-year events, 0.6 and 1.0 m/s speeds are assumed, respectively. An exponential current profile with a shape coefficient of 0.1429 is utilized. Where the specific wind-driven current is needed, (DNV-OS-J101, 2013) is used, with a conservative approach applying a k-value of 0.03.

4.1.2 Waves

Waves are assumed to be the dominant load on the TLB structures. The Upwind design basis provides a simple table for extreme wave heights, H_{max}, and extreme significant wave heights, $H_{s,max}$, as a function of the return period, T_{return} (Table 2).

Table 2: Extreme wave heights as a function of the return period (Fisher, et al., 2010)

T_{return} [Years]	$H_{s,max}$ [m]	H_{max} [m]	$T(H_{max})$ [s]
1	7.1	13.21	9.44
5	8.1	15.07	10.09
10	8.5	15.81	10.33
50	9.4	17.48	10.87
100	9.9	18.41	11.15

Correlation between directions is subject to discussion but those of extreme events are assumed to be uniformly distributed. Breaking waves are, as in the Upwind project, neglected. A band for the wave periods, T_p, is also defined by the following formula (Fisher, et al., 2010):

$$11.1\sqrt{\frac{H_s}{g}} \leq Tp \leq 14.3\sqrt{\frac{H_s}{g}} \qquad \textbf{Equation 3}$$

The results of Equation 3 for a selection of significant wave heights is shown in Table 3. As short periods are assumed to be most relevant, the minimum T_p is chosen.

Table 3: T_p in relation to Hs

H_s [m]	$T_{p,min}$ [s]	$T_{p,max}$ [s]
9	10.6	13.7
8	10.0	12.9
7	9.4	12.1
6	8.7	11.2
5	7.9	10.2
4	7.1	9.1
3	6.1	7.9
2	5.0	6.5
1	3.5	4.6

The Upwind documentation does not state that the Pierson-Moskowitz spectrum should be used for FLS and that a peakness factor of 3.3 should be used for the other DLCs. As the lower T_p band is used here, it is thought to be more correct to rely on the formulation in DNV RP-C205, which results in a peakness factor of 3.5 for the waves.

4.1.3 Wind

In addition to currents and waves, the Upwind design basis presents maximum 10-minute averaged wind speeds with respect to return period, as shown in Table 4. The wind speed is reported at a height of 90.4 m and a constant wind exponent factor of 0.14 is used for the shear profile due to insufficient data to estimate the shear profile at different wind speeds. Based on experience, the value is regarded as conservative for high wind speeds.

The extreme wind speed at a given recurrence period is calculated using Equation 4, derived from the Upwind design basis. Extreme wind speeds for various return periods are also listed in Table 4.

$$V_{hub,10min}(T_{return})=2.6446\ln(T_{return})+31.695 \quad \textbf{Equation 4}$$

Table 4: Extreme wind speeds at hub height as a function of the return period (Fisher, et al., 2010)

T_{return} [Year]	V_w (10 min) [m/s]	V_w (3 hour) [m/s]
1	32.74	29.466
5	36.85	33.165
10	38.62	34.758
50	42.73	38.457
100	44.50	40.05

As the TLB design requires relatively low Eigen-periods, preferrably less than 5 seconds, it is relevant to evaluate turbulence and 3-second gusts. The latter are estimated using a conversion factor of 1.26, and the recommended turbulence intensity is illustrated in Figure 5. For this study, the class 1C (IEC-61400-1-ed3, 2008) description is used to determine the turbulence at different wind speeds. Wake effects from neighbouring turbines are accounted for using data in Annex D with a turbine distance of 8 rotor diameters for the production cases.

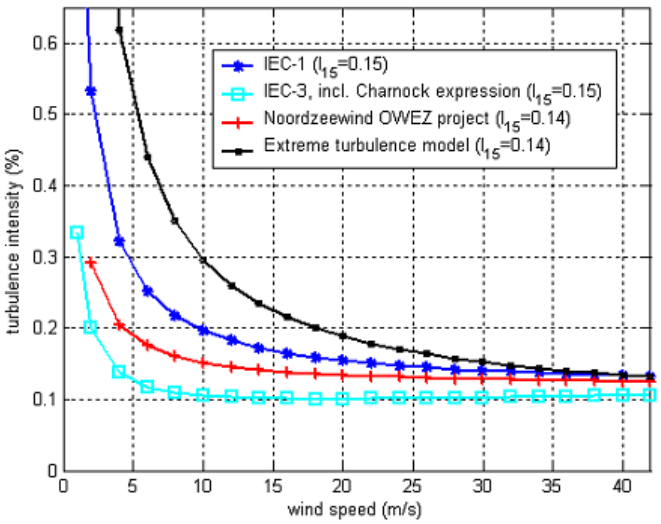

Figure 5: Turbulence intensities suggested for the K13 site (Fisher, et al., 2010)

To obtain an impression of the most severe wind states, it is relevant to investigate the wind force distribution on the system with respect to changes in wind speed. The relationship between wind force and height of attack in relation to the wind speed, obtained from simple calculations, is illustrated in Figure 6.

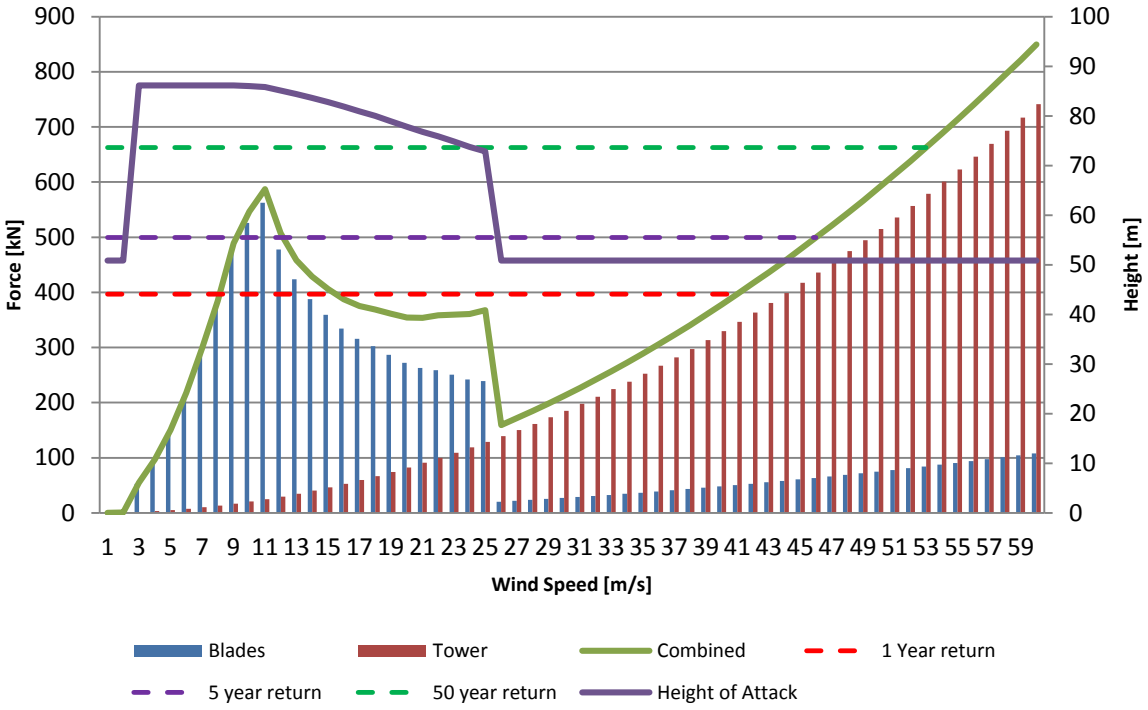

Figure 6: Wind load as a function of wind speed. Note that this is a simplified representation that does not account for wind shear. The wind drag factor on the tower is assumed to be 1.0 and the rotor thrust coefficient, Ct, is used to compute the rotor thrust

An interesting point is that 5-year peak gusts exert force at a lower point than a standard production incident around peak thrust for the turbine. Furthermore, although the 50-year gust is stronger, this will not necessarily result in the highest loads on the turbine as the height of attack is significantly lower when the rotor is not operating.

For the full wind field generated by TurbSim, a 195 by 195 m grid with 1600 points is used, with temporal resolution set to 20 Hz. The baseline analysis time is set to 1 hour and the wind field is looped in the coupled analysis, where the total simulation time is longer, in accordance with (IEC-61400-1-ed3, 2008). The Kaimal turbulence spectrum, in combination with a surface roughness of 0.0001, according to DNV-OS-J101, is used in the computations. The effective turbulence is influenced by the number of turbines located in the upstream wind field. In theory one could set up a specific field for each direction, but due to computation time limitations, and the analysis will not cover all of the turbines, an omnidirectional turbulence field influenced by wake is assumed. Wakes from two upstream turbines are assumed, located eight and 16 rotor diameters away.

Another factor is controller stability. The controller used is identical to the one used for the jacket foundation in the OC3 project. When there are turbulent winds it will not be able to obtain a steady thrust force due to pitch lag. Although, the rated power implies a thrust of about 580 kN, the peak

thrust is close to 900 kN. This is a temporary condition, but as a conservative approach the peak force is used in the optimization. However, a statistical evaluation in order to obtain a realistic combination factor is advised — particularly since the 50-year wave is used in the same load case and we want to model loads during combinations of events with 50-year recurrence, rather than loads that would be generated if all loads with 50-year recurrence occurred simultaneously.

4.1.4 Additional Site specific Data

In the design basis of the Upwind project, two different seabed conditions are assumed. This is relevant when choosing an appropriate anchor solution. The TLB designs are likely to be sensitive to anchor stiffness, but investigating the stiffness of possible anchor solutions is beyond the scope of this thesis. The anchors are assumed to be Vertical-Load-Anchors, as discussed in Paper 5. For this stage of the optimization we assume that the anchor points will have significantly higher stiffness than the mooring lines, and therefore neglect their contribution. However, it should be clear that this point needs further attention. Effects of scour, temperature and ice will also be neglected.

4.2 Design Load Cases

To verify a design, numerous load cases should ideally be checked (typically thousands of variations for an offshore wind turbine). In practice, it is not possible to optimize with respect to all load cases, especially in the time domain, and during the design phase it is not necessary to check all the variations; after all, only the final design needs to be fully verified. Instead, one addresses the most relevant load cases. These are usually selected by applying experience and relatively simple calculations, and differ in each stage of the design process. For a concept design, one typically uses zero to three load cases or states. For the next level, basic design, this is typically increased to around 10 before entering the final detail design phase with a full load case matrix. The main reasons for this progression are to enable efficient editing and rational improvements to the design.

The objective of this part of thesis is to generate a basic design by optimization. For this purpose the design load cases (DLCs) are split into three groups for: 1) frequency domain optimization, 2) time domain optimization and 3) verification. DNV-OS-J101 and DNV-OS-J103 are used as bases to determine the relevant load cases.

4.2.1 Frequency Domain Optimization

Frequency domain analysis is often used for designing fatigue limit states (FLS) as they can be solved quickly and therefore a waste number of DLCs can be analysed efficiently. However, earlier works have shown that fatigue is less of a design driver for TLBs than for most other concepts, typically with large pitch motions, as the tower is constrained just below the rotor plane. For all the analyses, the standard NREL 5 MW tower is used, and if that works for a concept constrained

where the transition is at + 10 meters, is should work when we constrain it at +30 meters. A fatigue optimization is likely to change the mass of the tower somewhat, but probably reduce it. Arguably, a frequency domain optimization of the tower should be included, but the focus of this work is to develop the floater concept. It should also be mentioned that the effect of a change in tower mass on the floater will be low and directly linked to the excess buoyancy. Therefore the time domain optimization will only run one load case to verify the global Eigen-periods of the design variation to be in acceptable regions.

4.2.2 Time Domain Optimization

For the optimization it is appropriate to reduce the number of load cases as much as possible in order to reduce simulation time. This may be done by isolating the dominating load cases. The TLB design relies on the Eigen-periods being shorter than wave periods in the high energy areas of the wave spectra. This is generally accepted as below four to five seconds and implies a direct first order response. The peak wave may be expected to cause the strongest wave excitation, but the largest response may be produced by small waves with periods closer to the resonant periods of the structure. Accordingly, the largest excitation by wind is expected to occur during the strongest gales in around three-second gusts. Therefore, the dominating ultimate limit state (ULS) load case is likely to involve a combination of the largest waves and highest wind speed. Load combinations are listed in Table 5. Ice loads are neglected, as are changes in water level since accompanying relative changes in Excess Buoyancy (EB) are minimal.

Table 5: Proposed load combination, based on (DNV-OS-J101, 2013)

		Environmental load type and return period to define characteristic value of corresponding load effect		
Limit State	**Load Combination**	**Wind**	**Waves**	**Current**
ULS	1	50 years	5 years	5 years
	2	5 years	50 years	5 years
	3	5 years	5 years	50 years

Accidental limit states are assumed to be less relevant and are treated in the verification step. Current is assumed to have negligible influence on the optimization and is not included. The optimization presented in Paper 4 indicated that waves were the main excitation agents. This is also likely to be the case at the K13 site as the 5-year and 50-year wind gusts produce similar moments on the structure due to the difference in height of attack. Load combination 2 is therefore chosen as the dominating load case. This corresponds to a state where the turbine is parked and hit by a gust wind of about 46 m/s over three seconds. The equivalent force on the structure due to wind is then about 500 kN. However, the thrust produced at rated wind speed is higher.

A statistical distribution approach should be used to determine the combination factor of the 3-second gust to the $H_{,max}$. As a conservative approach, the optimization thrust force at rated speed and the 50-year wave state is chosen. This results in a $H_{,max}$ of 17.48 m and minimum wave period from Equation 3, along with the peak production thrust of about 900 kN and a height of attack of about 86 m. In addition, the 5-year current of 1.0 m/s is applied. In comparison, for the extreme

North Sea conditions applied in Paper 3, the dominating case was 5-year gusty winds of 55 m/s and a 50-year $H_{,max}$ of 29 m.

4.3 Initial Design

The initial design of the TLB system can be easily established by a relatively crude approach. The proof-of-concept TLB B version addressed in Paper 3 is used here as a baseline for the optimization. It has a total mass of 1303 tons, including 190 tons for the anchors. The peak mooring line force is 16.7 MN and the peak vertical, horizontal and resultant forces on the anchor are 17.8, 23.3 and 29.3 MN, respectively.

4.3.1 Rotor-Nacelle Assembly and the Tower Structure

The baseline Rotor-Nacelle Assembly (RNA) for this study is the NREL-based OC3-5MW (Jonkman, et al., 2009); similar to that used in Paper 3 and the Upwind project. Its basic specifications are summarised in Table 6.

Table 6: Basic turbine RNA properties (Fisher, et al., 2010)

Turbine Parameter	Value	Unit
Rated power	5.0	MW
Rotor diameter	126.0	m
Mass of rotor and nacelle	350	ton
Cut-in wind speed	3	m/s
Rated wind speed	11.4	m/s
Cut-out wind speed	25	m/s
Nominal rotor speed	12.1	rpm
Lower bound rotor speed	6.9	rpm
Upper bound rotor speed	12.1	rpm

In the frequency domain, a full elastic rotor representation is used. The rotor is identical to the 5MW NREL assembly (Jonkman, et al., 2009) and the blades are pitched to zero degrees to simulate an operating state. Changes in Eigen-periods associated with changes in the blade pitch position are not considered here, although it is known to influence heave, pitch and roll. Further sensitivity studies should be performed to investigate their effects on fatigue. For the optimization, the RNA is replaced by a lump mass to simplify the geometry in order to enhance simulation speed. The verification cases are run with the flexible blades and the NREL OC3 pitch controller tuned for bottom-fixed wind turbines.

In the OC3 description of the tower structure, the tower arises from +10 m above the SWL. The lower diameter and wall thickness of the tower are set to 6.5 m and 0.027 m, respectively (Jonkman, et al., 2009). Due to the placement of the upper fairlead, the diameter and wall thickness are kept constant to 24.55 m. The tower then tapers to a diameter and wall thickness set to 3.9 and 0.025 m, respectively, below the nacelle flange. This has similarities to the NREL 5MW tower, with slight modification to accommodate a reasonable 1 bending mode period for the coupled

floater and tower structure. The Young's modulus is set to 210 GPa, the shear modulus to 80.8 GPa and the density is assumed to be 8500 kg/m^3 to account for paint, bolts, welds and flanges.

4.3.2 The Floater

The effects of varying floater shape have been addressed in all of the appended papers, and the results (particularly findings presented in Papers 3 and 5) suggest that complex floater solutions are not viable for the TLB system. For the optimization in Paper 3, with relatively harsh weather conditions, a tapered transition below the waterline was needed to secure EB while keeping the wave loads at a reasonable level. At the K13 site, however, the wave loads are expected to be significantly lower and the tapered section is not necessarily needed. The initial design features a simple cylindrical shape, from the floater-tower transition down to the bottom lid. The initial outer diameter at the waterline is identical to the tower bottom at +10 m. A tapered section, diameter increasing with depth, is located below the water line. The section above the tapering and below the tower has a wall thickness of 31 mm. Prior to optimization for the K13 site, the depth of the transition part is -19.3 m and the outer diameter of the lowest segment of the floater is 9.7 m with a wall thickness of about 40 mm. The initial draft is set to 40 m and the resulting steel mass is approximately 400 tons.

4.3.3 The Mooring System

The mooring system consists of nine mooring lines in total, distributed in two clusters of six and three at the bottom of the floater, just below the rotor plane, 24.55 m above SWL. In previous studies on TLB systems six mooring lines have been used in total: two sets of three lines attached at two heights (without considering yaw stability). Yaw stiffness was previously neglected or implemented either artificially or by bridle solutions. This work incorporates a further development of a bridle solution by letting the bridle intersection at the anchor point, thereby also increasing redundancy for mooring line failure, and using nine mooring lines: three at the upper level and six at the lowest level. The initial mooring radius is set to 75.0 m. Depending on soil type, suction- or gravity anchors should be considered as alternatives to the VLA anchors, but here the anchor points will be fixed. Mooring line diameters are 0.227 m for the upper lines, and 0.097 m for the lower lines, with a Young's modulus of 54.5 GPa. A standard Bexco DeepRope Dyneema mooring line type (BEXCO, 2015) is assumed.

4.3.4 Additional Specifications

Additional specifications may be considered, such as secondary steel structures and technical installations that are not dependent on the optimization process, notably the mass of the upper transition piece between the tower and the floater and ring stiffeners in the substructure. A mass of approximately 25 tons is added in the transition. 25 tons is also added at the upper fairlead in order to accommodate technical equipment for fixing the mooring lines. Penalties for the lower

fairleads, end-caps and transition changes in the floater are accounted for through couplings in the design variables.

4.4 Design Variables

To ensure the system is sufficiently stable to optimize within a reasonable amount of computation time, the number of design variables is kept at a minimum. This is also partly the reason for the two-step optimization in the frequency- and time-domains. This approach was initially introduced in paper 3, but has been further refined.

The design variables remain the same, but the link to the geometry and cost functions have been altered in order to improve results. Table 7 and The design variable rr1 is used to define the position of the anchors. Manipulation of rr1 implies a change in mooring line stiffness, due to both changes in the length of the line and the angle to the seabed. The variables allow identification of optimal mooring line size and angle in order to achieve acceptable Eigen-periods at the lowest possible cost.

Table 8 summarize the design variables used in the optimization:

Table 7: Design variables used in the frequency domain optimization

Item	Label	Unit
Anchor radius	rr1	m
Diameter of lower mooring lines	d1	m
Diameter of upper mooring lines	d2	m

The design variable rr1 is used to define the position of the anchors. Manipulation of rr1 implies a change in mooring line stiffness, due to both changes in the length of the line and the angle to the seabed. The variables allow identification of optimal mooring line size and angle in order to achieve acceptable Eigen-periods at the lowest possible cost.

Table 8: Design variables used in the time domain optimization

Item	Label	Unit
Depth to tapered section	ht	m
Outer diameter of floater	df	m
Pre-tension in the lower mooring lines	pre1	m/m
Pre-tension in the upper mooring lines	pre2	m/m

Depth to tapered section, ht, is the distance between the still water line and the top of the tapered section. The tapered section is assumed to be 5 m in height and the thickness depends on the outer diameter of the floater, df. The diameters are given by the floater body and the middle section penetrating the water surface. The thickness is tapered, and dependent on the diameter of each end. The thickness at the end points of the tapered section is given in Equation 5. A penalty for increasing diameter is added, as shown in Equation 5.

$$t = \frac{df}{500} + 0.024 \qquad \textbf{Equation 5}$$

The outer diameter of the floater, df, also governs the wall thickness in the floater body, as shown in Equation 6. The relationship is similar to the linearization applied in Paper 3, based on DNV RP-C202, and is assumed to be applicable for diameters between 6 and 10 m.

$$t = \frac{df}{500} + 0.018 \qquad \textbf{Equation 6}$$

The outer diameter of the floater is also used to define the mass of the bottom end-cap by the relationship shown in Equation 7.

$$t_{end-cap} = \frac{df}{384.16} + 0.0234 \qquad \textbf{Equation 7}$$

It would be potentially informative to incorporate the draft as a design variable, as a minimal draft is often a desired attribute. However, this would compromise the approach of splitting the optimization in the frequency and time domains because the connection of the lower fairleads strongly influences the global Eigen frequencies. Therefore it is not advisable to incorporate the draft in the time-domain optimization Configurations with different drafts could be included in an optimization for a specific site, but this is considered beyond the scope of this thesis, as the focus is more on the feasibility of the approach than finding the optimum draft.

4.5 Constraints

4.5.1 Frequency Domain Optimization

Two main constraints are applied in the frequency domain optimization:

1. All Eigen-periods should be below 3.5 seconds
2. All Eigen-periods should be outside 1.5 and 3.2 seconds

These constraints ensure that the Eigen-periods are located below the high energy part of the wave spectrum and outside the 1p (5.0 s – 8.3 s) and 3p (1.6 -2.9 s) period ranges of the rotor with a 10% margin. A penalty on the mooring line mass is also added to induce a tendency to minimize the mooring line diameter.

4.5.2 Time Domain Optimization

A single main constraint is applied in the time domain optimization:

1. Mooring line force should not be less than 500 kN

This constraint is set to avoid slack in the mooring lines with a reasonable margin. 500 kN is equal to about 10 % of the nominal pre-tension in the mooring lines. In addition a penalty is added to

the total mass to prompt a trend towards a minimum total mass. The mass of the anchors is also included in Equation 8, designed for VLA anchors in medium clay:

$$Anchor\ mass\ [N] = 3 \cdot \left(0.0022 \cdot F_{res,max} - 891.59\right) \quad \textbf{Equation 8}$$

4.6 Cost Functions

The *cost* of a variant in a given optimization step is derived from the constraints. There may also be several types of cost to consider for each constraint. Here, attempts are made to distinguish between material and non-material costs. Material costs are those that can be directly linked to a material property. For example, the cost of steel is directly related to the steel consumption. Likewise, the cost of production is related to the physical process of assembling the structure. However, the cost of GHG-equivalent emissions may be linked to the calculated amounts of emissions and their unit costs based on theoretical options, for instance to trade quotas, so they are hybrid costs. The non-material costs are linked to various other aspects like technology acceptance and readiness of the concept. There are several options to account for such intangibles in the optimization. For the level of this analysis, none of the design variables are assumed to affect non-material costs significantly, but the potential effects should be thoroughly evaluated when comparing different concepts (despite the subjectivity, uncertainty and variation with respect, for instance, to risk exposure involved).

Based on the design variables, the geometry of the structure may vary significantly between designs, with accompanying variations in complexity and constructability. However, in order to simplify the cost functions, this is handled with the design variables and included in the functions that determine the physical geometry of the construction as far as possible.

For the concept-specific optimization presented in this thesis, the different costs are summarized in order to compare the performance of each variant in the optimization stage. The cost functions used in the optimization do not necessarily have to be realistically parameterized (for comparative purposes), but when using several cost functions care must be taken to balance the weights. For this optimization, costs are based, as far as possible, on a benchmark wind farm with 100 turbines, as considered in Paper 5.

4.6.1 Material Consumption

Several types of material are used for different components of a wind turbine, but besides the RNA most of the structure is made from various grades of steel. Both Papers 4 and 5 show that the steel consumption is the major cost driver and main source of GHG-equivalent emissions. For this analysis we therefore focus only on steel consumption in the turbine. During the optimization, the total amount is not particularly important to assess, so the total mass reported from 3DFloat is used. Potential discrepancies in steel consumption for secondary structures are not considered. Based on the findings in Paper 5, the cost of steel, including fabrication, is assumed to be € 2100

per ton. This gives a simple linear relationship between total cost and steel consumption, but does not account for changes in complexity. Thus, this approach should only be used for comparisons of variants with small to moderate changes in geometry.

The TLB systems use synthetic fibre ropes that are neutrally buoyant in water. The mooring system radius and dimensions are altered in the optimization, resulting in changes in material consumption for the fibre ropes, which should therefore be included. Exponential approximation is utilised to estimate the cost per length of the fibre mooring ropes. The baseline cost per meter is estimated at € $91.681^{0.0113D}$ where D is the desired diameter. This is assumed to be applicable in a range of 90 mm to 300 mm. These assumptions are similar to those applied in Paper 5.

For the anchor system, similar approximations to those applied in Paper 5 are made, and a Stevmanta VLA system is chosen. The cost of the anchor is assumed to be 0.01417*F [N]*4.14, in the range 1000 – 2000 tons of resulting peak load.

4.6.2 Eigen-periods

The costs applied in the frequency domain optimization are abstract values, and only balanced to give reasonable results. For each Eigen-period within the bond of 1.5 and 3.2 seconds, a calculated TCOST is applied to the total cost, RCOST:

$$TCOST = TCOST + (30000 \cdot TTEMP^2) \quad \textbf{Equation 9}$$

where:
$TTEMP = The\ eigen\ period\ in\ seconds$

Several approaches with polyminal functions and double linear functions were tested in order to make a slope in both directions, but the optimization seemed sufficiently stable without it. However, a quadratic approach is used to avoid the upper constraint of 4.5 seconds for the Eigen-periods T. Equation 10 is used to compute the cost contribution to the total cost, RCOST.

$$\begin{aligned} &if\ T\ [S] \leq 4.5\ S: \\ &\quad RCOST = RMASS - STRUCMASS + TCOST \\ &else: \\ &\quad RCOST = RMASS - STRUCMASS + (CPENALTY \cdot (T - 7.D0)^2) \\ &\qquad\qquad + TCOST \end{aligned} \quad \textbf{Equation 10}$$

where:
$RMASS = Total\ mass$
$STRUCMASS = Floater, tower\ and\ RNA\ mass$
$CPENALTY = 1.E5$

4.6.3 Mooring Forces

The constraint of 500 kN for the mooing lines is not absolute as an exponential cost distribution is utilized. The total penalty id given by Equation 11.

$$
\begin{aligned}
&if\ F\ [N] > 500\ kN: \\
&\quad RCOST = \sqrt{-100000 - 500000 + (F\ **\ 2)} \\
&else: \\
&\quad RCOST = 2 \cdot \sqrt{-100000 + ((F - 500000)\ **\ 2)\ **\ 0.5}
\end{aligned}
$$

Equation 11

4.6.4 Stress and Fatigue

An evaluation of stresses and fatigue should be included in the optimization, although this is a complex and time-consuming feature to incorporate. The current optimization approach uses a linearized function to estimate proper wall thicknesses. In the calculations, a maximum stress of 100 MPa is assumed. Fatigue is mainly a challenge for the lower parts of the tower structure and areas subjected to large bending forces. The TLB structure counters the turbine moment with mooring lines at two heights, thereby reducing the moment transferred through the floater and floater-tower transition. In addition, the vertical component from the upper mooring lines provides a considerable pre-tension in the cross-section between the fairleads.

The dimensions of larger parts of the structure, especially the tower structure, can be expected to be governed by the need to avoid fatigue. A configuration including peak stress level in the cost function was tested, but it never significantly affected the output. This is likely to be the result of the application of the linearized wall thickness function. However, although stress is not included in the optimization fatigue will be evaluated in the verification step and the 100 MPa level should be revised if fatigue seems to pose a challenge.

4.6.5 GHG Emissions

Volumes of two materials are varied during the optimization: steel and dynema. The production of dynema is not particular polluting and due to the sheer difference in consumption (around 1000 tons of steel in comparison to 1-10 tons of Dynema), this is not distinguished in the cost functions.

4.6.6 Total Cost

Summing costs for a given variation provides a total cost, which only accounts for the fabrication of the floater hull and mooring system, but may also serve as a base for including other cost aspects for a floating wind turbine. In order to balance the evaluation of each concept, findings from Paper 5 are used to analyse the contribution of each component. Because of the construction complexity 1 kg of steel for anchors is 4.14 times more costly than 1 kg steel for the floater. This is reflected in the cost function. The anchor size will also influence the handling ability to some degree, but this is only accounted for in the LCOE analysis after the optimization.

The dimensions of the mooring lines and mooring radius are set in the frequency domain optimization, focusing on minimizing the mass with acceptable Eigen-periods. The time domain analysis does not inherit any ability to change the mooring lines. This may lead to a somewhat sub-optimal solution as one unit of anchor is considerably more costly than one unit of floater.

4.7 Simulation Setup

It is often challenging to find suitable parameters for complex time domain simulations. Usually, it is advisable to use wave tank tests to determine the hydrodynamic parameters. For the TLB concepts, the most important parameters are drag and added mass. Hydrodynamic damping is somewhat less important as the translations are small and should mainly be caused by first order motions. Extrapolated airy waves are used to compute the regular wave used in the optimization.

Extant literature, the IEA-OC4 project and findings reported in Paper 7 all indicate that drag- and inertia coefficients of 1.0 and 2.0, respectively, are valid settings, and thus are used for the simulations in this thesis. Axial drag and added mass are extracted and up-scaled from Paper 7, giving axial drag values of 0.1 and 0.5 for the tapered transition and the bottom end cap, respectively. The corresponding added mass parameters are set to 1.4. For descriptions of how 3DFloat handles the axial added mass, see earlier works. In addition, a linear damping heave of 230 kN/m is applied. The alpha and beta Rayleigh damping coefficients are set to 0.00182 and 0.0023, respectively, based on data from the wave tank experiments conducted in Brest. An additional structural damping of 2% of the critical mass is added to the mooring lines.

For the ALS, ULS and FLS verification runs, one-hour wind files were created with TurbSim. The simulation time was typically three hours with a time step of 0.01 seconds.

5 RESULTS AND EVALUATION

The design converges with relative ease towards an optimum balance of the design variables with respect to the given constraints and cost functions. This chapter evaluates the validity of the optimization and summarizes the resulting parameters for the optimized TLB B2 design. A verification of the design is presented in the following chapter. The optimized solution was obtained after 23 and 38 iterations in the frequency and time domains, respectively.

5.1 Optimized Geometry

One of the most important aspects of the TLB design is to keep the Eigen-periods in the acceptable regions, outside the high energy part of the wave spectrum and both the 1P and 3P regions. The resulting Eigen modes for the system, with the blades in feathered position, are listed in Table 9. It should be noted that the geometrical stiffness from the pre-tension in the mooring lines is not accounted for in the summary of frequency domain results, because it has weak influence compared to the element axial stiffness of the mooring lines in the system and thus is not deemed relevant to implement.

Table 9: Overview of the resulting design optimization variables, before and after time domain optimization

	Pre-time optimization		Post-time optimization (parked condition)						
	Feathered		Feathered		Blades at 0°		Without blades		
Mode	[Hz]	[s]	[Hz]	[s]	[Hz]	[s]	[Hz]	[s]	Shape
1	0.30	3.38	0.28	3.63	0.27	3.68	0.30	3.34	Surge/Pitch
2	0.30	3.30	0.28	3.58	0.28	3.63	0.30	3.34	Sway/Roll
3	0.62	1.60	0.67	1.48	0.58	1.73	0.71	1.41	Rotor torsion
4	0.63	1.59	0.70	1.43	0.67	1.49	0.71	1.41	1. bend (roll)
5	0.65	1.54	0.70	1.43	0.69	1.44	1.00	1.00	1. bend (pitch)
6	0.66	1.52	0.73	1.37	0.73	1.36	1.54	0.65	Blade twist
7	0.69	1.44	0.74	1.35	0.76	1.32	1.54	0.65	1 flapwise collective
8	0.70	1.43	0.87	1.16	0.84	1.19	2.33	0.43	Yaw
9	0.95	1.05	0.94	1.06	0.97	1.04	3.30	0.30	Heave
10	1.00	1.00	0.98	1.02	1.10	0.91	3.30	0.30	1 edgewise collective

There is a natural separation of roll and pitch periods due to the difference in stiffness between edge- and flap-wise direction on the blades. A 5% increase in pitch period is expected when the blades are turned fully into the wind, and an adequate distance to the 3P region should be maintained. Figure 7 illustrates the Eigen periods in relation to the allowed regions. For a detailed design, Eigen-periods should be investigated in detail with different pitch angles and nacelle positions.

Design in the frequency domain implies that Eigen modes should be placed somewhat apart in order to avoid coupled excitation. A typical level of separation is around 10%. This may be difficult to achieve for the TLB designs, as the structure is light, and the Eigen-periods are highly influenced by several parameters, such as water level and blade pitch. Mode 3 is of most concern, due to the

close proximity to the 1st bending modes. However, this will only be a concern during parked conditions, which have very limited durations relative to idling and production states. In order to get an impression of the influence, some FLS cases in the verification step will be run in parked condition. Modes 7 and 10 are of less concern as they will be influenced by the blade pitch angle.

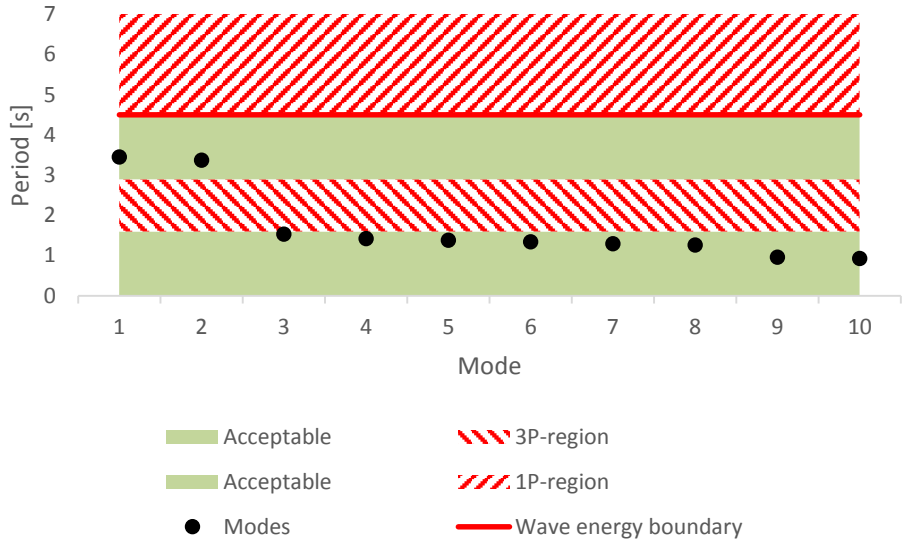

Figure 7: Visual interpretation of the location of the Eigen modes for the system

The time domain optimization influences the Eigen-periods of the system by less than 10%, which is deemed acceptable. However, the discrepancy is likely to be highly coupled to the closeness of the initial design to the optimized design and the optimization variables chosen for the time domain analysis. A final control of the Eigen-periods should always be performed after the time domain optimization. If the resulting Eigen-periods are not suitable, one should repeat the optimization loop, although this is rarely required, according to the author's experience with the setup.

5.1.1 Detailed Description of the Optimized Design

An overview of the resulting design variables is shown in Table 10.

Table 10: Overview of the resulting design optimization variables

Phase	Variable	TLB B2	TLB B - Initial	Unit
Frequency Domain	rr1	58.085	73.626	m
	d1	0.158	0.097	m
	d2	0.216	0.227	m
Time Domain	ht	-13.688	-19.271	m
	df	9.223	9.724	m
	pre1	2.92E-03	0.018	m/m
	pre2	3.48E-03	0.003	m/m

One of the major differences from the original optimization of TLB B, is the change in water depth. The optimal mooring radius for 50 m depth, with respect to stiffness distribution, is somewhat

larger than the water depth, but again the radius is roughly equal to the water depth for both TLB B and TLB B2.

The diameter of the floater is somewhat reduced, and the lower transition is moved closer to the surface, probably due to use of a lower extreme wave height in the environmental conditions, relative to the height used for the initial design. The resulting structural parameters are shown in Table 11.

Table 11: Overview of comparable results from the design optimization

Parameter	TLB B2	TLB B – Initial	Unit	Change
Floater mass	355	445	Tons	-20%
Top-side mass	701	667	Tons	5%
Anchor mass	103	190	Tons	-46%
Total mass	1068	1302	Tons	-18%
Wt floater	0.036	0.039	m	-7%
Wt transition	0.042	0.031	m	37%
Total buoyancy	2166	2 995	Tons	-28%
EB	1110	1 927	Tons	-42%
UML EA/L	21.70	21.72	MN/m	0%
LML EA/L	18.91	5.69	MN/m	232%

A 20% reduction of steel mass in the floater, to 355 tons, is consistent with expectations due to the reduction in environmental loads. The reduction from the initial design prior to the optimization was about 10%, down from 400 tons. This is somewhat lower than the TLB design proposed in (Sclavounos, et al., 2010), but expected as a more optimal depth and lower nacelle mass are used in this thesis. The anchor mass has been reduced by 46 % relative to the mass applied in Paper 3, which is desirable for the viability of the concept. The wall thickness in the tapered transition has somewhat increased due to the reduced value of ht, implying that the section will be subject to larger moments, and hence be more prone to fatigue damage. The increase in top-side mass is not due to the optimization, but results from the slight increase of the initial wall thickness of the tower top.

In addition, the mooring line dimensions have been increased, significantly for the lower lines. The initial TLB B design relied on the upper mooring acting as a stiff fixation point, resulting in relatively long surge and sway modes, while pitch and roll remained below the 3p region as the structure would pivot about the upper mooring. The increased size of the lower mooring lines, due to the yaw criterion, closed this option, and the surge and sway modes had to be placed together with pitch and roll for TLB B2, resulting in a considerable increase in stiffness for the lower mooring lines. This is not really a result of the optimization, but the desire to take the design a step forward by implementing more realistic constraints.

5.1.2 Visualisation

Schematic visualisations of the optimized design are shown in Figure 8 to Figure 12.

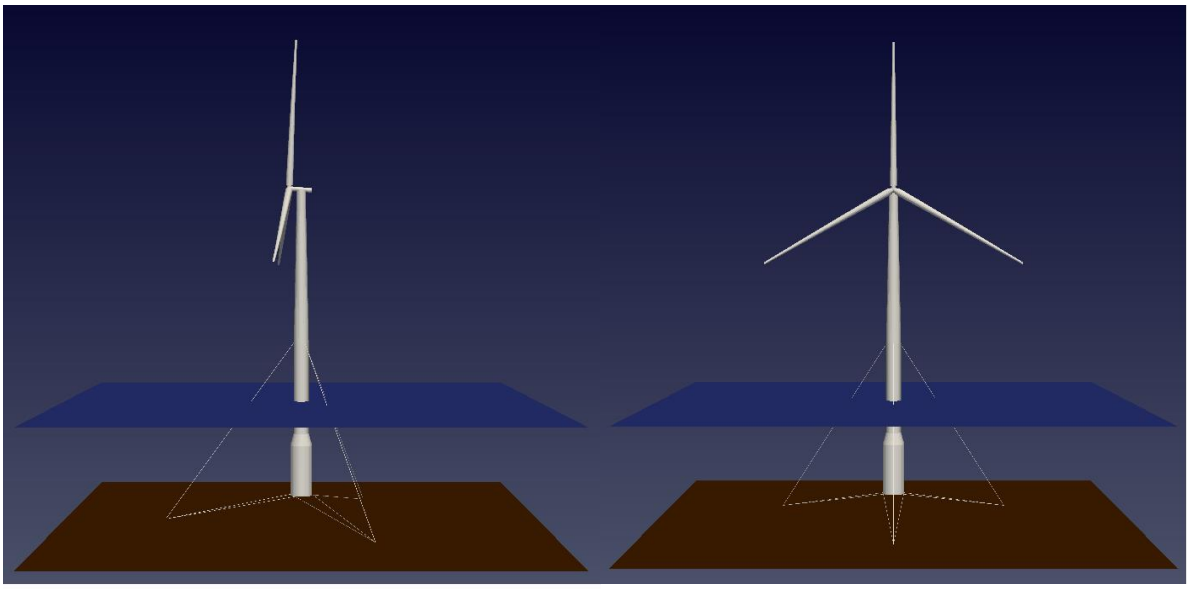

Figure 8: (to the left) x-z projection of the TLB B2 design
Figure 9: (to the right) y-z projection of the TLB B2

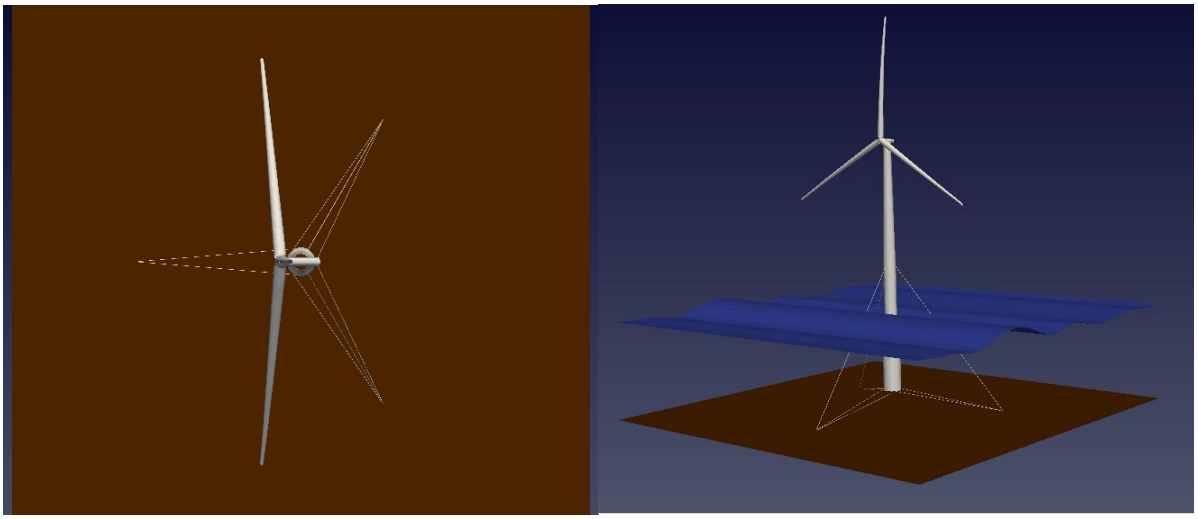

Figure 10: (to the left) x-y projection the TLB B2 design
Figure 11: (to the right) 3D-view of the TLB B2 design in an irregular sea state

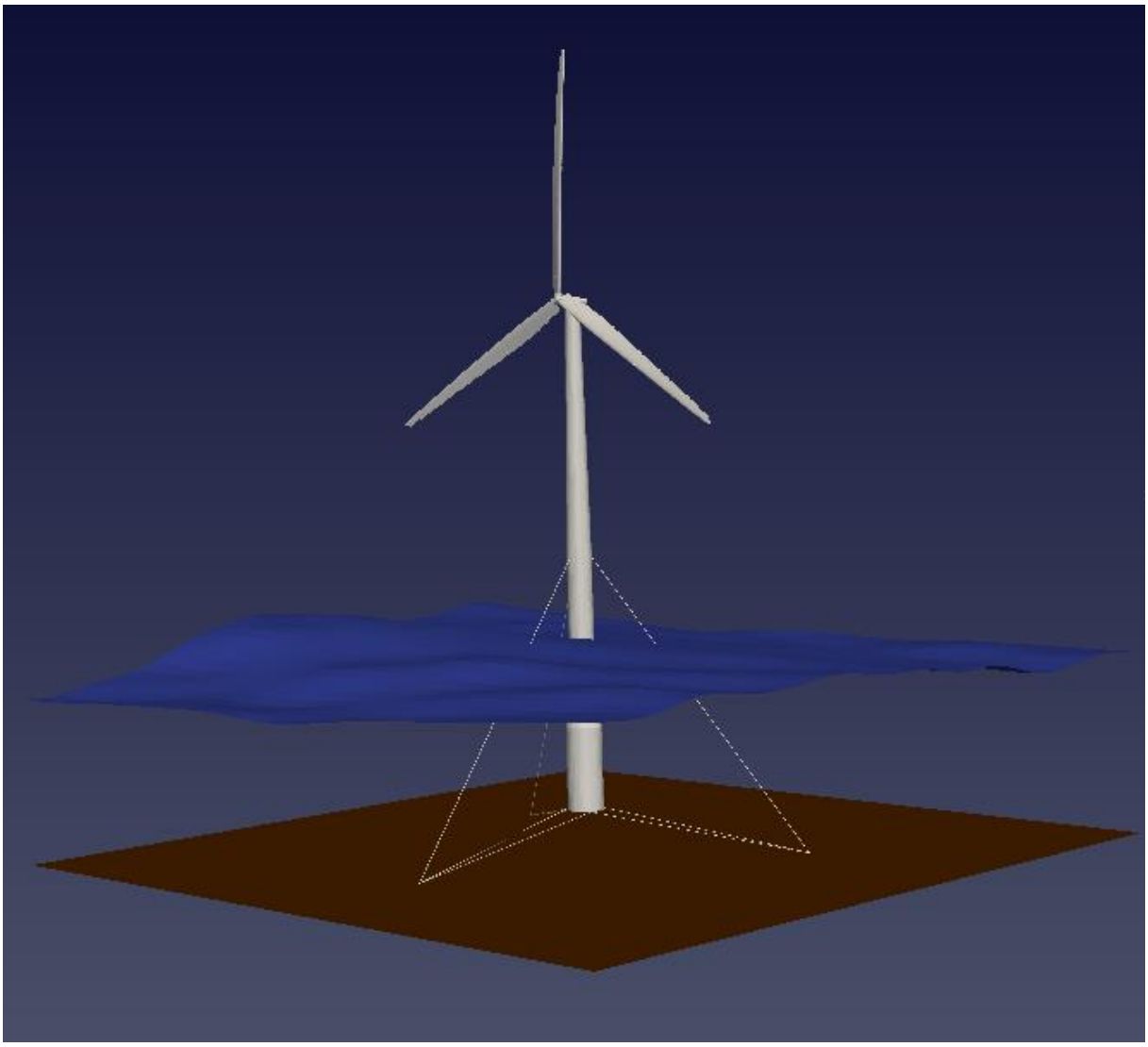

Figure 12: The TLB B2 in a rough sea state

5.2 Expected LCOE

The K13 Deep Water site in the Dutch North Sea, described in the Upwind Design Basis (Fisher, et al., 2010), is located at coordinates 53°13'04'' North and 3°3'13'' East, approximately 100 km north-west of the Dutch mainland.

In Paper 5 a baseline case with 100, 5 MW turbines was introduced. The distance to shore and relevant ports was assumed to be 200 km, relatively far offshore in comparison to parks that have been built in recent years. Later it was also pointed out that the discount rate and load factor were somewhat conservative. This resulted in relatively high LCOE for both the bottom-fixed concepts and the TLB systems, ranging from € 150 to € 160 per MWh. The concepts used in Paper 5 were not scaled to a specific site, but guestimates were applied to couple the mooring system and inter array cables to water depth. In order to elucidate probable outputs of a site-specific optimization

study more thoroughly, comparisons are applied here in two steps: first with the original baseline setup used in Paper 5, and then with the setup of the LCOE analysis optimized for the K13 deepwater site. The second step is performed to obtain the best LCOE estimate for the TLB system optimized towards a specific site. This will allow future concepts to be compared on equal terms as the K13 site has been thoroughly described and the data are publicly available.

5.2.1 Baseline of Paper 5 Comparison

The total CAPEX of all the concepts compared in Paper 5, and the newly optimized TLB B2, are shown in Figure 13. The total CAPEX is about 6 % higher for TLB B2 than for TLB B. As explained in the previous chapter, the K13 site favoured a different Eigen-period regime, for which an increase in mooring line diameter was found to be a cost-effective alternative through the optimization. The mooring radius is based on a 45 degree angle for the upper mooring lines in the LCOE scaling, thus any increase in depth will result in a significant increase in the length of the fibre rope used. It should also be noted that the additional set of three lower mooring lines is now implemented in the LCOE (as also described in the previous chapter), and they account for about 30% of the increase in total mooring line length, but as the anchor loads are also significantly reduced the total outcome is a reduction in total mooring costs.

A 6 % difference in CAPEX is within the area of uncertainty expected for the economic analysis. Closer inspection of the parameters in play during the optimization stage shows that optimizing for a different site in the 50 to 200 m depth range using linear extrapolation, based on maintaining the axial mooring line stiffness, may lead to up to 35 % variations in mooring and production costs. This supports the hypothesis that floating concepts, especially the TLB design, should be optimized for a site before comparing them in terms of economic performance with other designs. This is especially important when moving into sites with intermediate or shallow depths, where implementing typical catenary systems may prove to be very difficult and expensive. Catenary mooring, and possibly TLP, systems are assumed to be far easier to scale at depths increasing beyond 150 m.

None of the concepts compared in Paper 5 were optimized to the specific base case scenario, but the water depth sensitivity was documented and proved severe for the TLB design. Further comparison of the results for TLB B2 with the baseline scenario of Paper 5 seems futile as the design is only optimized for 50 m water depth.

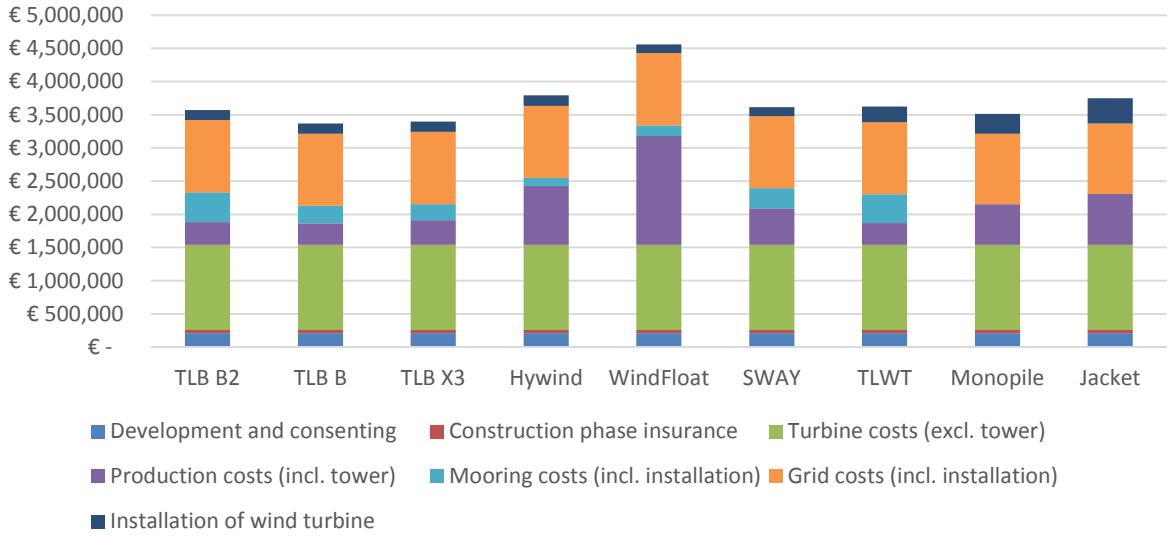

Figure 13: The CAPEX of all concepts compared in Paper 5 for a 500 MW wind farm in 120 meters of water depth and 200 km to shore, and TLB B2

5.2.2 CAPEX Evaluations for the K13 site

CAPEX estimations for the K13 site are shown in Figure 14. For TLB B and TLB2 they are almost identical (€ 3 102 855 and € 3 112 702, respectively). However, the TLB B system lacks the three additional mooring lines implemented in the TLB B2 to constraint in yaw motion[1]. The TLB B results should therefore be considered somewhat optimistic. However, interestingly, the CAPEX is now lower for the TLB design than for the bottom-fixed references situated in 30 m of water, as described in Paper 5. The CAPEX/MW for the TLB B2 design based on mooring plus production costs is even lower than the cost per MW solely of production for the monopile and jacket designs, by € 30 000 and € 186 000, respectively. The TLB B2 installation cost is also significantly lower. On the other hand, the shallow water prevents transport of the structure solely by towing, as assumed in the economic analysis. Although this has not been checked in detail, it seems reasonable to assume that a temporary secondary structure would be required stabilize the TLB B2 during tow-out due to the 50 m water depth. The shallow depth also implies that other installation options, such as jack-up vessels (as assumed for the bottom-fixed concepts) could be used for parts of the installation.

It should be noted that spar-concepts like the Hywind and SWAY are unlikely to be applicable at these water depths. The cost of catenary mooring systems, such as those for the WindFloat, should also be treated with considerable caution, as there are significant challenges in implementing traditional catenary mooring systems for large floating wind turbines at sites with intermediate depths.

[1] The typical increase in mooring line length is around 40 %, but it is depth-dependent. It will also influence the installation time. Thus, estimating the likely relative increase in CAPEX associated with increasing the mooring line length is far from straightforward.

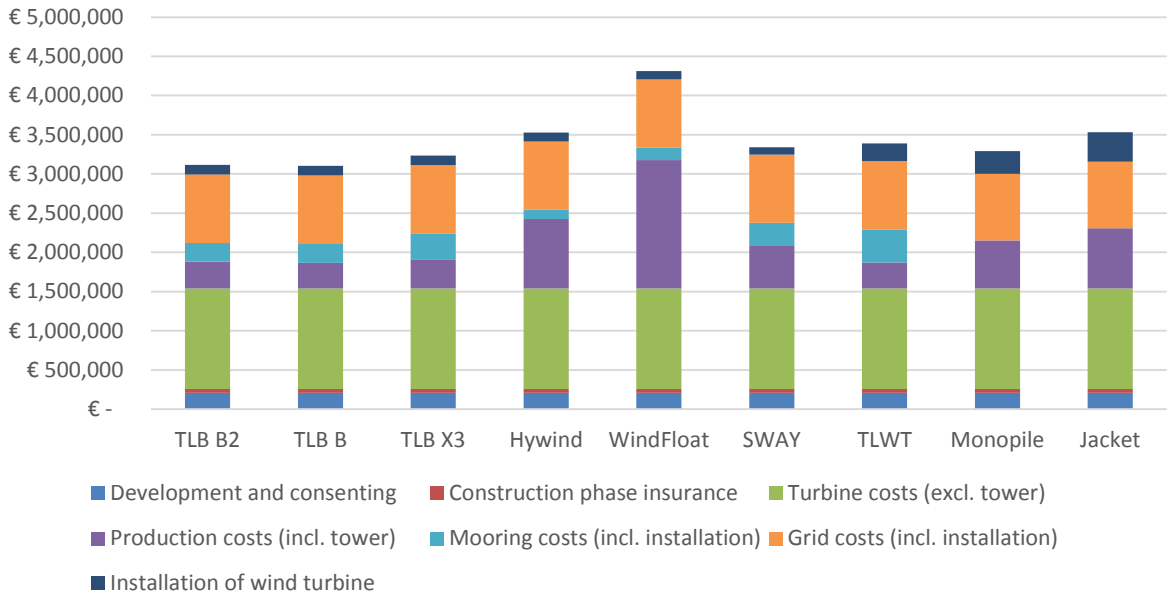

Figure 14: The CAPEX of all concepts compared in Paper 5 for a 500 MW wind farm in 50 meters of water depth and 100 km to shore, and TLB B2

The low CAPEX/MW for the TLB B2 shows that the gap in costs between offshore floating wind turbines and onshore turbines is starting to close. The turbine nacelle and rotor typically account for about 49 % of the CAPEX for a typical onshore turbine (Gielen, 2012), and now 41 % of the CAPEX for the TLB B2. In comparison, the turbine and nacelle only account for about 30 % of the CAPEX for the WindFloat. The largest discrepancy between the TLB B2 and the onshore systems is now in the grid costs, which account for over 28 % of the CAPEX for TLB B2 and just 11 % of the CAPEX for a typical onshore concept. The cost of onshore foundations should also not be neglected, as they typically account for about 16 % each (33 % in total) of the CAPEX of onshore turbines (Gielen, 2012). The substructure and mooring for the WindFloat contributes about 42 % of the CAPEX computed for the design, significantly more than for the onshore turbines. Due to the supporting mooring lines just below the rotor plane, the TLB B2 foundation & mooring costs only account for 19 % of its total CAPEX.

Typical offshore wind power CAPEX in the UK was reportedly € 3 367 985 in 2010 (Gielen, 2012). Thus, a CAPEX of around € 3 100 000 for the floating concepts suggests that they could be fierce competitors to bottom-fixed windfarms, but a low CAPEX is only an indicator of potential.

5.2.3 LCOE Evaluations for the K13 site

The reference scenario for the K13 site consists of a farm of 100 turbines with 25 years operational life. The distance to shore is set to 100 km and the wind farm is connected to the mainland grid by one transmission cable with HVDC connection to minimize the loss of energy. Reference values for the detailed input, such as material prices, vessel rates etc. are described in Paper 5.

Assuming a discount rate of 8 % and a net load factor of 47.5 % a baseline LCOE of € 106.3 ± 7 % (98.9 – 113.8) is computed for TLB B2. This is marginally lower than for the monopile at € 107.0 ± 8 % (98.3 – 115.9) and the jacket at € 113.0 ± 8 % (104.6 – 121.5). The variation is only based on changes in steel price, vessel day rates and turbine costs, as described in Paper 5. Variables such as desired discount rate, contingency level, component cost reduction and load factor are considered as *known* variables when establishment of a wind farm is being seriously considered. Nevertheless, the variation in LCOE from baseline caused by varying each of the parameters is presented in Figure 15 to illustrate its sensitivity to them.

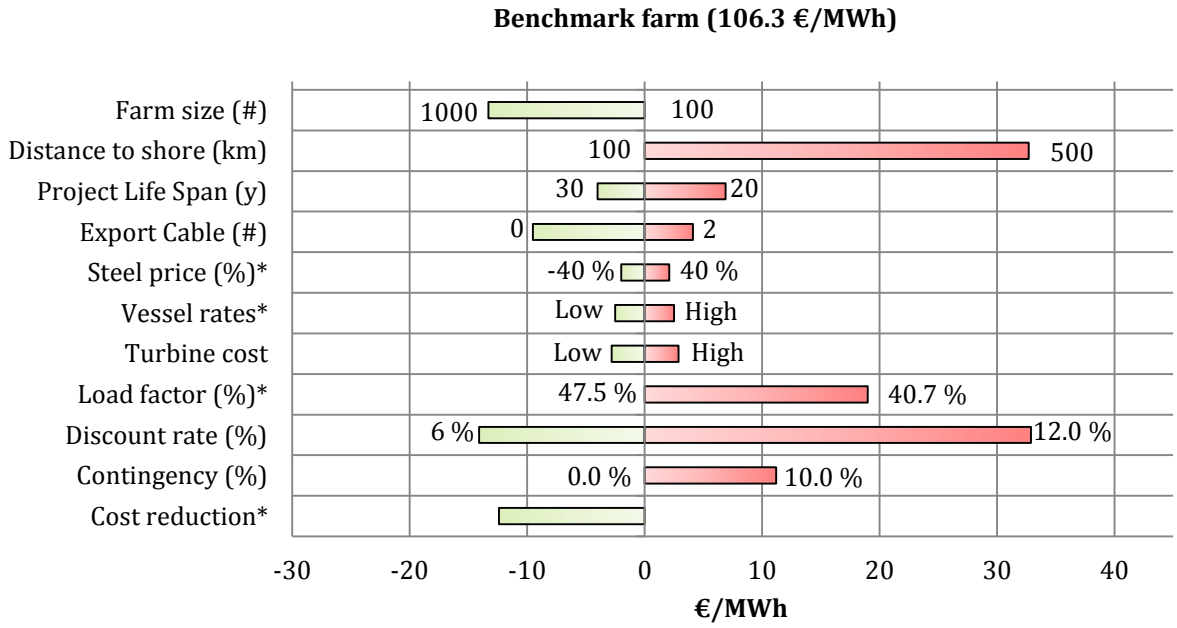

Figure 15: Variation in LCOE caused by varying the model parameters

The LCOE levels obtained here are about 50% less than those in Paper 5, largely due to use of a more realistic wind farm location (which reduces the LCOE by about € 10 per MWh), rather than the optimization of TLB B2. The optimization and further development of the TLB concept mainly help to reduce uncertainty regarding the concept, relative to the optimization presented in Paper 5. Reduction in the baseline discount rate from 10 to 8 % and the increase in baseline net load factor from 44.6% to 47.5 % also results in significant reductions of about € 15 and € 10 per MWh, respectively. The increase of the project life span lowered the LCOE by about € 5 per MWh.

The discounted cash-flow from CAPEX and OPEX contribute € 76.7 (72 %) and € 29.6 (28 %) per MWh to the total LCOE of € 106.3 for the TLB B2. DECEX is negligible, contributing less than € 0.1 per MWh, as the floater is made of steel and the towability enables efficient recycling. A quantified overview of the costs is shown in Table 12.

Table 12: A quantified overview of the costs for the LCOE

CAPEX	**Total wind farm**	**Per MW**
Development and consenting	€ 104,000,000	€ 208,000
Construction phase insurance	€ 25,000,000	€ 50,000
Turbine costs (excl. tower)	€ 640,500,000	€ 1,281,000
Production costs (incl. tower)	€ 171,300,000	€ 342,600
Mooring costs (incl. installation)	€ 118,770,845	€ 237,542
Grid costs (incl. installation)	€ 437,506,000	€ 875,012
Installation of wind turbine	€ 60,825,971	€ 121,652
Contingency	€ -	€ -
TOTAL CAPEX (EURO)	**€ 1,557,902,816**	**€ 3,115,806**
OPEX		
Annual operation & maintenance	€ 53,263,766	€ 106,528
Annual operation phase insurance	€ 8,750,000	€ 17,500
TOTAL OPEX (EURO/MW/annum)	**€ 62,013,766**	**€ 124,028**
DECEX		
Phasing		**€ 5,230**
TOTAL DECEX (EURO)	**€ 2,614,932**	**€ 5,230**
Energy Production		
Net energy production per MW (MWh)		**4,202**
NET Annual Energy Production - MWh	**52,521,163**	
Discount Rate (average over project lifetime)		**8.00%**
Discounted Cash flow		
Total CAPEX	€ 1,313,885,538	€ 2,627,771
Total OPEX	€ 507,408,637	€ 1,014,817
Total DECEX	€ 270,060	€ 540
Total discounted cash flow	**€ 1,821,564,235**	**€ 3,643,128**
Discounted net generation	**17,130,497**	**34,261**
Levelised Cost of Energy	**106.3**	**EURO/MWh**

A 2 % loss is assumed for an extreme, hypothetical loss of turbines due to a critical production fault in the mooring lines after 10 years. This would increase the total LCOE by 0.8 % when accounting for present value. An even more extreme hypothetical failure of 10 % of the mooring systems after 15 years would increase the total LCOE by ca. 2.3 %. In comparison, adding an extra set of mooring lines to the structure, for stability redundancy, increases the LCOE by some 4.4 % for the mooring lines and anchors, neglecting the additional cost of fabrication and additions to the main structure. This corresponds to the loss of almost 20 % of the turbines after

15 years and seems rather unrealistic. The results imply that even cheap redundant systems for offshore wind turbines should not be prioritized, as long as the probability of failure is relatively low or failure is most likely to occur late during their lifetime, but thorough analysis of failure likelihoods, modes and costs should be conducted to optimize the balance between redundancy costs and failure risks.

5.2.4 Offshore Floating Wind versus Other Markets

There are various support schemes for different types of renewable energy production in every country. Mapping the potential for a specific concept in all of the relevant countries and markets is therefore a substantial task, well beyond the core scope of this thesis. However, a basic assumption is that it must be able to compete with the alternatives. Several countries offer different levels of support for onshore and offshore wind systems, but in order to compete generally floating systems should be cheaper than the alternatives, which in many cases are onshore wind farms or, for countries with limited available land, bottom fixed offshore wind systems in shallow water.

The average capacity factor for onshore wind turbine farms in Europe ranges from 25 to 30 % according to the International Energy Agency (IEA, 2011). Figure 16 shows the relationship between estimated LCOE and capacity factor for onshore wind farms at several CAPEX values in 2011 and 2015. In 2011 the upper and lower bounds are set to € 1 544 256 and € 1 355 932, respectively. This is considerably lower than the CAPEX values obtained for any of the offshore concepts; the CAPEX for TLB B2 is nearly twice as high, thus the concept would need to deliver substantially higher production to achieve a favourable LCOE.

LCOE for onshore projects in high resource areas (USA, Brazil, Sweden and Mexico) averaged about € 51/MWh in 2011, but several of the projects installed in 2010 also produced LCOE up to € 100/MWh (Gielen, 2012). This is comparable to the values obtained for the TLB B2 at the K13 site. It should also be noted that grid costs account for over 20 % of the LCOE, thus a change in support schemes regarding grid connection can quickly make offshore wind farms an economically viable option in *any* country.

If we assume an optimistic average capacity factor of 30 % for onshore turbines in Europe, the average LCOE in 2011 was around US^{2010} 0.105 per kWh (about €^{2013} 79 per MWh, in the units applied in this thesis).The average LCOE for an offshore turbine in Europe in 2010 was considerably higher, about € 122 per MWh (Gielen, 2012). The baseline LCOE estimate for the K13 site is intermediate here, and not quite competitive with the average onshore wind farm, but probably competitive with onshore farms at sites where they produce energy at more than average costs. An important point is that the TLB B2 is more favourable than the average bottom-fixed solution in Europe, in addition to a significant proportion of the onshore wind farms.

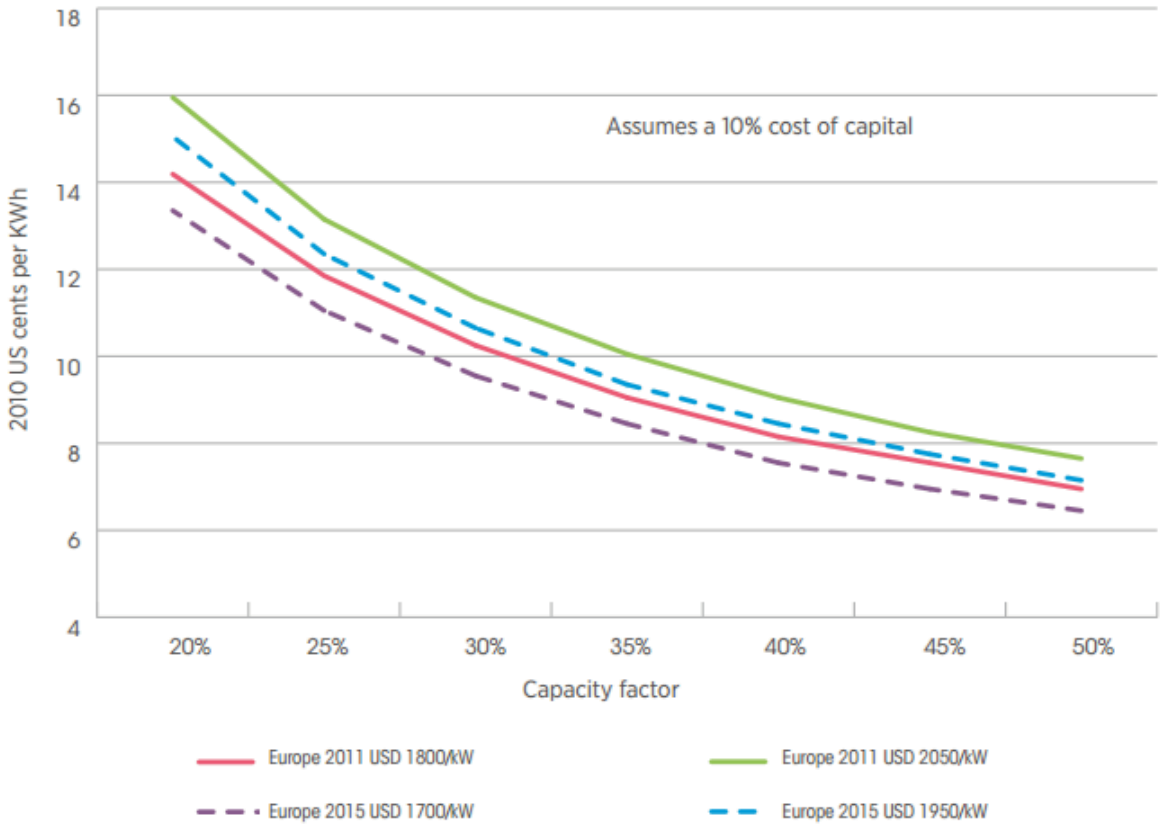

Figure 16: Estimated LCOE for onshore wind farms in Europe in 2011 and 2015 as functions of CAPEX and capacity factor
(Gielen, 2012)

The LCOE of onshore windfarms in the USA is estimated to be somewhat lower than in Europe, but somewhat higher in other markets suitable for offshore wind, such as Japan and Australia (IEA, 2011). Thus, if the TLB B2 is a competitive solution for Europe, it may be even more competitive in other markets, relative to onshore wind, and especially relative to other offshore wind options.

The Japanese and Australian onshore CAPEX per MW in 2010 was listed at around € 2000 and € 1800 /MWh (IEA, 2011). This is 30% and 17 % higher, respectively, than the upper limit quoted by Gielen for Europe. Assuming similar proportional contributions of CAPEX and OPEX, the equivalent LCOE for onshore turbines in Japan and Australia would be approximately € 110 and € 102 per MWh, respectively. Offshore LCOE at 45 m depth in Japan is assumed to be between € 122 and € 136 per MWh (GL Garrad Hassan, 2012). For a site like K13, the TLB B2 concept should be able to outperform both the onshore alternatives and existing offshore alternatives in Japan. It should also be able to compete with onshore turbines in Australia, but probably at somewhat higher energy prices than average onshore wind farm prices. It should be noted that local variations and extreme weather events, such as typhoons and cyclones, may significantly influence the results. Local adaption and optimization of the TLB B2 concept is advised based on the current findings.

6 VERIFICATION OF THE OPTIMIZED DESIGN

In order to determine the performance of the concept, the verification cases were thoroughly examined. For a TLB design with short resonant periods it is important to avoid excitation of the structure by significant amounts of energy at corresponding frequencies. The excitation within relevant frequency bands that can be endured strongly depends on the amount of damping in the system. The verification cases considered here are used as preliminary controls prior to a more thorough ULS, FLS and ALS study in a detailed design phase.

6.1 Verification of Dynamic Load Cases

The verification presented here still focuses on FLS and ULS cases, to confirm (*inter alia*) that the chosen optimization load case 1 covers the more complex and realistic load combinations. A normal safety class, implying a target safety level of 10^{-4} (annual probability of failure) according to DNV-OS-J101, is desired. This corresponds to the standard safety level for unmanned structures in DNV-OS-C101. Effects of several categories of events, in various combinations, should be investigated, e.g. extreme winds, waves and/or currents in operational, idling and parked modes. In addition spreading of waves and misalignments of wind, current and waves should ideally be considered. The limit state design proposed in DNV-OS-J101 is used as guidance.

Since first order excitation is most important, it is assumed that misalignment will reduce peak loads in the system and is therefore neglected. As $H_{,max}$ in the wave series results in the largest wave excitation, only a limited range of different wave heights is used, and the focus is on effects of extreme T_p, as responses to high frequency loads are of most interest.

A series of extreme load cases is used to demonstrate the survivability of the concept. Table 4-5 in (DNV-OS-J101, 2013) is used as a basis for establishing the load cases. Only those assumed to be most important for mooring and substructures are used to limit the extent of the verification. Ideally, responses across the 50-year contour line for combinations of 50-year wave conditions and various T_p values should be assessed, but to limit the number of load cases, only the mean T_p for each of the given significant wave heights will be computed. It is assumed that this will have limited influence on the results at this stage of the design phase.

Peak loads are expected during operation around rated wind speed (when thrust force is maximal) and during extreme events (when wave loads are maximal). In addition, power production at wind speeds in the region of 18-20 m/s is known to produce the largest yaw moments, although this is dependent on the rotor size, type of controller, turbine type and turbulence. For operational states, load cases 1.1 and 1.6a are used.

Load cases 2.x, 3.x 4.x and 5.x are neglected as no specific wind turbine supplier is used. Thus computation of these cases is not relevant. From experience, these cases are also most important for the design of upper parts of the tower and turbine blades.

For parked conditions, load case 6.1a is used with no misalignment. Parked conditions with pitch failure (load case 7.1a) is also included to demonstrate robustness and the relatively low importance of including misaligned cases.

Changes in water level are assumed to be irrelevant, as they have minor effects on the excess buoyancy and thus are not included in the variations. The selected load cases are summarized in Table 13.

Table 41 in (Fisher, et al., 2010) lists the extreme values, and Tp variations are implemented using formula 1. The shape parameter for the Jonswap-spectrum is set to 3.5, in accordance to (DNV-OS-J101, 2013). A complete compiled list is shown in Table 14.

Table 13: Summarized load cases

Design situation	Load case	Wind condition	Wave condition	Current	Limit State
Production	1.1	NTM	NSS	wind-gen	ULS
Production	1.6a	NTM	SSS	wind-gen	ULS
Parked	6.1a	EWM	ESS	50-year	ULS
Parked with fault	7.1a	EWM	ESS	1-year	ULS-Abnormal

Table 14: List of Ultimate Load Cases (ULS) for evaluation of performance

Turbine State	J101 DLC	DLC	Duration	Direction	Wave				Wind	Turbulence	Current
			[hours]	Uni[Deg]	Seeds	Hs [m]	Tp [m]	gamma [-]	U,100[m/s]	Ti [%]	V [m/s]
Production	1.1	ULS01	3	0	5	7.1	10.8	3.5	11.4	18	0.3
	1.1	ULS02	3	0	5	7.1	10.8	3.5	18	16	0.45
	1.1	ULS03	3	0	5	7.1	10.8	3.5	24	15	0.6
	1.1	ULS04	3	60	5	7.1	10.8	3.5	11.4	18	0.3
	1.1	ULS05	3	60	5	7.1	10.8	3.5	18	16	0.45
	1.1	ULS06	3	60	5	7.1	10.8	3.5	24	15	0.6
	1.6a	ULS07	3	0	5	9.4	12.4	3.5	24	15	0.6
	1.6a	ULS08	3	60	5	9.4	12.4	3.5	24	15	0.6
Parked	6.1a	ULS09	3	0	5	9.4	12.4	3.5	42.7	11	1.2
	6.1a	ULS10	3	60	5	9.4	12.4	3.5	42.7	11	1.2
Parked + fault	7.1a	ALS01	3	0	1	7.1	10.8	3.5	32.7	11	0.6
	7.1a	ALS02	3	60	1	7.1	10.8	3.5	32.7	11	0.6
	7.1a	ALS03	3	0	5	7.1	10.8	3.5	32.7	11	0.6

Limited data are supplied in (Fisher, et al., 2010) regarding the correlation between wave height and wind speed. The 1 year recurrence wave height is therefore applied to all wind speeds for DLC 1 to 6. This is assumed to be severely conservative for the cases with wind speeds below 24 m/s. 50-year wave conditions are assumed plausible with wind speeds around cut-out and are therefore used with ULS07 and ULS08. Effects of including a control mechanism that shuts down

power production during severe sea states are not considered. The corresponding return periods for the ULS cases listed in Table 14 are shown in Table 15.

Table 15: Recurrence periods corresponding to environmental loads in the ULS table

Turbine State	J101 LC	DLC	Return Period			Comment
			Wave	Wind	Current	
Production	1.1	ULS01	1	NA	Wind-driven	Rated wind speed
	1.1	ULS02	1	NA	Wind-driven	Above rated
	1.1	ULS03	1	NA	Wind-driven	Above rated
	1.1	ULS04	1	NA	Wind-driven	Rated wind speed
	1.1	ULS05	1	NA	Wind-driven	Above rated
	1.1	ULS06	1	NA	Wind-driven	Above rated
	1.6a	ULS07	50	Cut-out	Wind-driven	Production and SSS
	1.6a	ULS08	50	Cut-out	Wind-driven	Production and SSS
Parked	6.1a	ULS09	50	50	50	Extreme turb Wind @ 50 year SSS
	6.1a	ULS10	50	50	50	Extreme turb Wind @ 50 year SSS
Parked + fault	7.1a	ALS01	1	1	1	Pitch failure
	7.1a	ALS02	1	1	1	Pitch failure
	7.1a	ALS03	1	1	1	Lower mooring line failure

Fatigue is assessed by running the pre-defined FLS cases suggested in (Fisher, et al., 2010). This is run unidirectional and in-line with one mooring line, which is assumed to be the worst direction. This is considered to be a rather crude approach, which is likely to disfavour concepts that are sensitive to fatigue. The computed list of the FLS cases is shown in Table 16.

Stress is assessed at 13 cross-sections in the structure and fatigue damage at eight equally spaced points around the circumference. Total damage is assessed by Rainflow-counting and summed for each section over 25 years of life time. Stress concentration factors (SCF), in accordance with (DNV-RP-C203, 2010) are used. Sections are assumed to be conical sections welded from both sides. Doubler plates, hull penetrations and brackets are not considered. Thus, S-N (stress-cycle number) curve C1 can be used for the tower. The substructure is assumed to be fabricated with less precession and no grinding of welds. Thus, S-N curve D is assumed. For the tower, DNV-OS-C203 table 2-1 for S-N curves in air is used. For the substructure, table 2-2 for S-N curves in seawater with cathodic protection is applied. It is not necessary to implement a bi-linear approach as the number of cycles rather than high stress peaks drives fatigue for the TLB system.

The design fatigue factor (DFF) is assumed to be 3 in the design life calculations. This is in accordance with the low safety class in DNV-OS-J103 for non-accessible areas without planned inspections. No detailing of connections is performed, but the SCF is computed based on recommendations in section 3.3.7of DNV-OS-J101 (2013) (giving factors of 1.584 for positions in the tapered section in the floater, and 1.536 at other positions).

Table 16: List of Fatigue Limit State (FLS) cases for evaluation of performance

DLC	Hub Wind speed [m/s]	Turbulence [%]	Hs [m/s]	Tp [s]	Gamma [-]	Occurrence [hours/y]
FLS01	2	29.2	1.1	6.0	3.3	531.8
FLS02	4	20.4	1.1	5.9	3.3	780.6
FLS03	6	17.5	1.2	5.8	3.3	1230.6
FLS04	8	16.0	1.3	5.7	3.3	1219.7
FLS05	10	15.2	1.5	5.7	3.3	1283.7
FLS06	12	14.6	1.7	5.9	3.3	1250.2
FLS07	14	14.2	1.9	6.1	3.3	734.2
FLS08	16	13.9	2.2	6.4	3.3	728.5
FLS09	18	13.6	2.5	6.7	3.3	366.7
FLS10	20	13.4	2.8	7.0	3.3	304.8
FLS11	22	13.3	3.1	7.4	3.3	134.4
FLS12	24	13.1	3.4	7.8	3.3	85.3
FLS13	26	12.0	3.8	8.1	3.3	44.7
FLS14	28	11.9	4.2	8.5	3.3	17.7
FLS15	30	11.8	4.5	8.9	3.3	8.4
FLS16	32	11.8	4.8	9.1	3.3	4.4
FLS17	42	11.7	4.9	9.4	3.3	1.6

It should be noted that the main purpose of the verification step is not to fully document the concept, but to demonstrate the viability of the optimization approach. For the ULS results, an accuracy of ±15 % is assumed, due to lack of seed variation.

6.2 Verification of Results

One of the most potentially problematic aspects of the TLB system is that the mooring loads are relatively high. Thus, these loads are focal points of the ULS verification. Local buckling is not assessed at ULS as mooring pad eyes, equipment fixation, secondary structures and J-tube are not assessed at this stage.

6.2.1 ULS Verification

The ULS verification results are shown in Table 17 to Table 18. The extremals in each category are highlighted.

Table 17: Translations and rotations at the tower top during the verification ULS DLCs

vDLC	Heave [m]		Surge [m]		Sway [m]		Pitch [deg]		Roll [deg]		Yaw [deg]	
	Mean	Max	Mean	Max	Mean	Max	Mean	Max	Mean	Max	Mean	Max
ULS01	-0.20	0.21	0.40	0.70	-0.04	0.24	0.23	0.40	-0.03	0.14	0.01	0.23
ULS02	-0.20	0.21	0.23	1.04	-0.05	0.29	0.13	0.61	-0.03	0.16	0.01	0.37
ULS03	-0.20	0.21	0.21	**1.05**	-0.06	0.30	0.12	**0.58**	-0.04	0.18	0.02	0.49
ULS04	-0.20	0.21	0.24	0.47	0.32	0.66	0.14	0.26	0.18	0.35	0.01	0.23
ULS05	-0.20	0.21	0.16	0.65	0.17	**0.99**	0.09	0.37	0.10	**0.55**	0.01	0.36
ULS06	-0.20	0.21	0.15	0.57	0.15	0.81	0.09	0.32	0.08	0.47	0.02	**0.50**
ULS07	-0.20	**0.22**	0.21	0.79	-0.06	0.33	0.12	0.49	-0.04	0.19	0.02	0.48
ULS08	-0.20	**0.22**	0.15	0.52	0.15	0.68	0.09	0.30	0.08	0.40	0.02	**0.50**
ULS09	-0.18	0.20	0.08	0.91	0.00	0.35	0.04	0.53	0.00	0.20	0.00	0.08
ULS10	-0.18	0.20	0.02	0.48	0.04	0.62	0.01	0.26	0.02	0.31	-0.01	0.08

Table 18: Accelerations at the tower top during the verification ULS DLCs

vDLC	Heave [m/s²]		Surge [m/s²]		Sway [m/s²]	
	Mean	Max	Mean	Max	Mean	Max
ULS01	0.00	0.20	0.00	1.12	0.00	0.69
ULS02	0.00	0.31	0.00	1.76	0.00	0.89
ULS03	0.00	0.46	0.00	1.48	0.00	1.59
ULS04	0.00	0.21	0.00	0.75	0.00	1.34
ULS05	0.00	0.32	0.00	0.89	0.00	1.45
ULS06	0.00	0.46	0.00	2.36	0.00	1.27
ULS07	0.00	**0.48**	0.00	1.76	0.00	**1.61**
ULS08	0.00	0.46	0.00	1.58	0.00	1.40
ULS09	0.00	0.19	0.00	**2.47**	0.00	0.92
ULS10	0.00	0.18	0.00	1.20	0.00	1.45

These values are considered well within acceptable limits. The maximum horizontal acceleration is 2.47 m/s², within the targeted upper limit of 2.5 m/s². The rotations and translation are similar to levels of onshore turbines. Maximum heave occurs during interactions with the largest waves, and the surge and sway responses are similar, but peak at rated wind speeds in ULS03. It should be noted that the results are based on one three-hour seed, thus the values should be expected to have ± 20 % variation. A Gumbel distribution generated with several seeds is suggested to estimate 50-year extreme ULS responses accurately.

For the mooring lines, OS-E301 (DNV-OS-E301, 2010) states the following:

$$S_c - T_{c,mean} - T_{c,dyn} \geq 0 \qquad \textbf{Equation 12}$$

Where:

$S_c = Characteristic\ strength$
$T_{c,mean} = partial\ safety\ factor\ on\ mean\ tension \cdot mean\ tension$
$T_{c,dyn} = partial\ safety\ factor\ on\ dynamic\ tension \cdot dynamic\ tension$

The required stiffness (EA) according to the optimization is approximately 1.37E6 kN for the upper mooring lines. According to (BEXCO, 2015) this corresponds to a stock DeepRope of 187 diameter with a Minimum Breaking Load (MBL) of 24812 kN. OS-E301 requires the characteristic strength S_c to be considered as 95 % of the minimum break strength, which equals 23571 kN.

For the lower mooring lines, a stiffness of approximately 1.20 kN is required. This corresponds to a diameter of 177 mm and result in a characteristic strength of 20798 kN.

The partial safety factors for mean and dynamic tension of a mooring line in consequence class 1 assessed by dynamic analyses are 1.1 and 1.5, respectively. However, amendment D203 is used, multiplying the values by 1.2, as the redundant mooring line system has not been fully verified at this point. The resulting partial safety factors used for the ULS evaluation of the mooring lines are therefore set to 1.32 and 1.8 for mean and dynamic tension, respectively.

Table 19: Mooring line utilization during the verification ULS DLCs

vDLC	Lower mooring lines (worst)			Upper mooring lines (worst)		
	Mean [kN]	Dynamic [kN]	Utilization [%]	Mean [kN]	Dynamic [kN]	Utilization [%]
ULS01	**5269**	4125	40	3190	2205	23
ULS02	4719	4395	39	3509	2985	28
ULS03	4664	4725	40	3564	2730	27
ULS04	4620	2310	29	2420	4830	31
ULS05	4367	2775	30	2992	4740	33
ULS06	4367	2790	30	3058	4260	31
ULS07	4686	5505	43	3553	3195	29
ULS08	4378	2925	31	3036	6150	39
ULS09	4422	**6060**	**44**	**3630**	3870	32
ULS10	4103	4830	38	3421	**6780**	**43**

As expected, the mooring lines' utilization, shown in The partial safety factors for mean and dynamic tension of a mooring line in consequence class 1 assessed by dynamic analyses are 1.1 and 1.5, respectively. However, amendment D203 is used, multiplying the values by 1.2, as the redundant mooring line system has not been fully verified at this point. The resulting partial safety factors used for the ULS evaluation of the mooring lines are therefore set to 1.32 and 1.8 for mean and dynamic tension, respectively.

Table 19, increases with the sea state, but there is also a local peak around rated wind speed for production. Elements such as marine growth and additional forces from secondary structures have not been assessed, but are considered less significant for the mooring line response as the utilization is low. One can also conclude that stiffness rather than loads drive the mooring design as the utilization is low.

Reducing the anchor loads has been an important design driver for the continued development of the TLB concept. Characteristic anchor load results are presented in Table 20. The maximum vertical resultant (occurring when wave heights are most severe) is about 7 500 kN and anchor resultant forces peak when the worst wave conditions coincide with a production state at winds speeds close to cut-out. The utilization is based on a Vryhof Vertical Load Anchor (VLA) type

anchor with an ultimate holding capacity of 20 000 kN, excluding the computation of soil capabilities. Both the anchor and mooring line loads are now well within loads considered typical for offshore installations.

Table 20: Anchor vertical lift and resultant force during ULS verification

vDLC	Anchor vertical force		Anchor resultant force		Utilization
	Mean [kN]	Max [kN]	Mean [kN]	Max [kN]	[%]
ULS01	**4650**	5440	**8730**	13500	84
ULS02	4280	5440	8430	13900	87
ULS03	4250	5440	8430	13600	85
ULS04	4200	5530	7050	12000	76
ULS05	3080	5810	7340	11900	75
ULS06	3120	5690	7350	11900	75
ULS07	4270	5440	8470	**14600**	**93**
ULS08	3100	6900	7320	13800	89
ULS09	4110	5440	8460	**14600**	**93**
ULS10	3340	**7440**	7400	14100	91

With respect to directions, the 60 degree production cases result in approximately 10 % lower peak mooring line and anchor forces, but the total translation is somewhat larger. This implies that the system is slightly softer in this direction. Parked cases produce similar anchor forces, and as waves alone account for more of the forces in the system the lack seed variation increase the uncertainty of the results. For the lower mooring lines, no temporary slack events occurred during any of the simulations with the six-line configuration. For the upper lines, slack events occurred during some of the cases with wind speeds around cut-out and the turbine in production state. Traditionally slack lines are known to produce snapping loads, but no snapping loads appeared in the time series. An example from ULS07 is shown in Figure 17.

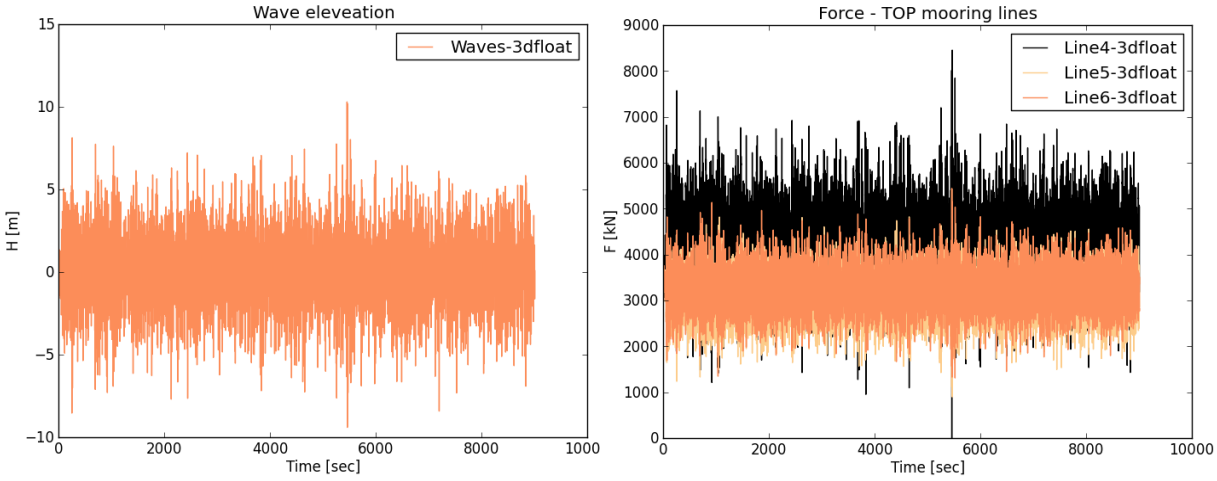

Figure 17: Force plots over time for the waves (left) and lower mooring lines (right) during the ULS07 DLC

A shell integrity control was performed based on DNV RP-C202. Shell, panel ring and column buckling was checked. The dimensioning moment and axial stress was checked for all the time series. The governing load case and the resulting utilization is shown in **Table 21** .

Table 21: Buckling utilization

Position [m]	Governing DLC	Utilization
-37.8	ULS07	**91%**
-20.1	ULS07	67%
-12.5	ULS07	62%
0.0	ULS07	67%
10.0	ULS02	56%
10.0	ULS02	69%
24.6	ULS02	**77%**
24.6	ULS02	**77%**
37.0	ULS02	70%
50.0	ULS02	63%
62.0	ULS02	52%
75.0	ALS01	43%
86.0	ALS01	43%

Overall, the buckling utilization is relatively low. For the lower part of the substructure, wave loads are dominating. Above the water line, typically high turbulence loads on the wind turbine result in extreme moments that produce the highest utilization.

The lowest section produce a high utilization, in general, due to a simplified approach, as no support from the bottom end cap structure is included, but a simple distribution of ring stiffeners was included. The vertical spacing was 3 m, and a generic stiffener with a height of 0.3 m and an average thickness of 0.025 m was assumed. No vertical stiffeners was assumed, although this might be beneficial for the submerged tapered section in the substructure. The resulting mass of the ring stiffener system was 26.1 tons.

6.2.2 ALS Verification

Three accidental load cases were assessed. The translation and rotational responses observed in these cases are summarized in Table 22 and Table 23. The responses are similar to those of the ULS runs, except for ALS03 (with a broken mooring line, where the yaw response was increased, but no extreme angles were observed).

The ALS03 DLC resulted in lower accelerations than the ULS runs, with peaks at about 1.56 m/s^2. The average peak acceleration through the time series is less than 1.0 m/s^2, but resonant peaks exacerbate the maxima, as shown in Figure 18. This is probably due to the change in rigid body Eigen modes, arising from the reduced stiffness in the horizontal plane for the lower mooring lines. This results in the surge and sway Eigen modes being closer to the lower wave periods and makes the structure more prone to resonant motion. A solution to this problem may be to allow

the rotor to spin, to increase aerodynamic damping of the system and thus reduce the resonant responses.

Table 22: Translations and rotations at tower top during the verification ALS DLCs

vDLC	Heave [m]		Surge [m]		Sway [m]		Pitch [deg]		Roll [deg]		Yaw [deg]	
	Mean	Max	Mean	Max	Mean	Max	Mean	Max	Mean	Max	Mean	Max
ALS01	**-0.18**	**0.19**	-0.01	0.64	0.02	0.29	-0.02	0.30	0.01	0.17	-0.12	0.20
ALS02	**-0.18**	**0.19**	-0.02	0.49	0.00	**0.59**	-0.02	0.27	-0.01	**0.30**	-0.12	0.21
ALS03	-0.16	0.18	**-0.18**	**0.72**	**0**.03	0.30	**-0.15**	**0.40**	0.02	0.18	-0.53	**0.91**

Table 23: Accelerations at tower top during the verification ALS DLCs

vDLC	Heave [m/s²]		Surge [m/s²]		Sway [m/s²]	
	Mean	Max	Mean	Max	Mean	Max
ALS01	0.00	0.14	0.00	**1.69**	0.00	0.89
ALS02	0.00	0.13	0.00	1.38	0.00	**1.56**
ALS03	0.00	**0.18**	0.00	1.54	0.00	0.90

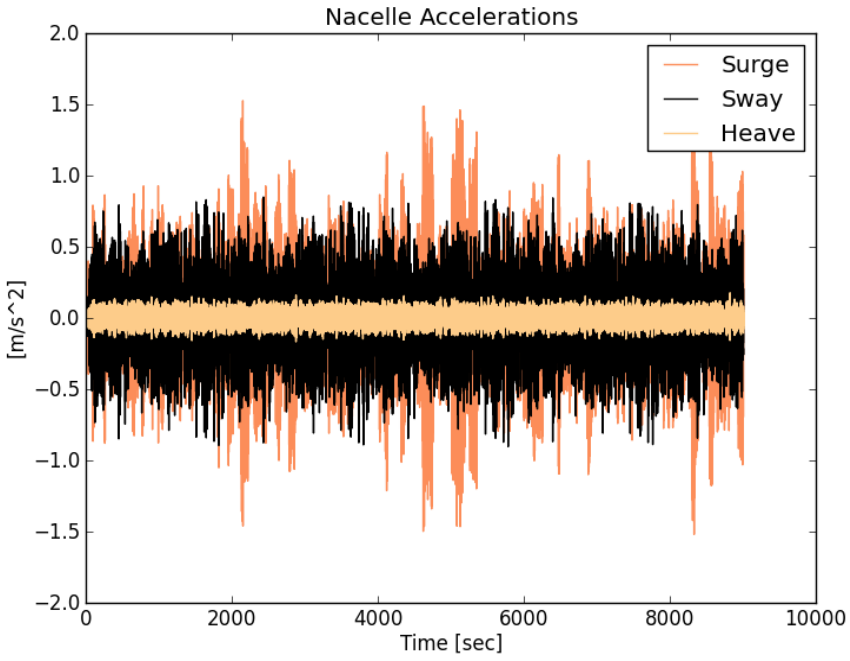

Figure 18: Nacelle accelerations during the ALS03 DLC

The corresponding partial safety factors for ALS in consequence class 1 are 1.0 and 1.1 for mean and dynamic tension, respectively, which are shown in Table 24. The low utilization factor indicates that increases in loads in the considered accidental states are limited.

Table 24: The highest mooring line utilization during the verification ALS DLCs

vDLC	Lower mooring lines (worst)			Upper mooring lines (worst)		
	Mean [kN]	Dynamic [kN]	Utilization [%]	Mean [kN]	Dynamic [kN]	Utilization [%]
ALS01	2690	1408	20	3930	3278	31
ALS02	2600	1804	21	3050	3949	30
ALS03	**3510**	**2288**	**28**	**4000**	**4048**	**34**

As shown in Table 24, the typical anchor utilization is lower in the ALS cases than in comparable ULS cases, demonstrating that the considered faults have very limited influence on the loads in the system. The reductions in partial safety factors more than outweigh the increased loads. This also shows that allowing the rotor to spin during an accidental state may be a valid option.

Table 25: Anchor vertical lifts and resultant forces during the verification ALS DLCs

vDLC	Anchor vertical force [kN]		Anchor resultant force [kN]		Utilization
	Mean	Max	[%]	[%]	[%]
ALS01	4040	5340	**8350**	**13000**	**67**
ALS02	3300	**6470**	7380	12700	66
ALS03	**4430**	5150	6960	12100	63

6.2.3 FLS Verification

Fatigue lives for the selected critical positions in the structure are shown in Table 26. Fatigue damage was calculated for eight points of each cross-section, and only values for the worst direction are shown in the table.

Table 26: Computed fatigue life for the structure with the original mooring line stiffness and sensitivity to 10 % changes in the modulus of elasticity

Cross-section		Height [m]	E-10%	Baseline	E+10%	
1	Close to lower endcap	-38	4.69E+11	4.75E+11	4.60E+11	Years
2	Below transition (under water)	-20	4.12E+03	4.05E+03	3.47E+03	Years
3	Above transition (under water)	-12	3.85E+01	3.88E+01	3.48E+01	Years
4	In the waterline	0	**2.53E+01**	**2.71E+01**	**2.28E+01**	Years
5	Below transition (+10m)	9	5.75E+01	5.07E+01	4.56E+01	Years
6	Above transition (+10m)	11	8.47E+01	7.63E+01	5.81E+01	Years
7	Below upper mooring	22	9.17E+01	6.87E+01	6.64E+01	Years
8	Above upper mooring	25	1.05E+02	7.06E+01	6.27E+01	Years
9	In tower	37	7.21E+01	4.06E+01	7.13E+01	Years
10	In tower	50	8.53E+01	7.12E+01	5.28E+01	Years
11	In tower	62	1.63E+02	1.21E+02	1.19E+02	Years
12	In tower	75	1.95E+02	1.82E+02	1.80E+02	Years
13	In tower	86	3.04E+02	3.00E+02	3.02E+02	Years

Positions 4 to 6 are respectively located at the still water line, below the tower flange and directly above the tower flange at 10.0 to 10.3 m. This part is reinforced with respect to slamming and collision, and thus has a 0.031 m thick wall. The tower section has a somewhat smaller thickness of 0.027 m up to the upper mooring lines. This section is also reinforced to avoid the 1P and 3P frequency of the rotor by stiffening the first tower mode. However, this is still the part of the structure with the highest fatigue damage. The current design fulfils the fatigue life requirement of 25 years.

In order to investigate the influence of changes in mooring line stiffness over time a simple FLS screening was applied. The mooring line elastic modulus was set to 90% and 110% of the original value in two complete FLS runs. The estimated fatigue life, for the worst direction at each cross-section, is also illustrated in Figure 19. The relative variation is high for the critical positions from the tapered section of the below the water line and up to cross-section 11 in the tower. Interesting features are that a reduction in stiffness seems to be beneficial overall for the fatigue lifetime, and a slight increase in Eigen periods reduces the accelerations and thus moments in the structure. However, this will only be valid as long as resonance can be avoided. A 10% variation is not sufficient to cause a significant increase in resonant behaviour.

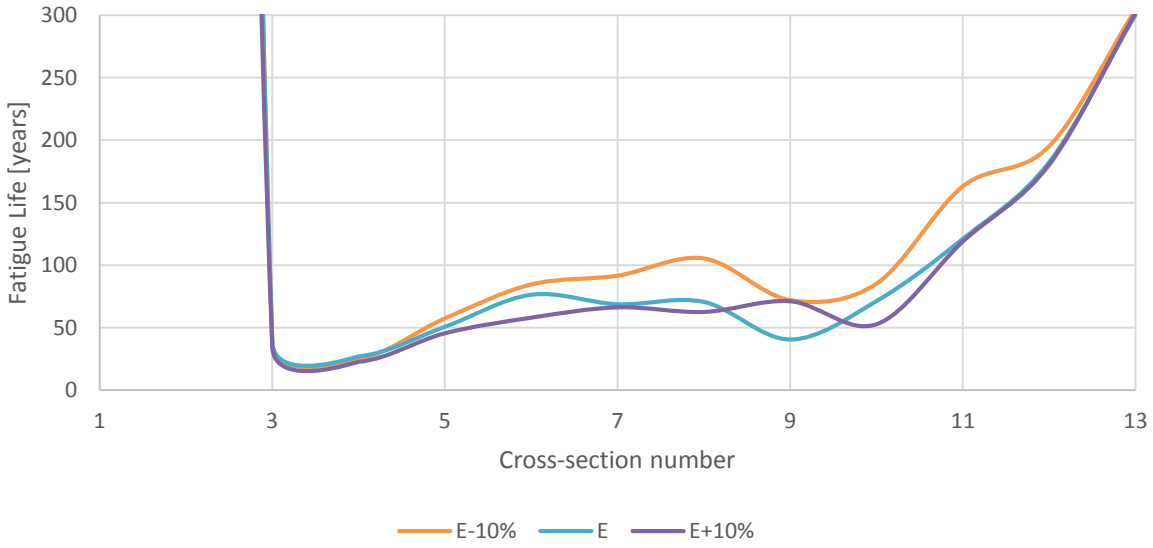

Figure 19: Fatigue life at each of the monitored cross-sections with ± 10 % variation in the modulus of elasticity of the mooring lines

An important aspect of the TLB concept is that much of the fatigue damage occurs in parked or low production load states, mainly because of waves with short periods that are closest to the Eigen-periods of the TLB system. When the rotor is parked, the aerodynamic damping is much lower than in a production state, increasing the damage from resonant behaviour. The results compiled in Table 26 are based on DLCs where the rotor is idle rather than parked with the brake enabled. If the rotor were to be continually parked, the lifetime with the current setup would be about 10 years, taking the DFF into account, implying that the rotor should be in parked state for less than 50 % of the time to avoid fatigue issues. A complete quantification of the damage from each of the FLS cases is shown in Table 27 and Table 28. The most damaging cases, with respect to fatigue, are shown in red.

Table 27: Fatigue damage for the substructure in cross-section 1 to 5 during the FLS DLCs

DLC	Section_1	Section_2	Section_3	Section_4	Section_5
FLS01	2.43E-14	7.74E-08	7.13E-06	1.93E-05	3.40E-05
FLS02	7.71E-14	5.49E-07	4.21E-05	9.08E-05	7.82E-05
FLS03	9.43E-14	1.69E-06	1.46E-04	4.59E-04	3.63E-04
FLS04	7.95E-14	2.57E-06	2.24E-04	6.31E-04	2.37E-04
FLS05	8.07E-14	8.62E-06	7.20E-04	1.27E-03	4.99E-04
FLS06	8.92E-14	1.11E-05	1.25E-03	1.83E-03	7.07E-04
FLS07	7.22E-14	1.08E-05	1.32E-03	2.66E-03	7.42E-04
FLS08	7.06E-14	1.24E-05	1.53E-03	2.60E-03	1.01E-03
FLS09	4.29E-14	1.08E-05	1.17E-03	2.73E-03	1.12E-03
FLS10	3.80E-14	1.16E-05	1.01E-03	2.85E-03	1.80E-03
FLS11	1.84E-14	5.85E-06	5.74E-04	1.29E-03	7.30E-04
FLS12	1.53E-14	5.82E-06	4.46E-04	9.36E-04	7.52E-04
FLS13	2.51E-15	2.15E-06	1.79E-04	7.00E-04	1.18E-03
FLS14	1.05E-15	8.04E-07	7.40E-05	2.19E-04	3.40E-04
FLS15	5.37E-16	4.00E-07	3.37E-05	8.39E-05	1.16E-04
FLS16	3.01E-16	2.85E-07	2.69E-05	8.97E-05	1.37E-04
FLS17	1.39E-16	1.37E-07	1.15E-05	2.79E-05	3.27E-05

Table 28: Fatigue damage for the tower in cross-section 6 to 13 during the FLS DLCs

DLC	Section_6	Section_7	Section_8	Section_9	Section_10	Section_11	Section_12	Section_13
FLS01	2.61E-05	6.85E-05	7.39E-05	8.55E-05	6.99E-05	2.47E-05	5.72E-06	1.72E-07
FLS02	5.05E-05	6.38E-05	5.71E-05	9.08E-05	5.23E-05	1.51E-05	2.55E-06	1.63E-06
FLS03	2.29E-04	3.57E-04	3.22E-04	4.73E-04	2.74E-04	1.08E-04	1.89E-05	3.22E-06
FLS04	1.87E-04	2.54E-04	1.88E-04	2.72E-04	2.42E-04	7.59E-05	2.70E-05	7.28E-06
FLS05	3.25E-04	2.34E-04	2.53E-04	2.92E-04	2.79E-04	1.44E-04	1.03E-04	5.04E-05
FLS06	4.87E-04	2.19E-04	3.25E-04	6.83E-04	3.04E-04	2.89E-04	2.79E-04	1.24E-04
FLS07	6.38E-04	2.01E-04	1.90E-04	1.41E-03	3.16E-04	2.39E-04	2.58E-04	1.52E-04
FLS08	8.18E-04	9.40E-04	8.47E-04	5.95E-04	3.76E-04	4.78E-04	4.86E-04	2.81E-04
FLS09	7.61E-04	3.12E-04	2.40E-04	9.90E-04	3.73E-04	3.38E-04	3.85E-04	2.55E-04
FLS10	8.92E-04	2.68E-04	2.87E-04	1.45E-03	4.44E-04	4.97E-04	4.62E-04	3.53E-04
FLS11	4.78E-04	3.30E-04	3.27E-04	2.53E-04	7.21E-04	3.14E-04	2.91E-04	2.25E-04
FLS12	4.95E-04	4.83E-04	3.25E-04	6.83E-04	2.60E-04	3.68E-04	2.78E-04	2.24E-04
FLS13	7.66E-04	2.39E-03	2.58E-03	3.61E-03	2.31E-03	9.08E-04	1.43E-04	5.26E-07
FLS14	2.13E-04	5.96E-04	5.60E-04	8.67E-04	5.51E-04	1.82E-04	2.60E-05	1.64E-07
FLS15	7.28E-05	1.99E-04	1.92E-04	3.04E-04	1.79E-04	6.66E-05	9.20E-06	6.82E-08
FLS16	9.24E-05	3.07E-04	2.62E-04	3.93E-04	2.53E-04	8.59E-05	1.38E-05	6.21E-08
FLS17	2.45E-05	5.99E-05	5.96E-05	9.02E-05	5.62E-05	1.85E-05	2.62E-06	2.35E-08

Sections 1 and 2 have been dimensioned to resist buckling, and easily endure the FLS cases. The shortest estimated fatigue life is 27 years for the substructure. The critical area is located around the water line and the driving load cases is typically at around rated wind speed and limited wave heights with low wave periods. For the tower structure, the governing load case is production at close to cut-out wind speed. The damage is likely to be caused by a combination of the horizontal load on the turbine and the increased accelerations from the wave response. Fatigue seem to be less detrimental, especially if one consider that the cases are run unidirectional, but may be important at other sites with different depths. The tower wall thickness parameter could then be

included in the frequency domain optimization. Regardless, the sensitivity to the parked cases has proven the importance of an integrated design in order to secure an optimal construction.

6.3 Additional Aspects

During the work in both the optimization and verification stages several other aspects of the concept have been documented.

1. Slack is observed in one of the lower mooring lines during extreme yaw events. Cable elements that do not exert any stiffness during compression, and thus any snapping effects that would appear during reloading, should be captured. As no peak force is observed during reloading, slack does not seem to be an issue.
2. During load cases with short waves the structure is prone to resonant behaviour. This is observed in both the FLS and ULS responses, and confirmed by further inspection of the time series. This is to be expected for a design such as the TLB, but it also emphasises the importance of correct damping levels and rigorous FLS verification. Sensitivity studies on the influence of changes in stiffness of anchor points, mooring lines, blade and nacelle positions should be conducted with respect to fatigue.

The TLB system is prone to produce resonant behaviour when rigid body modes such as surge, sway, pitch and roll are located close to the lower bond of wave periods in the sea state. The level of damping in the numerical model strongly influences the response, especially when there is limited aerodynamic damping, e.g. when the rotor is parked for maintenance. This is illustrated in Figure 20, by characteristic resonant behaviour observed during the FLS01 DLC. The level of damping in the system also governs the level of safety for the construction's Eigen-period upper limit. Currently this is set to 3.5 seconds. With increased damping, this limit could be elevated. In any practical case, this level will be set by the fatigue and accelerations in the system. Increasing damping may therefore be a cost-effective way of reducing extreme loads, fatigue, and responses.

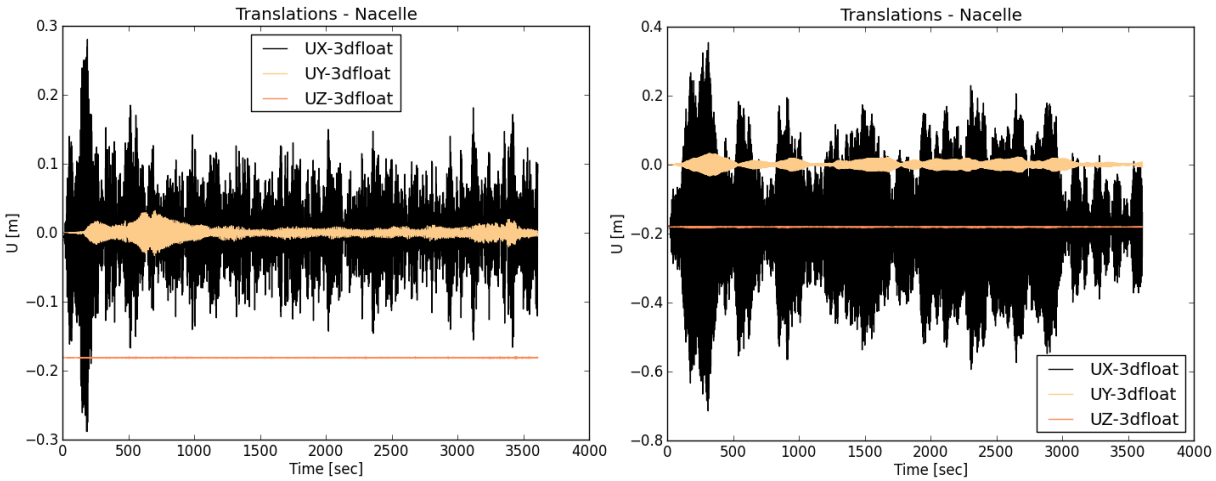

Figure 20: Translation for the nacelle during the FLS01 DLC with a parked rotor (right) and an idle rotor spinning slowly (left)

Vortex-induced motions (VIM) has been assessed with the use of DNV-RP-F105 (DNV, 2006). Onset of in-line VIM can be expected at current speeds of above 1.8 m/s for the 6.0 m diameter part of the substructure. This is significantly higher than the 1.2 m/s current with a 100 year return period for the K13 site. Due to the relatively low draft, full lock-in may also be neglected as surface waves will disrupt the phenomenon. However, lock-in should may considered for the lower part of the substructure, but with a diameter of 9.223 m the reduced velocity with a 100 year return period is only 0.45[2]. This is well below the onset level of 1.0 and 2.0 for in-line and crossflow VIM, respectively. The influence of VIM is considered irrelevant at this stage of the design, but should be assessed later, especially if a concept with longer rigid body Eigen periods is considered.

Ringing and/or springing issues have not been assessed in detail, but data obtained from the two wave tank tests indicate that they are of minor importance in the cases examined so far. As a rule of thumb, higher order effects are expected to be lower than 20% of the first order excitation, similar to the assumed accuracy of the ULS verification. However, this should be examined further, typically by establishing safe limits of operation.

Slamming effects in a 2D space is solved by a crude approach in 3DFloat. When the water plane intersects with the centreline of the element, both drag and added mass are applied instantly. 3DFloat does not account for partial immersion of the cross-section when applying drag and added mass, but it does account for the water plane elevation in time. Therefore, the instantaneous loads from the crude 2D approach is smoothed over time by the 3D nature of the problem when a wave is passing the structure. Based on the performed experiments, one can expect this to be a reasonable simplification at this design stage.

The double frequency response, documented in Paper 7, may pose a significant challenge during simplified optimization approaches that only cover a few sea state combinations. It is therefore advised to have a basic setup that is not prone to the double frequency response in order to ease the design process.

The extent of the rotor is large compared to the rest of the structure. The current Eigen value analysis covers only a few rotor position, but ideally it should be extended to include several positions as the position can have substantial effects, especially on blade pitch positon and variance in mooring line stiffness. Although the verification step will capture these variations, adapting it in the optimization is advisable as it is far less time-consuming to perform.

[2] This value was obtained without using a reduction of velocity with the current profile. It should be noted that the value is somewhat sensitive to the Eigen periods in the system and an increase of surge period to 5 s will increase the reduced velocity to above 1.0 and in the region of onset for in-line VIM.

7 CONCLUSION

This chapter briefly summarizes the results and pertinent lessons learned from experience during the studies underlying the appended papers and this thesis.

A 5 MW TLB concept has been optimized and developed. The design is based on the MIT Double Taut Leg, initially proposed by Professor Sclavounos of MIT in 2005. Six variants have been tested, in two wave tank tests, to prove the concept and aid validation of 3DFloat, the coupled aero-hydro-servo-elastic tool utilized for the numerical computations. A design approach, including a LCOE assessment, has also been developed in order to compare the TLB design with other concepts.

Two optimized designs are presented.

1. TLB type B for a harsh weather site in the North Sea basin
2. TLB type B2 for the K13 Deep water site in the Dutch North Sea

7.1 Concluding Remarks

The TLB concept is one of the first proposed designs for large offshore structures that meets the challenges and can deliver the advantages of mass production. The main focus is on driving the costs down, not only during the build, but during the whole lifetime of the structures to minimize the LCOE when producing enormous numbers of them. Simplicity and probabilistic design become important, but it is not easy to propose the construction of hundreds of these gigantic structures while acknowledging that some are likely to fail (and economically that may be an optimal outcome). As if the challenge was not already of epic proportions, there are also urgent needs to find viable solutions to minimize global warming. The TLB B2 design has so far proven a worthy candidate to solve this problem.

In terms of LCOE the TLB B2 shows potential to compete even with onshore wind turbines in Japan and Australia, and should be one of the better alternatives for offshore turbines in Europe at sites similar to the K13 site. The TLB design has demonstrated sensitivity to site optimization, and extrapolation of available data to other sites with different depths is challenging. However, during comparisons at different sites the optimization routine proposed in this thesis is advised to obtain a realistic impression both of the mooring system required and size of the substructure.

CAPEX comparisons of TLB systems with other concepts should preferably only involve mooring, production and installation costs, due to significant uncertainties and deviations among different estimations. It should be noted that CAPEX is not well suited for comparing TLB systems with technologies other than alternative offshore wind power systems. A thorough LCOE analysis should always be performed for a specific site in order to demonstrate advantages over alternative energy sources, due to significant differences in potential in relation to available area. It is also important to scale and evaluate each concept appropriately during comparisons as their sensitivity to environmental conditions and depth may vary widely.

From the previous optimization, the mooring loads have been reduced by over 50 % and the peak vertical load on the anchor points is now in the range of 7 500 kN for the 5 MW turbine. During the verification it has been found that a coupled simulation tool with elastic beam elements is required to capture the response of the TLB structures as the substructure is slim and flexible. Thus, an integrated design and software solution is highly important for safe, efficient development of the concept.

Of the remaining obstacles, establishing a reliable method to compute fatigue and predict changes over time in stiffness (stiffness degradation) of the fibre mooring lines is deemed most important, along with establishing a geotechnical model for computing stiffness and damping for the anchor points. At the current point this should be solved via sensitivity analyses covering the relevant parameter envelopes. Nevertheless, time domain analysis has proven to be an excellent tool for verification of offshore floating wind turbine platforms and a fatigue life of more than 25 years have been documented.

Lack of technological readiness has been previously regarded as one of the TLB design's downsides. However, taut leg tension platforms have been used for decades and synthetic mooring ropes have been used for high-risk lifting operations and as permanent mooring for ultra-deep water oil rigs. There are also plans to install a taut leg synthetic system, using 17 lines of 0.254 m polyester rope, on the Aasta Hansteen platform (Gabrelsen, 2012). As yet, the dynamic performance of such systems over 20 years has yet to be proven in the field, but a low-risk introduction on simpler constructions, such as MET-masts (which also have significantly shorter lifespans), may be possible.

We have developed and applied efficient designs for onshore wind mills for centuries, onshore wind turbines for half a century, and bottom-fixed wind turbines for decades, but we are still just beginning to prove the technical viability of floating concepts by utilizing offshore experience from the oil and gas sector. In order to further explore the possibilities in terms of reducing LCOE we must now move beyond relying on proven technology and start to adopt some of the basic principles of mass production. The price of the product can be reduced by building one extra unit rather than ensuring that all of the units never fail. After all, we are going to build thousands of them.

7.2 Suggested Improvements

A refinement of the mass distribution is recommended to improve knowledge of secondary steel consumption in TLB systems. This is particularly important for the upper mooring line tower connector and the tensioning system. However, this is likely to require detailed design of most of the major components in the system. The total mass is assumed to be in the range of 100 tons and can be integrated into the design by marginal adaptions to the floater geometry in order to secure the required increase in buoyancy.

Further studies should be performed to refine the load cases for the time domain optimization. When more data are collected on the concept, they may be used to find more realistic

combinations by statistical approaches. This will deliver higher utilization at the ULS, although the FLS utilization will also have to be integrated into the optimization.

Several new installation approaches for floating structures at sites with water depths around 50 m could be applied. Thus, further effort is needed to identify the optimal installation procedure at these depths (e.g. tow-out and installation of the substructure and tower in one operation, and use of a jack-up vessel only to mount the nacelle). If towing is to be used this also poses challenges for TLB systems, as a secondary stabilizing system will probably be needed during a towing operation with the structure in assembled position.

Floating turbines also pose new challenges with respect to dynamic loading on the blades and turbine housing. The TLB system is expected to provide similar (or better) performance than an onshore turbine, but nevertheless detailed study of both blade and machine fatigue is required.

Grid costs have proven to be major contributors to total costs of offshore wind systems. Thus, further effort is needed to identify integrated solutions that could reduce the overall LCOE for complete farms. This may involve integrating power electronics in the substructures or moving the power electronics subsea. The grid costs also seem somewhat overestimated in the LCOE estimates obtained to date (e.g. the CAPEX estimates for sites 10 km offshore are typically around € 875 000, while a European average is only € 536 000). This may be related to the expensive HVDC solution assumed in our calculation – and the costs obtained for it had large variance. Better data are needed to enhance the accuracy of the analysis.

Sensitivity studies are needed to determine optimal positions of the longest Eigen modes, such as sway and surge. As the Eigen-periods increase, the structure becomes more prone to resonant behaviour and thereby fatigue. Sensitivity studies are also needed to document the variation in response due to changes in both mooring and anchor stiffness over time.

7.3 Further Work

Clearly, much work remains to be done to optimize wind turbine designs generally, and TLB designs specifically. For efficient wind turbine design fully coupled and integrated computational tools are crucial. Significant progress towards the realisation of such tools has been made on the software side, with the development of 3DFloat, but several additional core features are still needed to enhance the accuracy of the design process, including:

1. Non-linear stiffness models that can account for synthetic mooring line test data in order to capture more realistic stiffness responses. This will also help to identify valid stiffness envelopes for sensitivity studies.
2. Better models of seabed interactions at anchor points to capture the anchor point stiffness and its expected envelope across the load spectrum accurately.
3. Further optimization of computation time, especially for more complex mooring models and models with large number of degrees of freedom.

Further improvements to the cost- and constraint models for the optimization are also needed to account for local support schemes, integrating the LCOE into the optimization step.

It has been established that the TLB B2 design would not survive a failure in one of the upper mooring lines without a redundant system to increase stability. Possible options to avoid such failure include emergency ballasting or increasing buoyancy. Analyses of both of these possibilities are warranted, but only after further risk and economic evaluations to test the current hypothesis, that to minimize LCOE failure must be allowed. Various optimizations should be performed with an increased substructure that allows failure of the upper mooring lines in order to establish the cost of redundancy for the stabilizing system.

Technology readiness is critical before a concept can be regarded a valid option. Pre-tensioned inclined mooring systems were introduced in the 1980s, but ignored due to uncertainties and lack of proof of concept. Anchor loads have also been previously cited as severe issues with the TLB concept, but offshore oil and gas systems have started to apply inclined taut pre-tensioned synthetic mooring lines. The next step will be to install such lines (at two heights) on a full-scale prototype to test their stabilizing effects. In addition, as both the grid and turbine costs are high a low level entry option may be to use offshore structures with lower CAPEX in full-scale prototype tests of the mooring system. Suitable, and recommended, candidates are offshore MET masts, due to their TLB characteristics, with limited translations, and capacity for towing to relatively shallow water sites (allowing floating full-scale masts to be used even for bottom-fixed wind farms). A MET-mast platform may also be suitable for testing a tensioning system for the mooring lines.

The issue of scalability has yet to be investigated for the TLB system. From the results so far, it has been established that the 5MW turbine during rated wind speeds produce about the same utilization in ULS as the most severe sea states. The results so far have established that utilization in ULS of the 5MW turbine at rated wind speeds is similar to the utilization in the most severe sea states, indicating that it is close to optimal in this respect, but data regarding different turbine sizes are limited. Increasing the turbine dimensions would definitely increase mooring loads and thus the mooring line dimensions needed to achieve the desired Eigen-periods. Experience to date with the TLBs indicates that the increase in top mass of a larger turbine is likely to pose more challenges than the increased thrust force, but this should be investigated further.

The layout and masses of the secondary steel structures must also be considered to develop the concept further. A standard single boat-landing can be utilized, but is relatively large and expensive to manufacture, contrary to the aims for the TLB design to reduce costs and masses as much as possible in order to minimise the LCOE. Further work should therefore be done to optimise solutions for moving maintenance crew to the turbine.

Other requirements for optimizing designs include site-specific environmental data and robust concept comparison tools. Several offshore wind farm contractors use in-house LCOE systems to evaluate concepts, but when they do not have access to site-optimized concepts it is considered challenging to find the most suitable concept for a specific site. Open site data, and even concept challenges for sites, may help drive offshore wind power costs down by stimulating progress towards more site-optimized concepts. The great challenge is not to optimize one concept for one site, but to find the optimal concept for each location

Further statistics on failure of the mooring system should be acquired and incorporated in both the LCOE analysis and optimization routine. Their influence on the LCOE is likely to depend on the site, and particularly ship traffic in the area (which may damage the mooring lines). The probabilities of fabrication errors and mooring line damage during installation and maintenance should also be assessed.

A non-linear geotechnical stiffness-model should be developed that includes the anchor point dynamic responses and time domain effects. A robust approach to ensure that the computed responses, including uncertainties, are adequate should also be developed.

Similarly, for the synthetic mooring lines, a function to establish the hysteresis in stiffness and damping should be created and implemented in the time domain analysis. This is likely to be necessary to avoid large safety factors and large stiffness envelopes for the mooring system driving up the total cost.

Scalability is desirable to optimize with respect to installation vessels, available turbine models and site conditions. The scalability of the system should be assessed further, with respect to both environmental conditions and other site conditions, such as depth and seabed conditions.

Damping is important for the fatigue life. Studies should be conducted to document realistic structural damping levels and more accurate damping contributions from interactions between the seabed, anchors, mooring lines and rotor.

Alternative installation methods are possible for sites with intermediate water depths and should be explored further in attempts to reduce risks and costs.

Hydrodynamic effects are important for global responses. Higher order effects such as VIV, sum frequency on the tendons, ringing and springing should be explored further and their impacts should be assessed.

8 REFERENCES

ARENA, 2013. *Australian Energy Resource Assessment,* s.l.: Australian Renewable Energy Agency (ARENA).

Armendáriz, J. A., Echarri, M., Nygaard, T. A. & Hoyos, D. M., 2011. *Development of OPASS Code for Dynamic Simulation of Mooring Lines in Contact with seabed,* Amsterdam: EWEA Offshore 2011.

Azcona, J. et al., 2010. *Aerodynamic Thrust Modelling in Wave Tank Tests of Offshore Floating Wind Turbines Using a Ducted Fan,* s.l.: Journal of Physics: Conference Series 524 (2014) 012089.

Bak, C. et al., 2013. *Description of the DTU 10 MW Reference Wind Turbine,* s.l.: DTU Wind Energy Report-I-0092, 2013.

BEXCO, 2015. *Deeprope Dyneema.* [Internett]
Available at: http://www.bexco.be/data/RGS%20489A-003.07%20Dyneema%20Parallel%20deeprope.pdf
[Funnet 25 02 2015].

Butterfield, S., Musial, W., Jonkman, J. & Sclavounos, P., 2005. *Engineering challenges for floating offshore wind turbines.* Copenhagen, Denmark, Proc 2005 Copenhagen Offshore WInd Conference.

Copple, R. W. & Capanoglu, C., 2012. *Tension Leg Wind Turbine (TLWT) Conceptual Design Suitable for a Wide Range of Water Depths,* s.l.: Proc 22nd International Offshore and Polar Engineering Conference (ISOPE), Rhodes, Greece. Vol. 1., pp. 396-403.

DNV, 2006. *Recommended Practice DNV-RP-F105 - Free Spanning Pipelines,* Oslo: Det Norske Veritas.

DNV-OS-C101, 2011. *Design of Offshore steel structures, General (LRFD method),* s.l.: DNV GL.

DNV-OS-E301, 2010. *Position Mooring,* s.l.: DNV.

DNV-OS-J101, 2013. *Design of Offshore Wind Turbine Structures,* s.l.: February 2013, DNV.

DNV-OS-J103, 2013. *Design of Floating Offshore WInd Turbine Structures,* s.l.: June 2013, DNV.

DNV-RP-C203, 2010. *Fatigue Design of Offshore Steel Strucutres,* s.l.: DNV GL.

Fisher, T., de Vries, W. & Schmidt, B., 2010. *Upwind Design Basis (WP4: Offshore Foundations and Support Structures),* Stuttgart, Germany: s.n.

Gabrelsen, Ø., 2012. *Aasta Hanstee - Worlds Largest SPAR,* Øystein Gabrelsen: Statoil.

Gielen, D., 2012. *Renewable energy technologies: cost analysis series,* s.l.: International Renewable Energy Agency (IRENA), Volume 1: Power Sector, Issue 5/5.

GL Garrad Hassan, 2012. *Cost of energy of floating wind,* s.l.: GL Garrad Hassan.

Govindji, A.-K., James, R. & Carvallo, A., 2014. *Appraisal of the Offshore wind industry in japan,* s.l.: Carbon Trust.

Graffy, N., 2010. *Historic Santa Barbara.* s.l.:HPN Books, ISBN: 1935377140.

Henanger, H. E., 2011. *Development of installation and mooring system for a floating offshore wind turbine,* Ås: UMB(NMBU) - Brage.

IEA, 2011. *2010 Annual Report,* s.l.: International Energy Agency, IEA WIND.

IEC-61400-1-ed3, 2008. *Wind turbines - Part 1: Design requirements,* s.l.: s.n.

IPCC, 2014. *Climate Change 2014: Impacts, Adaptions and Vulnerability. Part : Global and Sectoral Aspects. Contribution of Working Group II to the fifth Assessment Report of the Intergovermental Panel on Climate Change,* Cambridge, United Kingdom and New York, NY, USA: Cambridge University Press.

Jonkman, J., Butterfield, S., Musial, W. & Scott, G., 2009. *Definition of a 5-MW Reference Wind Turbine for Offshore System Development,* s.l.: Technical Report NREL/TP-500-38060, National Renewable Energy Laboratory (NREL).

Jonkman, J. et al., 2010. *Offshore Code Comparison Collaboration within IEA Wind Task 23: Phase IV Results Regarding Floating Wind Turbine Modeling,* Warsaw, Poland: Proc European Wind Energy Conference & Exhibition (EWEC).

Lu, X., McElroy, M. & Kiviluoma, 2009. *Global potential for wind-generated electricity,* s.l.: Proc of the National Academy of Sciences of the United States of America.

Maciel, J. G., 2010. *The WindFloat Project.* [Online]
Available at: http://www.wavec.org/content/files/11_Joao_Maciel.pdf
[Accessed 22 05 2015].

Main(e) International Consulting LLC, 2013. *Maine International Consulting. (2013). Floating Offshore Wind Foundations: Industry Consortia and projects in the United States, Europe and Japan,* s.l.: Main(e) International Consulting LLC.

Popko, W. et al., 2014. *Offshore Code Comparison Collaboration Continuation (OC4), Phase I-Results of Coupled Simulations of an Offshore Wind Turbine with Jacket Support Structure,* s.l.: Journal of Ocean and Wind Energy (ISSN 2310-3604), The International Society of Offshore and Polar Engineers, Vol. 1, No. 1., February 2014, pp. 1-11.

Powell, M. J. D., 2009. *The BOBYQA algorithm for bound constrained optimization without derivatives,* s.l.: Report DAMTP 2009/NA06, Centre for Mathematical Sciences, University of Cambridge, UK.

Robertson, A. & Jonkman, J., 2011. Loads Analysis of Several Offshore Floating Wind Turbine Concept. *proc of the International Offshore and Polar Engineering Conference (ISOPE) Vol. 1 pp. 443-450. Maui, Hawaii*.

Robertson, A. et al., 2014. *Offshore Code Comparison Collaboration Continuation Within IEA Wind Task 30: Phase II Results Regarding a Floating Semisubmersible Wind System,* San Francisco, California: proc 33rd International Conference on Ocean, Offshore and Arctic Engineering.

Robertson, A. et al., 2015. *OC5 Project Phase I: Validation of Hydrodynamic Loading on a Fixed Cylinder,* Kona, Hawaii: proc International Offshore and Polar Engineering Conference (ISOPE 2015).

Sclavounos, P. D., Lee, S. & DiPietro, J., 2010. *Floating Offshore Wind Turbines: Tension Leg Platform and Taught Leg Buoy Concepts Supporting 3-5 MW Wind Turbines,* s.l.: proc Europpean Wind Energy Conference (EWEC), Warsaw, Poland, EWEA, Vol 3., pp. 2361-2367.

Sørheim, E. A., 2002. *A user guide to INVALS: Inverse modeling of heat transfer of water film during DC-casting.,* s.l.: IFE-report IFE/KR/F-2002/007.

Spæren, A. O. E., 2013. *Development and construction of floating wind turbine models and test rig for wave tank test,* s.l.: Brage, (available from: http://brage.bibsys.no/xmlui/handle/11250/189018).

Spencer, J. A. & Camp, M. J., 2008. *Ohio Oil and Gas.* s.l.:Arcadia Publishing, ISBN: 0738551716.

STATOIL, 2015. *Hywind Scotland Pilot Park - Environmental Statement,* s.l.: Statoil, Document Number: A-100142-S35-EIAS-001-001 .

Stewart, G. M. et al., 2012. *Calibration and Validation of a FAST Floating Wind Turbine Model of the DeepCwind Scaled Tension-Leg Platform,* s.l.: Proc 22nd International Offshore and Poalr Engineering Conference (ISOPE), Rhodes, Greece, Vol. 1., pp. 380-387.

LIST OF APPENDICES

Appendix 1 – Paper 1: *A Comparison of two Conceptual designs for floating wind turbines*

Appendix 2 – Paper 2: *Experimental and Computational Comparisons of the OC3-HYWIND and Tension-Leg-Buoy (TLB) Floating Wind Turbine Conceptual Designs*

Appendix 3 – Paper 3: *Load Reductions and Optimizations on Tension-Leg-Buoy Offshore Wind Turbine Platforms*

Appendix 4 – Paper 4: *GHG emissions and energy performance of offshore wind power*

Appendix 5 – Paper 5: *Levelised Cost of Energy for Offshore Floating Wind Turbines in a Life Cycle Perspective*

Appendix 6 – Paper 6: *Experimental Results for Tension-Leg-Buoy Offshore Wind Turbine Platforms*

Appendix 7 – Paper 7: *Comparison of Experimental Results and Computations for Tension-Leg-Buoy Offshore Wind Turbines*

Appendix 1

A comparison of two conceptual designs for floating wind turbines

Tor Anders Nygaard, Anders Myhr and Karl J. Maus

Department of Mathematical Sciences and Technology,
Norwegian University of Life Sciences (UMB), 1432 Ås, Norway

email: tor.anders.nygaard@umb.no, anders.myhr@umb.no, karl.maus@umb.no

phone: +47-64965400, fax: +47-64965401

Abstract

By attaching pre-stressed mooring lines at several heights on a floating wind turbine, the need for restoring moment from the floater can be reduced or eliminated. The Njord concept has mooring lines attached at the bottom of the floater and essentially hub height, and a system to avoid conflict between the downwind mooring lines and the downwind rotor. The conceptual design examples presented in this paper have floater steel masses of 14 % and 34 % of the corresponding masses of the OC3-Hywind turbine defined in the IEA-OC3 project. Preliminary results from time-domain simulations with full coupling show lower load fluctuations for the Njord concept than OC3-Hywind, due to the constrained nacelle motions.

1 Introduction

A floating wind turbine must counteract the overturning moment due to the wind turbine thrust, tower drag, wave loads and currents. Nacelle motions may induce additional rotor loads and even instability, due to the strong coupling between aerodynamics, structural dynamics, hydrodynamics and control system. The floater overturning moment can be dealt with in several ways. A spar-buoy type with heavy ballast is shown in figure 1. Roll and pitch angles produce restoring moments due to the horizontal offset between center of buoyancy and center of gravity. SWAY [1] utilizes a downwind turbine, and a pre-stressed tower/floater spar that are allowed large surge/pitch motions. The restoring moment is due to the horizontal offset between the center of buoyancy and effective center of mass.

Another method to obtain restoring moment is to attach mooring lines (ML) at several heights on the structure. The Njord concept (NJ) shown in the figures 2

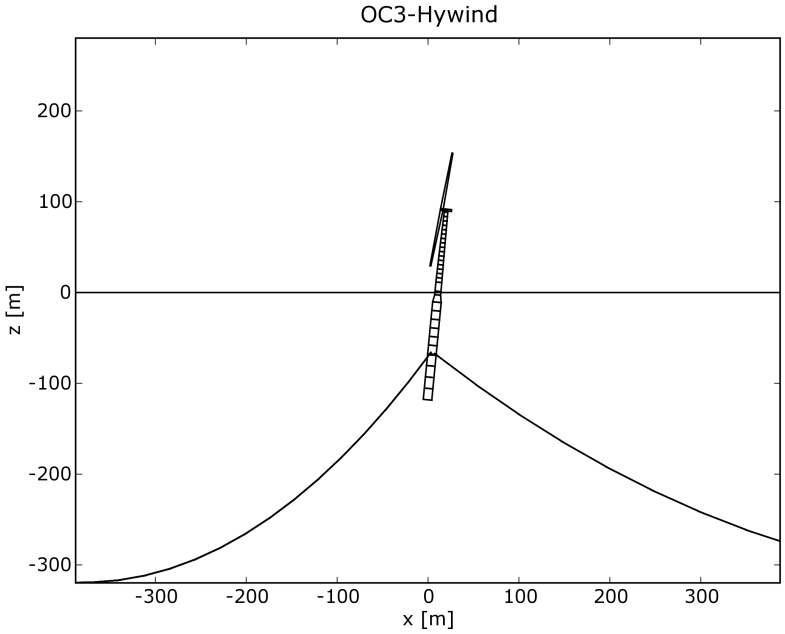

Fig. 1. OC3-Hywind Reference Floating Wind Turbine

and 3 has taut ML attached at hub height and at the floater. Conflict between the upper ML and the downwind rotor is avoided with a system lowering the effective height of the downwind ML. For wind direction changes requiring reconfiguration of the ML, the rotor is parked in a controlled manner (reducing the thrust force), one ML is moved down, the nacelle/rotor undergoes yaw motion, one ML is moved up, and the wind turbine goes back into operation. For a two-bladed rotor parked with the blades horizontally, the yaw motion may proceed with all ML in upper position. The aim of this paper is to report work in progress on a first examination of this method, with the aim of reducing the overturning moment on the floater, the nacelle motions, and the loads. The goal is to develop safe and cost-effective platforms for floating wind turbines, with similar dynamic properties as land-based towers, enabling existing rotor technologies to be adapted without major modifications.

2 Conceptual designs

The well documented OC3-Hywind (HY) floating wind turbine defined for the IEA-OC3 project (OC3) [2] is shown in figure 1. We use it as reference for comparison. The rotor is three-bladed, variable speed, with a diameter of 126 m and rated power of 5 MW. Rotor specifications are given in [3]. The pitch controller has been modified in OC3 to avoid negative aerodynamic damping above rated wind speeds during large nacelle motions [4]. The total mass above the Still Water Line (SWL) is 600 tons. Only overall data such as external

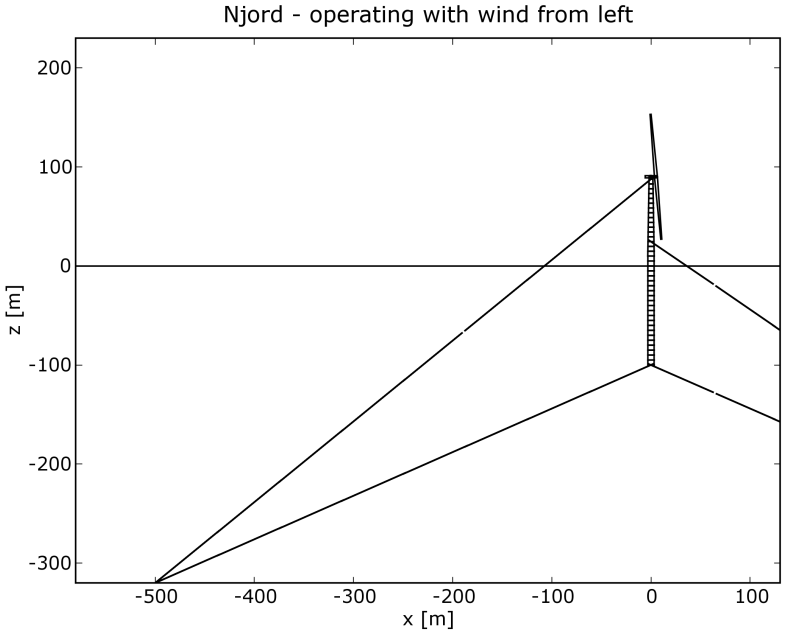

Fig. 2. Njord Floating wind Turbine - Operational

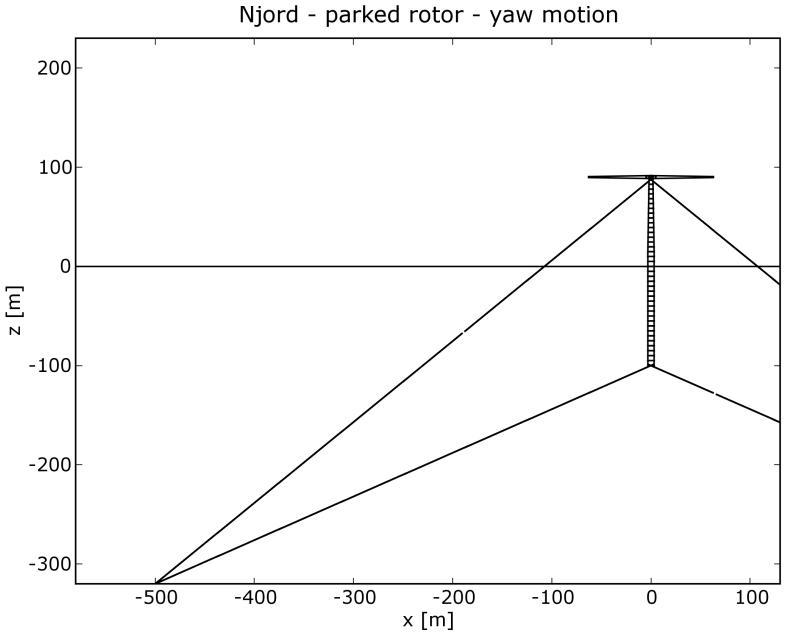

Fig. 3. Njord Floating Wind Turbine - Parked

geometry, total mass and inertias are available for the floater. The external diameter is 9.4 m below the taper at 12 m below SWL, and 6.5 m above the taper at 4 m below SWL. The total mass of the floater is approximately 7500 tons. We estimate roughly 1900 tons of steel, 3100 tons of solid ballast and 2500 tons of water ballast. The mooring system is three loosely connected

catenary lines.

The NJ wind turbines modelled in this paper have identical rotor/nacelle assemblies as HY, except for being of a downwind type. Two NJ floater examples are used in this paper. Version A is marginally stable without ML, but can increase stability with additional water ballast. The diameter is 6.3 m and the wall thickness 33mm. Additional mass due to stiffeners etc. is estimated by inserting ring stiffeners with wall thickness 33mm and inner diameter 5.5 m every third m. This gives a steel mass to deplacement ratio of approximately 0.2, which is similar to other steel floater designs. Version A has 1550 tons of solid ballast during normal operation, and up to 800 tons of water ballast during installation. Version B is a stripped down version that is unstable until installed with pre-stressed ML. Version B has only minor ballast required for adjustment to chosen mooring pre-stress. A comparison of overall characteristics is shown in table 1. The ML chosen initially for NJ are fiber ropes with

Table 1
Comparison of overall data

	OC3-Hywind	NJORD-A	NJORD-B
Hub height [m]	90	90	90
Draft [m]	120	100	40
Rotor/nacelle mass [ton]	350	350	350
Tower mass [ton]	250	250	250
Floater steel mass [ton]	1900	650	260
Solid ballast [ton]	3100	1850	0
Water ballast [ton]	2400	0-800	0

axial stiffness of 400 MN. The fiber ropes are slightly buoyant in water. The water depth is set to 320 m, identical with the OC3-Hywind cases. Four sets of ropes extend 700 m horizontally, diagonally to the viewing direction in figure 2. This ML configuration enables sharing of anchors in a wind farm, giving one anchor per wind turbine except at the edges.

3 Method

The different conceptual designs are compared with eigen-frequency and aero-servo-hydro-elastic time domain computations with the model 3Dfloat. 3Dfloat is a finite-element model (FEM). It utilizes Euler-Bernoulli beams with 12 degrees-of-freedom (DOF), and takes geometric nonlinearities into account with a co-rotated approach. The available loads are:

(1) Hydrodynamic forces (Morison), regular/irregular waves and currents
(2) Buoyancy
(3) Gravity
(4) Aerodynamic drag
(5) Wind turbine rotors applied to nodes
(6) Point forces applied to nodes

Newmark and Wilson time integration schemes are used for time domain simulation [5]. Linear algebra and eigen-solver routines are from the LAPACK library [6]. The rotor aerodynamic model is traditional blade-element/momentum theory (BEM), with enhancements for dynamic inflow and yaw errors. The module follows the methods in [7]. The drive-train and blades are for the computations in this paper assumed to be rigid. Tower/rotor interaction is not yet implemented. The element resolutions are 10 m and 5 m for the floaters and towers respectively. Each ML is modelled with 16 cable elements, where bending stiffness is turned off. The time step is 0.01 s.

4 Results

4.1 Eigen frequency analysis

The eigen frequency analysis is carried out with external forces and moments changes due to displacements represented as linearised stiffnesses added into to the stiffness matrix. ML are replaced with stiffnesses applied to the ML attachment nodes. The buoyancy and gravity are replaced by total buoyancy multiplied with metacentric height, in other words the restoring moment per radian roll or pitch angle. For NJ-A, the stiffness for the mooring was obtained by selecting a pre-strain giving the desired downforce, then perturbing the horizontal and vertical displacements of the mooring attachment, to obtain stiffnesses as the external force components per unit deflection. We used a deflection of 1 m. This choice is not trivial. For pre-strained ML, all initially contribute to a restoring force. For large deflections, however, ML losing tension no longer contribute to the stiffness. This nonlinearity, and the fact that damping reduces the eigen frequencies, should be taken into consideration when interpreting the results in table 2. HY has the solid body and flexible modes well separated on each side of the energetic part of the wave spectrum. NJ-A has a potential problem, since the surge/sway, and possibly heave/roll modes have periods with significant wave energy. We then selected ML axial stiffness for the lighter NJ-B by requiring eigen periods shorter than 5 s. The stiffnesses for ML were here estimated from the axial stiffness and geometry of the ML. The adjusted axial stiffness is 600 MN.

Table 2
Njord-A eigen periods [s]

	OC-HYWIND	NJORD-A	NJORD-B
Surge/Sway	124.5	10.4	6.8
Heave	30.3	6.95	3.4
Pitch/Roll	31.3	6.66	4.5
Tower 1st bending fore/aft	2.1	2.38	1.08
Tower 2nd bending fore/aft	0.28	0.71	0.39

4.2 Nonlinear time-domain simulations

The first load case has a constant wind speed (WS) at hub height of 11.4 m, a height exponent of 0.14, regular waves with wave height 2 m, and the turbine operating with the pitch control system enabled. At this WS the wind turbine has just reached rated power. Wave induced motion of the nacelle changes the relative WS seen from the nacelle, influencing the pitch control system, which again induces new motions and so on. Figure 4 shows a linear sweep on wavelength and thereby wave period over an interval of 1500 s. The wave period is plotted against the right y-axis with the blue line, starting at 20 s and ending with 5 s. The red and black lines show the blade root flapping moments for HY and NJ-B respectively. Overall, the moment fluctuations are 15 % for HY, and about 5 - 10 % for NJ-B. Larger fluctuations are observed for a wave period of 10 s for HY, and for 6 s for NJ-B. The load case shown in the figures 5, 6 and 7 has regular airy waves with wave height 2 m and period 10 s. The wind speed is steady at 11.4 m/s. The black line shows the Extreme Operating Gust (EOG) with amplitude 2 m/s and duration 10.5 s. The dip in WS immediately reduces the blade root flapping moment. The following increase in WS produces a peak in flapping moment before the pitch control takes over, but both turbines behave well and show no abnormal loads through this transient. The load variations for NJ-A due to waves is roughly half of the variations for HY, due to tight mooring lines restricting the nacelle motions. The EOG influence on the tower Still Water Line (SWL) bending moment is for HY both immediate due to the direct influence from the rotor thrust force, and indirect through the induced motions, for about one minute after the gust. NJ-A absorbs most of the bending moment due to the thrust force in the ML, but gets some indirect influence through the variation of ML down force and the following motions. The NJ-A SWL bending moment is about 10 % of the corresponding HY moment, due to the upper ML offloading the tower. The load variations in the NJ-A ML are significantly higher than HY. This is a consequence of the fundamentally different load paths. The loose catenary ML of HY let the structure average out load variations.

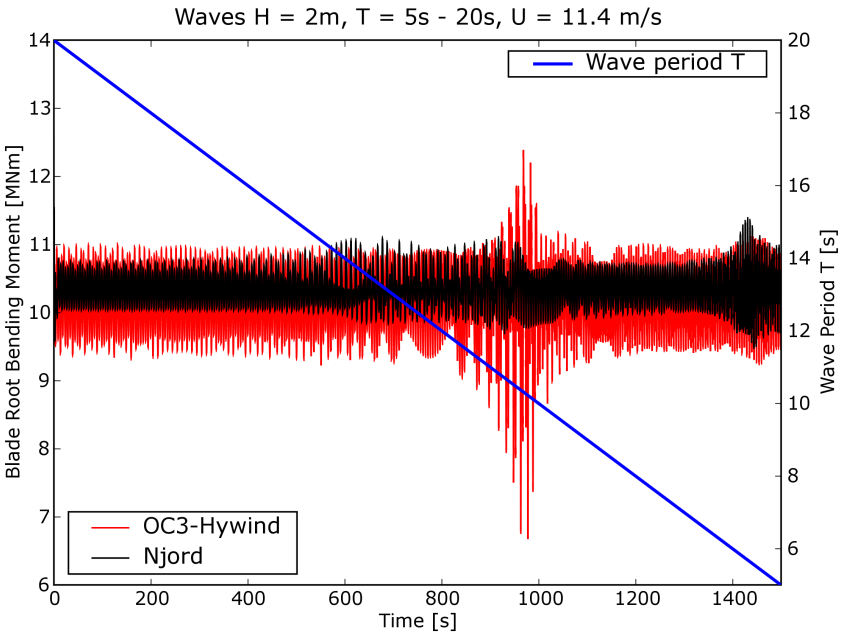

Fig. 4. Sweep on wavelengths, steady wind, pitchcontrol on

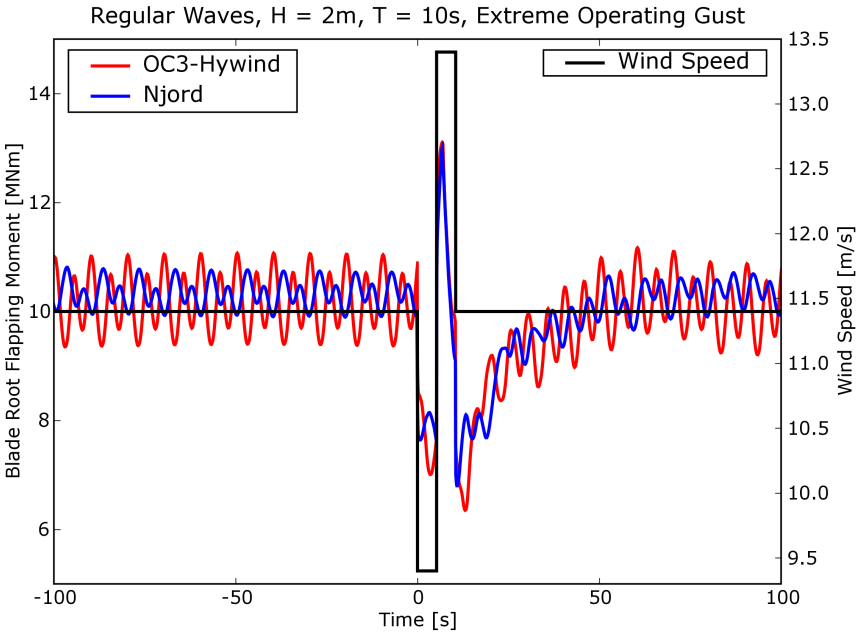

Fig. 5. Blade root flapping moment, extreme operating gust

5 Economics

The preliminary results obtained so far seem to support the initial assumption that taking the rotor thrust directly to the sea-floor with mooring lines would

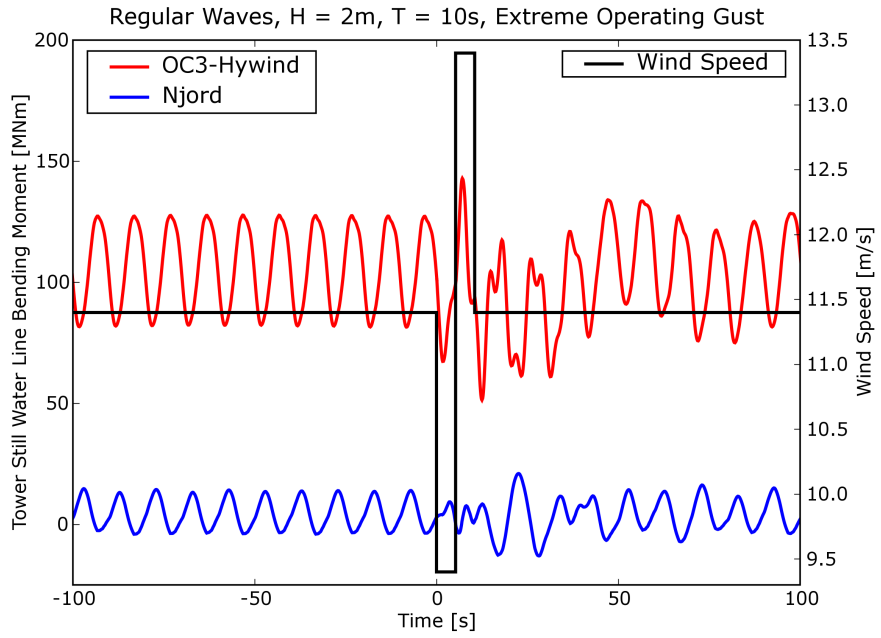

Fig. 6. Tower root bending moment, extreme operating gust,

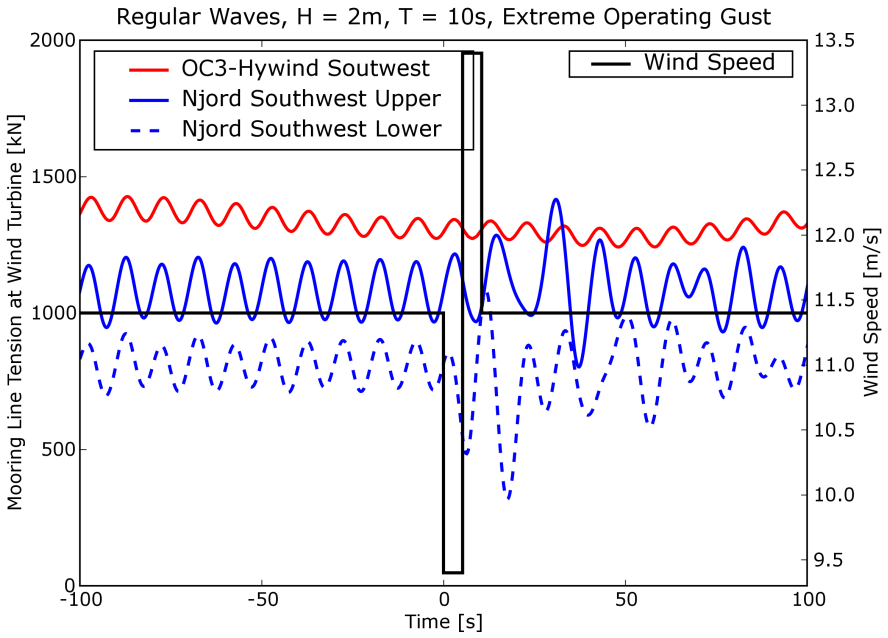

Fig. 7. Mooring line tension, extreme operating gust

allow a smaller floater, and give lower load fluctuations. Assuming that the floater accounts for more than 30 % of the total cost of a spar-buoy turbine, a saving of about 20 % of the total cost seems to be within reach. This saving can, however, easily be lost due to increased costs for ML, moving parts, safety systems and anchor systems subject to vertical forces. If the preliminary

findings are confirmed by the rest of the long list of load cases in OC3, the next challenge will be to design a simple, safe and cost effective mechanism for ML handling.

6 Conclusions

On a floating wind turbine, the floater overturning moment, nacelle motions and load variations may be reduced by taking the thrust force directly with a mooring line at hub height.

Two design examples result in floater steel masses of 14 % and 34 % of the estimated corresponding masses of the OC3-Hywind turbine defined in the IEA-OC3 project.

A load case with constant wind and regular waves, show lower load fluctuations for Njord through the range of wavelengths.

A load case with extreme operating gust and regular waves show stable behaviour for both OC3-Hywind and Njord. The load variations for Njord is typically 50 % of the corresponding variations for OC3-Hywind.

The model 3Dfloat used for computing the loads is currently assuming a rigid rotor, and ignores the rotor/tower interaction. These effects may reverse the preliminary findings in this paper.

Although the potential cost benefit appears to be high, the costs of moving parts, mooring lines, safety systems and anchors should be considered carefully.

The ultimate goal is to provide a platform with dynamic properties allowing existing rotor technologies developed onshore to be utilized offshore without major modifications.

References

[1] The Engineer (http://www.theengineer.co.uk). Ocean current, July 2008.
[2] Jonkman J. Definition of the Floating System for Phase IV of OC3. National Renewable Energy Laboratory (NREL), Golden, Colorado, February 2009.

[3] Jonkman, J., Butterfield, S., Musial, W. and Scott, G. Definition of a 5-MW Reference Wind Turbine for Offshore System Development. NREL/TP-500-38060.National Renewable Energy Laboratory, Golden, Colorado, February 2007

[4] Skaare, B., Hanson, T. D., and Nielsen, F. G. Importance of Control Strategies on Fatigue Life of Floating Wind Turbines. Proceedings of OMAE2007 26th International Conference on Offshore Mechanics and Arctic Engineering, 10-15 June 2007, San Diego, CA [CD-ROM], Houston, TX: The American Society of Mechanical Engineers (ASME International) Ocean, Offshore and Arctic Engineering (OOAE) Division, June 2007, OMAE2007-29277.

[5] Pai, P. F. Highly Flexible Structures: Modeling, Computation, And Experimentation. ISBN: 1563479176. AIAA 2007.

[6] Anderson, E. et al. LAPACK: a portable linear algebra library for high-performance computers. Supercomputing '90: Proceedings of the 1990 conference on Supercomputing. ISBN 0-89791-412-0, IEEE Computer Society Press, Los Alamitos, CA, USA.

[7] Bjorck A. Aerforce: Subroutine package for unsteady blade-element/momentum calculations. Technical Report TN 2000-07, FFA, Bromma, Sweden, 2000.

Appendix 2

Experimental and Computational Comparisons of the OC3-HYWIND and Tension-Leg-Buoy (TLB) Floating Wind Turbine Conceptual Designs

Anders Myhr and Karl Jacob Maus
Dept. of Mathematical Sciences and Technology, Norwegian University of Life Science (UMB)
Ås, Norway

Tor Anders Nygaard
Energy Systems Department, Institute for Energy Technology (IFE)
Kjeller, Norway

ABSTRACT

This paper describes Tension-Leg-Buoy (TLB) wind turbine floaters, in comparison with the OC3-HYWIND Spar-Buoy (SB). Wave tank experiments with TLB and SB conducted in a student project at the NTNU/MARINTEK MCLab are supplemented with computations with the models 3Dfloat and ANSYS. Although the small model scale of 1:100 and the scope of the test make quantitative comparisons between experiment and models difficult, the experiment and models agree reasonably well qualitatively. The main differences between TLB and SB in both experiments and computations are the smaller motions and the higher anchor loads of the TLB.

KEY WORDS: Offshore wind turbine; floating platform; spar buoy; tension-leg-buoy.

INTRODUCTION

The wind turbine technology has developed tremendously over the last three decades. The rated power for a large wind turbine has increased with a factor of 100, from 50 kW in the eighties to more than 5 MW in 2011. With a hub height of around 100 m, and a rotor diameter of more than 120m, a wind turbine is among the larger of mass-produced structures. Recent years, wind energy has been among the fastest growing energy technologies. With ambitious targets for renewable energy, the vast wind energy resource and available areas offshore are getting increased attention by energy planners and the wind energy community. This development was suggested first by Professor Bill Heronemus of Massachusetts Insititute of Technology (MIT) (Heronemus, 1972). After commercial wind turbines reached a size suitable for offshore applications around 2000, development of conceptual designs and computational tools started accelerating. Examples of floating wind turbine designs for areas with water depths in excess of 50m include 1) ballast stabilized Spar-Buoy (SB) floater with catenary mooring lines, 2) mooring line stabilized Tension Leg Platform (TLP), 3) buoyancy stabilized barge with catenary mooring lines, 4) semi-submersible platforms with one to four vertical columns, and finally the MIT double taut leg (Butterfield, Musial, Jonkman and Sclavounos, 2005). Butterfield et al. discuss different aspects of stabilizing the platform with a combination of ballast, buoyancy and mooring lines. For the spar-buoy, all platform degrees-of freedom (DOF) are inertia-controlled, and catenary mooring lines with low stiffness provide only station-keeping. This is achieved by a large floater with heavy ballast, keeping the rigid-body eigen periods above 30 s, outside the energetic part of the wave spectrum. The double taut leg, or Tension Leg Buoy (TLB) as it has been named later (Sclavounos et al., 2010), use excess buoyancy and mooring line stiffness to control all DOF. It can be argued that a TLB is more bottom-fixed than floating, since the vertical position is determined by the tendons, not the water level. Here, the eigen periods should be below the energetic part of the wave spectrum, below 5 s. The worlds first full-scale 2.3 MW floating wind turbine HYWIND was installed outside the Norwegian coast fall 2009. The OC3-HYWIND is a similar, public available definition of a 5 MW floating wind turbine used in the International Energy Agency (IEA) Offshore Code Comparison Collaboration project (OC3) (Jonkman et al., 2010). Although the HYWIND wind turbine has been a technical success, efforts are needed to reduce the costs, where one important cost driver is the steel mass of the structure. The steel masses reported in recent studies of TLB floaters (Sclavounos et al. 2010), (Nygaard et al. 2009), are significantly lower than for the OC3-HYWIND floater. Experimental data to support these results and development of computational tools, however, are lacking. The aim of this work is therefore:

1. The first analysis of experimental results from a wave tank test of one SB and two TLBs floaters, without wind loads.
2. Qualitative comparison of experimental results and computations with our in-house code 3Dfloat, and the commercial finite-element code ANSYS.
3. Compute full-scale versions of the SB and TLBs with wind turbine rotors, comparing motions and loads.

FULL SCALE 5MW CONCEPTUAL DESIGNS

All full-scale wind turbines defined in this paper have identical rotor/nacelle assemblies and towers above z = 10 m (10 m above the still water line (WL). The rotor is three-bladed, variable speed, with a diameter of 126 m and rated power of 5 MW (Jonkman et al., 2007). For the floating OC3-HYWIND platform, the blade pitch angle controller has been modified in OC3 to avoid instability above rated wind speeds (Skaare, 2007). The distributed properties of the tower for the OC3-HYWIND are founded on the base diameter of 6.5 m, which matches the top diameter of the platform, and the tower base thickness (0.027 m), top diameter (3.87 m) and thickness (0.019 m). The density of 8,500 kg/m^3 accounts for paint, bolts, welds, and flanges that are not accounted for in the tower thickness data. The radius and thickness of the tower are assumed to be linearly tapered from the tower base to tower top (Jonkman, 2009). The floater shapes are given in Table 1.

Table 1. Floater Shapes

Item	OC3-HYWIND	TLB A	TLB B
Depth to Platform Base Below WL (Total Draft)	120 m	100 m	52 m
Elevation to Platform Top (Tower Base) Above WL	10 m	10 m	10 m
Depth to Top of Taper Below WL	4 m	NA	NA
Depth to Bottom of Taper Below WL	12 m	NA	NA
Platform Diameter Above Taper	6.5 m	6.3 m	6.0 m
Platform Diameter Below Taper	9.4 m	6.3 m	6.0 m

Tension-Leg-Buoy (TLB)

The TLB floaters in this work come in two versions. Version A is marginally stable without mooring lines, but can increase stability with additional water ballast. The diameter is 6.3 m and the wall thickness 33 mm. Additional mass due to stiffeners etc. is estimated by inserting ring stiffeners with wall thickness 33 mm and inner diameter 5.5 m every third m. This gives a steel mass to deplacement ratio of approximately 0.2, which is similar to other steel floater designs. Version A has 1550 tons of solid ballast during normal operation and up to 800 tons of water ballast during installation.

Version B is a stripped down version that is unstable until installed with prestressed mooring lines. It has only minor water ballast required for adjustment to chosen mooring line pre-stress. The diameter is 6.0m from the tower base to elevation -20 m. Depending on the required excess buoyancy, the diameter further down can be increased. The scale model has constant diameter. A comparison of overall characteristics is shown in Table 2. The three conceptual designs are shown in Figure 1.

WAVE TANK TEST

The experiment was carried out in the Marine Cybernetics Laboratory (MCLab) at the Norwegian University of Science and Technology (NTNU)/MARINTEK in Trondheim, Norway. The MCLab is a towing tank with a single paddle wave maker, with significant wave heights up to 0.3 m. The length, width and depth are 40 m, 6.45 m and 1.5 m respectively.

Table 2: Comparison of overall characteristics

	OC3-HYWIND	TLB A	TLB B
Hub height [m]	90	90	90
Rotor/nacelle mass [ton]	350	350	350
Tower mass [ton]	250	250	250
Floater steel mass [ton]	1600 (estimated)	650	350
Solid ballast [ton]	3100 (estimated)	1850	0
Water ballast [ton]	2700 (balance)	0 – 800	0
Total mass	8000	3100	950
Overall center-of gravity (CG), below WL [m]	77.9	28.6	-28.1
Overall mass radius of gyration, pitch and roll [m]	50.7	57.6	45.6

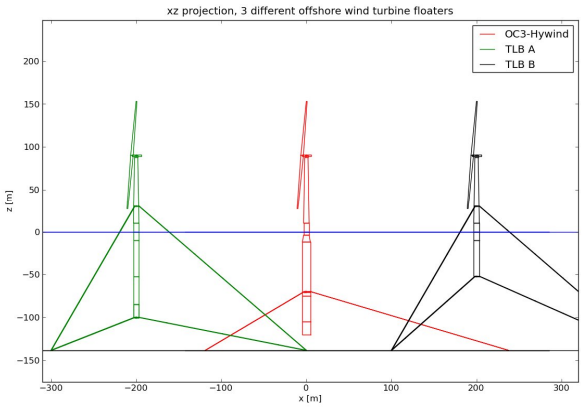

Figure 1: Conceptual designs OC3-HYWIND, TLB A and TLB B

Scaling

The test was scaled to preserve the ratio of inertial to gravity forces, or the Froude number, in geometrical scale 1:100. Table 3 shows the most important scale factors.

Table 3: Scale factors

Item	Factor
Acceleration, Keuler-Carpenter Number	1
Velocity, time, period, frequency	10
Geometry, wavelength, waveheight, stress	100
Reynolds number	1000
Forces, mass	10^6
Moments	10^8
Mass moment of inertia	10^{10}

Scale Models

The scale models are modular, with interchangeable towers and floaters in aluminium (Al), transition pieces in polyoxymethylene plastic (POM), nacelle and ballast containers in high density polyetylen plastic (HDPE) and gaskets of rubber, held together by threaded steel rods. One or more ballast containers can be held in position inside the floater by the threaded rods, to enable adjustment of overall mass, center of gravity (CG) and mass moment of inertias. The main difference between the defined full scale and the built model OC3-HYWIND is that the model mass moment

of inertias about CG, pitch and roll, are 14% too high. This is due to practical issues regarding placement of sensors and logging equipment, along with the challenge of keeping the model mass down. Figure 2 shows a sketch of the floater/tower experimental models.

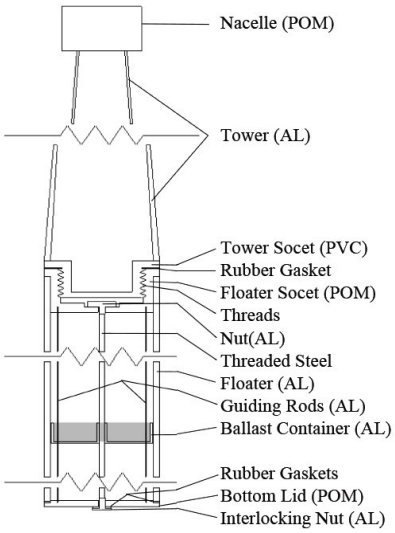

Figure 2: Experimental model sketch.

The OC3-HYWIND mooring system definition is given as 1) physical description of catenary mooring lines used at water depth of 320 m and anchor radius of 854 m, 2) resulting linearized spring stiffness matrix that can be applied to platform at WL and 3) nonlinear force-displacement relationships based on computations with a mooring line model (Jonkman, 2009). The resulting stiffness is very low, and simulations show that the time to reach a periodic solution would be long with the original mooring definition. The motions of the floater is, however, not sensitive to the mooring characteristics for OC3-HYWIND, since the mooring lines mainly contribute to station keeping. The mooring line stiffness was therefore increased with a factor of about 10. We applied linearized spring stiffness by attaching taut lines to the platform at an angle corresponding to the mooring line force in equilibrium position. The lines ran from the floater, over a wheel/spindle at the anchor radius, then vertically to a spring/strain gauge above the water line. Figure 3 shows the tower used to simulate the mooring stiffness. The tower consists of three 15 mm steel pipes held together by horizontal steel plates at four heights. Although the motions of the floater (except surge to equilibrium) are little influenced by the change of mooring line stiffness, the measured mooring line tension will show larger variations, and has little resemblance with the full scale mooring. The TLB mooring lines are taut, and can be directly modeled with the same towers, placed at the physical anchor radius. The model anchor radii in full scale are 113.5 m for OC3-Hywind and 200 m for the TLBs. In the model test, this corresponds to 130 and 75 mooring tower diameters, respectively.

Measurement System

For the tower root stress HMB XY101-3 120 Ω strain gauges were used. They were applied with HBM Z70 glue and covered with HBM SG250 for a first line of water protection. A second layer of protection was laid with ductile waterproof silicone. The monitors for mooring line tension were built with strain gauges from RS with model number N11MA512011 and also of 120 Ω resistance. These were applied on pre-cut stainless steel profiles that were machined to a semi-elliptic form for better sensitivity.

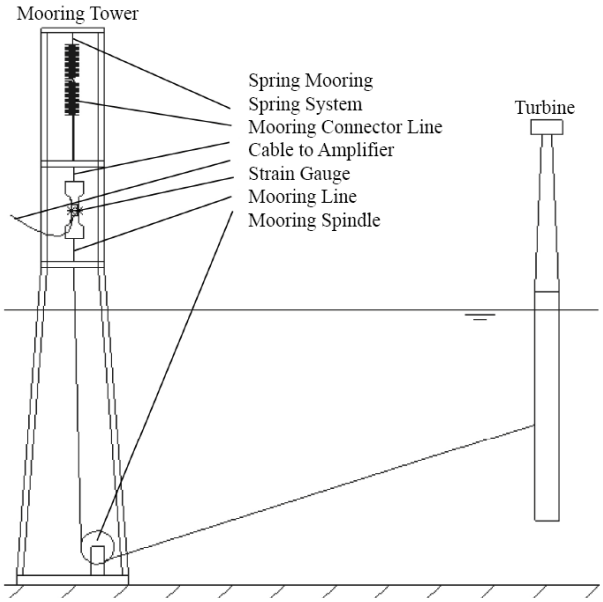

Figure 3: Mooring line configuration. The tower consists of three 15 mm steel pipes arranged in a triangular fashion.

To reduce internal stress in the material they were heat treated before the strain gauges were applied. To create a circuit for the strain gauges a M1000-6 amplifier from Micro Movements was utilized on 5 V. The variation in current was recorded with a USB-6210 multifunction data acquisition logger from National Instruments. This also recorded data from the wireless three axis accelerometer MMA7361LCR1 from Farnell with an amplitude range of 1.5g. The wireless bridge was created from a XBee XB24-Z7CIT-004 system with chip antennas. The water proofed strain gauges from HBM together with the wave height sensor were connected to a HBM MGC+ amplifying system. Motion tracking was applied at the tower top with the 6DOF real-time on-site motion capture system from Qualisys. All the inputs were connected to a computer with Labview used for logging and processing.

COMPUTATIONS

3Dfloat is an aero-hydro-servo-elastic finite element model (FEM) developed from 2006 at IFE and UMB for the computation of the dynamic response of offshore wind turbines. It is coded in FORTRAN90, with linear algebra routines from the LAPACK library (Anderson et al., 1990). 3Dfloat was one of the seven models compared in the IEA OC3 project (Jonkman, 2009).

Structural Model

The core of the model is a general FEM framework, where computational nodes are connected with elements. The model in this paper utilizes Euler-Bernoulli beams with 12 degrees of freedom (DOF). Tailored beam elements are used for cables (mooring lines). Tapered beams are approximated with linearly varying cross-sectional parameters defined at the end-nodes. Geometric nonlinearities are accounted for by a co-rotated FEM approach, where the reference configuration is a recently deformed state. The element equations are stated in a coordinate system attached to the midpoint of the element in the reference state, and then transformed to a common component coordinate system. This allows for the utilization of small-strain elements for large global deflections, as long as the element resolution is sufficient.

Loads

Loads from gravity, buoyancy, waves, current and wind are applied as distributed external loads on the structure. Forces are evaluated at Gauss points in the elements, and a Galerkin approach is used to evaluate consistent nodal loads. Wind is handled as a nonlinear drag term, and wave and current loads are computed using the relative form of Morison's equation (Sarpkaya, 1981). Terms involving acceleration (added mass) are added to the mass matrix, while all other loads are kept as applied loads on the right hand side (RHS) of the equation system. Point forces can be applied to nodes. A wind turbine rotor load model can associate rigid rotors to nodes, or provide aerodynamic loads to a flexible FEM representation of wind turbine rotors. The rotor aerodynamic loads are handled using unsteady blade-element/momentum theory (BEM), with extensions for dynamic inflow and yaw errors. Airfoil data are supplied as lookup-tables (Björck, 2000).

Control system

The generic control system in 3Dfloat is for a variable speed rotor, with fixed blade pitch angle below rated wind speed. Above rated wind speed, PI control of pitch angle is used to control rotational speed and power (Hansen et al., 2005). Alternatively, similar controllers developed in the IEA OC3 project for the NREL 5 MW reference rotor are implemented. One of these controllers has been tuned to maintain stability for the OC3-HYWIND floating wind turbine (Skaare et al., 2007).

Temporal Integration

The time domain computations are carried out using either the implicit Generalized-α method, the implicit Newmark scheme, or an explicit central difference scheme (Pai, 2007). For the implicit schemes, Newton sub-iterations are used for the convergence of the solution in each time-step, governed by a residual criterion. All Newmark and Newton parameters may be user-defined. In this paper, the generalized α-method with spectral radius 0.99 was used.

Eigen-frequency analysis within 3Dfloat is handled with all externally applied loads dependent on displacements linearized and added to the stiffness matrix at the relevant node. This includes the effect of buoyancy, mooring lines and restoring moment due to metacentric height.

Drag and inertia coefficients

The drag and inertia coefficients in the relative form of the Morison equation are often presented as function of the Keulegan-Carpenter and oscillatory Reynolds numbers (Sarpkaya, 1981). The Keulegan-Carpenter number (KC) is a measure of drag/inertial forces in oscillatory flows, and is the product of fluid velocity amplitude normal to the cylinder, and period, divided by cylinder diameter. The oscillatory Reynolds number (Re) is a measure of inertial/viscous forces, and is the product of fluid velocity amplitude normal to the cylinder and cylinder diameter, divided by the fluid kinematic viscosity. For case 1, the upper part of the floater, KC varies from about 0.5 to 3.0, and Re between 2000 and 12,000. The frequency parameter defined as Re/KC (Sarpkaya, 1981) is 3700 for case 1. From the figures 3.20 and 3.21 in (Sarpkaya, 1981) we take the inertia coefficient as 2.0, and the drag coefficient as 1.1 for case 1. For case 2, KC for the upper part of the floater, is in the range 4 to 8, and the oscillatory Reynolds number in the range 9000 to 16,000. The frequency parameter is 2300. The inertia coefficient is in the range 1.5 to 2.0. The drag coefficient is in the range 1.4 to 1.8. For case two, we used an inertia coefficient of 1.8 and a drag coefficient of 1.6.

The applicability of Morison equation for the full-scale version of OC3-HYWIND was addressed in OC3. It was concluded that Morisons equation is a good approximation because 1) diffraction effects are negligible in moderate to severe sea states, 2) radiation damping in most modes of motion is small and 3) flow separation will occur in severe sea states along the upper regions of the spar (Jonkman, 2009). Important parameters are the spar diameter to wavelength ratio, and the the Keulegan-Carpenter and oscillatory Reynolds numbers. For the scale model test, the Froude scaling preserves KC and the spar diameter to wavelength ratio, but reduces the Re with a factor 1000. Morisons equation is still applicable, but the drag term is more uncertain due to the reduced Re.

Spatial and Temporal Resolution

The simulations compared with the experiments are carried out in model scale, with a flexible FEM representation of the wave tank model. The results are presented in full size scale. One case with double resolution was carried out to check that the solutions are converged with respect to spatial resolution. The time step used for the all simulations is 0.01s, giving 100 steps per wave period for case1 in model scale. Several simulations with time step 0.001s were carried out to check that the solutions are converged with respect to temporal resolution.

RESULTS

Eigen Frequencies

Table 4 shows the computed ten longest eigen periods for the experiment scale model configurations, with mooring stiffness as measured during the test. In both the experiment and computations, the rotor/nacelle assembly is replaced with one clump mass. The results are presented in full scale.

Table 4: Computed eigen periods [s], full scale

Mode	OC3-HYWIND	TLB A	TLB B
Sway	54	3.7	3.4
Surge	54	3.6	3.3
Roll	37	2.8	3.9
Pitch	35	2.9	3.8
Heave	27	3.2	3.0
Yaw	11	8.5	8.2
First bending	0.027	0.025	0.014
Second bending	0.009	0.008	0.0045

The roll/pitch (and sway/surge) eigen periods are different due to the measured individual mooring line stiffness applied in the computations. The 'crow-foot' mooring line deltas that are used in the full scale version to control yaw motions were dropped in the experiment due to time constraints. This results in rather unfavorable eigen periods in yaw.

Overview of Cases

OC3 HYWIND, and the two TLBs were tested with no wind-load and regular waves with the following characteristics (for full scale):

Table 5. Cases

Case	Wave height [m]	Period [s]
1	5	10
2	10	18
3 TLBs only	30	18

Case 3 is meant to illustrate mooring snap loads for the TLBs. The scale model excess buoyancy is too low to maintain tension for this wave height. This paper will give a first analysis of case 1 and 2.

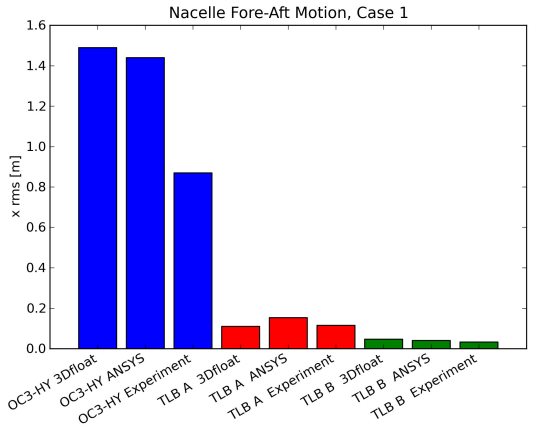

Figure 4: Nacelle fore-aft motion, case 1, presented in full scale.

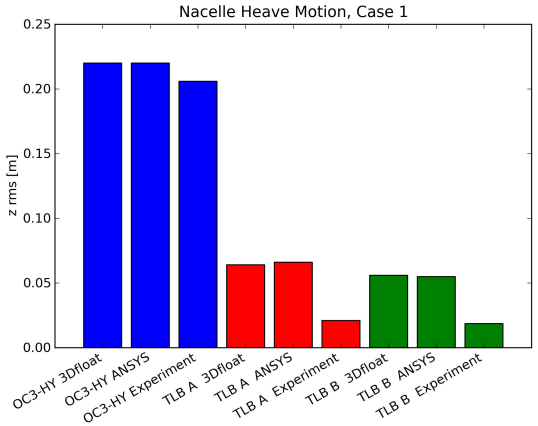

Figure 5: Nacelle heave motion, case 1

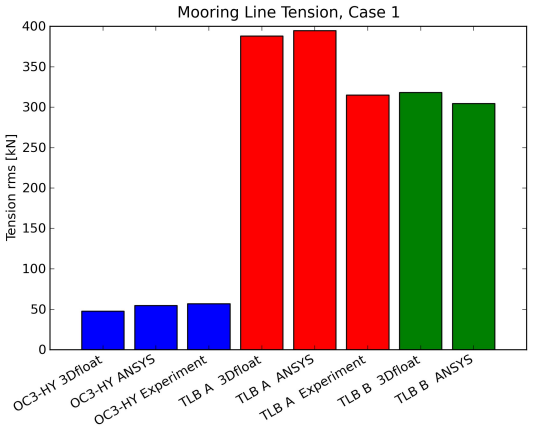

Figure 6: Mooring line tension, case 1

As measures of amplitudes, root-mean-square (RMS) of nacelle fore-aft motion (resulting from pitch and surge), heave motion and mooring line tension (average RMS of all mooring lines) are shown in the figures 4 through 9. For OC3-HYWIND, case 1, the heave motions and mooring line tensions agree well, but the fore-aft motions is lower in the experiment. In the computations, the pitch and surge motions are completely in phase. In the experiment, yaw motions induce roll motions and a phase shift between pitch and surge, reducing the resulting nacelle fore-aft motion. A closer look is provided later in the paper.

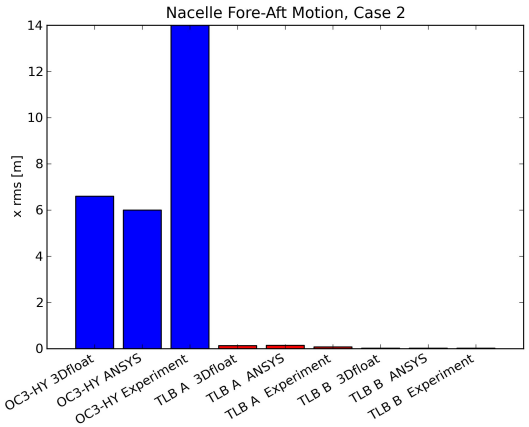

Figure 7: Nacelle fore-aft motion, case2

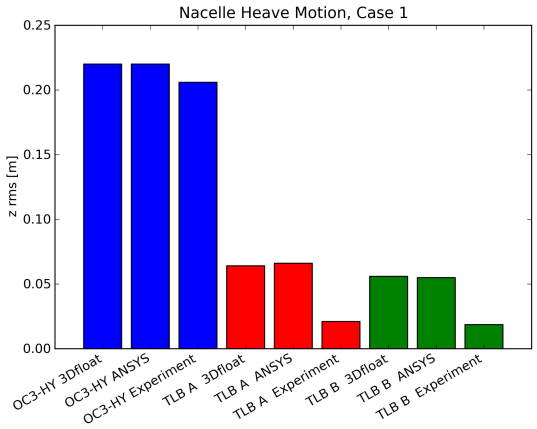

Figure 8: Nacelle heave motion, case 2

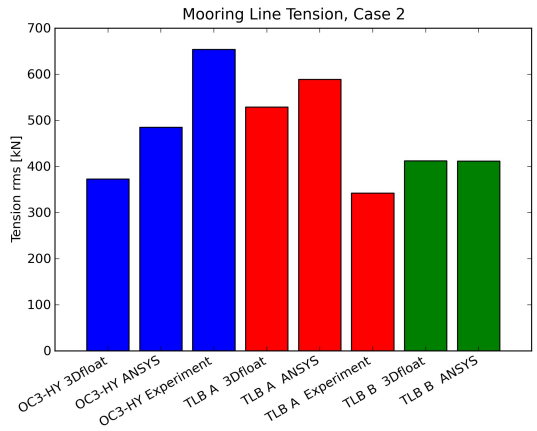

Figure 9: Mooring line tension, case 2

In case 2, the OC3 HYWIND experimental data show significantly higher fore-aft motions in the experiment. The reason for this is not yet fully understood, but we suspect that the effective mooring stiffness is higher in the experiment than the computations, bringing the inertia-controlled OC3-HYWIND closer to pitch resonance.

For TLB A, the first look at the results are best done for case 2, where the wave period is almost five times the highest platform eigen period, except for yaw. In this quasi-static case, heave motions are mostly determined by the wave elevation, and the axial stiffness in the mooring, which is the case in the model results. The experimental heave is more than a factor 4 lower. Possible sources of error are the friction in the mooring line spindle, the measurement of the mooring line stiffness, and the measurement of the very small heave motions. The fore-aft motions are also small and hardly seen in the figure. The experimental value is about 60 % of the computed. Sources of error here are the chosen drag- and inertia coefficients, and again the mooring system stiffness. A sanity check of the experiment mooring line tension was performed by adding the vertical components of all mooring line forces, and comparing the resulting amplitude with the buoyancy change induced by the wave. The match is good, giving some confidence in the measured tension RMS, which is about 60 % of the computed rms. This again points to force-model errors, e.g. the chosen drag- and inertia coefficients. For case 1, the chosen drag- and inertia coefficient seem to match the experimental results better. The fore-aft motions and mooring line tension match reasonably well. The experiment heave is less than half the computed, but the values are small, on the order of the laser tracker accuracy.

For TLB B, we have rejected the measured mooring line tensions, after performing the same sanity check as outlined for TLB A. For the rest of the results, the trends and discussions are the same as for TLB A.

A summary of the first overview of the results are as follows:

1. The stiffness-controlled TLBs have significantly smaller motions than the inertia-controlled SB.
2. Increasing mooring line stiffness reduces the motions for the TLB, whereas the inertia-controlled SB will be pushed towards resonance, and increased motions.
3. The inertia-controlled SB will smooth external load fluctuations, resulting in low anchor load fluctuations. In contrast, the TLB transfer loads directly to the anchors.
4. All motions except the pitch resonance were either accurately or over-predicted for the SB. All mooring line forces were either accurately or over-predicted for the TLBs. For the simple case used in this paper, the modeling approach is therefore conservative.

Selected results in some more detail

Figures 10 and 11 show a comparisons of experiment and computations for tower top total displacement in surge and heave direction, and mooring line tension for OC3-HYWIND. The computed motions agree well with the mainstream of the other models for a corresponding full scale case in OC3. The jagged lines for experiment tower top displacements are due to the sampling algorithm for the measurement system. The computed and measured heave motions agree well. The tower top displacement resulting from both surge and pitch has almost twice the amplitude in the computations. Platform pitch and surge are in phase, and contribute approximately equally to the tower top motion in the computation. The platform pitch signal is noisy in the experiment.

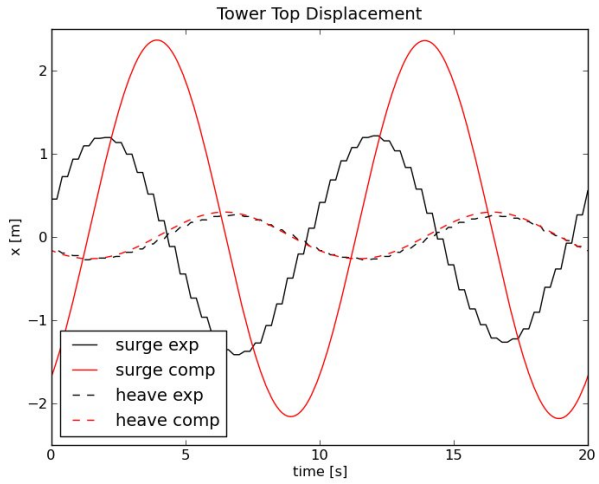

Figure 10: Experiment and Computed Tower Top Displacements for OC3-HYWIND, Case1.

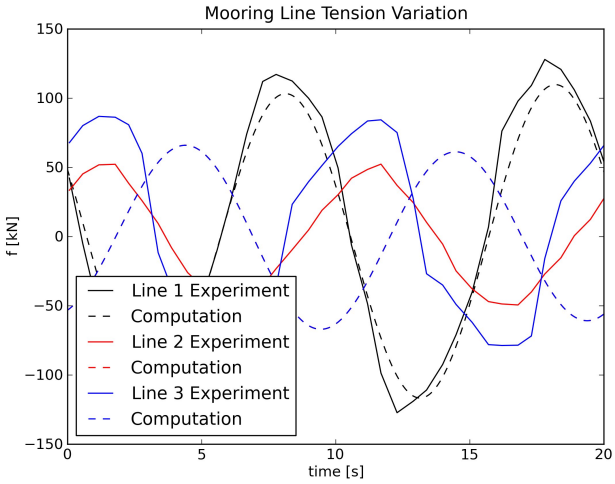

Figure 11: Experiment and Computed Mooring Line Tension Variations for OC3-HYWIND, Case1. Note: Line 2 computation is hidden by line 3 computation due to symmetry.

It has the same amplitude as in the computation, but is out of phase with platform surge, hence the lower total displacement. This is also seen as a phase shift in tower top surge motion between experiment and computation. Mooring line 1 is aligned with the waves, in the surge direction. Seen from above, line 2 and 3 are oriented counterclockwise from line 1. The measured and computed tension amplitudes agree well for line 1. The computed line 2 and 3 tensions are identical due to symmetry. The average of the experiment amplitudes for line 2 and 3 agree well with the computed amplitudes for line 2 and 3. Platform surge should therefore be similar for experiment and computation. The experiment phases for line 2 and 3 are not completely periodic, drifting in an out of phase in the rest of the time history not shown in Figure 4. The phase shift and differences in amplitudes are due to yaw motions in the experiment. The eigen frequency for yaw is only 10 % away from the wave frequency. Lowering the yaw damping in the simulations, and offsetting the CG of the nacelle from the centerline produces yaw motions and shifts in mooring line tension similar to the experiment. Overall, experiment and computations are in qualitative agreement. The differences can be explained by yaw motions in the experiment, and of

course the general high uncertainty due to both scaling, calibration and friction issues in scale 1:100.

The tower top (nacelle) motions and the mooring line tension variations of TLB A, case 1 are shown in the Figures 12 through 14.

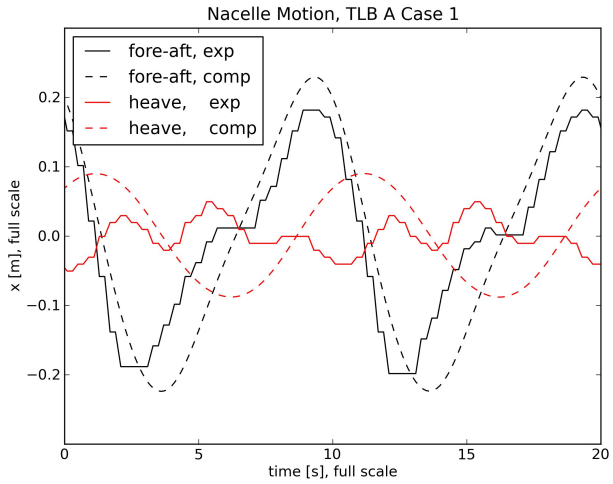

Figure12: Nacelle motion, experiment and computation, TLB A case 1

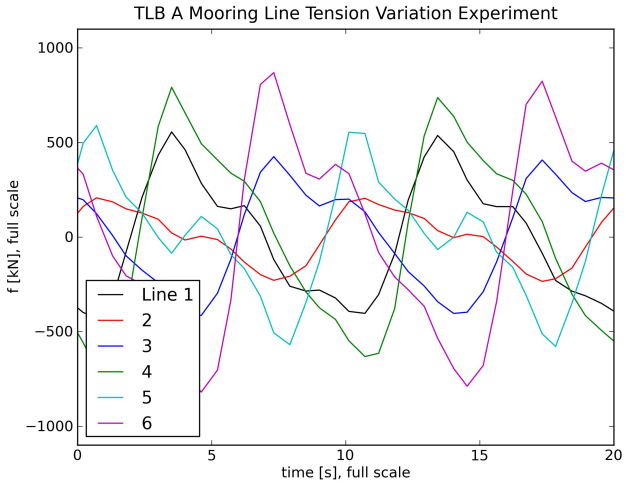

Figure 13: Mooring line tension experiment, TLB A, case 1

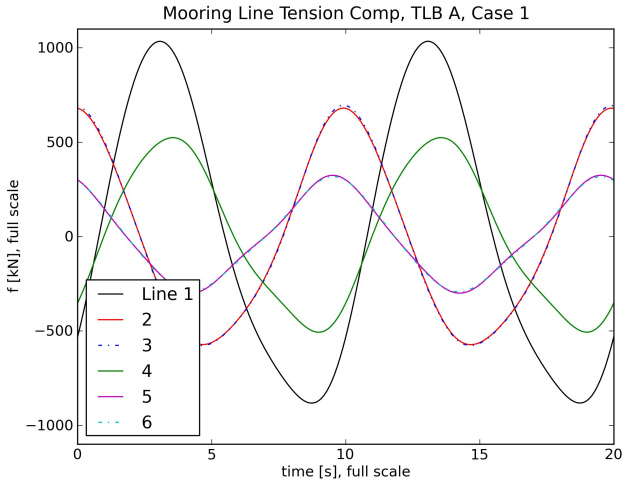

Figure14: Mooring line tension computation, TLB A, case 1

The nacelle fore-aft motions agree well between experiment and computation, both in amplitude and shape. The heave motions are significantly different, but the differences could be due to measurements issues as well, since the model scale motions here are less than 1 mm. Mooring line 1 is aligned with the waves, in the surge direction. Seen from above, line 2 and 3 are oriented counterclockwise from line 1. The lower mooring lines 3-6 are oriented in the same manner. In the experiment and computations, the upper and lower lines with the same orientation; 1/4, 2/5 and 3/6 are in phase. In the computations, the upstream lines 2/5 and 3/6 are almost in phase, whereas there is a significant phase difference in the experiment. This is again due to yaw and roll motions in the experiment, due to the ill placed eigen frequency in yaw. Another source of error is the initial orientation of the TLB in the experiment. Getting the correct pre-tension in all six lines and at the same time a vertical orientation of the floater is a tedious procedure. We ran computations with tilt 1 deg along the three mooring line directions without affecting overall RMS, but individual mooring line tension can be affected by initial tilt.

Conceptual Design Comparisons by Computation

The experimental results and computations in the previous section show different behavior of the inertia-controlled SB and the stiffness-controlled TLB in terms of motion and interaction between the floater and mooring system. In this section, computations with 3Dfloat are applied to OC3-HYWIND and TLB B to illustrate the interactions between the platforms and the wind turbine. In OC3, load case 5.1 we applied regular airy waves with wave height 6 m and period 10 s to the OC3-HYWIND, operating at a steady wind speed of 11.4 m/s. At this wind speed, the wind turbine has just reached rated power. Wave induced motions of nacelle cause power variations due to the change in wind speed relative to the rotor, which in turn trigger blade pitch control actions to control power, which in turn changes rotor trust, causing new motions, and so on. A pitch-controller for a bottom-fixed or land-based wind turbine may go unstable for wind speeds above rated power for a platform with large motions, like a SB. In OC3, this was overcome by tuning a conventional variable-speed controller. The real HYWIND prototype has a proprietary advanced controller, demonstrating significant reduction of motions compared to standard controllers. Figure 15 shows the rotor angular speed variations induced by the waves. For OC3-HYWIND, the variations agree well with the mainstream of the other models in OC3.

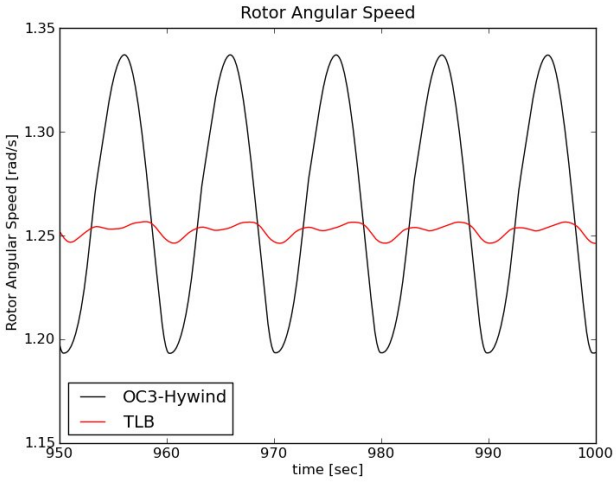

Figure 15: Rotor angular speed variations induced by regular waves

Due to the constrained nacelle motions, the TLB has significantly lower variations. Both standard and modified pitch-controllers gave stable operation of the TLB. The inertial forces from the heavy nacelle motions cause stress variations in the tower, where fatigue is an important issue for all wind turbines. Figure 9 shows the stress variations in the tower induced by the interaction of the waves, platform and wind turbine. The stress variations for the TLB are around 20 % of the corresponding variations for the SB.

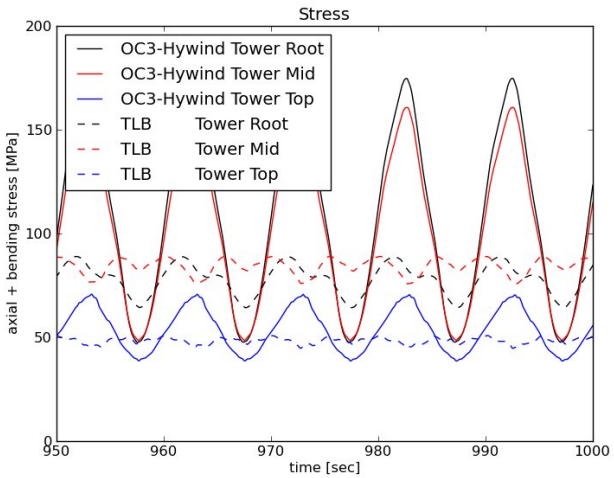

Figure 16: Tower stress variations induced, load case 5.1, OC3.

Overall, both the inertia-controlled OC3-HYWIND and the stiffness-controlled TLB seem to behave well. The restricted motion of the TLB results in lower stress variations than for the OC3-HYWIND.

CONCLUSIONS

1. An inertia-controlled Spar-Buoy (SB) and a stiffness-controlled Tension-Leg Buoy (TLB) have been compared in a wave tank experiment and by computations.
2. Although the experiment scale of 1:100 makes quantitative comparisons with the numerical models difficult, the qualitative agreement between experiment and model is reasonably good.
3. The agreement between the models 3Dfloat and ANSYS is good.
4. In both experiment and computations, the TLB motions are significantly smaller than for the SB.
5. The loads on the TLB tower are lower than on the SB. This is due to the taut mooring in two heights, taking loads directly to the anchors, and restricting motions, and thereby gravity and inertia loads.
6. The anchor loads for the TLB are significantly higher than for the SB.
7. The steel mass of the TLB B floater is 22 % of the OC3-HYWIND floater steel mass. This indicates a significant cost savings potential.

ACKNOWLEDGEMENTS

We gratefully acknowledge the support from Knut Arne Hegstad, MARINTEK, and the rest of the staff at MCLab. The test was in part funded by the Norwegian Research Council and UMB. The 3Dfloat computations were funded through the NOWITECH research program.

REFERENCES

Anderson, E. et al. (1990). "LAPACK: a portable linear algebra library for high-performance computers". *Proc 1990 conference on Supercomputing*. ISBN 0-89791-412-0, IEEE Computer Society Press, Los Alamos, CA, USA.

Björck, A (2000), "AERFORCE: Subroutine Package for unsteady Blade-Element/Momentum Calculations". FFA report TN 2000-07

Butterfield, S, Musial, W, Jonkman, J and Sclavounos, P (2005). "Engineering Challenges for Floating Offshore Wind Turbines". *Proc 2005 Copenhagen Offshore Wind Conference*, Copenhagen, Denmark October 26–28, 2005

Hansen, MH et al.(2005) "Control design for a pitch-regulated, variable speed wind turbine". RISØ-R-1500, 2005.

Heronemus, WE (1972). "Pollution-Free Energy From Offshore Winds," *Proc 8th Annual Conference and Exposition Marine Technology Society*, Washington D.C., September 11-13,1972

Jonkman, J, Butterfield, S, Musial, W and Scott, G (2007). "Definition of a 5-MW Reference Wind Turbine for Offshore System Development". NREL/TP-500-38060. National Renewable Energy Laboratory, Golden, Colorado, February 2007

Jonkman, J (2009). "Definition of the Floating System for Phase IV of OC3". National Renewable Energy Laboratory (NREL), Golden, Colorado, February 2009.

Jonkman, J et al. (2010). "Offshore Code Comparison Collaboration within IEA Wind Task 23". *Proc Europen Wind Energy Conference & Exhibition*, Warsaw, Poland, April 2010.

Nygaard, TA, Myhr, A and Maus, KJ (2009). "A comparison of two conceptual designs for floating wind turbines". *Proc European Offshore Wind Conference & Exhibition*, September 2009, Stockholm, Sweden.

Pai, PF(2007). "Highly Flexible Structures: Modeling, Computation, And Experimentation". ISBN: 1563479176. AIAA 2007.

Sclavounos, PD et al. (2010). "Floating Offshore Wind Turbines: Tension Leg Platform and Taut Leg Buoy oncepts supporting 3-5 MW Wind Turbines". *Proc European Wind Energy Conference EWEC 2010,* Warsaw, Poland 20-23 April 2010

Skaare, B, Hanson, TD., and Nielsen, FG (2007). "Importance of Control Strategies on Fatigue Life of Floating Wind Turbines". *Proc OMAE2007 26th International Conference on Offshore Mechanics and Arctic Engineering*, 10-15 June 2007, San Diego, CA [CD-ROM], Houston, TX: The American Society of Mechanical Engineers (ASME International) Ocean, Offshore and Arctic Engineering (OOAE) Division, June 2007, OMAE2007-29277.

Appendix 3

Proceedings of the Twenty-second (2012) International Offshore and Polar Engineering Conference
Rhodes, Greece, June 17–22, 2012

ISBN 978-1-880653-94–4 (Set); ISSN 1098-6189 (Set)

www.isope.org

Load Reductions and Optimizations on Tension-Leg-Buoy Offshore Wind Turbine Platforms

Anders Myhr
Norwegian University of Life Sciences (UMB)
Department of Mathematical Sciences and Technology, Ås, Norway

Tor Anders Nygaard
Institute for Energy Technology (IFE), Energy Systems Department
Kjeller, Norway

ABSTRACT

The stiffness-controlled Tension-Leg-Buoy (TLB) platform potentially has low steel mass and limited dynamic response compared to other deep water wind turbine platforms. The higher anchor loads, however, may offset the potential cost advantage of the TLB. The aim of this paper is to address important aspects of this issue, such as the Excess Buoyancy (EB) of the platform and the mooring line layout. The EB is required to keep the mooring lines taut throughout all events, and is therefore strongly influenced by the wave loads. An attempt to reduce the wave loads with a space-frame section in the wave action zone is presented. Optimization routines are utilized to adjust the geometry and mooring line layout for lower cost. The tools and procedures used for the optimizations and the resulting TLB conceptual design improvements are presented. As the trade-offs between different conceptual designs are studied closer, optimization should be helpful to enable more detailed comparisons under similar site specific conditions.

KEY WORDS: Offshore wind turbine; platform; Tension-Leg-Buoy (TLB); taut mooring; anchor loads; space-frame; aero-hydro-servo-elastic analysis

INTRODUCTION

A diverse portfolio of wind turbine platforms is currently being investigated for water depths exceeding 50 m. Examples include a bottom-fixed space-frame ("Jacket") at 50 m depth analyzed in the IEA OC4 project (Popko et al., 2012), a full-height bottom-fixed lattice tower at 60 m depth (Muskulus, 2012) and several floating platforms on water depths exceeding 200 m (Robertson and Jonkman, 2011).

The floating platforms include the Spar-Buoy such as the full-scale HYWIND wind turbine installed of the Norwegian coast in 2009. Recent studies indicate that this concept can be utilized in water depths from 150 m and deeper (Karimirad, 2012). Semi-Submersible platforms can be applied at water depths ranging from typically 50 m and deeper. Tension-Leg-Platforms (TLP) and TLBs are apparently floating, but the vertical position is determined by the tendons, and not the water level, so it can be argued that they are more bottom-fixed than floating. The TLP and TLB can both be applied at water depth exceeding 50 m (Sclavounos, 2010). The TLP system is well known from the oil and gas industries.

The TLB controls all Degrees-Of-Freedom (DOF) by the axial stiffness of taut mooring lines attached to the platform at two or more heights. In a wind energy context, it was first introduced under the name MIT double taut leg by Professor Sclavounos of Massachusetts Institute of Technology (MIT) (Butterfield et al., 2005). Later work includes application examples (Nygaard et. al, 2009) (Sclavounos et al., 2010) (Tsouroukdissian, 2011) and comparisons between a wave tank test and computations (Myhr et al., 2011).

The TLB has significantly lower steel mass in the floater compared to other platform types applied to water depths deeper than 50 m, and the cost is therefore potentially lower. However, due to the taut mooring lines and EB, the anchors are subject to relatively high mean horizontal and vertical loads. Furthermore, load variations due to wind and waves are transferred directly to the anchors. This leads to higher anchor costs than for conceptual designs with a catenary mooring line system.

The axial stiffness of the mooring lines and the anchor radius are governed by a requirement to keep all eigen periods of the system lower than three to five seconds, i.e. outside the energetic part of the wave spectrum. Also, no modes should interfere with the 1P and 3P ranges of the rotor. This problem is tedious to solve by trial-and error.

The EB is a major cost driver, directly for the steel mass of the floater, and indirectly for the anchors, due to the loads. It is therefore of interest to determine the minimum EB required to keep all mooring lines taut throughout extreme events, to avoid snap loads and failure.

The requirement for EB is driven by the maximum wave- and wind loads during extreme weather. For slender structures, the wave loads are largely determined by the projected area and volume of the structure in the wave action zone.

In this paper, we attempt to reduce the loads on TLB platforms by replacing the tubular part of the floater and tower in the wave action zone with a space-frame. This should lower the projected area and volume of the structure, and thereby the wave loads. This should again allow reduction of EB, since the wave loads during extreme events are reduced. Optimization is applied to the shape of the space-frame, the EB, and the mooring line axial stiffness and anchor radius. The extreme weather characteristics can if desired be site-specific, which is another way to potentially reduce the cost of wind energy. Optimization of the different conceptual designs to the same specific location before comparison will also benefit the understanding of the basic trade-offs.

APPROACH

When considering realization of floating wind turbine conceptual designs, our perspective is industrialization and large scale deployment of hundreds, if not thousands of wind turbines. In this perspective, reduction of the steel mass is a key factor in reducing the costs, along with simplifications in the geometry with respect to fabrication, transportation, installation and decommissioning. The main focus for this paper is reduction of mooring force amplitudes and steel mass.

For most floating wind turbines, the major part of the steel is located in the floater, and for the TLB also in the anchors. By reducing the EB and thereby the volume of the floater, the wall thickness and extent of stiffeners can be reduced accordingly to meet relevant design standards. For this paper the DNV-RP-C202 and IEC 61400-3 are used as a basis for the selection of wall thickness for a given outer diameter of a submerged cylinder, to ensure a structure that is viable for deployment at the chosen offshore location.

The computational comparisons of the different conceptual designs are carried out with environmental parameters corresponding to a location in the North Sea with harsh weather conditions and an intermediate water depth of 75 m. This is slightly deeper than the sites developed commercially for bottom-fixed wind turbines today and in our opinion a depth where floating wind turbines should be able to compete with bottom-fixed. Two approaches are examined in this paper:

1. Revisiting the fundamental design: A novel attempt to reduce the requirement for excess buoyancy by combining principles from semi-submersible vessels and offshore space-frames while still maintaining vital aspects regarding fabrication and mass-production. This reduces the wave loads due to the more transparent structure in the wave action zone and ensures a design that is suitable for large scale deployment.

2. Utilize optimization algorithms combined with aero-hydro-elastic computations to achieve designs that are optimized to a given condition for comparison under Ultimate Limit State (ULS).

Automated optimization routines replace elaborate hand-tuning of mooring-line stiffness and layout under eigen frequency constraints. In addition the optimization routine also handles the adjustment of floater buoyancy, height and key dimensions of the space-frame (the orange section in figure 1.) in addition to minimum mooring line tension under extreme wave conditions. The steel mass of cylinder end-caps is incorporated through rules for end-cap thickness based on the wall thickness. Additional steel mass is added for transitions between different cross sections. These masses are too complex to incorporate at a high precision level at this stage of the design process. The extra masses are therefore largely based on own experience and existing comparable designs.

Figure 1. Artists impression of the TLB Baseline (B) conceptual design. The figure does not include the “crow-foot” deltas providing yaw stiffness

The phases used during the optimizations are 1) eigen frequency analysis to determine mooring line layout and 2) simple and computationally efficient ULS cases applied with relevant safety factors to determine floater EB and main geometry. Finally, the optimized designs are tested with several other load cases (LC) to verify that the simple ULS provided a viable design. The aim of this work is to compare different approaches for load reductions, and the assumption is that simple ULS cases provide a useful first insight in the trade-offs between these approaches. A detailed design would of course involve the rest of the load cases in the design standards, such as fatigue, fault conditions etc.

COMPUTATIONAL TOOLS

3DFloat is an aero-hydro-servo-elastic simulation tool developed from 2006 at IFE and UMB for the computation of dynamic response of offshore wind turbines. It is coded in FORTRAN90, with linear algebra routines from the LAPACK library (Anderson et al., 1990). 3DFloat was one of the models applied to the OC3-HYWIND floating wind-turbine in the IEA OC3 project (Jonkman et al., 2010), and the bottom-fixed space-frame (“Jacket”) in the IEA OC4 project (Popko et al., 2012).

Structural Model

The core of the model is a general nonlinear Finite-Element-Model (FEM) framework, where computational nodes are interconnected with elements. The model in this paper utilizes Euler-Bernoulli beams with 12 degrees of freedom (DOF). Cable elements with reduced bending-stiffness are used for the mooring lines. Geometric nonlinearities are accounted for by a co-rotated FEM approach, where the reference configuration is a recently deformed state. The element equations are stated in a coordinate system attached to the midpoint of the element in the reference state, and then transformed to a common component coordinate system. This allows for the utilization of small-strain elements for large global deflections, as long as the element resolution is sufficient.

Loads

Loads from gravity, buoyancy, waves, current and wind are applied as distributed external loads on the structure. Forces are evaluated at Gauss points in the elements, and a Galerkin approach is used to evaluate consistent nodal loads. Wind is handled as a nonlinear drag term on the structure above the wave surface, except on the rotor blades, where lift- and drag lookup tables are used. The buoyancy for the wet elements is computed from the pressure field obtained from the wave kinematics model.

Regular wave kinematics is either linear finite water depth Airy-theory or stream functions up to order 12 (Chaplin, 1980). Irregular waves are obtained by superposition of Airy wavelets. The updated configuration of both the structure and sea surface is taken into account when applying buoyancy and wave loads to the wet elements. For the Airy waves, two approaches are implemented to provide wave kinematics to the wave surface. In the Wheeler stretching approach, the wave kinematics calculated at the Still Water line (SWL) is applied to the wave surface, stretching the distribution between the surface and the bottom. This creates variations in pressure extending further down than in the basic Airy formulation, influencing the heave excitation. In the extrapolated Airy theory, wave kinematics in the wave crest is assumed to be similar to the SWL, and elsewhere (for wet elements) as in the basic Airy theory. This modifies the kinematics only within the wave crests and troughs. In this work we use stream functions for the regular waves. The pressure in the stream function formulation is calculated by the Bernoulli equation applied in a reference frame moving with the wave celerity. In this frame, the pressure and velocity fields are steady, and the total pressure height is uniform.

Wave and current loads are computed on the wet part of the structure using the relative form of Morison's equation (Sarpkaya, 1981). Terms involving acceleration (added mass) are added to the mass matrix, while all other loads are kept as applied loads on the right hand side (RHS) of the equation system. Point forces can be applied to nodes. A wind turbine rotor load model can associate rigid rotors (or several if so desired), to nodes or provide aerodynamic loads to a flexible FEM representation of wind turbine rotors. The rotor aerodynamic loads are computed using unsteady blade-element/momentum theory (BEM), with extensions for dynamic inflow and yaw errors.

Control System

The generic control system in 3DFloat is for a variable speed rotor, with fixed blade pitch angle below rated wind speed. Above rated wind speed, PI control of pitch angle is used to control rotational speed and thereby power (Hansen et al., 2005). Alternatively, similar controllers developed in the IEA OC3 project for the NREL 5 MW reference rotor are implemented. One of these controllers has been tuned to maintain stability for the OC3-HYWIND floating wind turbine (Jonkman et al., 2010).

Temporal Integration

The time domain computations are carried out using either the implicit Generalized-α method, the implicit Newmark scheme, or an explicit central difference scheme (Pai, 2007). For the implicit schemes, modified Newton sub-iterations are used for the convergence of the solution in each time-step, governed by a residual criterion.

Eigen-frequency analysis with 3DFloat is handled with all displacement dependent externally applied loads linearized and added to the stiffness matrix at the relevant DOF. This includes the effect of buoyancy, mooring lines and restoring moment due to metacentric height. For the TLB, the mooring stiffness governs the motions as long as all lines are taut. The linearized force-displacements for the mooring lines are conveniently achieved by connecting the mooring lines to the structure with one element per mooring line.

Modeling Constants

The constants for the generalized α-method were evaluated as function of a spectral radius of 0.99 (Pai, 2007). The Rayleigh damping coefficients were chosen to give a structural damping of 1% of critical in the steel parts and 2% of critical in the fiber ropes used for the mooring lines. The drag- and inertia coefficients were given the standard values from the IEA-OC4 project of 1.0 and 2.0 respectively. This is assumed conservative for the hybrid structures in this study.

Optimization Module INVALS

The ALSIM package at IFE (Sørheim, 2002) contains an optimizer that has previously been used in an inverse procedure to optimize heat transfer coefficients in simulation model vs. experiment comparisons. In this project, the module was enhanced with the new optimization algorithms “Efficient Global Optimization (EGO)”, “Genetic Algorithm (GA)”, “Bound Optimization BY Quadratic Approximation (BOBYQA)” and “DIviding RECTangles (DIRECT)”. General and flexible capabilities were included to allow the module to communicate with other simulation models through text-files or scripts, without the need for linking of models. The design variables with limits are specified in the INVALS input, along with tags for identification of the design variables or derived quantities in the simulation model input templates. INVALS generate the 3DFloat input file from the template. The template is identical to the 3DFloat input file, except some header information, and formulas identifying how the selected input values are evaluated from the design variables. With the generated input, INVALS runs a script, that runs 3DFloat, and subsequently a cost function executable that parses through the output files of 3DFloat. The cost function is evaluated and exported to a text file that is subsequently read by the optimizer. The constraints are implemented as penalty functions in the cost model. INVALS can work on parallel systems, e.g. by sending one instance of a design configuration simulation to each processor.

A brief evaluation of the new algorithms in INVALS was performed on a benchmark problem from the casting industry. This confirmed the known characteristics of each of the methods. In the optimization problems of this paper, the BOBYQA method (Powell, 2009) seems to work well, and has been adopted without further comparisons with the other methods.

TLB WIND TURBINE PLATFORMS

The baseline for this study is the TLB B concept (Myhr et al., 2011) depicted in figure 1. It utilizes the OC3-5MW Rotor-Nacelle-Assembly (RNA) and reference tower from 10 meters above SWL (Jonkman et al., 2009). The draft is 50 meters for all platforms in this work. The three lower mooring lines (LML) are attached at the bottom of the floater. The three upper mooring lines (UML) are attached 24.5 m above SWL, just below the rotor plane. Further overview of the design is listed in table 6 and 7.

Redundancy against mooring line failure can be achieved by increasing the number of mooring lines, as for instance in a TLP platform. Redundancy for anchor failure can be implemented by increasing the number of anchors, e.g. with six mooring lines at each height. For this

work we ignore redundancy, since the focus is comparison of variations on the TLB concept.

A disadvantage for the TLB designs is the high loads in the mooring system. In order to avoid snap loads[1], the tension in the mooring lines has to be maintained, by the EB of the floater. Increasing EB leads to higher mean loads on the anchors.

The advantage of the TLB over inertia-controlled designs such as the spar-buoy and hybrid designs such as the semi-submersible platforms is the lower steel mass. In addition, the limited global translations and rotations exerted on the RNA, should result in less wear and fatigue.

TLB X

To reduce the wave loading we introduce changes in the middle section of the baseline TLB B system. There are two main components in wave loading, drag forces and inertia forces. The drag and inertia forces scale with the projected area and volume, respectively. Two designs are presented to reduce both these effects; TLB X4, a traditional 4 legged slim space-frame and TLB X3, a hybrid tripod to reduce bracings and ease fabrication. An illustration of the designs is shown in figure 2.

The space-frame designs extends to 15 meters above SWL. The tower structure above the space-frame is similar to TLB B. Optimization of the above tower structure is not taken into account in this paper.

The pretension of the mooring system implies that axial compression is transmitted through the space-frame. The relatively small projected areal also reduces wave drag significantly, thus the moment reactions on the space frame is low and we have a form of natural pretension giving the system a potential advantage with respect to fatigue.

The TLB X4 space-frame is based on the layout of the OC4 space-frame. The cross sections have been scaled to keep the stress levels at about the same level as the tower, just above the space-frame, taking into account approximate Stress Concentration Factors (SCF) for the joints. The space-frame has a fixed layout, with exception of the total height and the width. Thus, the frame is not verified according to proper standards, but by simplified stress calculations. The frame will have to undergo detailed optimization after the main geometry is set. Braces with a fixed diameter and a wall thickness of 0.4 m and 0.02 m respectively is utilized and distributed in three equally spaced sections.

The geometries undergo a simplified buckling control during the optimization. Due to the magnitude of the axial force in the columns and practical limitations with respect to wall thickness we see that buckling in general is not a major constraint for the X3 and X4 designs.

The TLB X3 is of great resemblance to TLB X4, but with three columns and no bracings. Less use of bracing members implies the use of a larger diameter for the vertical columns, but the total outcome is also dependent on several variables as the vertical extent of the space-frame, environmental conditions and Accidental Limit States (ALS). Using a slim three-column-configuration and mooring lines penetrating the free water surface, could raise concerns with respect to ALS but will not be examined in this work.

[1] Snap loads may occur when a pre tensioned mooring lose tension due to global displacement. If we assume this is due to a repetitive dynamical motion, the global stiffness will experience a temporary reduction in stiffness from the mooring line. This stiffness will be restored immediately when the mooring line is taut again and result in a large force with a short pulse.

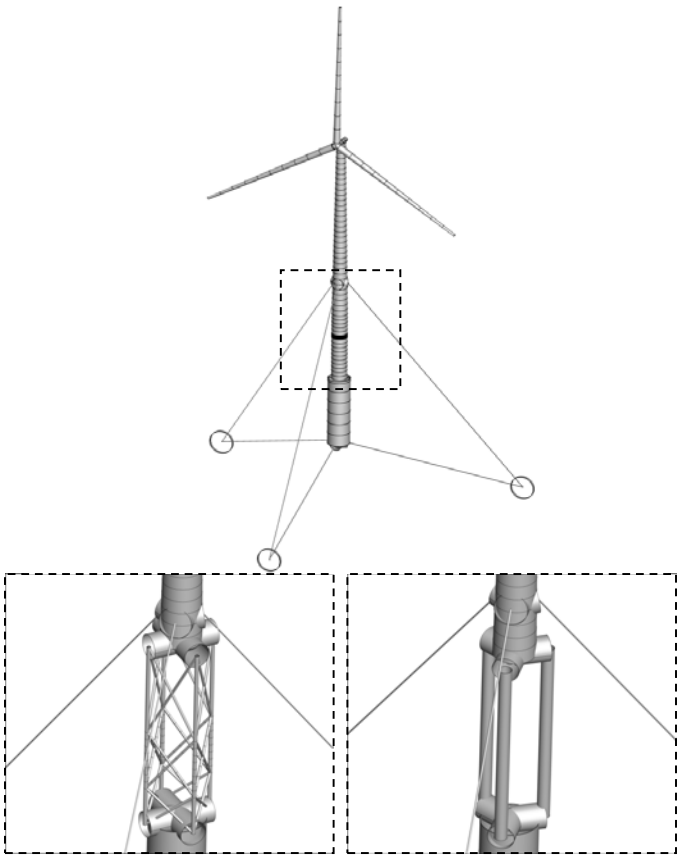

Figure 2. The baseline TLB B with plain cylinders on the top. Below are the changes made to the baseline illustrated; the traditional space-frame on TLB X4 and the tri-column solution for TLB X3

OPTIMIZATION

Frequency Domain Optimizations

The eigen periods will have to be situated outside the energetic part of the wave spectrum. In addition, one should also avoid the 1P and 3P excitation regions from the variable-speed rotor. 1P excitation can be caused by e.g. an unbalanced blade. 3P is the rate of which the rotor blades pass the tower shadow and turbulent eddies. The OC3-RNA has the following 1P and 3P regions:

Table 1. 1P and 3P excitation periods

	1P (s)	3P (s)
Max. 12.1 RPM	4.95	1.65
Min. 6.9 RPM	8.70	2.90

The 1P period-range lies within the high energy part of the wave spectrum (> 5 s). Thus, only the 3P region is relevant to avoid in addition to periods exceeding 5 seconds.

The eigen frequency optimization will mainly be used to adapt the mooring system to a defined geometry. To efficiently manipulate the mooring system with the least amount of variables the following design variables shown in table 2 was chosen.

Table 2. Design variables for the eigen period optimization

Variable	Explanation
rr1	Anchor radius (m)
d1	Lower mooring line (LML) diameter (m)
d2	Upper mooring line (UML) diameter (m)
yaw	Yaw stiffness (Nm/rad)

The "Crow-foot" delta connections for yaw-stiffness were omitted. Instead the yaw stiffness was applied to the center node at the bottom of the floater. This simplifies the geometrical aspects of attaching and optimizing the mooring system as we assume that the desired yaw stiffness can be obtained by selection of the split section length and fairlead geometry.

UML and LML travel in respective pairs down to the same anchor. In the numerical model, the anchor is simply a fixed node at the sea floor. No spring stiffness or damping has yet been applied to the anchors.

To summarize; the eigen period optimization of mooring line axial stiffness and anchor radius layout are performed with the total mooring line mass as cost function. The applied constraints are:

1. All eigen periods below 5 seconds
2. All eigen periods outside 1.7 – 2.9 seconds

The constraints are taken into account by including penalty functions in the cost functions. The baseline cost function, with only the first constraint, converged at a satisfactory level, but when introducing the second constraint this became more difficult. This is due to several aspects; First, there is now a region to avoid, in addition to an upper limit. Also the number of modes to control increase from one to a whole set, typically eight to ten, that could potentially fall within the 3P region. A hyperbolic function was first used to penalize the 3P region in addition to the initial baseline criteria. This approach gave convergence solutions to various local minimums and possibilities for rigid body mode periods below 1.7 s, leading to unnecessary stiff mooring lines. A linear function favoring the longer periods of the 3P region was used as a substitute. This produced solutions where most of the rigid body mode periods were located in the region 2.9 s– 5 s, and the rest below 1.7 s. This gave a tidy distribution of the eigen periods and reduced the mooring line axial stiffness.

An important note can also be made on the chosen stiffness setup for the TLB systems. Mainly, there are two governing setups that can be achieved by either having the UML or LML brought to a significantly higher horizontal mooring stiffness than the other. In a setup 1) with stiffer LML, the global rotation center of the turbine will shift down towards the lower mooring fairlead. This will increase periods for both pitch and possibly surge coupled modes. Using this setup, the system eigen periods seem to be more dependent on the geometry and are more sensitive to geometrical changes. To ease this early-stage optimization exploration we use a setup 2) where the UML are stiffer on all the designs. This will ensure lower eigen periods and less influence from changes made in the time domain optimization process.

Time Domain Optimizations

The mass of the floater can be calculated by the use of standards for a given main geometry. The main geometry is largely given by the fact that we have to keep tension in the mooring lines. An increase in EB will increase the mooring line tension, thus, we can manipulate the volume of the floater to influence EB. This is done by introducing a variable outer diameter, df, for the floater. Wall thickness of the floater section is coupled with the floater diameter and based on a linearization of the allowable wall thickness with ring stiffeners based on DNV RP-C202. Cylinder end caps and additional transition masses are also included and coupled to the floater diameter df. Together with data from existing designs we assume that the bottom cap thickness can be taken as 130 % of the appropriate wall thickness of a cylinder at the equivalent submerged location. To accommodate for additional stress from the anchor system we adjust the thickness to 140 %. Calculations suggest that transition changes between different cylinder dimensions are penalized with approximately 10 % additional mass per unit length.

As for the TLB X design, there are more complex transition pieces between the space-frame and the cylinders. For the submerged transition, a wall thickness of 140 % of the nominal value for the floater is used. The upper transition piece between space-frame and the tubular tower is of less complexity as no hydrodynamic loads will have to be accounted for. We assume that 120 % of the tower wall thickness will be sufficient for the transition. A solid circular disk with thickness 0.0338 m is attached in the model. The geometry of the tower is not changed and the transition piece will have a constant mass of 7.3 tons.

To optimize the wave loading on the structure, we will use the underwater height, ht, of the space frame as an input variable. Operating with a fixed draft of 50.0 meters, we also need the outer diameter of the floater variable to be able to freely regulate the EB. When changing ht, the center for the resulting force from the waves will also shift. In order to be able to reach a minimum force value in the mooring lines, we then also need to control the distribution of pretension between the UML and LML. This is done by manipulating the pre strain value of the lines having one design variable each for the upper and lower mooring lines. Additionally we also have the column spacing, dt, and diameters, ds, for the TLB X designs. In total we then have four to six design variables, for TLB B and TLB X respectively, in the time-domain optimization runs:

Table 3. Design variables for the time-domain optimizations

Variable	Explanation
df	Outer diameter of lower floater part (m)
ht	Height of the middle section below the water line (m)
pre1	Lower mooring line pre strain (%)
pre2	Upper mooring line pre strain (%)
dt*	Distance between column- and turbine centerline (s)
ds	Outer diameter of vertical column(s) in space-frame

* For TLB X4, dt is half the distance between the vertical columns

To summarize, the time-domain optimizations of space-frame extent, floater diameter and upper- and lower mooring line pre-strain are performed with the substructure steel mass as cost function. The following constraints are applied:

1. The minimum tension during the extreme events is 1000 kN for all mooring lines.
2. Maximum axial stress in the space-frame is 170 MPa.

Penalties are based on the distance from the constraint. All of the mooring lines are monitored, but penalty is calculated only for the one with the greatest distance to the constraint. This is done similar for the transition columns in the TLB X designs. Second order hyperbolic functions were used initially to ease convergence, but resulted in balancing issues when incorporating the second constraint. To compromise, a linear approach with scale factors was found to give the best result. Note that constraint two does not apply to TLB B as the

diameter is defined in the baseline geometry, but it is still optimized with the same form on the penalty function for the mooring lines.

There is no constraint for the change in offset caused by the manipulation of EB as this would further complicate the convergence. The drift in equilibrium position has been small in all optimizations so far. The optimization converges faster if the starting values for pre-strain are determined in an initial optimization in still water. The constraints are:

1. The equilibrium position is close to the design point
2. The tensions in the UML and LML are equal

If the floater mass change is significant between the frequency domain optimization and the time-domain optimization, another eigen analysis is run to check if the axial stiffnesses of the mooring lines need to be optimized again.

A thorough guide for choosing appropriate load cases is given in IEC 61400-3. Even a reduced set of load combinations, as used in (Robertson and Jonkman, 2011), results in an excess of 2000 load cases per concept. Previous experience from simulations on the TLB systems shows that the stiff mooring system is highly responsive to the loads. As most standards demands that irregular wave fields are run, most optimization routines will be time consuming due to the fact that the irregular wave field simulations will have to consist of a relatively long simulation time. We have earlier compared peak loads from 3-hour simulations of irregular sea state with 1) short simulations around the peak wave event and 2) regular waves with the same height as the peak wave event. The results for peak loads match well, and we use regular wave cases for the first comparisons of the conceptual designs. To achieve a quasi-static solution with regular waves on the TLB system, only three to four wave periods are typically required.

Based on descriptions on North Sea ocean basin recordings (Faltinsen 1990, Anderson et al. 2001) we assume the following load data and correlate them with the corresponding load cases in and IEC 61400-3 for the optimization routine as shown in table 4.

Table 4. Description of the chosen load cases with 50-year return period in accordance to the IEC 61400-3 standard

	Wind			Wave		
LC	Model	State	(m/s)	Model	State	(m)
6.1b	EWM	V_{50}	62	RWH	H_{red50}	26
6.1c	RWM	V_{red50}	55	EWH	H_{50}	29

Load case 6.1b and 6.1c are for now assumed to be design drivers for the TLB systems. No yaw misalignment was introduced in the optimization to reduce the amount of time steps needed. Instead, this is included a manual post optimization control of the design, also based on the IEC 61400-3 standard involving wind and wave misalignments. This is by no means intended as a final verification, but an extended initial control the optimized geometry in advance of the final design verification by a complete set of load case simulations. Table 5 illustrate the design values and load cases that will be incorporated.

Table 5. Description of the chosen load cases with 1-year return period in accordance to the IEC 61400-3 standard

	Wind			Wave		
LC	Model	State	(m/s)	Model	State	(m)
7.1b	EWM	V_1	35	RWH	H_{red1}	24
7.1c	RWM	V_{red1}	32	EWH	H_1	26

RESULTS

The chosen parameters for the tuning and optimization of the eigen periods were based on a sensitivity study of the input parameters. It was confirmed that the longer eigen periods, mostly the ones close to the high energy parts of the wave spectrum and the region of 3P, mainly were dependent on the mooring system configuration. There were also coupling effects, coupling the rigid body motions of pitch and surge with yaw. This implies that the system is sensitive to the yaw stiffness. This stiffness can be tuned, for all practical matters, by changing the distance from the fairlead to the floater center. Recheck of eigen periods post time-domain optimization also proved that the changes of geometry had no relevant influence on the eigen periods close to the 3P region or the limiting high energy parts of the wave spectrum.

Design Optimization Results

Currently, simplified versions of the LC 6.1c and 6.1b are assumed to be the design drivers suitable for fast optimization of the TLB systems. The wave dominant LC 6.1c has so far proven to be the definite governing case to determine the EB. By running the geometries optimized from LC 6.1c with LC 6.1b we also can confirm that the larger amount of EB indicates the worst LC. Since the 6.1c is the dominant LC it also implies that the wave loading is the governing force on the TLB geometry, regardless of whether a drag-force dominated space-frame or a larger inertia force dominated cylinder is chosen. The final design variable results are shown in the table below:

Table 6. Overview of the resulting design optimization variables explained in table 2 and 3

Phase	Variable	TLB B	TLB X3	TLB X4	Dim
Frequency Domain	rr1	73.626	76.705	78.429	m
	d1(LML)	0.097	0.137	0.102	m
	d2(UML)	0.227	0.248	0.266	m
	yaw	113.15	98.452	162.998	MNm/rad
Time-Domain	ht	-19.271	-8.025	-4.625	m
	df	9.724	9.996	10.547	m
	pre1(LML)	0.018	0.020	0.022	m/m
	pre2(UML)	0.003	0.003	0.003	m/m
	dt	0.000*	3.133	3.227	m
	ds	6.500*	0.837	0.648	m

* Fixed value based on tower properties

From the frequency domain results we can see that there are only minor differences between the designs except on the yaw stiffness. An interesting point here is that the needed yaw stiffness increases with the torsional stiffness of the space-frame, TLB X4 having the highest, and TLB X3 as the lowest.

It is apparent that the TLB X design desires to minimize ht to cover only a minimum of the wave action zone. Compared to the TLB B system, which suggest a larger ht, one can conclude that the low buoyancy to mass ratio of the truss, together with a desire to reduce the df, implies that the length of the space-frame should be kept to a minimum.

An important aspect is also the outer diameter of the columns in the transition of TLB X3 and X4. Even with extensive use of braces there is a relatively small reduction in outer diameter on the X4-brace design compared to the X3 without bracing. This confirms that the need for sufficient cross sectional area is the governing factor. To maximize the

cross sectional area a fixed wall thickness of 0.05 meters was chosen in the optimization due to fabrication aspects. The resulting designs of the optimization process are shown in table 7:

Table 7. Overview of comparable results from the design optimization

Parameter	TLB B	TLB X3	TLB X4	Dim.
Mass Floater	445467	521307	629408	kg
Mass Top Side	666609	606426	608826	kg
Mass Anchors	190486	173008	204243	kg
Total Mass	1302562	1300741	1442477	kg
Wt floater	0.039	0.038	0.039	m
Wt Col.transition	0.031	0.050	0.050	m
Total Buoyancy	2994609	3030886	4068389	kg
EB	1926620	1942048	2830155	kg
UML EA/L	21.72	21.485	24.219	N/m
LML EA/L	5.6851	5.5211	5.7205	N/m
Max ML Force	16.695	15.469	17.199	MN
Max Anc. V. Force	17.821	14.636	17.994	MN
Max Anc. H. Force	23.321	22.237	25.697	MN
Max Anc. R. Force	29.267	26.619	31.351	MN

The top side mass of TLB B is approximately 10% higher as the tower starts 10 meters above the waterline compared to 15 meters for the TLB X3 and X4. This is also reflected in the larger floater mass in the X3 and X4 designs. The slight variation in top side mass between X3 and X4 is due to the different dimensions of the mooring lines. Overall mass for the TLB B and X3 are approximately the same, but X4 stands out negatively.

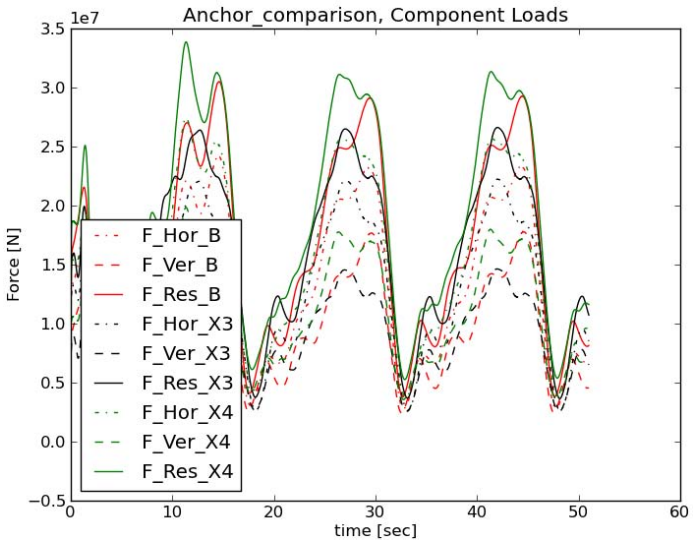

Figure 3. Component force for anchor subjected to the largest force for each design during the time domain optimization

Comparing the overall dimensions of the TLB B and X3 they perform very similarly, both with respect to steel-mass consumption, mooring line configuration, total buoyancy and then necessarily the EB. The X4 is distinguished from the rest, yet again in a negative way, by the need of 34 % more EB. The loads on the mooring system are considerably lower with the space-frame design of X3, but not as much as expected even if the vertical load reduction is close to 18 %. Further exploration with different setups is therefore needed. An interesting point is that the X4 design has not been able to produce a better result. This is probably due to the amount of braces, which forms the major part of the total projected area.

Post-Optimization Control

The control of the design optimization process was done in two steps; 1) by using a more correct version of LC 6.1c and 2) by using a simplified version of LC 7. Issues regarding yaw misalignment were used in the first step by introducing wind from -8, 0 and +8 degrees offset from the rotor orientation. A few coarse variations for the wave direction was also applied by using -30, 0 and +30 degree offsets from the wind direction, giving a total of 9 combinations. For the second step, wind and wave direction revolve 180 degrees around the turbine incrementally every 50 seconds by 30 degrees, alternated with a 30 degrees offset. No smoothing attempts or temporary damping is introduced between the shifts, thus transient effects are expected during the first 20-30 seconds of each shift in either wind- or wave direction.

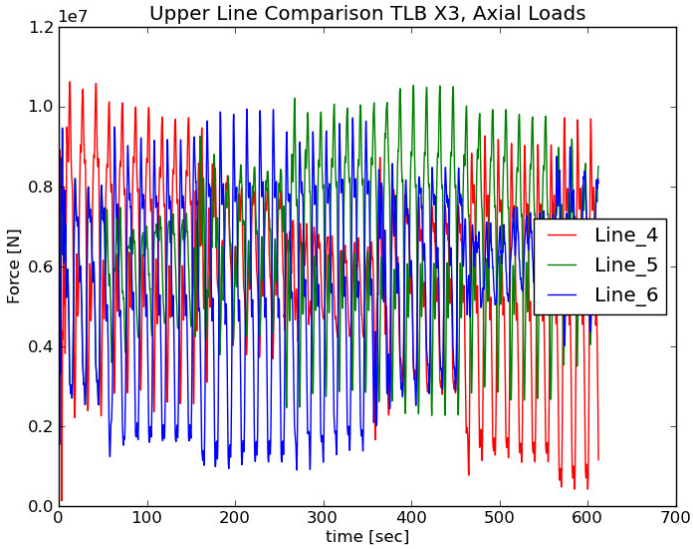

Figure 4. Axial force in UML on TLB X3 for LC 7 during the post-optimization load case control. Line 4 starting in down-wind position

As expected the minimum line tension of 1000 kN during the optimization was sufficient to maintain taut lines through the post-optimization checks with misalignments. The TLB X3 the design axial force constraint of 1000 kN is reduced to about 500 kN. For the TLB B and X4 system it is close to zero. It is apparent that the remaining margin differs for each concept, indicating that the margin of safety should be investigated thoroughly. The results also indicate that the initial assumption on the optimization LC is partly reasonable as the largest force occur at zero degrees offset. However, secondary load cases to locate minimum force situations are advised.

CONCLUDING REMARKS

From the results it is apparent that the TLB space-frame design may require about the same EB to maintain tension in the mooring lines during extreme events. However, the shape of the space-frame and the use of braces are important for the performance. It is also apparent that increased projected area of the space-frame influences the requirement for EB drastically. Results indicate that this probably is due to the buoyancy-to-mass ratio that is significantly less for the braced structure compared to TLB B and, to some extent, X3.

Replacing the cylinder in the wave action zone with a space frame may reduce the wave forces by a significant amount as long as bracing is either unused or kept to a minimum. For the TLB X3 a reduction of the peak resultant anchor loads of about 10 % is achieved, while the overall mass for the floater is about the same due to complications in transition pieces and the lower mass-to-buoyancy ratio for the space-frame structures. The load reduction in the vertical component on the anchor was, as expected, larger, due to less horizontal force exerted on the upper mooring lines and less water plane area.

To further reduce the steel-mass one should explore the possibilities of optimizing the space-frame to the design specific loads of the TLB system as the current results show potential for reduction of the mooring loads. The result is modest, but justifies further design optimization. Especially the different mooring line stiffness configurations that influence the global dynamic response are of great interest, but have been beyond the scope of this research.

The reduction in anchor mass is no exact calculation, and heavily site dependent as the TLB system currently makes use of drag embedded plate anchors. However, the anchor mass-to-stress ratio is approximately linear and will at least be indicative to the potential for material reduction.

It was confirmed that the eigen periods did not change significantly between the transient optimization runs and the initial eigen period optimizations. However, the authors suggest that should be included in the same optimization routine to directly verify that the optimized designs have proper eigen periods.

Automated optimization algorithms combined with aero-hydro-elastic computations for a limited set of specifically chosen LC has proven to be a good approach to investigate different conceptual designs. However, individual adaption as for lower mooring line force limit or possibly specific optimization LC for each concept should be explored further. For some designs, there could also be beneficial to implement more than one LC in the time domain optimization.

The current findings indicate that there is a significant potential to reduce the wave loads, and thereby the anchor loads, on the TLB system. At the current stage of the design process, some of the space-frame design parameters for both TLB X3 and TLB X4 are still predefined. Further work is needed to include this part in the optimization process. Other space-frame designs should also be considered as the load configuration on the TLB system is mainly axial, thus the need for supporting braces are less than for, i.e., bottom fixed jackets.

Further work is also suggested on Life Cycle Analysis (LCA) with respect to both costs and emissions as this will be needed to evaluate whether the space-frame is a viable option in large scale deployment of floating wind turbines.

ACKNOWLEDGEMENTS

We gratefully acknowledge the support from Einar Arne Sørheim, IFE, on the optimization module. The work was in part funded through the NOWITECH research program.

REFERENCES

Anderson, C. W. et al. (2001). "Wave Climate Variability and Impack on Offshore Design Extremes". Report for Shell International. Department of Probability & Statistics, University of Sheffield, UK.

Anderson, E. et al. (1990). "LAPACK: a portable linear algebra library for high-performance computers". *Proc of the1990 conference on Super-computing*. ISBN 0-89791-412-0, IEEE Computer Society Press, Los Alamos, CA, USA.

Butterfield, S, Musial, W, Jonkman, J and Sclavounos, P (2005). "Engineering Challenges for Floating Offshore Wind Turbines*". Proc 2005 Copenhagen Offshore Wind Conference*, Copenhagen, Denmark October 26–28, 2005

Chaplin, J. "Developments of stream-function theory," Coastal Engineering, 3, pp. 179–205, 1980.

Faltinsen, O. M. (1990). "Sea loads on ships and offshore structures." Cambridge: Cambridge University press. ISBN: 0521458706

Hansen, M. H. et al. (2005) "Control design for a pitch-regulated, variable speed wind turbine". RISØ National Laboratory report, RISØ-R-1500, 2005.

Jonkman, J., Butterfield, S., Musial,W., and Scott, G. (2009). "Definition of a 5-MW Reference Wind Turbine for Offshore System Development". Technical Report NREL/TP-500-38060, National Renewable Energy Laboratory (NREL).

Jonkman, J et al. (2010). "Offshore Code Comparison Collaboration within IEA Wind Task 23". *Proc Europen Wind Energy Conference & Exhibition*, Warsaw, Poland, April 2010.

Karimirad, M. (2012). "Feasibility of Application of Spar-type Wind Turbine in a Moderate Water Depth". *Proc of the 9th Deep Sea Wind R&D Seminar,* Trondheim, Norway, January 2012.

Muskulus, M. (2012). "The full-height lattice tower concept". *Proc of the 9th Deep Sea Wind R&D Seminar,* Trondheim, Norway, January 2012.

Myhr, A., Maus, K. J. and Nygaard, T. A. (2011). "Experimental and Computational Comparisons of the OC3-HYWIND and Tension-Leg-Buoy (TLB) Floating Wind Turbine Conceptual Designs". ". *Proc of the twenty-first (2011) International Offshore (Ocean) and Polar Engineering Conference*, Maui, Hawaii, ISOPE, Vol 1.

Nygaard, T. A., Myhr, A. and Maus, K. J. (2009). "A comparison of two conceptual designs for floating wind turbines". *Proc European Offshore Wind Conference & Exhibition,* September 2009, Stockholm, Sweden.

Pai, P. F. (2007). "Highly Flexible Structures: Modeling, Computation, and Experimentation". ISBN: 1563479176. AIAA 2007.

Popko, W. et al. (2012). "Offshore Code Comparison Collaboration Continuation (OC4), Phase I – Results of Coupled Simulation of Offshore Wind Turbine with Jacket Support Structure". *Proc of The Twenty-second (2012) International Offshore (Ocean) and Polar Engineering Conference*, Rhodes, Greece, June 2012.

Powell, M. J. D. (2009). "The BOBYQA algorithm for bound constrained optimization without derivatives". Report DAMTP 2009/NA06, Centre for Mathematical Sciences, University of Cambridge, UK.

Robertson, A. N. and Jonkman, J. M. (2011). "Loads Analysis of Several Offshore Floating Wind Turbine Concepts". *Proc of the Twenty-first (2011) International Offshore (Ocean) and Polar Engineering Conference*, Maui, Hawaii, ISOPE, Noll 1.

Sarpkaya, T. and Isaacson, M. (1981). "Mechanics of Wave forces on Offshore Structures". Van Nostrand Reinhold Co., New York, 1981

Sclavounos, P. D. et al. (2010). "Floating Offshore Wind Turbines: Tension Leg Platform and Taut Leg Buoy oncepts supporting 3-5 MW Wind Turbines". *Proc European Wind Energy Conference EWEC 2010,* Warsaw, Poland 20-23 April 2010

Sørheim, E. A. (2002). "A user guide to INVALS: Inverse modeling of heat transfer of water film during DC-casting. IFE-report IFE/KR/F-2002/007

Tsouroukdissian, A. R., Fisas, A., Pratts, P. (ALSTOM) and Sclavounos, P. D. (MIT) (2011). Floating Offshore Wind Turbines: Concept Analysis. American Wind Energy Association WINDPOWER 2011 Conference and Exhibition, Anaheim, CA, May 22-25.

Appendix 4

Renewable Energy 66 (2014) 314–324

Contents lists available at ScienceDirect

Renewable Energy

journal homepage: www.elsevier.com/locate/renene

GHG emissions and energy performance of offshore wind power

Hanne Lerche Raadal [a,*], Bjørn Ivar Vold [a,1], Anders Myhr [b], Tor Anders Nygaard [b]

[a] Ostfold Research, Gamle Beddingvei 2B, N-1671 Kråkerøy, Norway
[b] Norwegian University of Life Sciences (UMB), 1432 Ås, Norway

ARTICLE INFO

Article history:
Received 4 July 2013
Accepted 25 November 2013
Available online

Keywords:
Life Cycle Assessment
LCA
Offshore wind power
GHG emissions
Energy performance

ABSTRACT

This paper presents specific life cycle GHG emissions from wind power generation from six different 5 MW offshore wind turbine conceptual designs. In addition, the energy performance, expressed by the energy indicators Energy Payback Ratio (EPR) Energy Payback Time (EPT), is calculated for each of the concepts.

There are currently few LCA studies in existence which analyse offshore wind turbines with rated power as great as 5 MW. The results, therefore, give valuable additional environmental information concerning large offshore wind power. The resulting GHG emissions vary between 18 and 31.4 g CO_2-equivalents per kWh while the energy performance, assessed as EPR and EPT, varies between 7.5 and 12.9, and 1.6 and 2.7 years, respectively. The relatively large ranges in GHG emissions and energy performance are chiefly the result of the differing steel masses required for the analysed platforms. One major conclusion from this study is that specific platform/foundation steel masses are important for the overall GHG emissions relating to offshore wind power. Other parameters of importance when comparing the environmental performance of offshore wind concepts are the lifetime of the turbines, wind conditions, distance to shore, and installation and decommissioning activities.

Even though the GHG emissions from wind power vary to a relatively large degree, wind power can fully compete with other low GHG emission electricity technologies, such as nuclear, photovoltaic and hydro power.

1. Introduction

All electricity generation technologies consume energy and emit greenhouse gases (GHGs) to a greater or lesser degree. When assessing the environmental performance of electricity generation it is important to take a Life Cycle Assessment (LCA) approach. This enables assessment of both the investment and the operating impacts relating to the generation process, and means that the entire life cycle of the investigated power plant, including upstream and downstream processes, should be taken into consideration. Upstream processes include, for example, mining and transport activities relating to the extraction of fuel, as well as extracting and processing activities relating to the materials used for building the power plant. Typical downstream processes include activities related to building and operating the grid, as well as the management of waste from the power generation processes. For most renewable electricity technologies and nuclear power, upstream and downstream GHG emissions account for over 90% of the cumulative GHG emissions. For conventional fossil fuel technology, however, the upstream GHG emissions also impact on the total picture, as they can represent up to 25% of the direct emissions from the power generation [1].

According to the IPCC Special Report on Renewable Energy Sources and Climate Change Mitigation [2], wind energy offers significant potential for the reduction of near-term (2020) and long-term (2050) greenhouse gas (GHG) emissions. This is achieved by generating electricity from larger, grid-connected wind farms, deployed either on- or offshore. At the end of 2009, the total installed wind power capacity of 160 GW, of which 2.1 GW comprised offshore capacity, was capable of meeting roughly 1.8% of worldwide electricity demand. This contribution could increase to about 20% by 2050 if ambitious efforts were made to reduce GHG emissions and to address the other limiting factors for large-scale wind energy development [2].

Wind turbines with a rated power of 5–6 MW are now being designed and installed, mostly for offshore operation [3]. There seem, however, to be few available studies concerning the environmental assessment of these ratings in relation to offshore turbines. Weinzettel et al. [4] have analysed the environmental performance of a floating 5 MW offshore wind turbine (Sway

* Corresponding author. Tel.: +47 69351100; fax: +47 69342494.
E-mail address: hlr@ostfoldforskning.no (H.L. Raadal).
[1] Present address: Statkraft, Postboks 200, Lilleaker, 0216 Oslo, Norway.

0960-1481/$ – see front matter © 2013 Elsevier Ltd. All rights reserved.
http://dx.doi.org/10.1016/j.renene.2013.11.075

concept), and Tveten [5] has analysed wind power generation based on 5 MW offshore turbines in Scandinavia. Schleisner [6], Voorspools et al. [7], DONG Energy [8], Jungbluth et al. [9], Bauer et al. [10], Chataignere and Le Boult [11] and Vestas ([12] and [13]) have all assessed offshore wind power LCAs with turbine ratings from 0.5 MW to 3 MW. In the case of onshore wind power, however, there are several existing studies [14–21].

The aim of this paper is to present LCA GHG emissions and energy performance of six different offshore 5 MW wind power conceptual designs. The paper focuses on exploring the variations of the concepts rather than making a detailed ranking of the various different concepts. In addition, comparisons with relevant wind power LCA data are presented. The work has been carried out as a part of the research project Energy Trading & Environment 2020 [22].

The paper is organised as follows: Section 2 gives a short presentation of the Life Cycle Assessment methodology and the investigated energy indicators. Section 3 describes the offshore conceptual designs which have been investigated, while the resulting GHG emissions and energy performance are presented in Section 4. The results are compared with relevant literature data in Section 5, while Section 6 presents the conclusions.

2. Life Cycle Assessment (LCA) methodology

Life Cycle Assessment (LCA) represents a structured, comprehensive and internationally standardised (ISO 14044:2006 [23]) method for quantifying environmental and health impacts, resources consumed and resource depletion associated with any goods or services. In accordance with the International Reference Life Cycle Data System (ILCD) Handbook [24], Life Cycle Thinking and LCA create the scientific approaches behind modern environmental policies and business decision support relating to sustainable production and consumption.

Every electricity technology has an outage probability, whether it consists of a system of geographically dispersed wind farms, a hydro power station with a reservoir, or a fossil-fuelled power plant. The effect of adding new capacity can be quantified by the capacity credit. This is the capacity of conventional plants displaced by the new capacity, with an unchanged probability of failure to meet the reliability criteria of the system [25]. With high penetration levels of renewable energy, the capacity credit of different technologies such as wind energy, solar energy and bio energy could differ significantly. These differences have been ignored in this study. This simplification does not affect the comparison between the various different offshore wind turbine conceptual designs, but should be taken into account when comparing wind, solar and conventional energy technologies.

2.1. Analysed environmental indicators

This paper presents the environmental indicators GHG emissions and energy performance related to wind power generation. The GHG emissions have been calculated as Global Warming Potential (GWP), presented as g CO_2-equivalents. With regard to energy performance, two of the most common energy indictors for renewable electricity generation have been calculated: Energy Payback Ratio (EPR) and Energy Payback Time (EPT). A short description of these indicators is given below.

Energy Payback Ratio (*EPR*) expresses the amount of delivered energy during the power plant's lifetime, per energy unit invested in infrastructure and extraction/transport processes. It should be noted that the literature uses various different expressions for the EPR indicator. Examples of these are 'energy ratio', 'external energy ratio' and 'energy return on investment (EROI)', all of which refer to the same basic calculation as EPR [26]. In accordance with Hall [27], the EPR indicator refers to the amount of energy returned from one unit of energy invested in an energy-producing activity. A high EPR value means high energy efficiency. It should be mentioned that the energy being included in the fuel which represents the energy source (such as coal or gas) for thermal power plants is not included as invested energy in EPR calculations. This makes comparisons difficult between thermal and non-thermal electricity technologies due to the relatively high losses in the electricity conversion step for thermal power generation.

Energy Payback Time (*EPT*) expresses the amount of time in months or years, taken to "pay back" the energy invested in infrastructure and extraction/transport processes. A low EPT value means high energy efficiency. As in calculations for EPR, the energy being included in the fuel which represents the energy source is not included as invested energy in the calculation of EPT.

EPR represents a good energy indicator for assessing whether a wind turbine actually produces more energy than it consumes during its life cycle. EPT, on the other hand, measures the amount of electricity-producing months or years, which are required in order to pay back the energy invested in the wind power plant. It should be emphasised that EPR is dependent on the lifetime assumed for the power plant while EPT is independent of this parameter. The relationship between the parameters is expressed using the following equation:

$$\mathrm{EPR} = \mathrm{Lifetime}/\mathrm{EPT} \quad (1)$$

Raadal et al. [28] present a detailed investigation and discussion of different energy indicators for electricity generation.

3. The investigated offshore wind power concepts

Table 1 shows the analysed six offshore wind turbine concepts, comprising five floating and one bottom-fixed.

All concepts use the NREL 5 MW offshore reference wind turbine Rotor-Nacelle-Assembly (RNA), based on Jonkman et al. [33]. The hub height is 90 m and the rotor diameter is 126 m. The water depth is 200 m for the floating concepts and 50 m for the bottom-fixed concept. The wind farm (bottom-fixed or floating) is assumed to be located 200 km off the British Coast, at Doggerbank (independent of the real water depth), and consists of 100 wind turbines installed in a square layout (10*10 turbines). Fig. 1 illustrates the different concepts.

The Sway Tension-Leg Spar (TLS) is a single spar with excess buoyancy, one vertical tendon and a downwind turbine. The tower structure utilises external axial stiffening rods. More information can be found in Ref. [29].

The UMaine Semi-Submersible concept was developed in the DeepCwind project at the University of Maine. The concept consists

Table 1
Overview of the analysed concepts.

Concept	Name	General description	Reference
Floating	SWAY	Tension-Leg-Spar (TLS) similar to the SWAY concept	Borgen [29]
	UMaine Semi-S	UMaine Semi-Submersible	Robertson and Jonkman [30]
	UMaine Spar	UMaine Spar-Buoy (same as OC3-Hywind, at water depth of 200 m)	
	UMaine TLP	Tension-Leg-Platform with vertical tendons	
	MIT TLB	MIT Tension-Leg-Buoy (TLB),	Sclavounos et al. [31]
Bottom-fixed	OC4 Jacket	IEA OC4 Jacket	Vorpahl et al. [32]

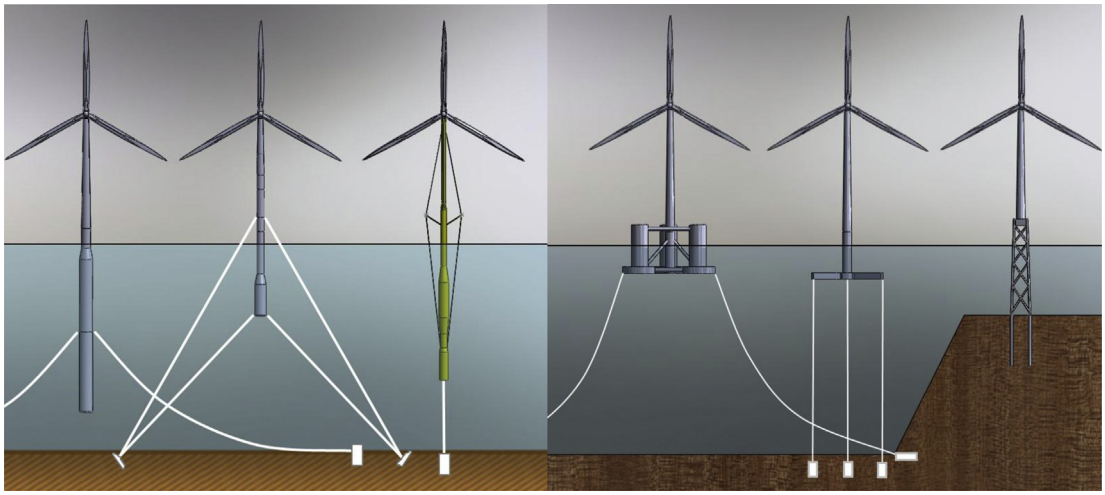

Fig. 1. Illustration of the concepts, from left to right; UMaine Spar, MIT TLB, SWAY, UMaine Semi-Sub, UMaine TLP and OC4 Jacket.

of a generic semisubmersible platform with the tower on a central column and three larger offset vertical columns connected by slender pontoons. The column stabilised platform has an overall draft of 20 m and utilises a catenary mooring system, water ballast and heave damper plates [30].

In the IEA OC3 project, the OC3-HYWIND was defined and made available to the research communities [34]. The UMaine spar buoy is essentially the same, but applied at a water depth of 200 m with a mooring system designed for that depth. The OC3-HYWIND was again largely based on the HYWIND concept and combined with an adapted version of the NREL 5 MW tower and turbine. The spar buoy relies on ballast stabilisation, deep draft and a catenary mooring system with crow-foot delta connections.

A small and relatively low mass TLP system is represented by the UMaine TLP consisting of a ballasted cylindrical platform with three horizontally extended legs, supporting the vertical tethering tendons, from its base. The concept relies on excess buoyancy to ensure taut tendons as in both the Sway TLS concept and MIT TLB.

The MIT TLB is a hybrid platform based on the same concept as Sway TLS but with a different solution for the mooring system. Two sets of inclined mooring lines are attached at two heights. One set of mooring lines has crow-foot deltas to control the yaw motions of the platform. All platform degrees-of-freedom are thereby stiffness-controlled, and all eigen periods are below the energetic part of the wave spectrum [31].

The OC4 Jacket is a space-frame installed at 50 m depth. The transition piece connecting the platform and the tower is made of concrete. The structure was designed for the IEA OC4 project [35].

The default wind farm is assumed to have a 20-year lifetime and a Capacity Factor (CF) of 46%. The CF expresses the actual annual electricity generation divided by the maximum possible annual electricity generation (operating at full power). It is expressed as a fraction, or a percentage. The functional unit for the analyses in this study is 1 kWh electricity generated and fed to the grid onshore. Thus, the GHG emissions and energy performance correspond to the generation of 1 kWh of wind power delivered to the grid onshore. The system boundaries include all the relevant life cycle stages, e.g. production of raw materials, transport, installation and decommissioning etc. Recycling credits from end of life treatment have not been included. This is in line with the Product Category Rules for electricity generation, in accordance with the International EPD System [36]. Grid losses through cables from offshore to onshore have not been included.

Table 2 lists the masses for the components above the substructure. The interface between the substructure and the tower is 10 m above the still water line. Table 3 lists the masses for the different substructures.

Low density concrete (2190 kg/m^3) has been used as grout material (included in the bottom-fixed foundation), while a density of 2380 kg/m^3 has been assumed for standard offshore concrete. The Ecoinvent processes “Poor concrete, at plant/CH U” and “Concrete, normal, at plant/CH U” have been used, respectively [37]. The applied steel density is 7850 kg/m^3 (the analyses do not adjust for bolts and flanges). Coatings are not included in infrastructure. For standard offshore steel and rebar steel, the Ecoinvent processes “Steel, converter, low-alloyed, at plant/RER U” and “Steel, low-

Table 2
Materials and masses for the adjusted NREL 5 MW offshore turbine [33] and corresponding Ecoinvent processes [37] used in the analyses.

Turbine NREL 5 MW (all values in tons per WT)	Rotor (hub and blades)	Nacelle	Tower structure	Sum	Ecoinvent processes used in the analyses [37]
Steel	60	197	234	490	Steel, converter, low-alloyed, at plant/RER U (rotor and nacelle), Steel, low-alloyed, at plant/RER U (tower)
Aluminium		8	5	13	Aluminium, primary, at plant/RER S
Electronics			4	4	Electronics for control units/RER U
Plastic			4	4	Polyethylene terephthalate, granulate, bottle grade, at plant/RER U
Copper		32	2	35	Copper, at regional storage/RER U
Oil			2	2	Lubricating oil, at plant/RER U
Glass reinforced plastic	50	2		53	Glass fibre reinforced plastic, polyamide, injection moulding, at plant/RER U
Sum	110	240	250	600	

Table 3
Materials and masses for the various different foundation/platform concepts [29–32].

Foundation/platforms, anchor and mooring cables (tons per WT)	Steel					HDPE	Concrete		
	Platform		Anchor	Mooring cables	Total steel	Mooring cables	Platform		Total concrete
	(Standard offshore)	(Reebar)	(Standard offshore)				(Standard)	(Grout)	
OC4-Jacket	539	67	153		759		59	66	126
SWAY	1050		188	20	1258				
Umaine Semi-S	3000	2	45	294	3341		205		205
Umaine Spar	1600	1	60	204	1865		143		143
Umaine TLP	525		354	60	939				
MIT TLB[a]	400	25	121		546	78			

[a] Increased tower mass (reebar steel) due to upper mooring line tethering system.

alloyed, at plant/RER U" have been used, respectively [37]. For the HDPE mooring cable for the MIT TLB, the Ecoinvent "Polyethylene, HDPE, granulate, at plant/RER U" process has been used [37]. All the floating concepts use water as ballast material, except the Umaine Spar which uses olivine.

The type, composition and weight of the offshore internal cables, typically three-phase 30–36 kV cables, are provided by Nexans [38] and Kaiser & Snyder [39]. The external cable (high voltage transmission cables) represents 145 kV, based on data from Statoil's external cable at Sheringham Shoal [40]. Based on the provided data, respective production processes for the cable material have been constructed by the use of representative Ecoinvent materials and corresponding processes.

One 500 MVA offshore substation is assumed to support the 100 5 MW turbines. The data have been provided by upscaling one 220 MVA offshore substation based on Tveten [5].

The calculation of the acquired fleet, time and fuel consumption relating to installation and decommissioning has been based on a combination of information from Sanden & Vold [41], Nielsen [42], Reitan [43] and Stuart [44]. For reasons of simplicity, the run of the installation of the floating concepts has been assumed to be equal and consists of towing, stabilising and installing activities. The run of the installation of the bottom-fixed platform includes transport and installation. For the same reasons, the operational time for installing the bottom-fixed and floating wind turbine concepts is assumed to be the same. However, the bottom-fixed operational window is assumed to be 65% which is 5% higher than for the floating concept, due to more complex operations. Maintenance is also assumed to be the same for all the concepts and is based on data from Sanden and Vold [41].

With regard to decommissioning and waste treatment of the wind turbines after end-of-life, the following assumptions have been drawn:

- Concrete: 15% to landfill, 85% to recycling
- Steel: 10% to landfill, 90% to recycling
- Glass reinforced plastic (in nacelle and rotor): 100% to recycling
- Aluminium (in nacelle, tower and transformer): 10% to landfill, 90% to recycling
- Copper (in nacelle, tower and transformer): 10% to landfill, 90% to recycling
- Cables (internal and external): 66% to recycling and 34% to energy recovery
- HDPE (mooring cable for MIT TLB): 100% to energy recovery

In accordance with [36], the environmental burdens relating to recycling shall not be included in the analysis since these burdens shall be allocated to the user of the recycled material. Therefore, transport and waste treatment burdens are only included for landfill and energy recovery activities. Data for relevant Ecoinvent processes [37] have been used for these processes. Other important data and assumptions with regard to the analyses are described in detail in Raadal and Vold [45].

When considering the realisation of the conceptual designs for the floating wind turbines, the study's perspective has been that of industrialisation and the large scale deployment of hundreds, if not thousands of wind turbines. When taking this perspective, installation procedures and equipment can be tailored to the various different conceptual designs. Relatively low costs have been assumed for maintenance compared to those we see today because of the large scale perspective chosen for the study. Later in the paper, a sensitivity analysis on emissions during installation is put in perspective in relation to the other emissions, showing that this rather crude approach is a useful first approximation. When considering installation of the first offshore floating wind farms, the differences in installation will be much more significant. Some conceptual designs, such as the semi-submersible, can be assembled in port and towed out. For the MIT TLB, the installation procedures are not yet fully developed and proven. For more detailed studies, and for evaluation of the first wind farms, differentiation on installation and maintenance would be required.

4. Resulting GHG emissions and energy performance for offshore wind

4.1. GHG emissions

The presentation of the GHG emissions results has been separated into the life cycle stages as shown in Table 4.

Fig. 2 shows the resulting GHG emissions (grams CO_2-equivalents/kWh) for the investigated offshore wind farm concepts in relation to the life cycle stages described in Table 4.

As seen from the figure, the total GHG emissions from the investigated offshore concepts vary between 18.0 (MIT TLB) and 31.4 (Umaine Semi-S) g CO_2-equivalents/kWh, a difference which represents a 75% increase in relation to the MIT TLB concept (representing the lowest GHG emissions).

Further, the figure clearly shows that the turbine and foundation/platform materials contribute most to the overall GHG emissions. The platform contribution varies between 6.3 (MIT TLB) and 19.7 (Umaine Semi-S) g CO_2-equivalents/kWh, corresponding to 35% and 63% of the total GHG emissions from each installation, respectively. The variations between the concepts are placed in this category, since the tower and RNA are identical. The different platform concepts are further analysed in order to investigate the most important parameters affecting these GHG emissions. This is presented in Fig. 3.

As seen from Fig. 3, the main contributor to the overall platform GHG emissions for all the concepts is steel production (separated into steel relating to the platform and anchor/cables, respectively). The steel production activity contributes from 50% to 89% of overall platform GHG emissions, depending on the concept. Generally,

Table 4
Short description of the life cycle stages included in the analyses.

Life cycle stage	Description
Installation (fuel)	Fuel consumption related to the transportation of all the equipment from shore to offshore site in order to install the wind farm.
Turbine materials	Production, processing and transport of all the infrastructure material related to the turbine production. Disposal of materials is also included (credits from material to recycling are not included).
Platform materials	Production, processing and transport of all the infrastructure material related the platform production, including production of internal and external (from offshore to shore) cables. Disposal of materials is also included (credits from material to recycling are not included).
Maintenance (fuel)	Fuel consumption related to the transportation from shore to offshore site due to maintenance.
Maintenance (infrastructure/reinvestment)	Production, processing and transport of all the material used for maintenance during the lifetime of the wind farm. The reinvestments needed are given annually and multiplied with the lifetime. Disposal of materials used for maintenance is included in this life stage.
Maintenance (others)	Production, processing and transport of support materials used for maintenance (oil, cotton etc.) and treatment of waste.
Decommissioning (fuel)	Fuel consumed for decommissioning the wind farm. For simplification the decommissioning is assumed equal to the installation (fuel) and operation (reversed). Disposal of materials is included in the life cycle stages Turbine and platform materials, respectively.

apart from the MIT TLB, the second largest platform contributor is the production of aluminium in connection with internal and external cables. Overall contribution from external cables is 1.95 g CO_2-equivalents/kWh.

As shown in Fig. 2, the GHG emissions relating to the turbine materials (assumed to be equal for all the concepts) are 4.7 g CO_2-equivalents/kWh, thus contributing to a range between 15% (Umaine Semi-S) and 26% (MIT TLB) of the total GHG emissions. The main parameters affecting the turbine GHG emissions are presented in Fig. 4.

The figure clearly shows that the main materials affecting the turbine GHG emissions are steel and glass fibre, contributing to 55% and 27%, respectively. In addition, it can be seen that the main components of the turbine (tower, rotor and nacelle) contribute about one third each to the total turbine GHG emissions.

From Fig. 2 it can also be seen that the installation and decommissioning life cycle activities contribute respectively 6.2 and 5.8 g CO_2-equivalents/kWh for the bottom fixed and floating concepts. This represents a range varying from 18% to 33% of total GHG emissions relating to each installation.

4.2. Sensitivity analyses GHG emissions

4.2.1. Sensitivity analyses capacity factor (CF) and lifetime (LT)

An increase in CF (better wind conditions or higher availability) or lifetime (LT) will reduce the GHG emissions per unit electricity (GHG emissions per kWh). The change relative to a reference is expressed as:

$$\text{GHG emissions per kWh}/\text{GHG emissions per kWh}_{ref} = \left(CF_{ref}/CF\right)*\left(LT_{ref}/LT\right) \quad (2)$$

Fig. 5 shows the relative GHG emissions per kWh as a function of the relative CF. The significance of CF can also be seen in traditional economic decision metrics such as Net Present Value (NPV). One of the pitfalls with NPV is that a large cost at the end of the project, such as decommissioning, can be obscured, especially if a high rate of return is used in the calculations. This can influence decisions exposing a company to considerable risk.

The capacity factor of different offshore wind farms is shown to vary between 29% and 53% in the literature [46]. These values represent relative CF's of 0.63 and 1.15, respectively (related to the default CF of 0.46), corresponding to a relative GHGE in the range

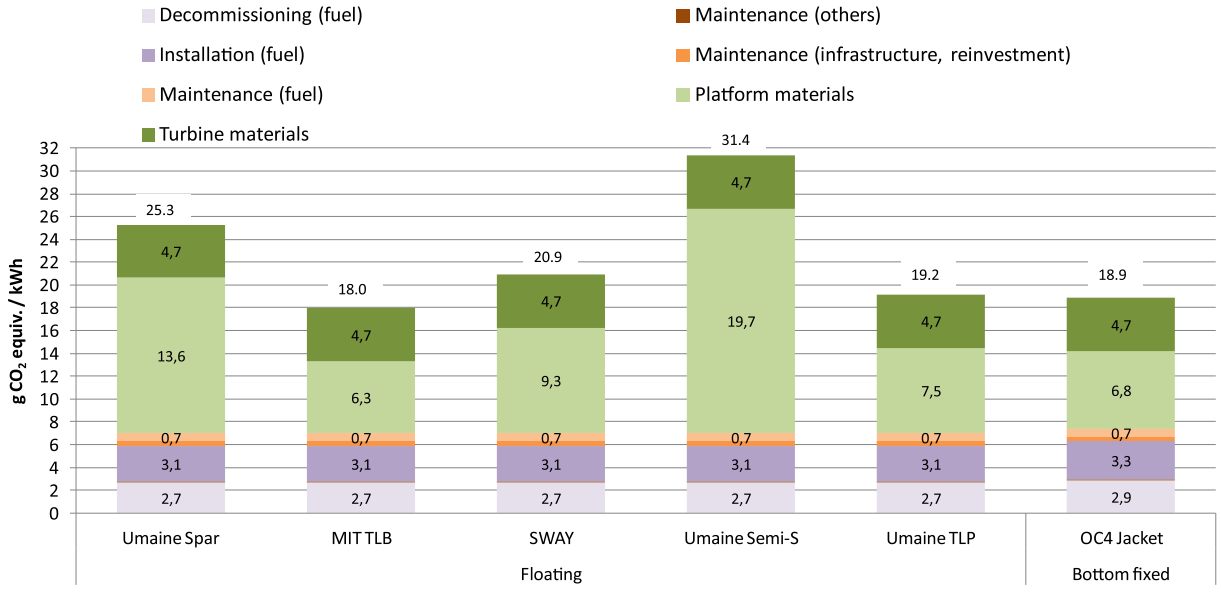

Fig. 2. GHG emissions (g CO_2-equivalents/kWh) for the investigated offshore wind farm concepts in relation to the different life cycle stages.

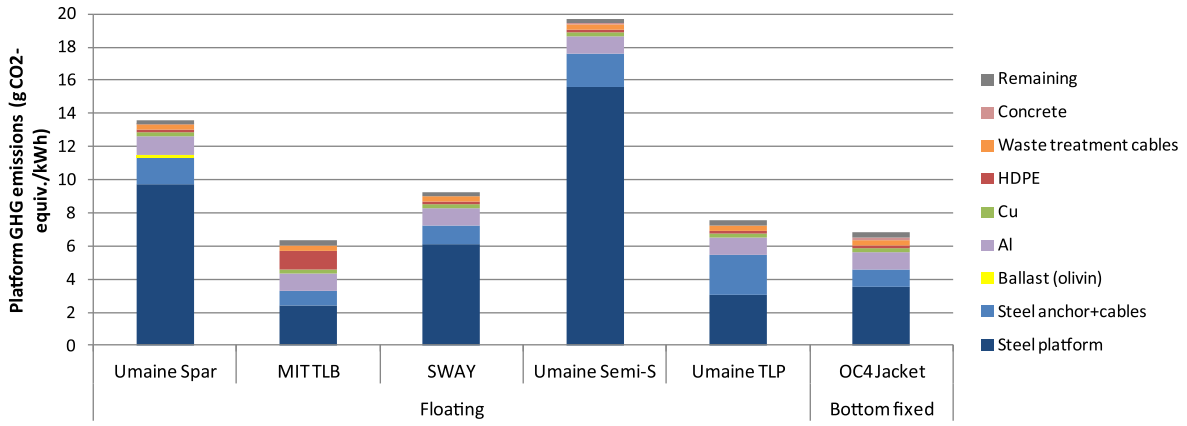

Fig. 3. Platform GHG emissions grouped into the main contributors.

0.87–1.58. Similarly, an increase of LT from 20 to 25 years (relative LT 1.25) will lead to a reduction in GHGE of 20% (relative GHGE emissions 0.8).

4.2.2. Sensitivity analysis with respect to steel masses

As described in Section 4.1, the materials relating to the foundation/platforms (including external/internal cables) are the main contributors to overall GHG emissions, representing a range from 35% to 63% of the total GHG emissions (dependent on the concept under consideration). Furthermore, from Fig. 3 it can be seen that the GHG emissions per kWh from the steel production of the foundation/platforms (see Table 3, excluding external/internal cables) represent between 36% and 79% of the total platform GHG emissions per kWh. Thus, the overall impact of the platform steel varies between 12% and 50% of the total offshore concepts' GHG emissions per kWh. This means that changing the platform steel amounts by 1% results in changes in GHG emissions of between 0.12% and 0.5% (depending on the concept under consideration). Fig. 6 shows the total GHG emissions dependent on the relative changes in platform steel masses. It should be emphasised that the two investigated cases OC4 Jacket and Umaine TLP cannot be clearly distinguished in the figure because they coincide.

As seen in Fig. 6, the Umaine Semi-S and the MIT TLP concepts are those which are, respectively, to the greatest and smallest degree, affected by a relative change in the platform steel masses. This is to be expected as these concepts represent the largest and smallest steel masses. The figure also shows that a significant change in the platform steel masses may alter the ranking of the conceptual design with regard to GHG emissions. This can be exemplified by a 53% reduction of platform steel masses in the Umaine Spar concept, which would result in GHG emissions per kWh equal to the Sway default concept.

This paper does not intend to rank the platforms according to GHG emissions per kWh, since all the conceptual designs with open data can be considered as 'first-generation designs'. New versions of floaters are being designed with significantly reduced steel masses as the industry gains experience, and one can similarly expect significant cost reductions for offshore floating wind turbines as those already seen for onshore wind turbines. The study nevertheless demonstrates the importance of overall steel masses on GHG emissions and energy performance.

4.2.3. Sensitivity analysis with respect to fuel consumption during installation and decommissioning

The installation and decommissioning life cycle stages represent the second largest contributor to the overall GHG emissions, ranging from 18% to 33% for the various different concepts. In order to investigate the robustness of the main assumptions in relation to these life cycle stages, a sensitivity analysis has been performed by increasing/decreasing the fuel consumption by 25%. The results are shown in Fig. 7.

As seen from the figure, a 25% increase/decrease in fuel consumption in relation to installation and decommissioning of the wind farms has comparatively little impact on the overall GHG

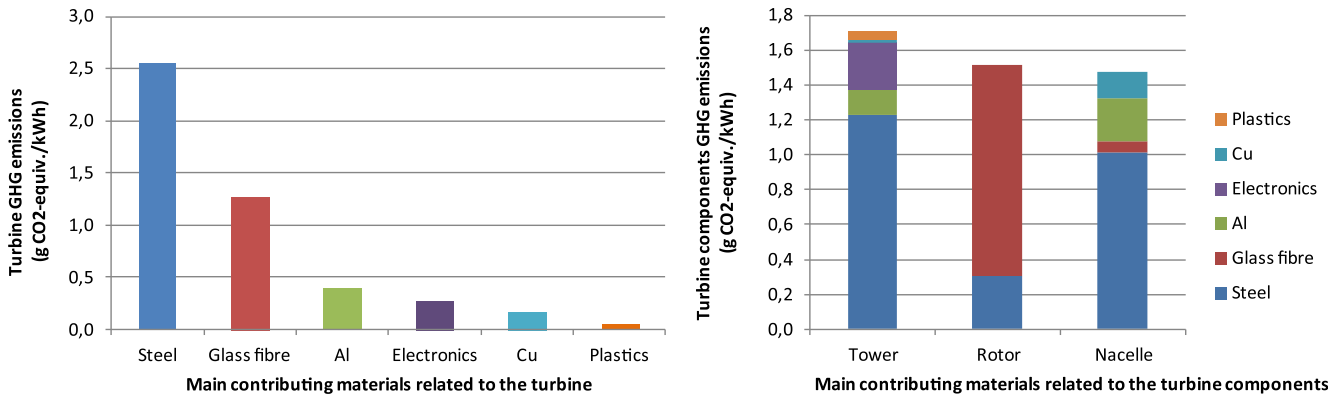

Fig. 4. Turbine GHG emissions grouped into the main contributors.

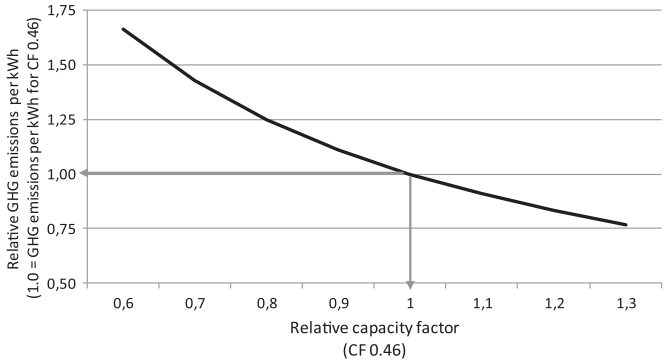

Fig. 5. Sensitivity analysis showing variations in relative GHG emissions per kWh as function of relative capacity factor (CF).

emissions. The increase/decrease in the overall GHG emissions ranges between 5% and 8% dependent on the analysed concept.

4.3. Energy performance

The energy indicators EPR (Energy Payback Ratio) and EPT (Energy Payback Time), as defined in Section 2.1, are presented in Fig. 8. The greater the EPR indicator value, the better the energy performance, while the opposite applies in the case of EPT (the smaller the value the better the performance).

The figure shows that the investigated concepts achieve EPR and EPT values of between 7.5 and 12.9, and 1.6 and 2.7 years, respectively. The MIT TLB and OC4 Jacket give the best performance, being in line with the results for GHG emissions. This is to be expected since the use of conventional energy within an analysed system generally represents the main contributor to GHG emissions.

5. Comparison of GHG emissions and energy performance with relevant data

The GHG emissions and energy performance results for the investigated offshore concepts have been compared with relevant LCA literature data in order to put the investigated wind power cases and concepts in perspective.

5.1. GHG emissions

The results for GHG emissions (g CO2-equiv/kWh) have been compared with relevant LCA data [4–11,30,36–42] and categorised according to turbine size and capacity factor.

The literature data have been adjusted as follows, in order to ensure comparability: data representing lifetimes other than 20 years ([9,14,15] (2 cases) and [16]) have been adjusted for 20 years, and data including benefit from recycling of materials [18,19] have been adjusted to exclude these benefits. Some cases [12,13] have been excluded from the comparisons because the benefits from recycling included in the analyses have been too challenging to adjust. It should be emphasised, however, that lack of transparency in the underlying assumptions in the literature can mean that some unmodified data may still be included in the comparisons. The results are shown in Fig. 9, presenting onshore and offshore data as blue and red bullets (in web version), respectively. The offshore concepts investigated in this study are highlighted by circles. It should be noted that the values of the two investigated concepts Umaine TLP and OC4 Jacket (representing 19.2 and 18.9 g CO_2-equiv./kWh, respectively) coincide in the figure and are therefore hard to distinguish from each other.

Fig. 9 shows that there is a tendency for a decrease in GHG emissions where there are, respectively, increased turbine size and capacity factors. This is in accordance with results from other studies [1,15,20,46,47]. Despite this general tendency, Fig. 9 shows that the variations in the data are still relatively large. Such variations can be explained by differing presuppositions concerning the wind farm. These can include lifetime; end-of-life treatment of wind turbine components; the energy invested to build and install the wind turbines; reinvestment rates and maintenance; whether current or future conditions have been analysed as well as the type of analysis[2] (Process analysis or Input–output analysis).

As described above, the data in Fig. 9 have been adjusted with regard to the two first mentioned parameters (lifetime and end-of-life treatment) in order to make them comparable. As regards the impact of the type of analysis on the results, GHG emissions reported for wind power appear to increase when changing from Process analysis to Input–output analysis [46]. This corresponds with the results from a multivariate regression analysis, examining the influence of methodology, scope and technological maturity [15]. They show that the results of the energy intensity (and GHG emissions) increase during a change from Process to Input–output analysis. The literature data presented in this study include both analysis types, and the variations may be affected by this. Another source of scatter in the data could be that wind farms are optimised for minimum energy costs and not minimum GHG emissions.

In addition, Fig. 9 shows that the offshore concepts investigated in this study (highlighted by circles) generally result in higher GHG emissions when compared with other offshore wind power studies. This is further investigated using a more detailed comparison of these concepts and relevant offshore data, as shown in Fig. 10 (the investigated cases are presented as red bullets, in web version).

As seen in the figure, there are only two comparable offshore cases with regard to turbine size (Weinzettel et al. [4] and Tveten [5], highlighted by black circles) as the others represent turbines smaller than 2.5 MW. This shows that the results of the six conceptual offshore designs investigated in this study give valuable additional environmental information regarding large offshore wind power. The two above mentioned cases represent a Sway concept [4] and a “representative offshore concept in Scandinavia” [5] with corresponding GHG emissions of 12.2 g and 20.6 CO_2-equivalents/kWh, respectively ([5] adjusted for 20 years lifetime).

In order to compare the results for equal capacity factors, the two cases have been adjusted for the default capacity factor used in this study (46%). The respective modified GHG emissions, presented in Fig. 10 (right part) by the “stars” depicted in the graph, become 14.1 [4] and 16.8 [5] g CO_2-equivalents/kWh. This shows that both cases result in lower GHG emissions when compared with the investigated conceptual designs. The distances to shore in the comparable cases are, however, 75% [4] and 85% [5] shorter when compared with the distance (200 km) in this study. In order to assess the importance of distance to shore, the Sway conceptual design in this study has been modified by assuming 50 km distance to shore (a 75% reduction). The resulting GHG emissions of 18 g CO_2-equivalents/kWh represent a reduction of 14%, thus showing that distance to shore also affects the results and should be taken into consideration when comparing offshore wind concepts.

[2] A process analysis assesses the value chain of the system in a holistic manner, focussing on all significant processes based on mass and energy relations (bottom-up approach). An input–output analysis (IOA) assesses the environmental aspects of products and services by dividing a product into its economic components (machinery, chemistry, services, etc.) as the basis for performance calculation (top-down approach).

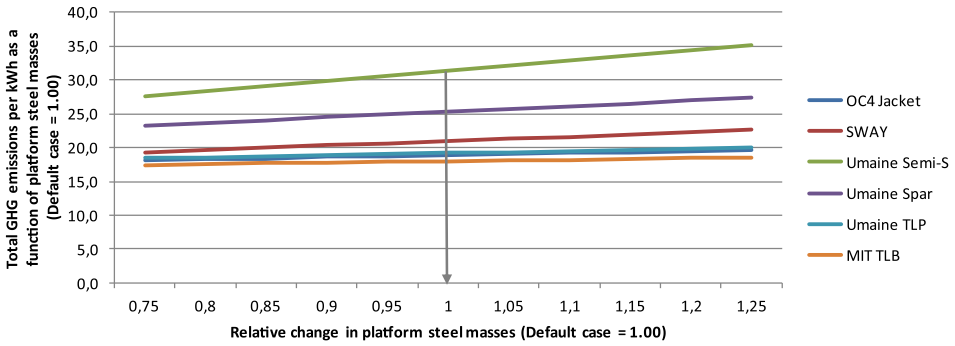

Fig. 6. Platform steel masses' impact on the offshore conceptual designs' overall GHG emissions.

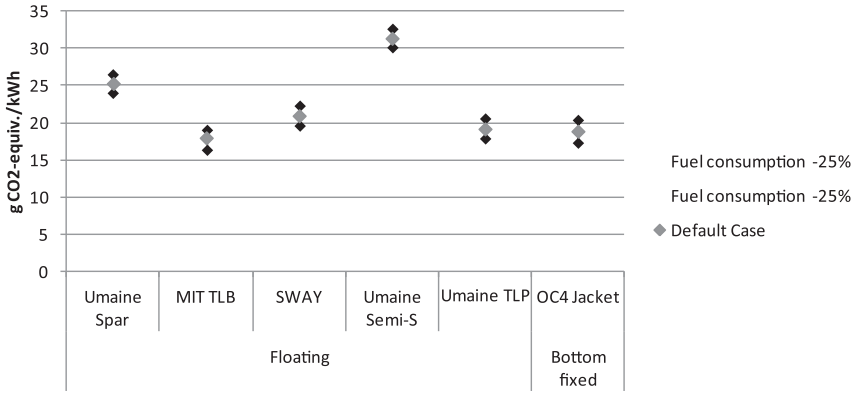

Fig. 7. Sensitivity analyses regarding fuel consumption for installation and decommissioning for the different offshore concepts.

The difference in the resulting GHG-emissions between the Sway case investigated in this study and the case described in Ref. [4] has been reduced from 33% to 22% by modifying equal conditions with regard to capacity factor and distance to shore. The difference in the remaining GHG emissions (22%) can partly be explained by the steel masses being 19% less in the Weinzettel et al. [4] case compared with the Sway concept analysed in this study. A more detailed analysis of this 19% difference in steel masses shows that the case investigated in Ref. [4] has not included steel masses relating to anchor and anchoring cables. In the Sway concept analysed in this study, these steel masses represent 210 tons, which accounts for 63% of the steel masses difference between the two Sway cases. Other differences between these cases which may be of importance for the results are transport to offshore (towing boats being the only vessels included in Ref. [4]), infrastructure maintenance (5% extra infrastructure material [4] when compared with 2%) and solid ballast material (included in Ref. [4]) when compared with water.

The comparisons and modification of the offshore concepts show that wind conditions and distance to shore are important factors to be taken into consideration when comparisons of offshore wind concepts are carried out. It confirms, furthermore, that the required steel infrastructure masses have great importance for the resulting GHG emissions.

It should be noted that Tveten [5] has used an Extended Input–Output LCA for the analysis. The use of these broader system boundaries would imply that increased GHG emissions could be expected, when compared with the Process LCA method used in

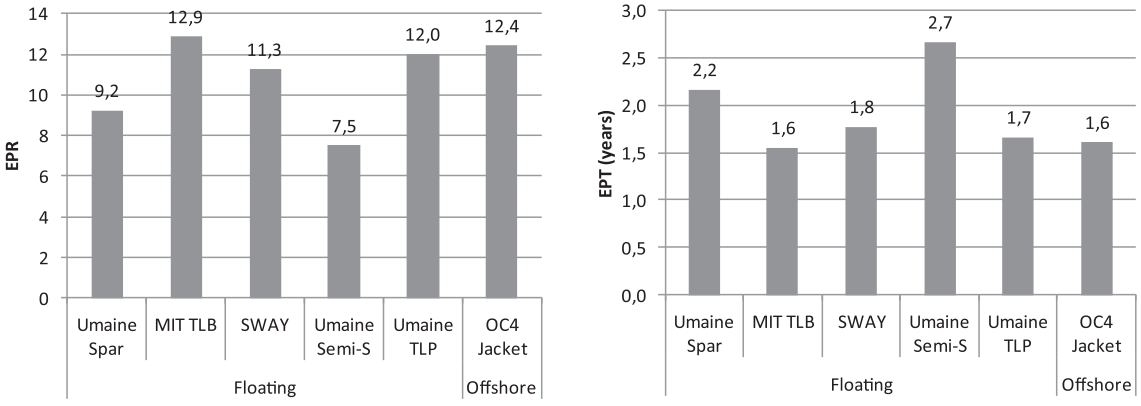

Fig. 8. Energy Payback Ratio (EPR) and Energy Payback Time (EPT) for the different offshore concepts.

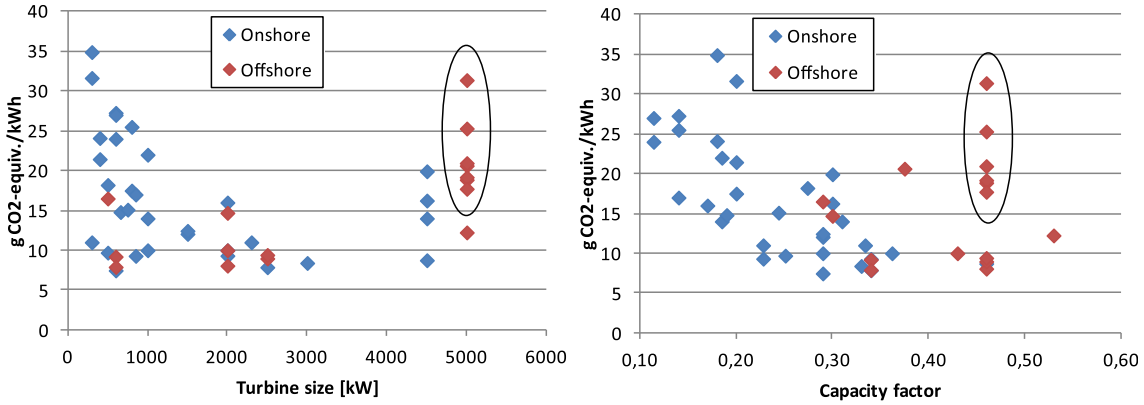

Fig. 9. Comparisons of GHG emissions of the investigated offshore cases with relevant LCA literature, categorised in accordance with turbine size (left) and capacity factor (right).

this study. This is, however, not the case; the principal reason being, in all probability, that, lacking specific data [48], Tveten [5] has chosen to simplify the platform data. Instead of using specific material and masses relating to the platform, a total mass of 1000 tons, comprising "foundation/ballast and mooring", has been applied. In addition, the data relating to this category have been based only on cost data for "proxy sector from the background system". Compared with the conceptual designs analysed in this study, the relating specific platform steel masses (including anchor and mooring cables) represent a range of between about 550 tons and 3350 tons (see Table 3). The corresponding GHG emissions represent a range of between 3.3 and 17.6 g CO_2-equiv./kWh, which account for 18%–56% of the total wind turbine GHG emissions. Thus it can be seen that specific platform steel masses have significance for the resulting GHG emissions.

Within the EU-supported NEEDS (New Energy Externalities Developments for Sustainability) project [8], projected future offshore wind turbine ratings have been considered. These are between 8 MW and 32 MW, and from 2005 until 2050. The scenarios represent various differing assumptions with regard to the development of future technology. Examples include improved steel production, increased share of renewables in the electricity mixes etc. for water depths varying between 10 and 30 m (2005), 20–60 m (2025) and >100 m (2050). The projected future technology models have been based on up-scaled data from the reference technology (Horns Rev Offshore Wind farm, 2 MW) and result

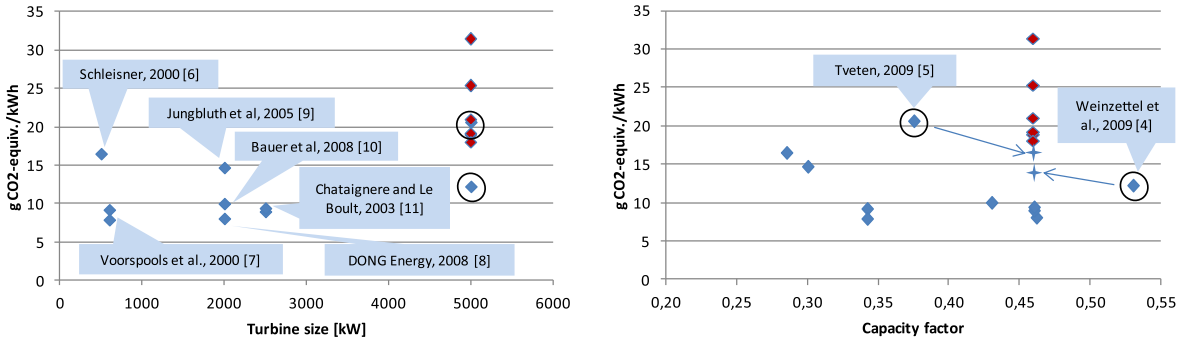

Fig. 10. Comparisons of the investigated offshore concepts with relevant LCA literature, categorised in accordance with turbine size (left) and capacity factor (right).

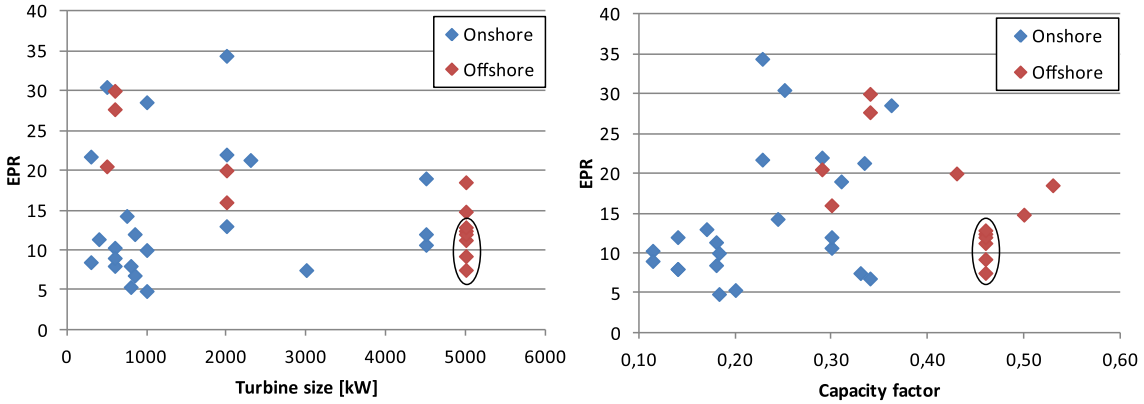

Fig. 11. Comparison of EPR (Energy Payback Ratio) for the investigated offshore cases with relevant literature, categorised in accordance with turbine size (left) and capacity factor (right).

in GHG emissions varying between 2.9 and 7.9 CO_2 -equivalents// kWh. The principal conclusions from this study are that the material used in the manufacture of wind turbine components is crucial for the overall environmental impact of a wind turbine.

5.2. Energy Payback Ratio (EPR)

In order to put the concepts in this study into perspective, the energy performance results or Energy Payback Ratio (EPR) have been compared with relevant LCA literature, just as with the GHG emissions.

The EPR results have been compared with relevant LCA data [4,6,7,9,10,30,37–41,45] and categorised in accordance with turbine size and capacity factor. The data have been standardised according to a 20 year lifetime and no credits from recycling have been included. The results are shown in Fig. 11, the offshore conceptual designs investigated in this study being highlighted by black circles. As emphasised for Figs. 9 and 10, the values of the two investigated concepts Umaine TLP and OC4 Jacket (representing 19.2 and 18.9 g CO_2-equiv./kWh, respectively) coincide in the figure and these concepts are therefore hard to distinguish from each other.

Lenzen and Munksgaard [15] confirm that small wind turbines of 1 kW require about three times more life-cycle energy per unit power than large wind turbines of 1 MW. Thus, it might have been expected that the EPR indicator would generally increase in accordance with increased turbine size (just as GHG emissions decrease with turbine size). It can be seen, however, from Fig. 11, that there exists a lack of correlation, both between EPR and turbine size and between EPR and capacity factor. This is in line with the conclusions drawn by Davidsson et al. [49], stating that there is an inconsistent use of terminology and concepts regarding wind power energy performance. The need for discussion on the way in which environmental impact, energy performance, and natural resource use of renewable energy recourses should be assessed is addressed by the authors [49]. The existence of this inconsistency in energy performance assessment is supported by Modahl et al. [50]. They conclude that assessing the energy indicator Cumulative Energy Demand (CED) for a product or service is more dependent on the LCA practitioner's knowledge and competence about the CED assessment method, than on other methods for assessing environmental indicators, e.g. carbon footprint. It is important to check whether resources are accounted for as material resources/ feedstock or as energy resources. This is because the pre-defined CED methods which are available in LCA software tools often differ with regard to the challenges connected to feedstock issues. If they are not, then the energy resources may be handled differently, leading in turn to diverging results (Modahl et al. op.cit).

Davidsson et al. [49] point out another complicating issue with regard to energy performance assessment. Some studies include a conversion factor (reflecting the efficiency of the conventional electricity generation) relating to the produced electricity. This is in order to convert the produced wind power to the primary energy which would otherwise have been produced in a conventional power plant. There is no consensus, however, on how conversion to primary energy should be handled, or even if and why it should be done. It must be emphasised that the literature data in this study have been modified in order to exclude potential conversion factors, but lack of transparency may have resulted in unmodified data. The data have been modified by multiplying them with the given efficiencies related to the assumed conventional power plants. Davidsson et al. [49] summarise that the use of different methods, lack of transparency, and variations in the presentation of results, e.g. including and not including a conversion factor, make it difficult to compare studies with each other and with other renewable sources. The "disturbed picture" of energy performance shown in Fig. 11 confirms the above mentioned inconsistency in energy performance assessment.

Fig. 11 also shows that, the investigated offshore concepts generally show lower values than the offshore literature data, which means lower energy performance. This is in line with the results for the GHG emissions, as shown in Section 5.1.

6. Conclusions

There are currently few LCA studies in existence which analyse offshore wind turbines with rated power as great as 5 MW. The results, therefore, from the investigation into the six conceptual offshore designs used in this study, give valuable additional environmental information concerning large offshore wind power. The resulting GHG emissions vary between 18 and 31.4 g CO_2-equivalents/kWh while the energy performance, assessed as EPR and EPT, varies between 7.5 and 12.9, and 1.6 and 2.7 years, respectively. The relatively large ranges in GHG emissions and energy performance are chiefly the result of the differing steel masses required for the analysed foundation/platforms.

In comparison with the relevant existing offshore studies, the six conceptual designs result in larger GHG emissions and lower energy performance. The principal reason for this is that more complete and accurate data for steel masses relating to the platform, anchor and mooring cables have been included in the analysis. Thus, one major conclusion from this study is that specific platform/foundation steel masses are important for the overall GHG emissions relating to offshore wind power. Other parameters of importance when comparing the environmental performance of offshore wind concepts are the lifetime of the turbines, wind conditions, distance to shore, and installation and decommissioning activities.

The offshore wind power conceptual designs which have been investigated here, give larger GHG emissions and a lower energy performance when compared with the corresponding average values of the onshore wind power data. This can indicate that the extra energy invested in offshore plants, as a result of the need for additional platform infrastructure, may not be beneficial.

This study confirms the results from other research [15] which shows a tendency for GHG emissions to decrease in relation to an increase in turbine size and capacity factor. It should be noted, however, that despite this general tendency, relatively large variations within the data still remain. These variations can mainly be explained by the following: varying assumptions/conditions relating to the energy invested to build and install the wind turbines; the type of analysis (Process LCA or Input/Output); whether the turbine is located on or offshore, and varying reinvestment rates and maintenance activities.

In the case of energy performance of wind power, the study confirms the inconsistencies with regard to energy performance assessment methods which have been documented by Davidsson et al. [49] and Modahl et al. [50]. There is a need for an increased effort in work on standardising energy performance calculations methods.

Even though the GHG emissions from wind power vary to a relatively large degree they are small in relation to those from fossil electricity generation technologies. Wind power can fully compete with other low GHG emission electricity technologies, such as nuclear and photovoltaic power, and hydro power. GHG emissions from wind farms are small in relation to those from fossil electricity generation technologies.

Lastly, it should be emphasised that GHG emissions and energy performance represent only two environmental indicators. With regard to decision making and guiding policy, several other environmental indicators need to be taken into consideration. These

include land use, visual aspects, biodiversity and noise. This is particularly relevant when comparing onshore and offshore turbines.

Acknowledgements

The authors would like to thank Amy Robertson and Jason Jonkman, at the National Renewable Energy Laboratory (NREL), for reviewing the major assumptions for the analyses. In addition, the Research Council of Norway is acknowledged for financially supporting the research project Energy Trading & Environment 2020 through the RENERGI programme.

References

[1] Weisser D. A guide to life-cycle greenhouse gas (GHG) emissions from electric supply technologies. Energy 2007;32:1543–59.
[2] IPCC. IPCC special report on renewable energy sources and climate change mitigation. In: Edenhofer O, Pichs-Madruga R, Sokona Y, Seyboth K, Matschoss P, Kadner S, et al., editors. Prepared by working group III of the intergovernmental panel on climate change. Cambridge, United Kingdom and New York, NY, USA: Cambridge University Press; 2011. p. 1075.
[3] Sieros G, Chaviaropoulos P, Sørensen JD, Bulder BH, Jamieson P. Upscaling wind turbines: theoretical and practical aspects and their impact on the cost of energy. Wind Energy 2012;15:3–17.
[4] Weinzettel J, Reenaas M, Solli C, Hertwich EG. Life cycle assessment of a floating offshore wind turbine. Renew Energy 2009;34:742–7.
[5] Tveten ÅG. Life cycle assessment of offshore wind electricity generation in Scandinavia. Master thesis. UMB; 2009.
[6] Schleisner L. Life cycle assessment of a wind farm and related externalities. Renew Energy 2012;20:279–88.
[7] Voorspools KR, Brouwers EA, D'haeseleer WD. Energy content and indirect greenhouse gas emissions embedded in 'emission-free' power plants: results for the low countries. Appl Energy 2012;67:307–30.
[8] DONG Energy. NEEDS (New energy externalities developments for sustainability). RS 1a: life cycle approaches to assess emerging energy technologies. Final report in offshore wind technology; 2008.
[9] Jungbluth N, Bauer C, Dones R, Frischknecht R. Life cycle assessment for emerging technologies: case studies for photovoltaic and wind power. Int J Life Cycle Assess 2005;10:24–34.
[10] Bauer C, Dones R, Heck T, Hirschberg S. Environmental assessment of current and future Swiss electricity supply options. In: Proceedings of international conference on the physics of reactors 'nuclear power: a sustainable resource', Interlaken, Switzerland 2008.
[11] Chataignere A, Le Boult D. Wind turbine (WT) systems. In: ECLIPSE environmental and ecological life cycle inventories for present and future power systems in Europe 2003.
[12] Vestas Wind System A/S. Life cycle assessment of offshore and onshore sited wind power plants based on Vestas V80-2.0 MW turbines; 2004.
[13] Vestas Wind System A/S. Life cycle assessment of offshore and onshore sited wind power plants based on Vestas V90-3.0 MW turbines; 2006.
[14] Hondo H. Life cycle GHG emission analysis of power generation systems: Japanese case. Energy 2005;30:2042–56.
[15] Lenzen M, Munksgaard J. Energy and CO_2 life-cycle analyses of wind turbines–review and applications. Renew Energy 2002;26:339–62.
[16] Burger B, Windkraft Bauer C. Final report ecoinvent. Ecoinvent No. 6-XIII, v2.0. Paul Scherrer Institut and Swiss Centre for Life Cycle Inventories Switzerland; 2007.
[17] Crawford RH. Life cycle energy and greenhouse emissions analysis of wind turbines and the effect of size on energy yield. Renew Sustain Energy Rev 2009;13:2653–60.
[18] Martínez E, Sanz F, Pellegrini S, Jiménez E, Blanco J. Life-cycle assessment of a 2-MW rated power wind turbine: CML method. Int J Life Cycle Assess 2009;14:52–63.
[19] Tremeac B, Meunier F. Life cycle analysis of 4.5 MW and 250 W wind turbines. Renew Sustain Energy Rev 2009;13:2104–10.
[20] Ardente F, Beccali M, Cellura M, Lo Brano V. Energy performances and life cycle assessment of an Italian wind farm. Renew Sustain Energy Rev 2008;12:200–17.
[21] Tryfonidou R, Wagner HJ. Multi-megawatt wind turbines for offshore use: aspects of life cycle assessment. Int J Global Energy Iss 2004;21:255–62.
[22] Fortum Market and Ostfold Research. The energy trading & environment 2020 research project. Available from: http://ostfoldforskning.no/prosjektsider/49/energy-trading-and-the-environment-2020.aspx. [accessed October 2010].
[23] International standard ISO 14044:2006 environmental management – life cycle assessment – requirements and guidelines; 2006.
[24] European Commission. European Commission (2010) international reference life cycle data system (ILCD) handbookIn General guide for life cycle assessment - detailed guidance. 1st ed. Luxembourg: Joint Research Centre, Institute for Environment and Sustainability; March 2010. Publications Office of the European Union, EUR 24708 EN.
[25] The European Wind Energy Association (EWEA). About wind energy - the facts. Part II grid integration [Online]. Available from: http://www.wind-energy-the-facts.org/en/; 2009 [accessed November 2012].
[26] Gagnon L. Energy payback ratios for electricity generation [Online]. Available from: http://lightbucket.wordpress.com/2008/04/30/energy-payback-ratios-for-electricity-generation/; 2008 [accessed June 2011].
[27] Hall CAS. Introduction to special issue on new studies in EROI (Energy return on investment). Sustainability 2011;3:1773–7.
[28] Raadal HL, Modahl IS, Bakken TH. Energy indicators for electricity production. In: Comparing technologies and the nature of the indicators energy payback ratio (EPR), net energy ratio (NER) and cumulative energy demand (CED). Ostfold Research, OR 09.12; 2012.
[29] Borgen E. Floating wind power in deep water - competitive with shallow-water wind farms. Mod Energy Rev 2010;2:49–53.
[30] Robertson AN, Jonkman JM. Loads analysis of several offshore floating wind turbine concepts. In: The international society of offshore and polar engineers 2011 conference, Maui, Hawaii June 2011.
[31] Sclavounos PD, Lee S, DiPoetro J, Potenza G, Caramuscio P, De Michele G. Floating offshore wind turbines: tension leg platform and taught leg buoy concepts supporting 3–5 MW wind turbines. In: The European wind energy conference EWEC 2010, Warsaw, Poland 2010.
[32] Vorpahl F, Popko W, Kaufer D. Description of a basic model of the 'UpWind reference jacket' for code comparison in the OC4 project under IEA wind Annex XXX [Online]. Available from: http://www.iwes.fraunhofer.de/en/publications/list_of_publication/publikationen_veroeffentlichungengesamt/2011/description_of_abasicmodeloftheupwindreferencejacketforcodecompa/_jcr_content/pressrelease/linklistPar/download/file.res/UpWind%20Reference%20Jacket%20Description%20for%20OC4.pdf; May 2011 [accessed June 2012].
[33] Jonkman JM, Butterfield S, Musial W, Scott G. Definition of a 5-MW reference wind turbine for offshore system development; 2009. NREL/TP-500–38060.
[34] Jonkman JM, Larsen T, Hansen A, Nygaard TA, Karimirad M, Gao Z, et al. Offshore code comparison collaboration within IEA wind Task 23: phase IV results regarding floating wind turbine modelling. In: The European wind energy conference & exhibition Warsaw, Poland April 2010.
[35] Popko W, Vorpahl F, Zuga A, Kohlmeier M, Jonkman JM, Robertson AN, et al. Offshore code comparison collaboration continuation (OC4), phase I - results of coupled simulation of offshore wind turbine with Jacket support structure. In: The 22nd international offshore and polar engineering conference (ISOPE), Rhodes, Greece June 2012.
[36] The International EPD System. Product category rules, CPC 171 electrical energy CPC 173 steam and hot water. PCR 2007:08 version 2.01; 2011.
[37] Swiss Centre for Life Cycle Inventories. The EcoInvent database for processes, products and transport. Integrated in the life cycle software tool SimaPro (Pré). Available from: http://www.ecoinvent.ch/; 2011.
[38] Nexans. Data internal cable. Available from: http://www.nexans.no/eservice/Norway-no_NO/navigateproduct_537256501/TSLE_72kV_1x240AQ_35.html#; 2010.
[39] Kaiser MJ, Snyder BF. Offshore wind energy installation and decommissioning cost estimation in the U.S. outer continental shelf, U.S. Dept. of the interior, bureau of ocean energy management. Herndon, VA: Regulation and Enforcement; 2011.
[40] Mathisen T. Personal email correspondence from Tom Mathisen, Seatrench AS, to Bjørn Ivar Vold (Ostfold research) December 19, 2011.
[41] Sanden IL, Vold BI. Life cycle analysis of floating wind turbines with regard to internal and external factors compared with bottom-fixed wind turbines. UMB/IMT; 2010. Master thesis.
[42] Nielsen OJW. Installation data bottom-fixed platform. Personal communication (email) with Vold BI. January 2012.
[43] Reitan H. Data crane vessel maintenance. Personal communication with Vold BI. February 2012.
[44] Stuart F. Data crane vessel. Personal communication (email) with Vold BI. February 2012.
[45] Raadal HL, Vold BI. GHG emissions and energy performance of wind powerIn LCA of two existing onshore wind farms and six offshore wind concepts. Ostfold Research, OR 24.12; 2012.
[46] Raadal HL, Gagnon L, Modahl IS, Hanssen OJ. Life cycle greenhouse gas (GHG) emissions from the generation of wind and hydro power. Renew Sustain Energy Rev 2011;15:3417–22.
[47] Dones R, Heck T, Hirschberg S. Greenhouse gas emissions from energy systems, comparison and overviewIn Encyclopedia of energy. New York: Elsevier; 2004. pp. 77–95.
[48] Tveten ÅG. Personal communication. 2012.
[49] Davidsson S, Höök M, Wall G. A review of life cycle assessments on wind energy systems. Int J Life Cycle Assess 2012;17:729–42.
[50] Modahl IS, Lyng KA, Raadal HL, Askham S. Cumulative energy demand - how valid and comprehensive are our CED practice today?. In: The SETAC Europe 22nd annual meeting/6th SETAC world congress, Berlin 2012.

Appendix 5

Renewable Energy 66 (2014) 714–728

Contents lists available at ScienceDirect

Renewable Energy

journal homepage: www.elsevier.com/locate/renene

Levelised cost of energy for offshore floating wind turbines in a life cycle perspective

Anders Myhr*, Catho Bjerkseter, Anders Ågotnes, Tor A. Nygaard

University of Life Sciences (UMB), Department of Mathematical Sciences and Technology, Box 5003, Drøbakveien 31, 1430 Ås, Norway

ARTICLE INFO

Article history:
Received 27 September 2013
Accepted 18 January 2014
Available online 12 February 2014

Keywords:
HYWIND II
TLB
WindFloat
LCOE
LCA
Floating wind turbines

ABSTRACT

This report presents a comprehensive analysis and comparison of the levelised cost of energy (LCOE) for the following offshore floating wind turbine concepts: Spar-Buoy (Hywind II), Tension-Leg-Spar (SWAY), Semi-Submersible (WindFloat), Tension-Leg-Wind-Turbine (TLWT) and Tension-Leg-Buoy (TLB). The analysis features a generic commercial wind farm consisting of 100 five megawatt turbines, at a far offshore site in a Life Cycle Analysis (LCA) perspective. Data for existing bottom-fixed turbines, both jacket and monopile concepts are used as reference values for adaptation to the generic wind farm parameters. The results indicate that LCOE values are strongly dependent on depth and distance from shore, due to mooring costs and export cable length, respectively. Based on the findings, depth is the dominant parameter to determine the optimal concept for a site. Distance to shore, Load Factor and availability are amongst the significant factors affecting the LCOE. The findings also indicate that LCOE of floating turbines applied in large scale and in intermediate depths of 50–150 m is comparable to bottom-fixed turbines. Floating turbines for increasing depths generally experience increased LCOE at a lower rate than bottom-fixed turbines. An optimal site, situated 100 km offshore would give LCOE in the range of € 82.0–€ 236.7 per megawatt-hour for the conceptual designs in this paper.

1. Introduction

During the last decade, the European wind energy sector has grown from an annual energy capture of 23 TWh in 2000 to 177 TWh in 2010 [1]. A significant part of this production is land-based. However, over the last few years, the number of offshore wind farms is increasing. Important drivers for this include increased wind potential and environmental aspects [2].

The offshore commercial wind farms are, as of yet, constructed with bottom-fixed wind turbines. Depending on depth and soil conditions, various concepts are utilised, but most common is the monopile. However, at increasing depths, typically around 30 m, the monopile design reaches engineering limits with respect to pliable diameters and wall thicknesses. For deeper waters, the more expensive jacket foundation is a valid option. It is limited to depths of less than 50 m, not due to engineering limitations, but economic viability [3].

One may argue that the depth limitations for bottom-fixed turbines exclude the possibility to utilise the vast quantities of offshore wind resources. For deeper waters, one will need to approach different foundation concepts such as floating platforms. New concepts deployed in new territories may imply increased costs, but floating platforms may also at the same time offer beneficial aspects with respect to improved wind conditions, reduced wave loading, reduced installation cost and less visual impact.

The main barriers for installation of floating wind turbines are high capital- and operating expenditures (CAPEX, OPEX), but there has also been a lack of accurate simulation tools capable of analysing and optimising these complex systems. Nevertheless, increased offshore knowledge through experience with bottom-fixed turbines and recent development of simulation codes have led to the development of several different floating platforms.

The scope of this work is not to assess the mechanical properties and viability of each concept, but rather to investigate the LCOE of current state-of-the art offshore floating concepts. We assume deployment in a large-scale, both for the floating and bottom-fixed wind farms. We use the term 'floating' also for concepts where the floater elevation is given by the taut mooring system rather than the mean sea level, such as the TLS, TLP, TLWT and TLB.

* Corresponding author. Tel.: +47 95106883.
E-mail address: anders.myhr@umb.no (A. Myhr).

0960-1481
http://dx.doi.org/10.1016/j.renene.2014.01.017

2. Approach

This work is based on the master thesis of Catho Bjerkseter and Anders Ågotnes [4], graduating summer 2013 at the University of Life Sciences, Norway. Their work consisted mainly in gathering data and the development of a computer tool to aid in the comparison of different floating offshore wind turbine concepts. A thorough review of their work has been conducted and the scope of this work is to present updated findings and results. Much of the same approach is employed; including the complex calculation methods, but with revised and updated values based on recent reviews and newly acquired experience. Some new features and boundary conditions are also included, in addition to a new concept.

There are several important parameters to consider when trying to determinate an optimal source for energy production. Local resources, national commitments, emissions and environmental impacts are all important. One may discuss the importance of each of these factors, but when considering large-scale deployment, a project is not likely to be completed if at an economic disadvantage. Thus, the cost of energy production should presumably be a dominant factor. The approach to obtain this cost of energy is similar to the one described in Ref. [4] and only the main important aspects and edited features will be presented in this work.

When considering the cost of energy, there are several perspectives and approaches to consider. OPEX and CAPEX are the main features examined to evaluate the economic potential of the project. These factors are often used for initial review of larger investment projects, but are not suited for distinguishing between several concepts with significant discrepancies concerning the mentioned features. This is especially apparent when evaluating capital-intensive projects that will accumulate the income over a longer period – much like the common offshore wind farm. When considering a wide time span, in example 20–30 years, quantification of the expenses in different phases of the project becomes important due to capital costs and risk placement. This is often referred to as a Life Cycle Cost Analysis (LCCA) or Cradle to Grave (CG) and is both a convenient way and widely used method to evaluate the potential economic performance [5,6].

For this work, an LCCA analysis will be conducted on each of the concepts. The LCCA is divided into five main phases, distinguished by the different operating conditions and capital intensity;

1. Development and consenting (D&C)
2. Production and acquisition (P&A)
3. Installation and commissioning (I&C)
4. Operation and maintenance (O&M)
5. Decommission (DECOM)

To increase the significance of the LCCA concerning concept comparison it is advisable to utilise a levelised cost in order to define a similar reference for value of money at different stages of a project. It is convenient to level the LCCA results by expected energy production. This allows for a better analysis and evaluation of risk and total cost during the life span is often referred to as a Levelised Cost of Energy (LCOE) Analysis. The similar reference value of money is obtained by discounting the costs to a given date[1] by the annuity method. Once obtained, the LCOE may be interpreted as the minimum unit price of energy and is a suitable variable in order to evaluate the performance of different concepts. The following equation is used to calculate the LCOE and is derived from Ref. [7]:

$$\mathrm{LCOE} = \frac{\sum_{t=0}^{n} \frac{I_t + M_t}{(I_0+r)^t}}{\sum_{t=0}^{n} \frac{E_t}{(I_0+r)^t}} \quad (1)$$

where I_t denotes investments at time t; M_t denotes operation and maintenance costs at time t; E_t denotes energy generation at time t; r denotes the evaluation discount rate; t denotes the time, ranging from zero to n.

The discount rate should reflect the market value of both equity and debt. In addition, project risk and return yield should be considered. This combination is often referred to as Weighted Average Cost of Capital (WACC). For this work, the WACC is set to a base case of 10%, with high- and low cases at 8% and 12%, respectively, in addition to an assumed inflation interest of 2.5%. Momentary values are stated in Euros and PV and converted to 2013-Euros (1st of January) before inflation by the Industrial Producer Price Index (PPI). No contingency is used in the analyses of the concepts.

Future cost reduction potential was not covered. The model was compared to existing literature, from both onshore [8,9] and offshore [10–12], in Ref. [4] and produced satisfying results. Additional comparison to Ref. [13] resulted in limited discrepancies, especially for the production cost estimations.

Six conceptually different floating concepts are investigated in this work. Variation in underlying conditions typically makes comparison difficult. Two bottom-fixed wind turbine setups are therefore included for increased value and comparability to similar work.

It is likely that the different concepts are under different stages of development, ranging from small prototypes to conceptual phase with full-scale deployment. In this analysis it is assumed that all the concepts are fully developed. Cost of development and scaling effects are included. Further, a reference case, consisting of 100 5 MW turbines localised in a 10 by 10 km grid with a sub-station in its centre, placed 200 km offshore is used as a benchmark. The reference case also features a given turbine tower and topside[2]. The reference turbine is rated at a power of 5 MW.

The calculation of steps one to three, in addition to step five, is handled internally by the developed simulation tool. Step 4, O&M is partially solved by utilising external software, in example the Operation and Maintenance Cost Estimator (OMCE-Calculator) developed by the Energy Research Centre of the Netherlands (ECN) (reference). This simulation tool computes the results prior to performing sensitivity analysis on high- and low scenarios to identify the main contributions to risk and uncertainty in each of the proposed concepts. This results in an optimised suggestion for which turbine concept that is the most suitable under given conditions when differentiated by LCOE.

3. The concepts

In total, nine different wind turbine concepts are investigated. The floating concepts consist of four spar concepts, a semi-submersible and a tri-floater. Ballast, displacement, mooring lines or a combination of these may stabilise a floating system. Floating systems become available in waters from 30 to 40 m and deeper.

[1] Also known as present value (PV).

[2] Refers to installation above tower level, usually interpreted as hub-height, and include nacelle, hub and rotor. Power electronics inside the turbine tower is also taken as included.

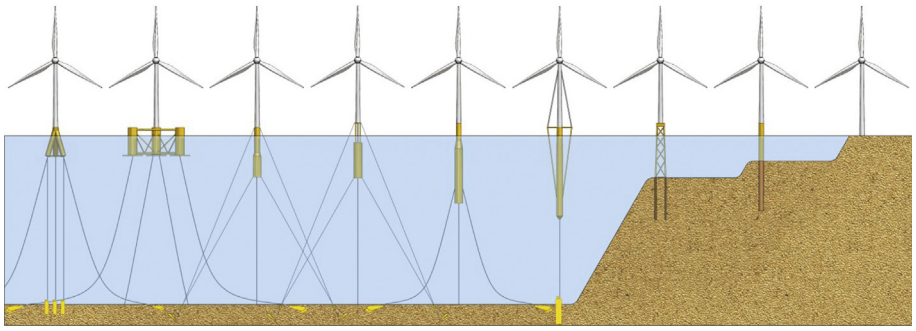

Fig. 1. Illustration of the different concepts, from left to right; TLWT, WindFloat, TLB B, TLB X3, Hywind II, SWAY, Jacket, Monopile and the onshore reference. The mooring systems are not to scale in the horizontal direction.

The bottom-fixed foundation concepts consist of a jacket, utilised at intermediate depths (30–50 m of water), and a monopile suitable for shallower water. All of the systems are illustrated in Fig. 1 and then explained briefly.

The conceptual Tension-Leg-Wind-Turbine (TLWT) utilised in this work achieves stability through displacement and mooring lines. It is developed by the International Design, Engineering and Analysis Service (I.D.E.A.S) [13] and in based on the Tension-Leg-Platform (TLP) system, a favoured solution in the offshore oil-sector. The TLP concept is well known for its performance, utilising vertical tendons to constraint motion along the vertical axis, and several similar concepts have been investigated [14]. However, the TLWT features a reviewed and optimised structure and spaced tri-floater sub-structure. The TLWT may utilise a set of three inclined tendons under specific conditions, but the setup used in this work features three vertical tendons held by suction anchors. A second catenary mooring system is used for horizontal station keeping and redundancy.

The WindFloat [15] system by Principle Power was successfully deployed with a full-scale 2 MW turbine off the coast of Portugal in late 2011. The prototype uses buoyancy for stabilisation, implying a complex and steel-intensive sub-structure with a mass of about 2500 tons, but the concept is favoured for its good towability.[3] A catenary mooring system of four mooring lines, comprising of both steel wire and chain, held by four Drag-Embedded Anchors (DEA), provide the station keeping.

The Tension-Leg-Buoy (TLB) systems benefit from a stabilising system consisting of six taut Dyneema fibre robes held by three Vertical Load Anchors (VLA). The high axial stiffness mooring lines are kept taut by excess buoyancy. The high stiffness results in minimal motion, comparable to or even less than for onshore turbines, but also increased mooring cost – especially for increased depths. TLB B and TLB X3 [16,17], developed at the University of Life Science in Norway, are based on the original works presented in Ref. [18]. The revised versions utilised in this work are derived from Ref. [16]. The reason for implementing two different TLB concepts is to identify if one can justify measures to reduce the wave loading on the structure in order to reduce the total load on the anchors. Not shown in Fig. 1 TLB X3 features a slim lattice transition piece, with an increased complexity factor, located in the wave action zone. In comparison, the TLB B utilise a more traditional conical transition. The total steel mass of the platform is about the same (445 and 521 tons respectively).

The Hywind II system is an optimised version of the original Hywind system that has been operating off the coast of Norway since 2009. Data used for the Hywind II in the analysis is based on engineering work performed in Refs. [17,19,20] and personal communication with representatives from Statoil ASA [21]. The solution features proven technologies, but with a large mooring footprint with a three line catenary system similar to WindFloat, in addition to a relatively high sub-structure steel mass of about 1700 tons to accommodate ballast and sufficient stability.

In 2011, SWAY AS deployed a 1:6 scaled prototype of the coast of Norway. The SWAY concept features a tension-leg-spar (TLS) construction with one tendon attached to a suction anchor. Excess buoyancy ensures tension and acceptable motions for the downwind rotor assembly. There is no apparent transition from tower to floater, and the tower–floater construction is reinforced by an external wiring system. This allows for optimisation of the body to save materials resulting in a total steel mass of about 1100 tons for the supporting body [19,22].

The chosen bottom-fixed reference system is the well-known jacket structure developed in OC4, the follow up project of Offshore Code Comparison Collaboration (OC3) managed by the International Energy Agency (IEA) Wind Task 27 [23]. Typical jacket structures are complex and labour-intensive due to the lattice construction. It is suited for intermediate water depths, beyond the reach of monopiles.

The second bottom-fixed reference is the monopile. It is a simple design compared to the jacket substructure. The steel mass rises sharply for water depths beyond 30 m, affecting the costs and installation procedures. A simplified generic system based on several existing wind farms is developed to obtain an approximation of total substructure mass at a given depth.

4. Underlying conditions

To compute the LCOE for each of the concepts we split the common set of underlying conditions and boundaries into three

Table 1
Site assumptions for the reference wind farm.

Years of development	2013–2018
Year of commissioning	2018
Years of operation	20
Number of turbines	100
Installed capacity	500 MW
Water depth – floating concepts	200 m
Water depth – bottom-fixed concepts	30 m
Distance to port and grid connection	200 km
Average wind speed at hub height	10 m/s
Soil conditions	Homogenous medium clay

[3] Towability: A factor used to describe how easily a concept may be transported at sea. This factor will take into account the need for support vessels, impact of weather conditions, towing resistance and total draft under transportation.

categories; 1) The general reference wind farm, 2) General resources and 3) Vessel specifications.

4.1. General reference wind farm assumptions

It is assumed that installation takes place on a large scale, and that a resourceful company with general offshore experience, able to handle the entire supply chain, rich in both capital and general offshore experience, will handle large parts of the supply chain and operate the wind farms when completed.

Assumptions in Table 1 are used to define the general reference wind farm. The location used is taken as a generic Northern European site. A Weibull probability distribution, derived from Ref. [24] and illustrated in figure 30 of Ref. [4] is utilised to quantify wind speed. Wave loading conditions, where appropriate, is based on the generalised site conditions for the northern parts of the North Atlantic described in Ref. [25].

The 5 MW reference turbine is derived from the well-known generic 5 MW offshore turbine developed by the National Renewable Energy Laboratory (NREL) [26]. A quantification of materials was performed by Raadal et al. [27]. The summarised results are shown in Table 2. The power production is assumed similar to the Repower 5 MW offshore turbine [28] in which the NREL-reference is partly based on and the Power Capacity Factor (PCF) is set to 53 ± 3% for the high- and low sensitivity.

Power output to the grid is substantially less than what one can expect from the capacity factor alone. This is due to several sources of loss, such as wake losses, losses in the power electronics and downtime. The resulting grid output factor is calculated to 44.0%, corresponding to 3859 annual hours of maximum load, based on the values displayed in Table 3, as discussed in Ref. [4], and often referred to as the net Load Factor (LF).

4.2. General resources

The overall consumed resources are simplified and quantified to steel- and fuel consumption as well as needed personnel and commodity resources. One of the main assumptions is that costs for the floater and tower structure can be calculated by evaluating the steel mass only as this covers the majority of the mass in the different structures. However, power electronics, electric cabling and mooring are added separately to the cost calculation.

Steel prices are volatile and vary greatly between countries, locations and other various factors. A base price of € 775 per ton for bulk steel is assumed. Adding to the complexity, there is a variety of different grades, quality and transport options. The base case price, including transport cost, is increased by € 225 per ton to account for Marine quality treated S355 quality steel. The resulting base price is set to € 1000 per ton, accordingly. To account for volatility, the high- and low scenarios are set to ±40%. [4].

During the recent years, bunker fuel cost has experienced as much as 100% fluctuation compared to the average baseline and should be considered as particular volatile. However, the overall fuel consumption cost is found low compared to the operating day-rates of the offshore vessels in question and thereby of less significance. Variation is thereby assumed included in the high- and low scenarios for the vessel costs. A flat fuel cost of € 640 per ton is therefore used in the analysis [4].

Offshore personnel is assumed to work 182.5 days per year with an annual cost of € 67k, resulting in day-rates of € 370 based on discussion in Ref. [4]. High- and low scenarios are set to ±8%.

Table 2
Properties for the generic 5 MW turbine.

Rotor diameter	126 m
Hub height	90 m
Rotor mass	110 tons (of which 54% steel)
Nacelle mass	240 tons (of which 82% steel)
Tower mass	250 tons (of which 93% steel)
Rated speed	11.4 m/s
Operational wind speed limits	3.5–30 m/s
Generator type	Double-fed, asynchronous, 6-pole

Table 3
Overview of the quantified losses to form LF based on the chosen PCF.

Wind farm availability	93.8%
Aerodynamic array losses (wake effects)	7.0%
Electrical array losses	1.8%
Other losses	3.0%

4.3. Vessel specification

Specific vessel costs are limited to vessels in direct use for the three last steps of the project, installation, O&M and decommission. Thus, vessels for weather surveys etc. are not quantified. Due to the contract-based nature of each stage, one distinguishes between installation- and service vessels and appropriate tables listing each category are displayed in Tables 4 and 5 respectively. Installation vessels are also assumed used for the decommission phase.

Additionally, crane vessels for larger maintenance work where larger turbine components are resupplied, Cable-laying vessels or AHTS vessels for cable maintenance, PSVs for component and helicopters for special transport are assumed to be used, but chartered at shorter contracts and are not evaluated as fixed costs [4].

5. Basis for life cycle cost analysis

LCA results for each given phase of the project are calculated before the LCOE approach is applied. Each phase has several quantifiable sub categories presented in Ref. [5]. This section will mainly present the results of the discussion and resulting values from Ref. [4]. Changes and reviewed evaluations will also be presented.

5.1. Development and consenting

The base case D&C was set to an averaged value of € 104,106k, with high- and low scenarios of +20% and −27%, respectively, for the reference wind farm of 500 MW. As there are no available data for deep offshore wind farms, the averaged values were derived from several sources of bottom-fixed sites and will thereby pose some uncertainty. Nevertheless, Fig. 2 shows the assumed distribution of costs for this initial phase.

Table 4
Approximate day-rates, in thousand €, of the different vessels suitable for installation purposes, including mean fuel consumption, excluding labour as discussed in Ref. [4].

Vessel type	Low-case	Reference base-case	High-case
Crane vessel	431	531	631
Inshore crane barge	45	55	65
Jack-up vessel	161	196	231
Anchor handling, tug and supply (AHTS)	81	91	101
Tug boat	16	17	18
Platform supply vessel (PSV)	43	46	49
Onshore mobile crane	5	6	7

Table 5
Annual fixed costs, in thousand of €, for maintenance vessels, including mean fuel consumption, excluding labour as discussed in Ref. [4].

Vessel type	Low-case	Reference base-case	High-case
Specialised maintenance vessel	1850	1900	1950
Mother vessel	12,800	13,100	13,500

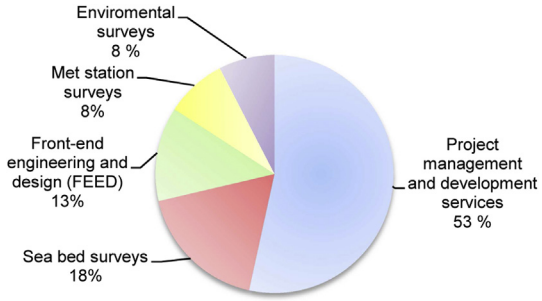

Fig. 2. Development and consenting cost breakdown for the 500 MW base-line farm [4].

For the sensitivity study, it is reasonable to assume that D&C is influenced by the number of turbines to be constructed. Fig. 3 illustrates the utilised cost to number of turbine dependency.

Contingencies are not included for this analysis as this is regarded more of a tool when taking the Final Investment Decision, rather than a basis for the LCOE. The contingency level will also be dependent on the available information. The quality of the available information is described through the sensitivity study and the high- and low scenarios that directly influence the LCOE. For lowered risk, a construction phase insurance is assumed to € 50k per MW based on estimations from Ref. [10]. High- and low scenarios are set to ±10%.

5.2. Production and acquisition

One of the major cost driving components is the turbine. An averaged value of € 7475k is used for the tower and the turbine combined. All of the concepts are in general assumed to use identical turbines and tower configurations. The exceptions are TLB X3, SWAY and the bottom-fixed concepts. The interface between floater and tower is 15 m above the water line for SWAY and 10 m for the other concepts. Correction for changes in zero level for the tower is made by volumetric interpolation with respect to height and is based on the reference turbine tower. The SWAY concept consists of a combined floater and tower. A reduced turbine cost of € 6405k, where the tower is deducted, is employed. High- and low scenarios are set to ±20%.

Table 6
Production cost estimates for the bottom-fixed substructures [4].

	Monopile	Jacket	
		Lattice structure	Piles
Material consumption [tons]	1200	510	315
Material cost [€]	1200k	510k	315k
Manufacturing complexity factor	100%	400%	100%
Manufacturing cost [€]	1200k	2040k	315k
Total production cost [€]	2400k	3180k	

5.2.1. Substructures

Substructures for the bottom-fixed reference systems are based on interpolation of available empirical data as it would require substantial efforts to design specific solutions for the different scenarios in this work. For monopiles, it is obvious that both depth and soil conditions influence the cost substantially. Scaling of available empirical data, with respect to turbine size, is solved by estimated peak thrust forces expected for the relevant rated power. Thus, reference values are all with 5 MW turbine size to obtain an equal reference scenario. The reference monopile-substructure is calculated to a mass of 1200 tons, including the transition piece. The reference jacket at 30 m is developed for the 5 MW turbine with a total mass of 825 tons, where of 510 tons is in the main lattice work and 315 tons is from piles. Costs for the secondary steel components and the transition piece for the jacket are not quantified, but assumed to be included through the complexity factor influencing the fabrication costs [4,29].

In this work, manufacturing costs are evaluated through a complexity factor and related to the bulk steel price. The value reflects not only the complexity with respect to fabrication, but how suitable the design is for mass production. Secondary elements and equipment are also to be included in this factor. Justification and evaluation of these factors for each of the concepts are thoroughly discussed in Ref. [4] and an overview is displayed in Tables 6 and 7. These tables also feature the assessed material masses per floating concept. The masses are results from computations, personal consultations, reverse engineering, experience or a combination of these [4]. It is not possible to disclose all of the material used in the evaluation, but it may be mentioned that no negative feedback has been received from the contacted stakeholders to indicate that any of the concepts are deviating from its specifications.

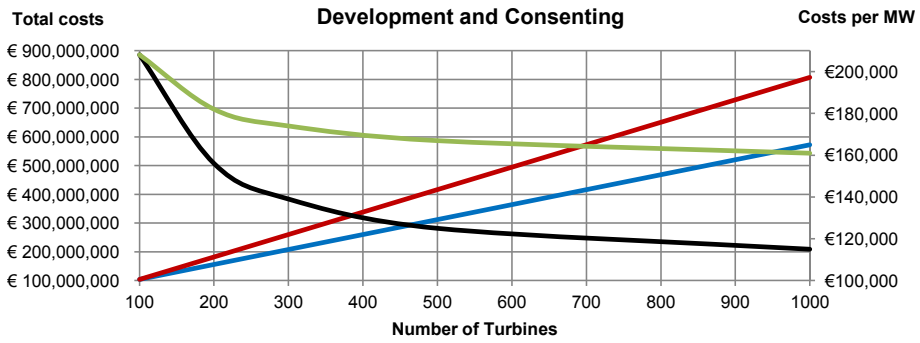

Fig. 3. Illustrating the dependency between farm size and D&C, where the total cost is shown in red (Bottom-fixed) and blue (Floating) (left *y*-axis) and cost per MW is shown in green (Bottom-fixed) and black (Floating) (right *y*-axis). (For interpretation of the references to colour in this figure legend, the reader is referred to the web version of this article.)

Table 7
Production cost estimates for the floating substructures [4].

	TLB B	TLB X3	Hywind II	WindFloat	SWAY	TLWT
Material consumption [tons]	445	521	1700	2500	1100	417
Material cost [€]	445k	521k	1700k	2500k	1100k	417k
Manufacturing complexity factor	110%	130%	120%	200%	150%	130%
Manufacturing cost [€]	489.5k	677.3k	2040k	5000k	1650k	542.1k
Total production cost [€]	934.5	1198.3k	3740k	7500k	2750k	959.1k

5.2.2. Mooring

The perspective of this work is large-scale deployment in soil conditions consisting of medium clay. This somewhat restricts the mooring options. For instance, for one-off constructions, dead-weight anchors may be container shaped and filled with scrap steel as a cheap alternative. This may be acquired at costs down to a tenth of the cost of a high capacity suction anchor. However, the sheer amount of scrap metal needed to moor a wind farm of more than 100 turbines, where the vertical holding capacity is in the range of 500–1000 tons per anchor, is unrealistic. Advanced anchor systems are therefore assumed for all of the concepts. The taut moored TLB concepts each utilise three Vryhof Stevmanta VLAs while the catenary systems of Hywind II and WindFloat make use of similar simpler DEAs of the Vryhof Stevshark type. The TLB X3 features approximately 10% less resulting anchor force compared to TLB B and is adjusted by linear interpolation. The redundant station-keeping system of the TLWT also uses a similar anchor technology. The vertical tendons of SWAY and the TLWT are held by high capacity suction anchors. All of the systems are further described and evaluated in Ref. [4] while the base case for mass estimation and cost is displayed in Table 8. High- and low values are ±25%.

Different mooring lines are utilised for each concept. All of the catenary mooring systems utilise a combination of steel wire and chain while SWAY uses a steel cylinder. Mooring line consumption is dependent not only on the number of anchors and mooring lines, but also depth. Calculating the respective mooring line lengths of the different systems is a complex operation. Thus, some simplifications are utilized. For instance, a linear approximation for growth in wall thickness of vertical tendons is assumed for SWAY. Cost is estimated by bulk price and a complexity factor of 150% ± 25% is used.

For the catenary systems, cost of the chain is approximated to € 250 and 126.5 kg/m at a diameter of 76 mm suitable for both Hywind II and the WindFloat. Correspondingly, a 6 × 41 strand steel wire with a diameter of 61 mm and a mass of 29 kg/m is utilised for these concepts. The estimated base cost of this wire is € 45 per meter. Vertical tendons for the TLWT are assumed of similar type for at a depth of 50 m and are increased linearly in order to maintain vertical stiffness with increasing depth.

Table 8
Baseline costs for the anchors utilised for each concept.

Concept	Type	Mass [tons]	Complexity	Count [n]	Total cost [€]
TLB B	Stevmanta VLA	40	870%	3	1042.5k
TLB X3	Stevmanta VLA	36	870%	3	938.4k
Hywind II	Stevshark Mk5	17	670%	3	342k
WindFloat	Stevshark Mk5	17	670%	4	456k
SWAY	Suction pile	140	1025%	1	1435k
TLWT – taut	Suction pile	50	1025%	3	1537.5k
TLWT – catenary	Stevpris Mk6	3	1833%	3	165k

Table 9
Calculated line lengths for the base case at 200 m depth.

Concept	Total line length [m]	Total line cost [€]
TLB B – upper fibre rope	956	433,987
TLB B – lower fibre rope	811	440,864
TLB X3 – upper fibre rope	956	421,031
TLB X3 – lower fibre rope	811	599,804
Hywind II – steel wire	1800	81,000
Hywind II – chain	150	37,500
WindFloat – steel wire	2640	118,800
WindFloat – chain	200	50,000
SWAY – steel cylinder	101	191,313
TLWT – vertical steel wire	528	35,505
TLWT – catenary steel wire	1980	44,550
TLWT – chain	150	18,750

The TLB systems make use of synthetic fibre ropes that are neutrally buoyant in water. Exponential approximation is utilised to estimate the cost per length of the fibre mooring ropes. The baseline cost per meter is estimated at € $91.681^{0.0113D}$ where D is the desired diameter and assumed applicable in a range of 90–300 mm. At 75 m the following line thickness is used for the upper and lower lines of TLB B and TLB X3 respectively; 0.1416, 0.1495, 0.1388 and 0.1754 m.

The reduced anchor loads for TLB X3 could indirectly lead to a lower mooring line cost, but at significant depths the minimum line stiffness due to eigen frequency requirements governs the line diameter. The TLB system is mainly dependent on the line axial stiffness, thus both the length and cross sectional area scale linearly with depth. The result is a quadratic increase in cost. For the catenary systems, maintaining the stiffness is not as important, and no scaling of the cross section is applied. However, calculating the necessary mooring line length to avoid anchor uplift complicates the calculations severely also for catenary systems. Some approximations are performed to achieve a realistic prediction of the mooring line length for all concepts as further explained in Ref. [4]. Total mooring line lengths and base case costs for the reference wind farm in 200 m of water are shown in Table 9. All high- and low cases for the mooring systems is set at ±25%. The total line length of the TLB system is calculated with a fixed angle of the upper mooring lines of 45°. An additional 25 m per line is added to account for the distance between the seabed and anchor. One may expect that the lower mooring lines would be reduced somewhat in size with increasing depth, due to an increasing vertical component, but this is not accounted for.

5.2.3. Grid connection

It is natural to distinguish between export cables and inter-array cables. The inter-array grid is divided into 20 strands, each accommodating 5 turbines with a 33 kV 300 mm^2 copper core conduction cable. The distance in the reference grid is 1 km between each turbine. Connecting inter-array cable lengths are assumed to be 1.4 km in length. To adjust for the operating water depth, this is added to the length. Based on the evaluation and grid description in Ref. [4] the base case inter array cable cost is set to € 281k/km with high- and low cases at ±15%. Total inter-array cable length for the base case of 100 turbines is approximated to 191.6 km, resulting in a maximal power loss of 0.68% with an average theoretical loss of 0.31%.

The export cables are substantially larger and more expensive than the inter-array cables. This analysis focus on larger distant offshore wind farms and Direct Current (DC) is arguably the better option. For the sensitivity study, the distance to shore is reduced, but Alternating Current (AC) transition will not be considered in order to maintain the overall scenario as argued in Ref. [4]. For the

Table 10
Estimated installation cost for monopile concept wind turbines [4].

Component	Operation	Count	Duration	Unit cost [€]	OW	Total cost [€]
Substructure installation	Quay-side lifts	2.00	0.13	196k	75%	65k
	Transportation	0.22	0.82		75%	47k
	Substructure installation	1.00	2.00		50%	784k
	Stationed personnel	30.0	2.95	370	52%	63k
Turbine installation	Quay-side lifts	1.00	0.17	196k	80%	42k
	Transportation	0.11	0.82		80%	22k
	Turbine installation	1.00	1.20		50%	470k
	Stationed personnel	30.0	2.19	370	54%	45k
Total installation cost per monopile wind turbine utilising a specialised jackup-vessel						1538k

Table 11
Estimated installation cost for jacket-type wind turbines [4].

Component	Operation	Count	Duration	Unit cost [€]	OW	Total cost [€]
Substructure installation	Quay-side lifts	2.00	0.13	196k	75%	65k
	Transportation	0.22	0.82		75%	47k
	Substructure installation	1.00	3.00		50%	1176k
	Stationed personnel	30.0	3.94	370	52%	84k
Turbine installation	Quay-side lifts	1.00	0.17	196k	80%	42k
	Transportation	0.11	0.82		80%	22k
	Turbine installation	1.00	1.20		50%	470k
	Stationed personnel	30.0	2.18	370	54%	45k
Total installation cost per jacket wind turbine utilising a specialised jackup-vessel						1951k

benchmark test, a single 320 kV 1500 mm^2 High-Voltage DC system is used with a baseline cost of € 443k/km. Appropriate cross sections and/or dual cables are chosen for the sensitivity analysis, depending on the optimal solution with respect to optimal values for the LCOE. High- and low values for grid cables are set to ±20%.

When using HVDC, the current is transformed from AC to DC in a substation. There is also a need for stepping up the current to a suitable voltage in order to minimise the losses, in this case from 33 kV of the inter array to the 320 kV in the export system. The total offshore substation cost for a 500 MW unit, not including installation, is approximated to € 143.0 M and € 161.7 M for bottom-fixed and floating wind farms, respectively, as discussed in Ref. [4]. The equivalent onshore recipient is added a cost of € 71.5 M regardless of concept. Where suitable, a 1000 MW unit with an estimated cost of € 235.6 M and € 271.7 M for bottom-fixed and floating solutions is applied, respectively.

5.3. Installation and commissioning

A thorough exploration of the economic aspects of several approaches to installation of the different wind turbine systems was performed in Ref. [4]. For this work, only the approach identified as the optimal solution for each concept will be commented. Wind farm commissioning costs, e.g. the costs associated with finalisation and testing of the wind farms, are assumed included in the presented results.

Table 12
Offshore OW and time consumption for components in the lifting strategies [4].

Component	Time consumption [h]	Maximum operational wind speed [m/s]	OW [%]
Individual rotor blade	4	8	43
Assembled rotor	5	8	43
Nacelle	4	10	58
Tower	6	12	59
Complete turbine	12	7	35

5.3.1. Bottom-fixed installation

The installation operation features a high-capacity jack-up vessel with 4 days of mobilisation time. 15 employees, working 12-h shifts, are assumed required to perform the installation, resulting in a total of 30 workers stationed on the vessel in addition to the vessel crew. Estimated total installation costs for both monopiles and jackets in the benchmark wind farms are shown in Tables 10 and 11, where number of operations, duration in days and Operational weather Windows (OW) are also shown. A vessel capacity of nine main turbine components, i.e. pile, substructure component[4] or turbines is assumed. Three hours per quay-side lift and a transit speed of 11 knots are also assumed.

5.3.2. Floating installation

Several horizontal transportation methods have been suggested to reduce the installation cost of offshore wind power. This includes horizontal transportation of the nacelle and the pre-joining of tower and nacelle [13,19]. It is not evaluated as this is still uncertain concepts and require turbine manufacturers to adapt the turbines significantly. Two main installation strategies were evaluated in Ref. [4]; 1) Assembly inshore, towing of complete turbine and 2) Towing of substructure and assembly offshore. Strategy 2 features both pre-joined turbines and a strategy where floater and tower is pre-joined, and only the turbine is installed offshore. The options of strategy 2 are denoted 2.1 and 2.2 respectively. The main strategies 1 and 2 are further expanded by evaluating five different lifting strategies for each of the components. Appropriate OWs for the components in the expanded set are shown in Tables 12 and 13.

[4] By substructure component it is referred to either pile, transition piece and jacket. The minor foundation piles for the jacket are taken as one substructure component.

Table 13
Concept-depending towing speed and OW for AHTS vessels. Similar assumptions are made for the TLB B, TLB X3 and the TLWT.

	TLB & TLWT		Hywind II		WindFloat		SWAY	
	Speed [knots]	OW [%]	Speed [knots]	OW [%]	Speed [knots]	OW [%]	Speed [knots]	OW [%]
Self-transport	15	90	15	90	15	90	15	90
Towing complete turbines	4.5	45	3	50	5	55	3.5	45
Towing pre-joined floater and turbine	5.4	50	4.2	55	6	65	3.9	60
Towing only floater horizontally	5.9	65	4.6	60	6.5	70		

The most economical viable option was chosen for each concept. Common assumptions for the analysis are the same as for the bottom-fixed concepts in addition to the following remarks:

1. Quay-side launch of floaters treated as one qua-side lift though with an OW of 80%
2. Up-ending of floaters take 12 h with 60% OW, applying to all concepts except WindFloat
3. One AHTS can tow either one complete turbine or two floaters
4. All towing operations are assisted by two tug boats
5. PSV transit speed is 18 knots with OW of 70% with a capacity of three turbines
6. Loading of solid ballast for Hywind II, SWAY and WindFloat is performed inshore by a minor crane vessel with an OW of 60%
7. In general inshore OW are increased by 20% compared to operations performed offshore
8. Time consumption to attach the mooring system is assumed to six hours per line, OW 55%
9. Four hours of mobilisation for the offshore crane vessel between turbines, OW 65%
10. Two hours of mobilisation for the inshore crane vessel between turbines, OW 75%

For all of the concepts, inshore assembly, and turbine assembly in two parts is advantageous. The two-part turbine lift is by complete tower and assembled nacelle with rotor. This implies that it is convenient to assemble most of the major parts on ground level, minimising lifts and the need for larger crane facilities. In general, offshore assembly of the turbines is three to four times more expensive than inshore assembly and towing of the complete structure. The total cost to mount the turbine on the TLB- and TLWT concepts is calculated to € 768k. For Hywind II, WindFloat and SWAY the corresponding cost is € 786k, € 644k and € 655k, respectively.

5.3.3. Mooring system installation

Logistical operation challenges concerning several vessels operating within the wind farm at the same time are not considered and anchors are assumed installed prior to the arrival of each turbine. Turbines are not allowed to share anchors in the economical model.

Anchors for both catenary- and taut mooring systems are installed by a sole AHTS. The detailed process of installing each specific anchor type is described in Ref. [4]. Key assumptions are as follows;

1. Eight hours of installation time for each of the DEA
2. Nine hours of installation time for each of the VLA
3. 12 h of installation time to place one suction anchor
4. 30 min per 100 m of depth is added to the installation time
5. AHTS available deck space for storage of anchors is 630 m^2
6. Available deck space is assumed to decrease by 1 unit per 100 m of depth
7. OW for transit is 75%, while anchor installation OW is set to 60%

One assumes that the DEA and VLA anchors are more suitable for stacking on deck than the cylindrical suction pile anchors. The suction anchors for the TLWT is somewhat smaller than the single large version used for SWAY. However, it also requires three smaller drag embedded anchors. For convenience, it is assumed that the occupied space of one small drag embedded anchor, in addition to the smaller suction pile, equals about half the space occupied by the larger suction pile fitted for SWAY. Further elaboration on the consumption of deck space for each anchor type is discussed in Ref. [4].

5.3.4. Electrical Infrastructure Installation

Electrical infrastructure is quantified in three sub sections; export cables, inter-array cables and the offshore substation. A single trenched export cable is assumed at the high- and low case cost estimations of € 354k/km to € 826k/km. Minimum distance to the wind farm in the sensitivity analysis is 100 km, hence no scale economics are either expected nor implemented in the analysis. The inter-array cables are set to a cost of € 190k/km with high- and low cases at ±10%.

The offshore substation installation is dependent on the choice of foundation. Base cost for the 500 MW units are approximated to € 23.8 M for bottom-fixed wind farms and € 18.6 M for floating, when assuming jacked- and WindFloat (semi-submersible) type foundations. The corresponding values for the 1000 MW unit are € 36.6 M and € 28.5 M, respectively. Assumptions for high- and low cases are discussed in Ref. [4].

5.4. Total capital expenditures

Total CAPEX results for the reference scenario is summarised in Fig. 4.

Total CAPEX for the bottom-fixed turbines in the reference scenario is € 1750–1875 M for the base case. This result is in line with existing generic sources, ranging from € 1800 to 1900 M [30–32]. However, these sources are for wind farms closer to shore than the reference scenarios used for this work, but may feature different interest rates and do also include contingencies, which are not included in this work. Thus, the analysis results seem reasonable with respect to the total CAPEX.

5.5. Operation and maintenance

Calculation and optimisation of O&M and downtime are performed using the OMCE-Calculator, and described in detail in Ref. [4]. One distinguishes between the floating- and bottom-fixed wind farms, but the foundation variation of each is not assumed to influence costs significantly and thereby not evaluated. Three types of O&M-strategies are used in the optimisation; 1) calendar based preventive, 2) condition based preventive and planned

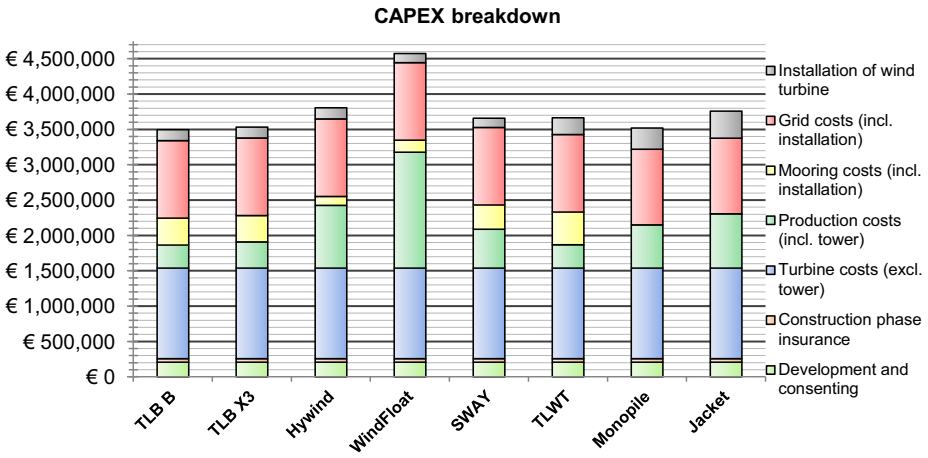

Fig. 4. Base case CAPEX quantification per MW for each concept in the reference scenario.

Table 14
Fixed annual labour cost for the benchmark wind farm [4].

Category	Number of employees	Fixed annual cost [€]	Total annual cost [€]
Offshore O&M technician	60	67k	4020k
Offshore O&M managers	2	118k	236k
Offshore O&M administrative	6	60k	360k
Onshore technical	3	50k	150k
Total annual	82		4766k

corrective, and 3) unplanned corrective. The OMCE-calculator implements opportunity based maintenance strategies.[5] The following assumptions were applied;

1) Annual maintenance of 24 h per turbine with three technicians assisted by small maintenance vessel. A larger preventive maintenance every 10 years is also assumed, requiring twice the time. In addition subsurface inspection every 3 years assisted by a diving vessel is required.
2) Condition based replacement of smaller components with predictable wear is expected to take eight hours by three technicians. Replacement of larger parts is assumed to take twice the resources.
3) All of the operations are expected performed at site. Minor incidents can be repaired without the assistance of a crane vessel, opposed to major repairs, which do. Corresponding expected repair time is 4 and 48 h with the aid of three and six technicians respectively.

The failure rate of subsea cables is expected to 0.1 per 100 km/year, resulting in a wind farm total availability of 97% and 0%, if either an inter-array- or export cable fails, respectively. Based on the results of the OMCE-Calculator, an average of about 870 events per year in category 1 is expected to occur for bottom-fixed and floating respectively. Categories 2 and 3 are independent of foundation and contribute 4 and 120 occurrences, respectively. The total downtime accounts for 54,082 and 58,070 h per year for floating and bottom-fixed wind farms respectively. The total corresponding availability is 93.8% and 93.4% and loss of power production is 143,621 and 155,585 MWh.

[5] Opportunity based maintenance allows maintenance in all categories on several turbines simultaneously, thus reducing the mobilization costs of external vessels.

Table 15
Decommissioning cost in relation to installation cost.

Description	% of installation cost
Complete wind turbine – floating	70
Complete wind turbine – bottom-fixed	80
Subsea cables	10
Substation	90
Mooring systems	90

Insurances for the operating phase are also added to the O&M costs. High- and low cases of € 15–20k/MW are chosen while the base case is set to € 17.5k/MW [4].

5.5.1. Personnel, accommodation and port facilities

This analysis features the choice of a mother vessel, operating within the wind farm through the operational phase. A team of 60 technicians and two managers, in addition to the vessel crew, work rotating shifts on fixed contracts to man the mother vessel. Shifts are 6:00 am to 6:00 pm and maintenance is only initiated if technicians can spend a minimum of 2 h on site. For peak workload scenarios, similar to when performing condition-based maintenance, one assumes additional crew at the rate of € 70 per hour. In addition, an onshore staff of six administrative personnel and three technicians is assumed for the benchmark wind farm. Estimated costs for the different personnel are shown in Table 14.

Short-term storage of supplies and crew accommodation is solved by the mother vessel, though additional port facilities are needed. This cost is assumed to € 2.3 M/year as described in Ref. [4] with high- and low cases at ±11%.

5.5.2. Vessel and equipment requirements

To maintain the offshore wind farm, the following assumptions are made;

Table 16
Distribution of CAPEX, in percent, with respect to year 0 of commissioning [4].

Phase	−4	−3	−2	−1	0	1
Development and consenting	56%	10%	11%	11%	12%	1%
Construction phase insurance	0%	25%	25%	25%	25%	0%
Turbine cost, excluding tower	0%	0%	19%	39%	42%	0%
Production cost, including tower	0%	0%	19%	39%	42%	0%
Mooring costs, including installation	0%	0%	0%	40%	60%	0%
Grid costs, including installation	0%	20%	75%	5%	0%	0%
Installation of wind turbine	0%	0%	0%	36%	64%	0%

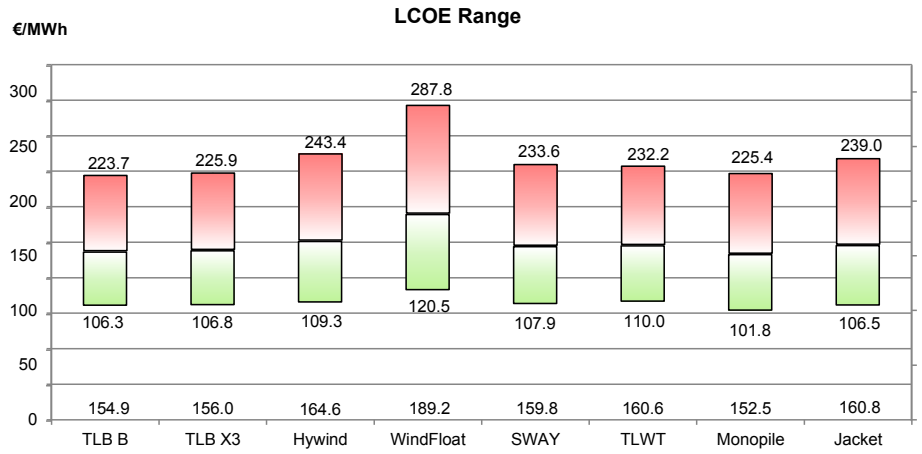

Fig. 5. LCOE for the reference wind farm for each of the concepts with indications on both best- and worst-case scenarios.

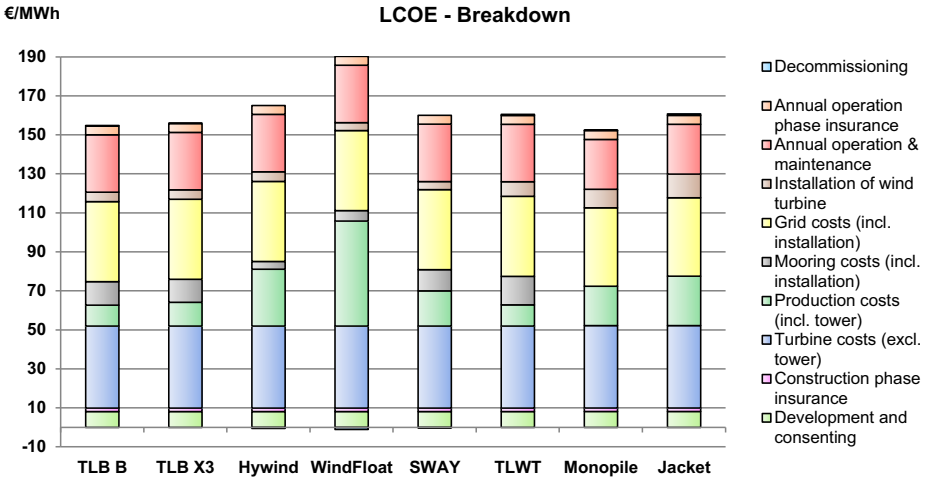

Fig. 6. LCOE cost breakdown for the base case of the reference case.

1. Two specialised maintenance vessels stationed on the mother vessel. Average travel time to turbine is set to one hour and the vessel is able to transport parts of up to 2 tons. Additional similar vessels are chartered, if required, to perform condition based maintenance.
2. Replacement of larger parts requires a larger crane vessel, assumed chartered on the spot market. A specialised maintenance vessel is assumed to assist the operation.
3. Repair of cables is performed by chartering a cable-laying vessel on the spot market. Preventive maintenance on cables is performed with an ATHS that features diving support and ROV.
4. Subsurface inspection and repairs are assumed performed by a diving support vessel chartered on the spot market.
5. Helicopter is chartered to transport technicians when required

The cost of the specialised maintenance vessels is assumed to have a base case price of € 1.9 M/year with ±2.4% as high- and low case. The larger crane vessels needed for maintenance operations is assumed to be somewhat smaller than the ones required for

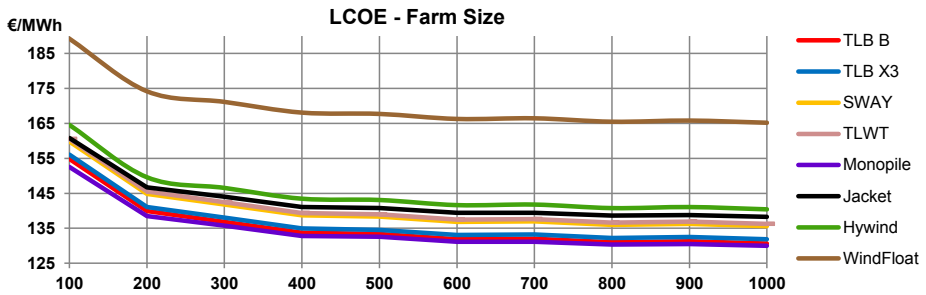

Fig. 7. LCOE changes with increasing number of turbines with the reference wind farm as basis.

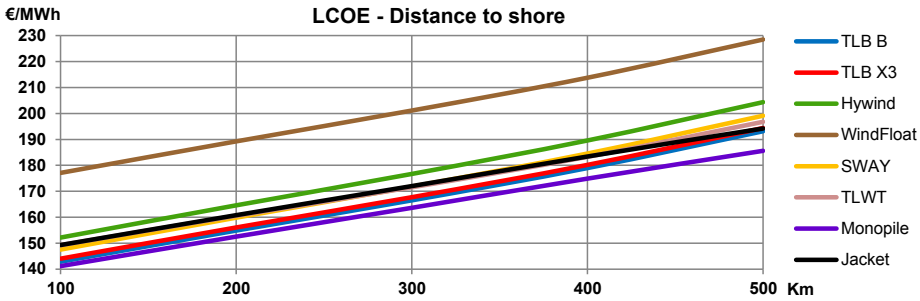

Fig. 8. Change in LCOE with respect to the distance to shore for the reference scenario with base case values.

installation. The cost is assumed to be € 196k/day and € 300k/day for jack-up and a floating crane vessel, respectively. One month of mobilisation is estimated for the larger maintenance vessels and the cost is set to four day-rates.

The total OPEX, including operation phase insurances, are calculated to € 131 and 115k/MW for the floating and bottom-fixed turbines, respectively. Vessel rates for unplanned maintenance seem to account for the majority of the difference. Jack-up vessels, used in the bottom-fixed wind farm, may be chartered for approximately two thirds of the day-rates of comparable floating cranes. The calculated values are somewhat higher than the € 45–50 M/year indicated in Refs. [30–32]. The difference is likely to be a result of the increased distance, influencing maintenance on the export cable, increased transport costs and the introduction of a mother vessel.

5.6. Decommissioning

To simplify the analysis, one assumes that the substructures are not reused, but rather recycled and sold for scrap. Cables are cut below the sea-bed and the remaining inter-connecting lengths are left. A reverse installation process is used to estimate the cost of bringing the components ashore. However it is assumed that this process can be performed simpler and faster. The matrix in Table 15 indicates the assumed decommissioning cost by comparison to the installation.

Linearization of the steel scrap price over the last 13 years result in an averaged estimation of 323.4 €/ton in 2013, and a linearized increase of 17.4 €/year is used to estimate the scrap value at the time of decommissioning. It is apparent that some of the more steel intensive structures may have a negative decommissioning cost.

6. Levelised cost of energy results

The LCOE results are based on the discounted values of CAPEX, OPEX and DECEX before being distributed relative to the energy generation. Additionally, ranges of the high- and low cases are presented. As mentioned earlier it was assumed that the final investment decision is to be taken in 2013 and the operating phase to start five years later, in 2018. CAPEX values are distributed according to Table 16, derived from Ref. [4], where year zero denotes the year of commissioning.

O&M costs are assumed evenly distributed over the 20 years of operation and DECEX are assumed to be distributed 100% at year 21 after commissioning. The following ranges, shown in Fig. 5, for LCOE can then be calculated for the reference wind farm, including the high- and low cases to indicate best- and worst-case scenarios.

For the reference wind farm, where bottom-fixed concepts at 30 m are compared to the floating concepts in 200 m of water, SWAY, TLWT and the TLB concepts are virtually at the same LCOE, considering the analysis accuracy. The large ranges of each high- and low case result in LCOE ranges that span beyond ±50% of the expected base case. Thus, the current spans are too large if one are to get a more reliable prediction to the final LCOE. A review of the high- and low cases is performed to identify which factors contribute the most to the uncertainties. The cost breakdown of the LCOE for the base case values in the reference wind farm is shown in Fig. 6.

The aim of this work was to differentiate the concepts, though a significant part of the breakdown indicates costs that are not concept dependent, such as turbine, grid and O&M.[6] This leaves the production, mooring and installation cost. The more expensive mooring systems of the TLB, TLWT and SWAY indicate similar cost as the installation of bottom-fixed systems. Basically, this implies that installation and production cost of floating concepts should be equal or lower than production cost of bottom-fixed in order to compete. Steel mass, being one of the major contributors to the production cost along with complexity, should therefore be minimised as one can notice for the concepts that are able to compete with the bottom fixed-concepts.

Decommissioning costs are relatively insignificant in perspective to the total LCOE. For Hywind, WindFloat and SWAY they reduce the LCOE as the scrap value outweighs the decommissioning cost and thereby shown in the lower end of the columns in Fig. 6.

It should be emphasised that this is for a site located far offshore which contribute significantly to increase the LCOE through increased grid costs. Further analyses on the sensitivities regarding the reference scenario are conducted in the following sections.

6.1. Farm Size

Fig. 7 shows that increasing the number of turbines to 200 would lower the LCOE by approximately 10% and that semi convergence is achieved from about 600 turbines, resulting in an LCOE reduction of 10–15%. The analysis resolution is per 100 turbines and shifts are observed with change in the utilisation and number of mother vessels and required chartering of vessels. In addition the configuration of substations(s) somewhat influence the result.

6.2. Offshore distance

An increasing distance to shore implies a nearly linear increase in LCOE as shown in Fig. 8. Slight shift in the trend is observed due to the change in transportation distance during installation and

[6] Distance to shore is excluded. In future work, one should strive to distinguish the concepts also with respect to O&M. It is likely that the different geometries will experience independent challenges with respect to availability, specific maintenance, fatigue on turbine, etc.

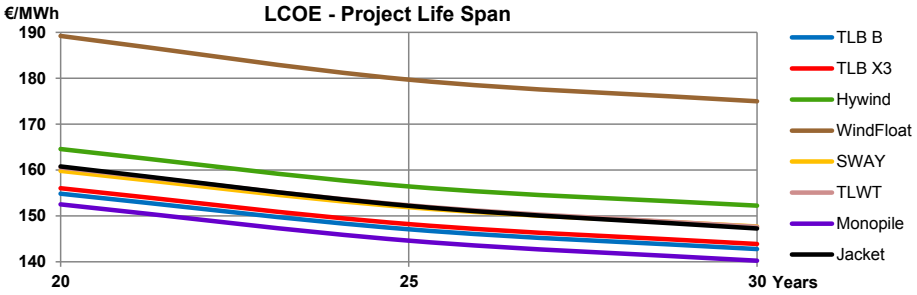

Fig. 9. LCOE changes with offshore distance for the reference scenario with base case values.

rotation of the labour force. Mobilisation times of chartered vessels are not affected by the change in distance. A minimum distance of 100 km is set to maintain a realistic perspective when assuming HVDC connection. The bottom-fixed concepts are less affected by the increasing distance as the installation vessels carry several turbines per trip while the floating concepts need to be towed individually.

6.3. Project life span

Based on the assumptions of this analysis, one expects to find an economical advantage with respect to LCOE when increasing the turbine lifetime to 30 years. The result is plotted in Fig. 9 and the analysis account for increased maintenance, but no increased turbine cost to accommodate the increased lifetime. A reduction is observed with increasing lifetime, though the effect is reduced when closing up to 30 years. The amount of increase in the wind turbine cost is uncertain, but not likely to outweigh the advantages of an increased lifetime to 25 years. When increasing the lifetime to 30 years, it is reasonable to assume that there will be no gain when accounting for the increased investment cost. It should also be noted that increased lifetime also increases the probability of severe weather conditions, which in turn may also influence the overall material consumption in the substructures. A more thorough assessment is necessary in order to evaluate if increased lifetime is beneficial.

6.4. Water depth

One of the parameters expected to distinguish the different floater concepts is the change in water depth and the corresponding changes of the mooring systems. Especially the TLB systems are sensitive to depth, as the effective stiffness at the fairleads and angle of the mooring lines have to be maintained. The results are shown in Fig. 10.

The catenary mooring systems produce an increased LCOE when moving into shallower waters as the mooring line length increases [4]. The mooring system of the TLWT should be more robust than the SWAY system as the depth increases. This is not showing in the analysis due to simplifications in the mooring system of SWAY. The dimensions of the mooring column for SWAY are not likely to be a result of maintaining the stiffness conditions, but also increasing loads. Another issue, not being addressed, is increasing installation complexity for SWAY as this rigid column increases in length and thickness. Using only stiffness determined mass growth by depth and no additional modification to installation cost is considered severely conservative, especially for increasing depths above 200 m.

When comparing with monopiles, the TLB systems are the only floating concepts being able to produce a competitive LCOE. The LCOE of the floating systems all increase with depth, but at a far slower rate than for the bottom-fixed systems. In general, concepts with low steel-mass perform the best in shallow depths, while concepts of larger steel mass become more optimal with increasing depths. This indicates positive trade-offs for more complex mooring systems in shallower waters in order to reduce total production cost.

Both TLB concepts, SWAY and the TLWT perform better than the comparable jacket concepts in waters below about 250 m. The Hywind system is also comparable, but at a slightly higher level before achieving an advantage in deeper waters of 4–500 m. Due to large steel mass and high production costs, the WindFloat concept is relatively expensive, but also experience minimal increase in cost with increasing depths. The TLB X3 system has 10% reduced anchor

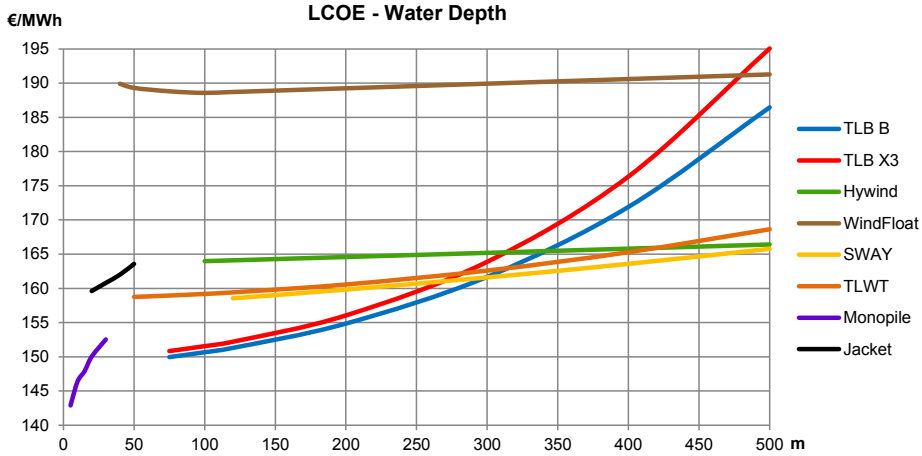

Fig. 10. LCOE changes with depth for the reference scenario with base case values.

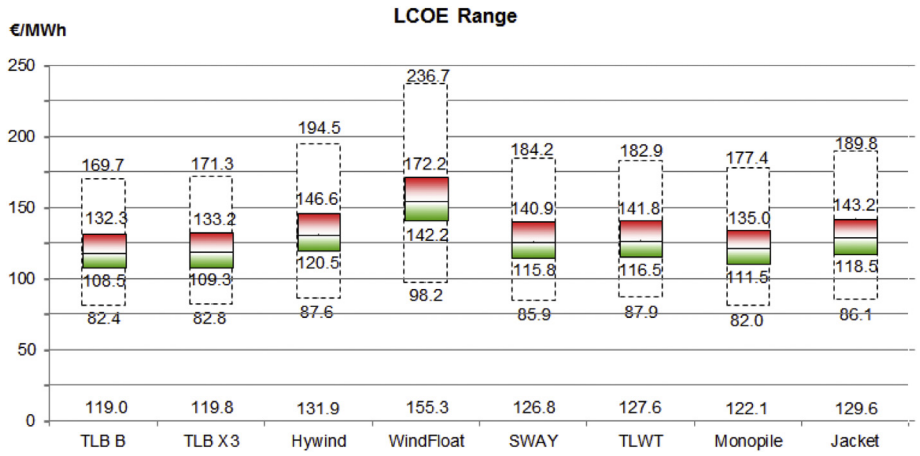

Fig. 11. LCOE for the optimised reference wind farm. All high- and low cases included (dotted lines), while the reduced intervals are shown in colour.

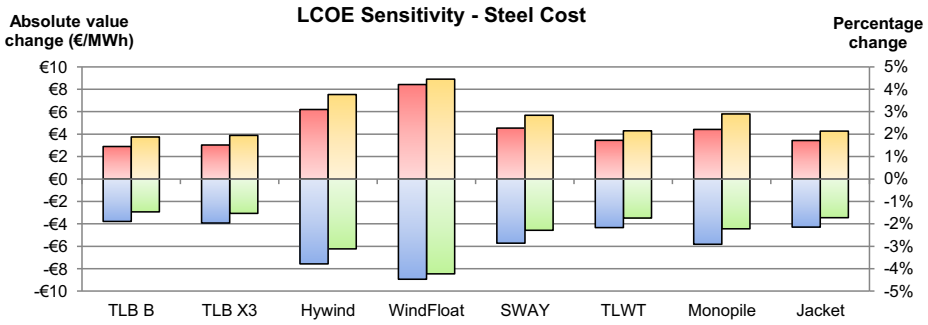

Fig. 12. Indicates influence of the high- and low cases of steel cost on each concept. Columns in yellow and blue are represented in percentage on the *y*-axis on the right side. (For interpretation of the references to colour in this figure legend, the reader is referred to the web version of this article.)

loads compared to TLB B. However, this does not reduce the mooring costs enough to accommodate the additional complexity featured by its space-frame section. Additionally, the TLB X3 demands somewhat higher mooring line stiffness as a result of reduced stiffness in the space-frame. Due to the scaling effects with depth to maintain the correct axial mooring line stiffness, the distance between LCOE of TLB B and TLB X3 increase with increasing depths.

6.5. Optimised results

The reference case is not particularly suitable to estimate the LCOE of wind energy. Optimised site conditions for each of the concepts are therefore utilised to better describe this, and to further quantify the sensitive cost contributors. An optimised reference wind farm is assumed, consisting of 300 turbines with 25 years lifetime and a location 100 km offshore. Monopile depth is 5 m, jacket depth is 20 m, while the TLWT, TLB systems, SWAY and catenary systems are located at depths of 50, 75, 120 and 100 m, respectively. The LCOE is lowered by 30–40%, compared to the base scenario, and is shown in Fig. 11. The following assumptions were made:

1. D&C, insurances, turbine cost, production cost, mooring system acquisition cost and electrical component costs are expected to be known, thus kept at base case level.
2. The high- and low cases of capacity factors and availability is reduced to ±1%
3. Short term vessel contracts can be acquired at fixed price, i.e. installation costs are fixed at base case values, while O&M- and decommission costs are unchanged

The monopoles and TLBs have the lowest costs. The differences up to the other concepts are small, considering the remaining uncertainty of roughly ±10%. Only a minor part of these are concept dependent, as shown when cost drivers are quantified further in the next section.

6.6. Quantified cost drivers

The results of the reference wind farm analyses indicate that the cost of the export cable is a major component of the LCOE. High- and low cases, altering the cost per meter, indicate a potential increase of about 6% or a reduction of about 13%. The overall vessel cost contributes surprisingly little, much due to the fact that the installation step contribute relatively little to the overall LCOE. High- and low cases result in changes of about 2–2.5% change in LCOE. The influence on steel cost is dependent on concept, where the steel intensive are more sensitive and shown in Fig. 12.

The overall influence of the steel price is still relatively low, at around 2% for the concepts with low steel mass. Figs. 13 and 14 show that the importance of accurate prediction of the load factor and the set discount rate sensitivities influence the LCOE in the range of about ±10% for the high- and low cases. The high- and low cases for Load Factor indicate a corresponding increase of 9.8–10.7% or a decrease of 7.3–7.9% of the LCOE. However, it is

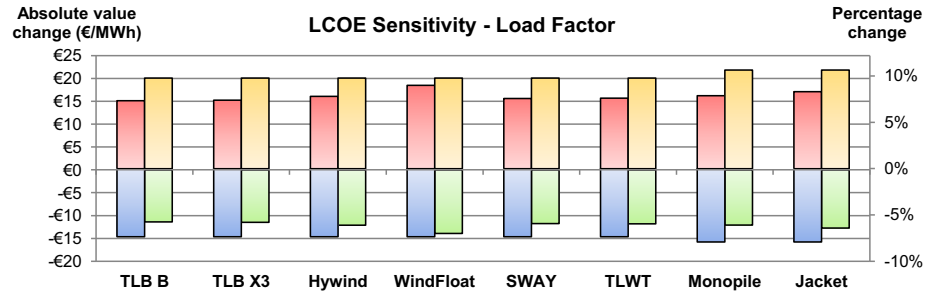

Fig. 13. Indicates influence of the high- and low cases for change in load factor on each concept. Columns in yellow and blue are represented in percentage values on the *y*-axis on the right side. (For interpretation of the references to colour in this figure legend, the reader is referred to the web version of this article.)

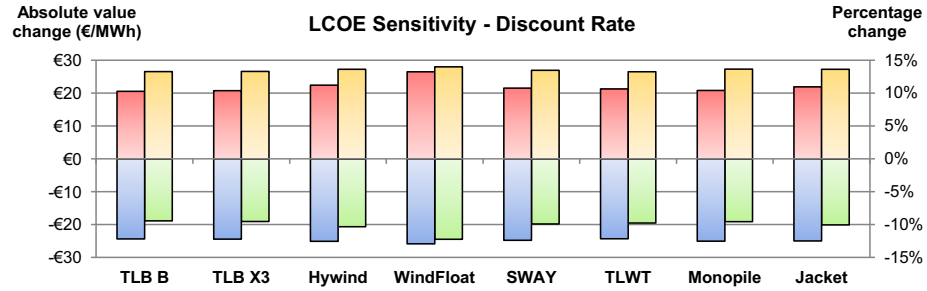

Fig. 14. Indicates influences of the high- and low cases for the discount rate of each concept. Columns in yellow and blue are represented in percentage values on the *y*-axis on the right side. (For interpretation of the references to colour in this figure legend, the reader is referred to the web version of this article.)

important to keep in mind that, the suggested high- and low cases for the load factor is based on both low quality supplier details and scarce weather information. In a realistic case, local weather surveys and detailed supplier contracts will reduce the variation considerably.

The discount rate is pre-set and in such terms not a subject of uncertainty. However, it is an interesting point that the initial high- and low cases of ±2% contribute with an increase of 13.3–14.0% or and decrease of 12.2–12.9% of the LCOE, making the capital intensive and long lifetime offshore wind farms sensitive to expected capital return.

7. Concluding remarks

The results indicate that energy from floating wind turbines, in comparison to bottom-fixed concepts, may be produced at equal or lower LCOE. Several key cost driving aspects have been identified for both bottom-fixed and floating wind farms. One can distinguish between site dependent and thereby predictable aspects and uncertain aspects. Of the predictable aspects, discount rate, distance from shore, farm size and depth is of the highest sensitivity to the LCOE. Of the more uncertain aspects, accuracy of load factor and variation in steel price is two of the main factors most influential to distinguish the foundation concepts.

Optimised conditions for all the concepts were identified. General aspects indicate that farm sizes of 400–500 turbines as close to shore as possible is beneficial. This is due to the fact that the sheer size allows for larger specialised support and maintenance vessels to operate solely in the wind farm. Based on the optimised results, one can also assume the optimal turbine concept for each water depth. The current findings indicate that the TLWT should be used in its deployable operating depth of 40 m and up to 75 m where the TLB systems can be installed. The increasing mooring costs with depth for the TLB system allow the TLWT and SWAY to be more cost effective solutions from about 300 m of depth. SWAY and the TLWT are comparable at all depths, but there are reasons to assume that the mooring costs of SWAY, especially for depths exceeding 200 m, to be optimistic.

In general, the concepts with the lowest steel mass have the best performance with respect to LCOE. This is also apparent with increasing depth, where the concepts of lowest mass reach optimum at an early stage, before a concept of larger mass takes over with increasing depth. This may indicate a trade-off between steel mass and mooring costs.

It is apparent that even if the lattice cross-section of TLB X3 reduces the anchor loads, there is no reduced cost for the mooring lines as they are determined by stiffness conditions rather than peak loads. Thus, there is no significant reduction in LCOE by initiating this measure. However, this may not be the case for a different site or turbine size, but indicates that the focus should be to reduce the demand for line axial stiffness in order to compete in deeper waters.

The overall performance of the analysis is robust, and the reference results for the bottom-fixed concepts are found in line with available literature. However, improvements are needed in order to further quantify anchor costs, and one should implement different mooring options and soil conditions. Further work is suggested on the implementation of cost saving potentials and scaling effects, especially for mass produced components like turbines, mooring lines and anchors. Further investigation is also suggested on effects such as turbine lifetime extension.

Additionally, further work should be considered in order to ensure that each of the compared concepts is optimised for equal weather and site conditions. This is especially important for the concepts of low steel mass, where small changes separate the results of each concept.

References

[1] Iuga D. Contribution of wind power to electricity generation and generation capacity in the EU-27. Belgium: European Wind Energy Association; 2013 [chapter 3].

[2] EWEA. Wind energy – the facts: a guide to the technology, economics and future of wind power; 2009. London, UK.
[3] Borgen E. In: Briefings LT, editor. Floating wind power in deep water – competitive with shallow-water wind farms?; 2010.
[4] Bjerkseter C, Ågotnes A. Levelised cost of energy for offshore floating wind turbine concepts. Department of Mathematical Sciences and Technology, University of Life Sciences; 2013. p. 206.
[5] Shil NC, Parvez M. Life cycle costing: an alternative selection tool. J Bus Res 2007;9:49–68.
[6] Kawauchi Y, Rausand M. Life cycle cost (LCC) analysis in oil and chemical process industries. Trondheim: Norwegian University of Science and Technology; 1999.
[7] Gielen D. Renewable energy technologies: cost analysis series – wind power. In: Gielen D, editor. IRENA working paper. International Renewable Energy Agency (IRENA); 2012.
[8] Tegen S, Hand M, Maples B, Lantz E, Schwabe P, Smith A. 2010 cost of wind energy review (Technical report NREL/TP-5000-52920); 2012.
[9] Liebreich M. Bloomberg new energy finance summit. In: Bloomberg new energy finance, the future of energy summit 2013, New York, USA; 2013.
[10] P. (PVC). Offshore wind cost reduction pathways study. In: Finance work stream. London, UK: The Crown Estate; 2012.
[11] Howard R. Offshore wind cost reduction pathways project – simple levelised cost of energy model. London, UK: The Crown Estate; 2012.
[12] Delay T, Jennings T. Offshore wind power: big challenge, big opportunity. London, UK: The Carbon Trust; 2008.
[13] Copple RW, Capanoglu C. Tension leg wind turbine (TLWT) conceptual design suitable for a wide range of water depths. In: International offshore and polar engineering conference. Rhodes, Greece: International Society of Offshore and Polar Engineers (ISOPE); 2012.
[14] Robertson AN, Jonkman JM. Loads analysis of several offshore floating wind turbine concepts. In: International offshore and polar engineering conference (ISOPE). Maui, Hawaii, USA: International Society of Offshore and Polar Engineers (ISOPE); 2011.
[15] Weinstein J, Roddler D. WindFloat – a floating support structure for large offshore wind turbines. In: European wind energy conference & exhibition 2010, Warsaw, Poland; 2010.
[16] Myhr A, Nygaard TA. Load reductions and optimizations on tension-leg-buoy offshore wind turbine platforms. In: The twenty-second (2012) international offshore and polar engineering conference. Rhodes, Greece: International Society of Offshore and Polar Engineers (ISOPE); 2012.
[17] Myhr A, Maus KJ, Nygaard TA. Experimental and computational comparisons of the OC3-HYWIND and tension-leg-buoy (TLB) floating wind turbine conceptual designs. In: International offshore and polar engineering conference. Maui, Hawaii: International Society of Offshore and Polar Engineers (ISOPE); 2011.
[18] Sclavounos P, Tracy C, Lee S. Floating offshore wind turbines: responses in a seastate Pareto optimal designs and economic assessment. Department of Mechanical Engineering, Massachusetts Institute of Technology (MIT); 2007.
[19] Moss DW, Myhr A. Concept for installation of floating offshore wind turbines. Department of Mathematical Sciences and Technology, University of Life Sciences; 2009.
[20] Nygaard TA, Myhr A, Maus KJ. A comparison of two conceptual designs for floating wind turbines. In: European offshore wind conference & exhibition, Stockholm, Sweden; 2009.
[21] Byklum E. In: Bjerkseter C, editor. Personal correspondence with Eirik Byklum in Statoil ASA regarding Hywind properties; 2013.
[22] Jorde J. In: Ågotnes A, editor. Personal correspondence between Jørgen Jorde from Inocean/SWAY AS. Bergen/Ås: Inocean/SWAY AS/Jørgen Jorde; 2013.
[23] Jonkman JM, Musial W. Offshore code comparison collaboration (OC3) for IEA task 23 offshore wind technology and deployment. USA: National Renewable Energy Laboratory; 2010.
[24] Bierbooms W. Offshore wind climate. In: 0E5662 offshore wind farm design. Delft University of Technology; 2010.
[25] Faltinsen OM. Sea loads on ships and offshore structures. Cambridge University Press; 1990.
[26] Butterfield S, Jonkman JM, Musial W, Scott G. Definition of a 5-MW reference wind turbine for offshore system development. Washington DC, USA: National Renewable Energy Laboratory; 2009.
[27] Raadal HL, Vold BI, Myhr A, Jonkman JM, Robertson AN, Nygaard TA. GHG emissions and energy performance of offshore wind power. Renew Energy; 2013 [in press].
[28] REpower Systems. In: Systems R, editor. 5M the 5-megawatt power plant with 126 metre rotor diameter. http://www.repower.de/fileadmin/download/produkte/RE_PP_5M_uk.pdf; 2013.
[29] Popko W, Vorpahl F, Zuga A, Kohlmeier M, Jonkman J, Robertson A, et al. Offshore code comparison collaboration continuation (OC4), phase I – results of coupled simulations of an offshore wind turbine with jacket support structure. In: I.S.o.O.a.P.E. (ISOPE), editor. The twenty-second (2012) international offshore and polar engineering conference. Rhodes, Greece: International Society of Offshore and Polar Engineers (ISOPE); June 17–22, 2012.
[30] Douglas Westwood. Offshore wind assessment for Norway. Aberdeen: Douglas Westwood; 2010.
[31] Scottish Enterprise. A guide to offshore wind and oil & gas capability. Glasgow, Scotland: Scottish Enterprise; 2011.
[32] The Crown Estate. A guide to an offshore wind farm. London, UK: The Crown Estate; 2010.

Appendix 6

Journal of Ocean and Wind Energy (ISSN 2310-3604)

Vol. 1, No. 4, November 2014, pp. 217–224

http://www.isope.org/publications

Experimental Results for Tension-Leg-Buoy Offshore Wind Turbine Platforms

Anders Myhr
Department of Mathematical Sciences and Technology, Norwegian University of Life Sciences (NMBU)
Ås, Norway

Tor Anders Nygaard
Energy Systems Department, Institute for Energy Technology (IFE)
Kjeller, Norway

Several simulation tools for analysis of offshore wind turbine dynamics are under development. However, there are limited experimental data available for validation. This paper presents wave trials for three different Tension-Leg-Buoy (TLB) systems at scale 1:40. The presented results include decay tests, plus regular and irregular wave trials. Data are displayed using Response Amplitudes Operators (RAO). Both the model geometries and test setup are described in detail. The time series of the results will be made available to the offshore wind community in order to contribute to further development and validation of offshore wind turbine simulation tools.

INTRODUCTION

The application of bottom-fixed turbines is currently moving from the test phase, where turbines are counted by the tens, into large-scale deployment by the hundreds. Floating offshore turbines have yet to move from the prototype stage and into large-scale deployment, but several types of platforms are currently in different stages of development. Sufficient stability to support the wind turbine can typically be achieved by ballast, buoyancy, mooring lines, or by a combination thereof. Examples include Hywind, a full-scale 2.3 MW spar buoy, WindFloat, which features a semisubmersible platform active ballast system, the 1:6 prototype Sway, and several different Tension-Leg-Platform (TLP) and Tension-Leg-Buoy (TLB) systems, as discussed by Robertson and Jonkman (2011), Weinstein and Roddier (2010), Copple and Capanoglu (2012), Myhr and Nygaard (2012), and Jonkman and Matha (2011).

To investigate the potential for large-scale deployment of offshore wind turbines, Simulation Tools (STs) capable of predicting the dynamic performance of the various concepts are needed. Extensive work has been performed in order to develop both existing and new STs for this purpose in the IEA project Offshore Code Comparison Collaboration (OC3) (Jonkman et al., 2010) and the follow up project OC4 (Popko et al., 2014). However, the approach in OC3 and OC4 has so far been verification through comparison in order to perform a stepwise approach, but also due to lack of experimental data. Recent validation of the code FAST for a TLP (Stewart et al., 2012) illustrates the need for experimental data to validate the STs. Validation of the STs should ultimately be performed on full-scale systems. However, wave tank trials in confined basins are attractive due to several aspects: the controlled environment, lower costs, and the opportunity to test different concepts under similar conditions.

The mooring-stabilized TLB systems are known for their low steel mass and stiffness-controlled dynamic response. The TLB was first introduced as a platform for wind turbines under the name MIT Double Taut Leg by Professor Sclavounos of the Massachusetts Institute of Technology (Butterfield et al., 2007; Sclavounos et al., 2010). Taut axial mooring lines are utilized to stabilize the turbine and to control the eigen periods, which are all to be less than 4–5 s, while also avoiding the rotor periods and other relevant periodic loading. Tension in the six mooring lines is achieved through excess buoyancy in the floater, and safe operation is dependent on tension in all of the mooring lines at all times to avoid snap loads. Therefore, design of TLB systems is dependent on accurate STs capable of computing the complex dynamic response of an elastic body subjected to irregular loading from both wind and waves. Subsequent work on the TLB systems includes application examples (Nygaard et al., 2009; Sclavounos et al., 2010; Tsouroukdissian et al., 2011), comparisons between a wave tank test and computations (Myhr et al., 2011), and optimization of TLB systems (Myhr and Nygaard, 2012).

APPROACH

The experiment had two main goals: (1) To further investigate the dynamic performance of TLB systems, and (2) to obtain and share high quality data on scaled floating offshore wind turbines for further development of simulation tools. Three geometries were selected and designed (Fig. 1) to cover both inertia- and drag-dominated loading, as well as aspects related to measures for reduced wave loading.

The Deep Wave Basin of 12.5 m by 50.0 m at the IFREMER facilities in Brest was made available for two weeks to conduct the wave trials. The depth range was 10 to 20 m with maximum wave height (H_{max}), crest-to-trough, of up to 0.5 m. Recent works and optimization shown by Nygaard et al. (2009), Myhr et al. (2011), and Myhr and Nygaard (2012) on the TLB systems indicate that an angle between 35 and 50 degrees between the upper mooring lines and the seabed is optimal. Together with the need for absolute control of the mooring points, it was decided to use a surface-mounted, pre-tensioned structure with a small footprint in order to fix the mooring lines at a significantly shallower and more accessible depth of a few meters.

This allowed for high-precision load cells (FLINTEC Type SB6) to be mounted above water, and the axial loads of all the mooring lines could be measured in the vertical direction after passing through a pulley system at the desired mooring point. The vertical mounting was also necessary to practically mount precision linear

Received July 24, 2014; revised manuscript received by the editors October 10, 2014. The original version was submitted directly to the Journal.
KEY WORDS: Offshore wind turbine, experimental results, Tension-Leg-Buoy (TLB), taut mooring, space-frame.

prototype actuators, based on the LINAK LA23, to remotely control the pre-tension of each mooring line. Each mooring line ran from the floater down to the anchor point pulley and vertically upward to a special coil spring concept with adjustable stiffness. The spring/load-cell actuator system allowed convenient manipulation of the stiffness in each mooring line. Both the load cells and the actuators should ideally be located within the model for full-scale systems, but to increase the model accuracy, it was moved to the opposite, static end of the mooring lines. The in-house Qualisys motion tracking system was used to capture motions at the top of each model.

The models selected for the test, TLB B and TLB X3 (Fig. 1), are based on previous development by Myhr and Nygaard (2012) and optimized for a site in harsh weather conditions. However, the mooring line configuration was adapted on-site to ease the experimental setup with regards to the available facilities at IFREMER. Therefore, the dynamic response shown in this experiment does not represent a well-designed full-scale system, but should nevertheless be suitable for STs validation. To increase model accuracy and ease fabrication, some modifications and simplifications were made on the original designs. In addition, a simplified reference model, the TLB S, was introduced. It consists of a uniform rigid cylinder with draft and mooring points similar to TLB B and TLB X3. It can be represented in STs with little effort.

Previous testing by Myhr et al. (2011) revealed that the scale 1:100 was challenging due to the elastic behavior and the relatively small motions of the TLB systems. Due to the low mass of the full-scale systems, accurate 1:100 models were also fragile, expensive to fabricate, and cumbersome to represent in STs. Therefore, it was decided that the models should be as large as possible and fabrication methods should favor easy modeling in the simulation tools for increased accuracy. The upper limit was determined by the extent of the basin and its wave-making capabilities. Larger models would include a wider and deeper mooring setup and a lowering of the relative wave height, thus reducing the forces acting on the model. As a compromise, the scale was set to 1:40.

Digital signal data from the Qualisys system and analog signal data from the load and wave sensors were recorded at 100 Hz by Labview. The central tracking and reference point is located 157 mm above the top level of each model. The mass of the optical tracking system was measured at 82 g and is assumed to be evenly distributed from the top level of the model down to the reference tracking height. Tuning of the models in the basin was done prior to the tests. This included tuning of the mooring system to ensure correct neutral position, buoyancy, orientation, mooring line stiffness, and pre-tension. The mooring line stiffness was tuned based on eigen-period computations performed by Myhr and Nygaard (2012), but deviating somewhat due to discrepancies in mooring radius. Verification that the longest of the eigen periods corresponds to 5 seconds in full-scale was performed to ensure when we could provoke resonant behavior during the trials.

The results for the wave trials are presented by the use of Response Amplitude Operators (RAO). Additionally, video was recorded by a high definition (HD) camera mounted at the side of the basin, close to the top height of TLB B and TLB X3. A second video feed from a submerged camera somewhat downstream was also recorded. Wave gauges were placed both upstream and to the side of the models.

EXPERIMENTAL SETUP

The structure supporting the mooring system, sensor equipment, and actuators was based on extruded square aluminium lattice profiles of 0.2 m by 0.2 m-type Mast 4420 from Lattix AS. The selected towers feature high transparency, resulting in low wave reflection. Three towers were used, one for each pair of mooring lines spaced every 120 degrees around the model, with one located directly downstream. To maintain the correct position of the anchor points, three distance-wires were secured in the horizontal plane between the anchor points. The distance-wires were pre-tensioned by connecting two additional wires at each tower, inline with the distancing wires, and fixating them at the surface. The final mooring point positions are shown in Table 1, with the x-axis in the wave direction. The lines are distributed in a clockwise

	Number	X [m]	Y [m]	Z [m]
	1	3.835	0.030	−1.868
Lower lines	2	−1.891	−3.336	−1.868
	3	−1.943	3.306	−1.868
	4	3.835	−0.030	−1.868
Upper lines	5	−1.943	−3.306	−1.868
	6	−1.891	3.336	−1.868

Table 1 An overview of the final mooring point location

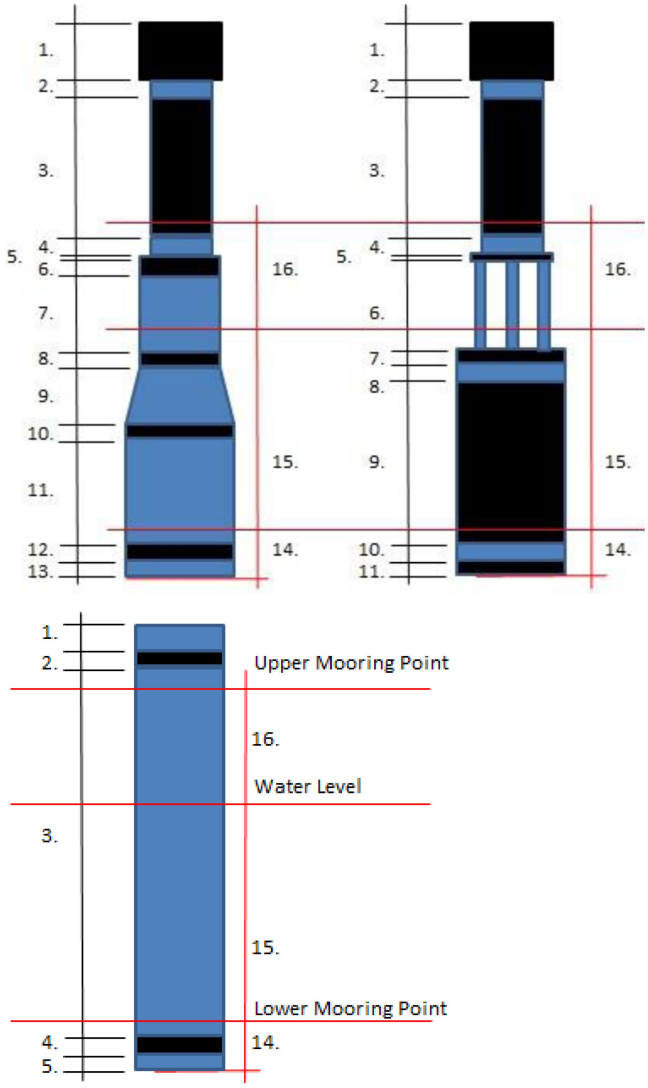

Fig. 1 Individual sections of the geometries for (a) TLB B, (b) TLB X3, and (c) TLB S. The reference system has origin in the centerline at the still water level.

direction from the bottom up with lines 1 and 4 downstream on the tower.

Models

To increase the quality of the recorded data, a significant effort was made to simplify the TLB conceptual original models developed by Myhr and Nygaard (2012), which, in turn, were based on the NREL 5MW reference turbine developed by NREL (Jonkman et al., 2009). Several compromises were made to achieve robust, durable, and predictable models with a reasonable distribution of stiffness and masses, while retaining solutions that could be implemented in the simulation models with ease and high accuracy. The RNA was simplified by the use of a lump mass, and the center of mass was located along the central axis of the turbine. This allowed for module-based, precision-engineered, multi-material models, where TLB B and TLB X3 share the same tower to reduce model discrepancy. Polycarbonate, polyvinyl chloride (PVC), and various aluminium compounds were chosen for the main structure. Data supplied are based on product sheets. A detailed overview of the models is shown in Figs. 1a, 1b, and 1c with corresponding section descriptions in Tables 2, 3, and 4, respectively.

Section 1 replaces the total mass of the NREL 5MW RNA assembly, but yaw inertia is not preserved, as there is no physical rotor attached. Sections 1 to 4 for TLB B and TLB X3 are identical, as they utilize the same tower. The tower was fitted to the floater by tightly fitted, fine-threaded connectors. The remaining connections were glued with appropriate epoxy-based adhesives or cyanoacrylate upon receiving a thick coat of water-resistant paint. Glued connections overlapped by 10 to 20 mm to ensure sufficient surface area for the glue to achieve a safe transition.

Mooring Lines

Three mooring lines, spaced at 120 degrees in the horizontal plane, were attached at each mooring height. The axial stiffness was significantly higher than the scaled mooring line stiffness in order to accommodate compliance from transition changes, mooring line terminals, and connectors. In addition, it was also convenient to have some room for final tuning of the spring system. One-millimeter multistring stainless steel wire was used for the mooring line. Tuning of the mooring lines was done by using the actuators to enforce known displacements while monitoring the loads and adjusting the springs. The resulting line stiffness for each mooring line is shown in Table 5.

Calibration of the lines was performed by arresting the end of each mooring line while connected to the pre-tensioned towers and pulley system, and with all the connectors and terminals installed. Thus, any stiffness compliance from the installation rig should be included. The pre-tension in the mooring lines is shown in Table 6. Sufficient pre-tension in each mooring line is essential in order to achieve correct neutral position and to avoid snap loads.

During the installation of TLB B, one of the mooring lines failed. There was no visible damage to the equipment, but a recalibration of the load sensors post-experiment indicated a slight offset in the zero level in one of the sensors. The results have been updated

TLB B Item	Length [mm]	D outer [mm]	Thickness [mm]	Mass [g]	E-mod [Mpa]
1	83.7	162.5	81.3	4681	69000
2	20.0	150.0	75.0	832	69000
3	1780.0	150.0	4.0	3922	2380
4	20.0	150.0	9.0	170	69000
5	5.0	160.0	17.0	120	69000
6	20.0	160.0	10.0	159	69000
7	843.0	160.0	5.0	3174	3275
8	20.0	160.0	8.0	154	69000
9	123.0	NA	4.5	1201	69000
10	18.0	298.3	5.5	276	69000
11	582.0	298.3	2.5	3877	69000
12	10.0	298.3	5.5	102	69000
13	7.0	297.0	148.5	745	69000
14	33.0	360.0		126	
15	1217.0				
16	646.0	210.0		66	

Table 2 Geometry description of TLB B

TLB X3 Item	H [mm]	D outer [mm]	Thickness [mm]	Mass [g]	E-mod [Mpa]
1	83.7	162.5	81.3	4681	69000
2	20.0	150.0	75.0	832	69000
3	1780.0	150.0	4.0	3922	2380
4	20.0	150.0	12.8	213	69000
5	4.0	200.0	37.8	640	69000
6	576.0	22.0	3.0	837*	69000
7	5.0	260.5	130.3	1021	69000
8	8.0	261.0	4.5	96	69000
9	1025.0	261.0	2.5	5959	69000
10	8.0	261.0	4.5	88	69000
11	5.0	260.5	130.3	577	69000
14	35.0	321.0		66	
15	1217.0				
16	645.0	210.0		66	

*The summarized mass of the three rods used in the space frame

Table 3 Geometry description of TLB X3

TLB S Item	H [mm]	D outer [mm]	Thickness [mm]	Mass [g]	E-mod [Mpa]
1	3.0	250.0	125.0	216	2380
2	5.0	250.0	125.0	237	2380
3	1824.0	250.0	5.0	7956	2380
4	5.0	250.0	125.0	240	2380
5	3.0	250.0	125.0	218	2380
14	40.0	310.0		90	
15	1054.0				
16	717.0	310.0		90	

Table 4 Geometry description of TLB S

	1	2	3	4	5	6
TLB B & S	2.899	2.842	2.870	2.341	2.320	2.299
TLB X3	2.494	2.479	2.425	2.312	2.325	2.234

Table 5 Showing line stiffness calibration values in N/mm

	Line 1	Line 2	Line 3	Line 4	Line 5	Line 6
TLB B	164.80	164.10	159.70	188.89	184.26	178.66
TLB S	200.73	195.14	197.14	184.79	177.58	179.66
TLB X3	149.51	147.99	142.60	185.55	180.19	173.26

Table 6 List of initial mooring line forces in Newton

	LC 1	LC 2	LC 3	LC 4	LC 5*
Tp [s]	3.04	1.58	3.04	2.53	1.26
Hs [m]	0.28	0.13	0.28	0.28	0.08
Gamma	1.05	2.87	1.05	2	1.05

*LC only run on TLB X3

Table 7 An overview of the irregular wave load cases where JONSWAP spectrums were used

H [m]	Period [s]					
	0.95	1.26	1.58	1.8	2.5	2.8*
0.13	LC 6	LC 7	LC 9	LC 11	-	LC 15
0.3	-	LC 8	LC 10	LC 12	-	LC 16
0.5	-	-	-	LC 13	LC 14	LC 17

* LC only run on TLB X3

Table 8 An overview of the regular wave load conditions

with the re-calibrated values, but it resulted in a slight offset in the initial position of TLB B, as obtaining the vertical orientation of the turbines was done by evaluating the mooring line forces.

Load Cases

Each load case (LC) was run for 60 and 300 seconds for regular and irregular runs, respectively. A compromise between maximum wave height and diversity of wave periods was made to ensure good quality waves and maximum wave loading to reduce the relative error. The LCs are shown in Tables 7 and 8. Seawater was utilized in the basin, and the corresponding density was assumed to be 1025 kg/m^3.

Figure 2 shows the corresponding measured wave spectrum for each of the irregular load cases in Table 7, as recorded by the side wave gauge. LC 1 and LC 3 are identical in order to verify whether different realizations of the wave fields have repeatable spectrums.

RESULTS

Decay Tests

The eigenmodes of stiffness-controlled platforms are fundamentally different from floaters with catenary mooring lines, where the

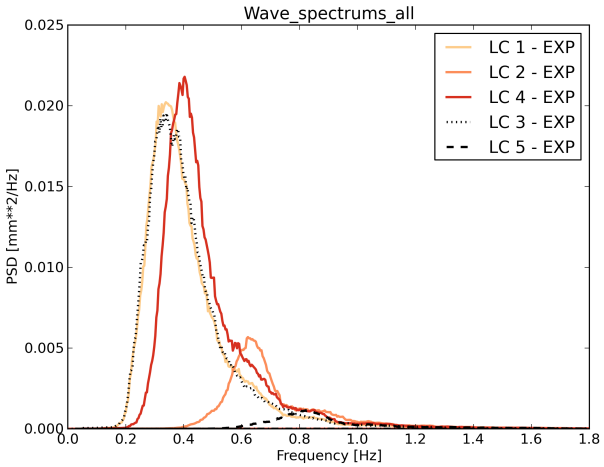

Fig. 2 Wave spectrums computed from the data recorded by the side-mounted wave height sensor

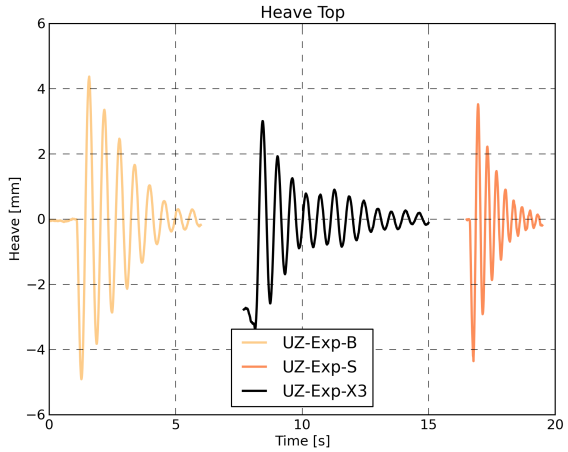

Fig. 3 Plot of heave motion during the decay tests for TLB B, TLB X3, and TLB S

couplings between the rigid body surge, sway, heave, roll, pitch, and yaw modes are weak. The taut mooring lines introduce strong couplings interacting with the elasticity of the platform, except in heave. Heave was introduced by adding a mass to the top of the model and quickly removing it again. For one of the pitch-surge modes, the tower top horizontal deflections in the downstream direction due to platform pitch rotation and surge motions were in phase. For this pitch-surge mode, the motion was introduced by exerting force in the upstream direction on the very top of each turbine, rim of nacelle for TLB B and TLB X3, and top lid for TLB S. A clean yaw rotation of the platform should only couple with heave. Yaw was introduced by exerting force on the upper mooring point. This introduced some pitch and surge, and even slight heave motions. Computations of these combined modes are perhaps best achieved in the time domain by replicating the experiment rather than performing an eigenanalysis only. The results of the heave, pitch-surge, and yaw decay tests are shown in Figs. 3, 4, and 5, respectively.

The heave eigenfrequencies in the experiment for TLB S, TLB B, and TLB X3 are estimated to be 2.9, 1.7, and 1.7 Hz, respectively. The corresponding damping ratios, looking at the decrements, are estimated to be 8%, 6%, and 4% of critical, respectively. TLB X3 experiences a temporary increase in the heave decay amplitude after 6 to 7 cycles. This is likely the result of influence from an observed pitch and roll motion after 4 to 5 seconds, and is caused by the selected method of applying the initial displacement.

The pitch-surge decays for TLB S and TLB X3 are clean with limited coupling to other modes. The surge-pitch eigenfrequencies

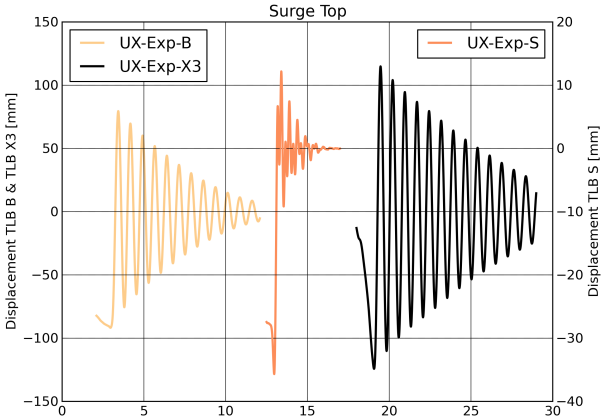

Fig. 4 Surge motions during pitch-surge decay tests

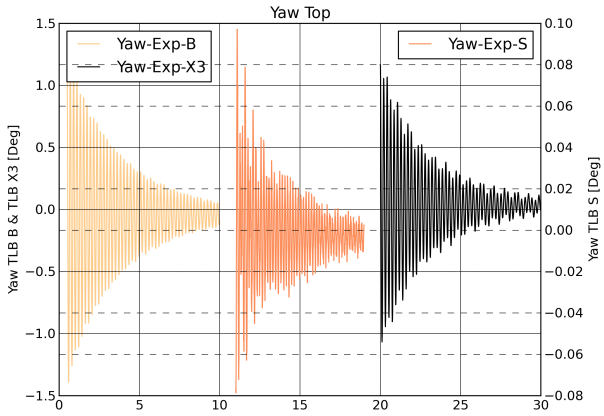

Fig. 5 Plot of rotation during yaw tests

are estimated to be 2.34, 1.34, and 1.35 Hz for TLB S, TLB B, and TLB X3, respectively. The corresponding damping ratios are calculated to be 8%, 3%, and 1% of critical, respectively. However, for TLB S, the pitch-surge decay is complex with interaction between the flexibility of the floater and the mooring lines. This is due to the combination of a stiff mooring system and a floater with low mass. TLB S posed similar challenges in yaw, but data with reasonable quality were captured. The yaw eigenfrequencies are calculated to be 4.8, 6.0, and 4.6 Hz for TLB B, TLB S, and TLB X3, respectively.

Wave Trials

The RAO for both regular and irregular load cases are obtained by the absolute value of the Fourier amplitude of the response divided by the absolute value of the Fourier amplitude of the wave elevation (side wave gauge) at the same frequency. The RAO plots summarize all the load cases for the three platforms. In order to reduce noise, the plotted frequencies are collected from a limited range, depending on LC. For LCs 1 to 5, the intervals used are 0.2–0.8, 0.5–1.7, 0.2–0.8, 0.3–0.8, and 0.6–1.7 Hz, respectively.

Tower Top Translation and Rotations

Recordings of surge, heave, and pitch relative to the tracking point are presented in Figs. 6, 7, and 8, respectively. Minor motions in sway, roll, and yaw are not analyzed in this work. TLB X3 is showing significantly higher RAO than TLB B and TLB S in the heave direction. The dynamic pressure on top of the floater and the

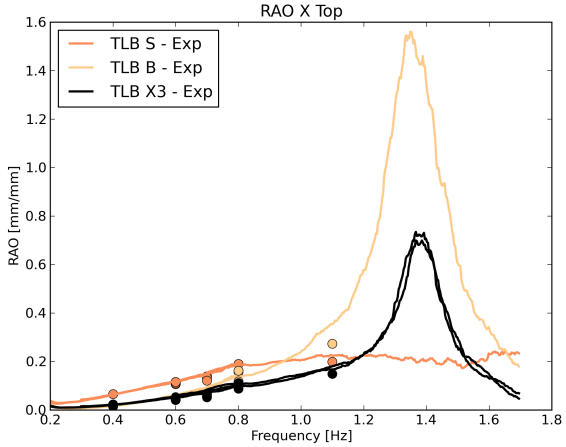

Fig. 6 Tower top surge motions where dots are regular LCs

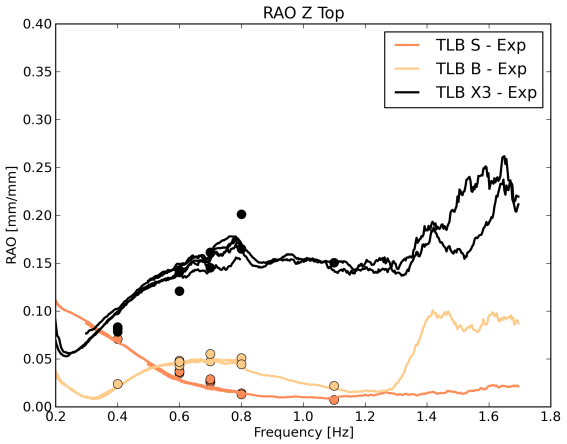

Fig. 7 Tower top heave motion where dots are regular LCs

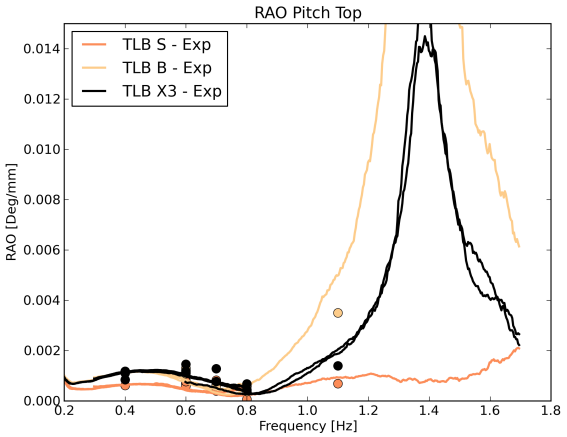

Fig. 8 Top pitch rotation where dots are regular LCs

lower water plane area are the main contributors to this difference. Increased variation can be observed for higher frequencies where both the excitations and responses are low.

The eigenfrequencies identified in the decay tests correspond well to the peaks in Figs. 6, 7, and 8. The RAO obtained for TLB X3 differ somewhat between the LCs beyond 1 Hz. This is probably due to complex nonlinear fluid dynamics phenomena occurring at the sharp transition between the floater and the space-frame, as shown in Fig. 1 and Fig. 15. Figure 15 shows air bubbles originating from a pocket of air behind the floater. At lower frequencies, some deviation is observed for LC 2 and LC 5 as a result of the wave distribution being focused at higher frequencies for these LCs.

Forces in the Mooring Lines

Tension for the lower mooring lines, denoted as lines 1 to 3 with line 1 located downstream, is shown in Figs. 9, 10, and 11. Lines 2 and 3 should produce the same results due to symmetry. Until eigenfrequencies are encountered at around 1.4 Hz, mooring lines 2 and 3 for TLB S and TLB X3 have similar results, although some discrepancy can be observed for TLB B. Studying the full dataset, one can see that TLB B experiences somewhat more yawing motion in frequencies at and above 1 Hz. Simulations suggest some yawing is to be expected due to a small asymmetry in the mooring line stiffness. Unfavorable distribution of friction in the pulley system has the possibility to further enhance the effect, but coherent results for all of the irregular cases suggest that the influence is relatively small. Line 1 is aligned with the waves and has a higher response

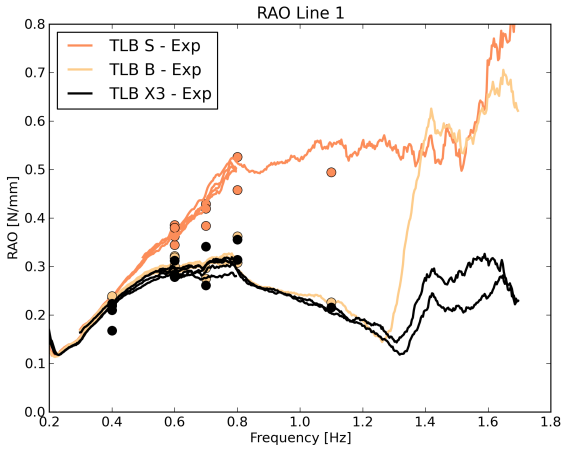

Fig. 9 Axial force of line 1 where dots are regular LCs

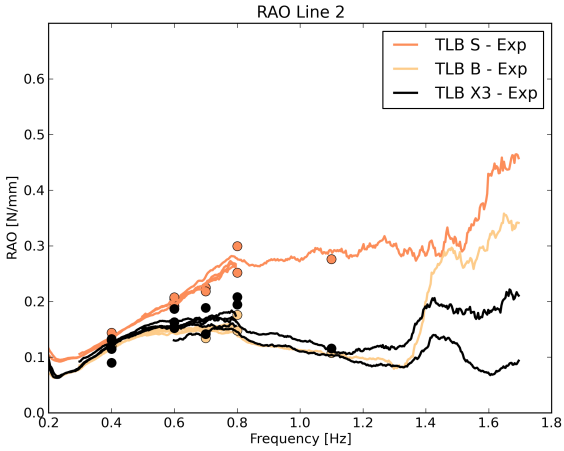

Fig. 10 Axial force of line 2 where dots are regular LCs

than lines 2 and 3. An interesting effect, where the forces decrease when approaching the range of 0.7 to 1.3 Hz, is due to partial cancellation of the lower fairleads motions due to surge and pitch. The TLB S has less mass than TLB B and TLB X3, and the center of mass is located close to the center of buoyancy. This explains why TLB S does not benefit significantly from the cancellation effect.

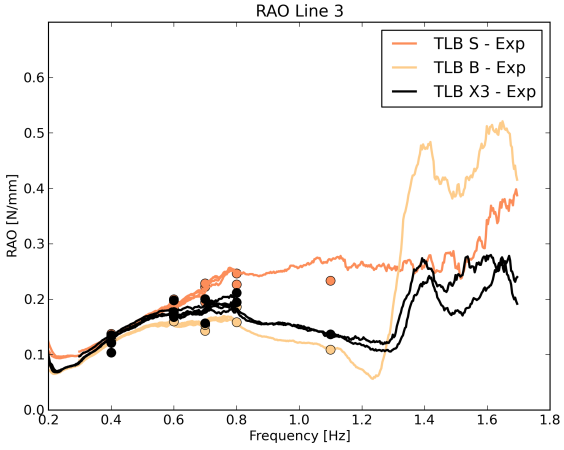

Fig. 11 Axial force of line 3 where dots are regular LCs

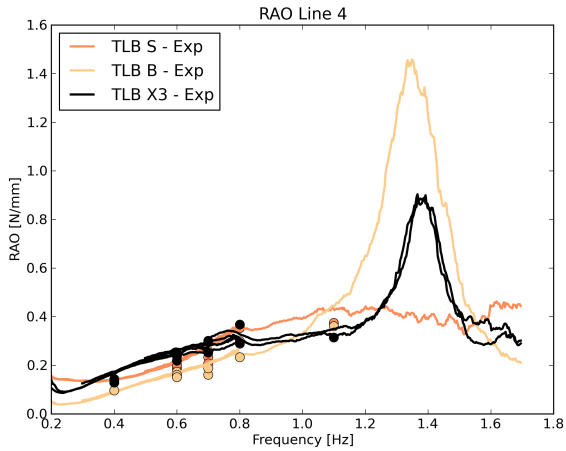

Fig. 12 Axial force of line 4 where dots are regular LCs

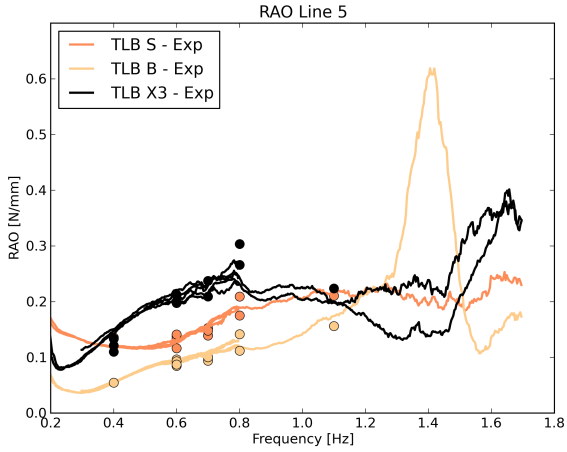

Fig. 13 Axial force of line 5 where dots are regular LCs

Plots for the upper lines, numbers 4 to 6 where line 4 is located downstream, are shown in Figs. 12, 13, and 14. At the lower fairleads, the motions due to surge and pitch add up rather than cancel, and we do not get the lower response in the range of 0.8 to 1.2 Hz, as seen for the lower lines. The RAO peaks of TLB B and TLB X3 are less distinct, especially for TLB X3. This is assumed to be from the same disturbance caused by the end cap lids, as previously mentioned. There is also a discrepancy between lines 2

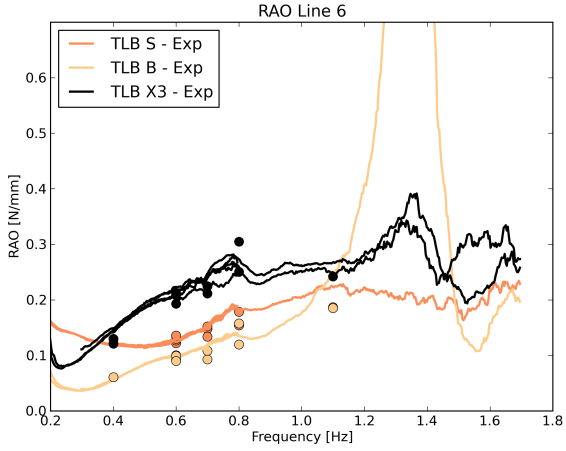

Fig. 14 Axial force of line 6 where dots are regular LCs

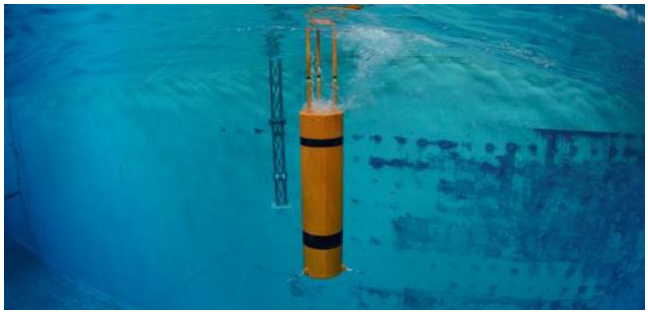

Fig. 15 Photo showing low pressure effects over the top lid on the floater body while relatively large waves are passing

and 3 for TLB B in the upper lines, but opposite of that observed for the lower lines. This indicates an offset between the lower and upper mooring line orientations in yaw, which, in this case, would introduce a yawing motion under horizontal loading. Overall, the mooring line force amplitude responses are as expected. The total variations are assumed to be small, and the results for both regular and irregular runs are taken as consistent and reliable.

Other Aspects

Multi-harmonics were observed visually during the tests. Both first and second bending modes of the model structure were observed. The stiffness of the scaled models is not far from what is expected for similar full-scale systems. The observation of these effects illustrates the importance of simulation tools that are capable of capturing the internal elastic behavior when simulating slim complex systems such as floating wind turbines.

The RAO results are noisy below 0.4 Hz and above 1.0 Hz. The selected JONSWAP spectrums for some of the LCs have low energy outside this range. One could increase the run-time to reduce the noise, but this would also increase the transversal wave motion in the basin. Despite the noise, these frequencies are included in the results for completeness.

Decent resolution for both high and low frequencies was achieved through the selected irregular load cases. However, for comparison with simulations, it would be preferable to select a limited range of frequencies around the specified wave period of each irregular LC. When comparing the irregular LCs, it is apparent that the range between 0.4 and approximately 1.2 Hz is of the best quality with respect to resolution and wave distribution. Overall, the regular LCs are in agreement with the irregular wave trials.

SOURCES OF ERROR

Error types, such as wave train irregularities, signal noise, or other sources suitable for filtering, may be documented and possibly eliminated by statistical methods based on a high number of load cases. However, for this experiment, the wave tank was only available for a limited amount of time (two weeks). Analyzing three different floaters was deemed more important than the number of load cases at this stage. This was based on the assumption that controlled variation in geometries would lead to fewer errors when comparing the full set of results to a simulation code. Using different geometries also gave further possibilities of validation, as they address different challenges with respect to development of the simulation codes.

The most important sources of errors are: (1) friction in the mooring system due to the pulleys, (2) alignment of the tracking system, (3) accuracy in model construction, (4) signal noise, (5) model orientation, and (6) exact stiffness in the mooring lines. For issue 1, the friction in only two of the six pulleys was tested in detail. For the pulley systems that were investigated, it was noted, based on simple tests, that the static friction under a load of 200 N was less than 0.25%; thus, the total contribution of error to the experimental results is assumed to be low, at least for low frequencies. However, simulations show that modeling the hysteresis friction in the mooring line pulleys is crucial for a realistic damping of responses at the pitch-surge eigenfrequencies.

During the installation of the models, the nacelle with the tracking system had to be attached prior to the final position of the model, resulting in issue 2. The alignment with respect to yaw angle was only visually confirmed. A pure pitch motion may therefore be recorded as a coupling between pitch and roll motion. From visual inspections, it was assumed that the total yaw offset was less than 1 degree, and therefore the total contribution to the recorded pitch values was close to none.

With respect to issue 3, uncertainty regarding material properties is considered most influential. Glued and threaded connections are assumed to be rigid. Material properties, as specified by the producer, are used without further verification at this point. With regards to the description of the geometries, the mass of the glue is not accounted for directly in the transitions. Also, a coat of paint was applied to the physical model for waterproofing. The amount of paint and glue was calculated by measuring mass pre- and post-application. Assuming an even distribution, the density of each part is adjusted accordingly.

For the issue of signal noise, we experienced an overall low influence and variation of both white noise and irregularities. This can be identified during calm water, prior to each case. Minor offsets in mooring line pre-tension were observed upon pre-tuning the models, typically in the range of $\pm$0–3%. This is a possible indicator of an offset in the horizontal neutral position. This is likely a sum of errors in mooring line length, final placement of mooring points on models and rigging, friction, yaw offset between upper and lower mooring points, and overall model geometry imperfections. The yaw offset is assumed to be less than 3 degrees. The largest difference was found for TLB X3, which has the most complex geometry, while almost perfect equilibrium was found for TLB S. It is assumed that offsets of the magnitude mentioned are of less importance with respect to the quality of the dataset, as they are likely to have little to no effect on the overall load amplitudes.

None of the sources of errors discussed above are taken into account in the presented results. Issue 6 represents the main contribution to the extent of errors in the results. The stiffness of the spring system was calibrated without the mooring lines to ease the operation. Numerous mooring lines were tested to find an acceptable combination of axial stiffness and low bending stiffness to reduce the energy lost in the pulley system. A 1-mm steel wire was the final choice. Robust wire clamps and carbine hooks were used as connection terminals. A single terminal was tested and found to give no relevant compliance contribution. However, this was not true for a complete mooring line and spring setup, as it was discovered that there was a significant compliance influencing the total line stiffness. A post-trial stiffness control calibration was performed on TLB X3. Each load sensor was connected to only one unique mooring line that was used for all the models successively. Mooring line stiffnesses for TLB S and TLB B were adjusted based on the findings from the control performed on TLB X3. When performing the control mooring, line 5 accidentally broke. No data were collected for this line, and an average of the remaining lines was used for its compliance contribution.

CONCLUSIONS

The experimental data agree well with previous experience and simulations presented earlier for TLB systems. The scaled models and the experimental setup performed up to specification and expectations. The quality of the results should therefore be suitable for further verification of simulation codes. Three different geometries were tested under similar scale and conditions to further document the effects of geometry changes in the wave-action zone. This is intended to support the further development of simulation codes to handle different and more complex geometries. From the results we can also conclude that the TLB design is robust and reliable, even when severe changes are made to the initial conditions, such as altering the mooring line radius.

Further work in a separate paper will include: computations, detailed comparisons with the experimental data, and identification of model weaknesses. Time series of the experimental data will eventually be available for other research groups.

ACKNOWLEDGEMENTS

Support was provided through the EU Seventh Framework Program (FP7)-funded MARINET project to conduct wave trials on three different TLB floaters at the IFREMER test facilities in Brest, France. We gratefully acknowledge the support from Amund Føyn for the actuator system algorithms and Anders Spæren for aid with constructing the rigging and models. Acknowledgement is also offered to Joakim Berg, Catho Bjerksether, and the team at IFREMER in Brest for helping to conduct the wave trials. Finally, we also acknowledge the support from Institute for Energy Technology (IFE) and NOWITECH.

REFERENCES

Butterfield, S, Musial, W, Jonkman, J, and Sclavounos, P (2007). *Engineering Challenges for Floating Offshore Wind Turbines*, Technical Report NREL/CP-500-38776, National Renewable Energy Laboratory, Golden, CO, USA, 13 pp.

Copple, RW, and Capanoglu, C (2012). "Tension Leg Wind Turbine (TLWT) Conceptual Design Suitable for a Wide Range of Water Depths," *Proc 22nd Int Offshore Polar Eng Conf*, Rhodes, Greece, ISOPE, 1, 396–403.

Jonkman, JM, and Matha, D (2011). "Dynamics of Offshore Floating Wind Turbines—Analysis of Three Concepts," *Wind Energy*, 14(4), 557–569.

Jonkman, J, Butterfield, S, Musial, W, and Scott, G (2009). *Definition of a 5-MW Reference Wind Turbine for Offshore System Development*, Technical Report NREL/TP-500-38060, National Renewable Energy Laboratory, Golden, CO, USA, 23 pp.

Jonkman, J, et al. (2010). *Offshore Code Comparison Collaboration within IEA Wind Task 23: Phase IV Results Regarding Floating Wind Turbine Modeling*, Technical Report NREL/CP-500-47534, National Renewable Energy Laboratory, Golden, CO, USA, 23 pp.

Myhr, A, and Nygaard, TA (2012). "Load Reductions and Optimizations on Tension-Leg-Buoy Offshore Wind Turbine Platforms," *Proc 22nd Int Offshore Polar Eng Conf*, Rhodes, Greece, ISOPE, 1, 232–239.

Myhr, A, Maus, KJ, and Nygaard, TA (2011). "Experimental and Computational Comparisons of the OC3-HYWIND and Tension-Leg-Buoy (TLB) Floating Wind Turbine Conceptual Designs," *Proc 21st Int Offshore Polar Eng Conf*, Maui, HI, USA, ISOPE, 1, 353–360.

Nygaard, TA, Myhr, A, and Maus, KJ (2009). "A Comparison of Two Conceptual Designs for Floating Wind Turbines," *Proc Eur Offshore Wind Conf Exhibition,* Stockholm, Sweden, EWEA, 3, 1685.

Popko, W, et al. (2014). "Offshore Code Comparison Collaboration Continuation (OC4), Phase I – Results of Coupled Simulation of Offshore Wind Turbine with Jacket Support Structure," *J Ocean Wind Energy*, ISOPE, 1(1), 1–11.

Robertson, AN, and Jonkman, JM (2011). "Loads Analysis of Several Offshore Floating Wind Turbine Concepts," *Proc 21st Int Offshore Polar Eng Conf*, Maui, HI, USA, ISOPE, 1, 443–450.

Sclavounos, PD, et al. (2010). "Floating Offshore Wind Turbines: Tension Leg Platform and Taut Leg Buoy Concepts Supporting 3-5 MW Wind Turbines," *Proc Eur Wind Energy Conf (EWEC 2010)*, Warsaw, Poland, EWEA, 3, 2361–2367.

Stewart, GM, Lackner, MA, Robertson, A, Jonkman, J, and Goupee, AJ (2012). "Calibration and Validation of a FAST Floating Wind Turbine Model of the DeepCwind Scaled Tension-Leg Platform," *Proc 22nd Int Offshore Polar Eng Conf*, Rhodes, Greece, ISOPE, 1, 380–387.

Tsouroukdissian, AR, Fisas, A, Pratts, P, and Sclavounos, PD (2011). "Floating Offshore Wind Turbines: Concept Analysis," Presented at *WINDPOWER 2011 Conf Exhibition*, Anaheim, CA, USA, American Wind Energy Association.

Weinstein, J, and Roddier, D (2010). "WINDFLOAT—A Floating Support Structure for Large Offshore Wind Turbines," *Proc Eur Wind Energy Conf (EWEC 2010)*, Warsaw, Poland, EWEA, 5, 3949–3950.

Appendix 7

Journal of Ocean and Wind Energy (ISSN 2310-3604)

Vol. 2, No. 1, February 2015, pp. 12–20

http://www.isope.org/publications

Comparison of Experimental Results and Computations for Tension-Leg-Buoy Offshore Wind Turbines

Anders Myhr
Department of Mathematical Sciences and Technology, Norwegian University of Life Sciences (NMBU)
Ås, Norway

Tor Anders Nygaard
Energy Systems Department, Institute for Energy Technology (IFE)
Kjeller, Norway

This work compares wave tank experimental results in scale 1:40 and hydro-elastic computations of three different Tension-Leg-Buoy (TLB) offshore wind turbine platforms. The results include comparisons of time-series of displacements for free-decay tests, time-series of tower top motion and mooring line tension for selected regular wave cases, Power Spectral Densities (PSD) for one irregular wave case, and Response Amplitude Operators (RAO) for tower top motion and mooring line tension for all the regular and the irregular wave cases. The experimental results and computations agree well, and both capture interactions between hydrodynamic loading, flexible motion of the floater/tower, and the tower top motions. The time series of the experimental results will be publicly available for further development and validation of computational tools for offshore wind turbine platforms.

INTRODUCTION

Several new floating offshore wind turbine concepts are under development. Some commonly known examples are the SWAY Tension-Leg-Spar (Karimirad and Moan, 2013), the full-scale WindFloat system (Roddier et al., 2010), and the HYWIND system (Tande et al., 2014), where a single turbine has been operating full-scale since 2009. Several concepts are also in the early prototype development stage, such as different Tension-Leg-Buoy (TLB) and Tension-Leg-Platform (TLP) systems, but trials for these concepts have so far been limited to wave basins (Myhr and Nygaard, 2012; Robertson and Jonkman, 2011; Stewart et al., 2012; Copple and Capanoglu, 2012).

The evolution from onshore to offshore bottom-fixed wind turbines increases computational complexity through the inclusion of wave loading and the need for more complex soil models. Floating structures such as TLPs and TLBs have similarities to bottom-fixed structures due to the stiff mooring system. Nevertheless, they represent another level of complexity because of mooring lines and larger motions. Finally, large floaters like semisubmersibles need consideration of detailed hydrodynamic models to account for effects such as diffraction and radiation. “Floater” here refers to the part of the substructure below the tower/floater interface, typically at 10 m above the still water line in full scale. Due to the large number of load cases (LC) needed to check the feasibility of a design, computational tools must be efficient. In addition, high accuracy is necessary to reduce the risk of failure and to achieve a cost-optimized design.

The International Energy Agency (IEA) Wind Task 23 projects known as Offshore Code Comparison Collaboration (OC3) (Jonkman et al., 2010) and the follow-up project OC4 (Popko et al., 2012) are important drivers for the development and verification of computational tools for offshore wind turbines. The lack of publicly available experimental results means the activity so far has been limited to verification through comparisons of computational results from different codes. In the ongoing OC5 project, model validations against wave tank results and full-scale data are just starting. The FAST code (Jonkman, 2007) was recently validated against experimental results for a TLP platform. It produced good results but also discrepancies that could not be explained at the time (Stewart et al., 2012). In order to support model validation, we recently conducted wave tank experiments on three different TLB floaters at the IFREMER wave tank in Brest, France through the MARINET project. In this paper, we compare some of the results with corresponding computations with the in-house simulation tool 3DFloat at IFE.

APPROACH

The experimental results herein include time series of wave height, tower top motion, and mooring line tension, as well as video recordings. The LCs include decay tests and regular- and irregular-wave cases (Myhr and Nygaard, 2014). For a full-scale floater, most of the wave excitation is in the range 0.05 to 0.2 Hz, corresponding to 0.3 to 1.3 Hz for the 1:40 scale model. The results are presented as PSDs and RAOs. For the RAO computations, the absolute value of the Fourier amplitude of the response is divided by the absolute value of the Fourier amplitude of the wave height.

The comparisons are performed in three steps:

(1) Decay tests: They are particularly useful for checking the modeling of the structural and added mass, plus the stiffness of the mooring system, through comparison of the eigenperiods. The obtained damping ratios allow tuning of the parameters affecting the damping, such as the drag coefficient in the Morison force model, linear damping applied to the floater, the hysteresis damping applied to the fairleads, and structural damping in the mooring lines.

(2) Regular wave cases: From these one can make direct and detailed comparisons of time series results, peaks and amplitudes for both motions, and mooring line tension.

Received July 24, 2014; revised manuscript received by the editors December 23, 2014. The original version was submitted directly to the Journal.
KEY WORDS: Offshore wind turbine, experimental results, Tension-Leg-Buoy (TLB), hydro-elastic computations.

(3) Irregular wave cases: These are presented with PSDs and RAOs in order to give a quick overview of the platform responses to loading with a combination of different frequencies.

COMPUTATIONAL TOOL

3DFloat is an aero-servo-hydro-elastic simulation tool developed at IFE and NMBU for the computation of dynamic response of elastic structures subject to combined wind and wave loading, such as offshore wind turbines and suspension bridges (Myhr and Nygaard, 2012). It is coded in FORTRAN90 with linear algebra routines from the LAPACK library (Anderson et al., 1990).

The core is a general nonlinear Finite Element Method (FEM) framework. The load models include hydrodynamics and rotor aerodynamics. 3DFloat is one of the tools verified with the OC3-Hywind floating wind turbine in the IEA OC3 project (Vorpahl et al., 2013), the bottom-fixed space-frame ("Jacket") in the IEA OC4 project (Popko et al., 2012), and the semisubmersible platform in the IEA OC4 project (Robertson et al., 2014). An optimization example and further details of the model are given in Myhr and Nygaard (2012).

EXPERIMENTAL SETUP

The data sets utilized for validation in this work were obtained in experiments in the IFREMER wave tank in Brest, France. The experimental data and setup are described in a separate paper (Myhr and Nygaard, 2014). An overview of the setup is shown in Fig. 1 and Fig. 2.

Simplifications

The main simplification of the geometry in the Simulation Model (SM) is ignoring the fairlead brackets (with a mass of 0.022 kg and dimensions of 20 mm by 30 mm). The sum of the mass for all brackets amounts to about 0.150 kg. The SM beam model has rigid, massless connectors from the center of the floater to the fairleads. The connectors for the Physical Model (PM) are small 50 mm stainless carabiners, each about 0.01 kg.

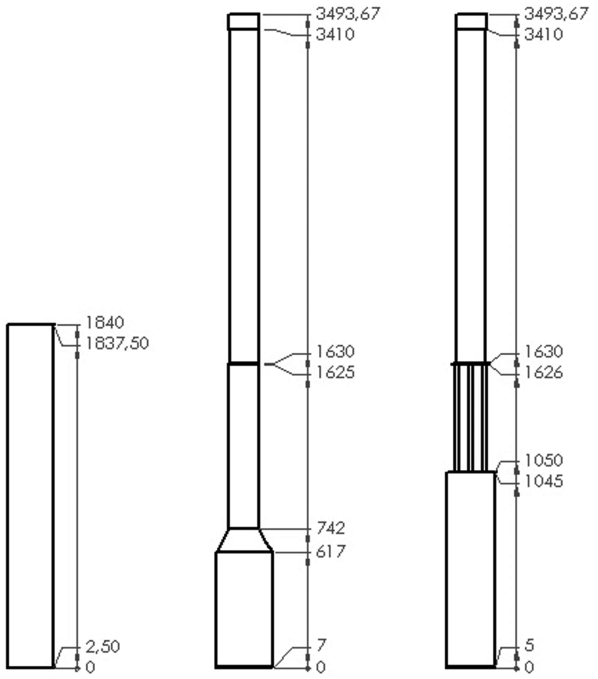

Fig. 1 Sketches of the selected geometries (from left to right): TLB S, TLB B, and TLB X3. The indicated height levels [mm] correspond to transitions in mass and/or diameter (Spæren, 2013).

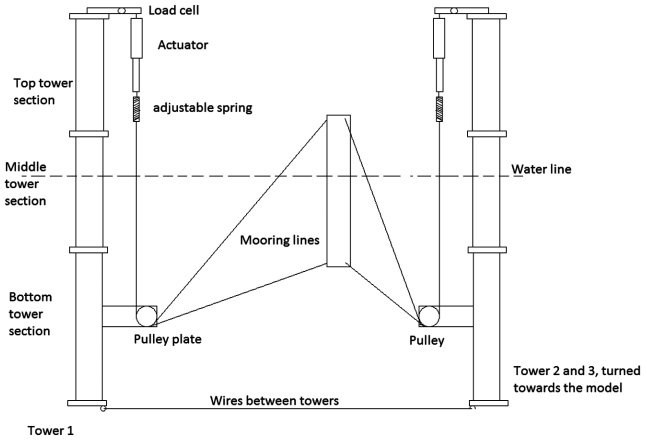

Fig. 2 Experimental setup with load cell, actuator, pulleys, and supporting towers. A spacing wire between the towers is shown, but additional pretension wires have been removed for clarity (Spæren, 2013).

	LC 1	LC 2	LC 3	LC 4	LC 5*
Period [s]	3.04	1.58	3.04	2.53	1.26
Hs [m]	0.28	0.13	0.28	0.28	0.08
Gamma	1.05	2.87	1.05	2	1.05

*LC 5 was only run with TLB X3

Table 1 The irregular LC Jonswap spectrums. LC 1 and LC 3 have identical wave characteristics in order to check the consistency of the test.

H [m]\Period [s]	0.95	1.26	1.58	1.8	2.5	2.8*
0.13	LC 6	LC 7	LC 9	LC 11	—	LC 15
0.3	—	LC 8	LC 10	LC 12	—	LC 16
0.5	—	—	—	LC 13	LC 14	LC 17

*LC only run on TLB X3

Table 2 Regular wave load conditions

Load Cases

Tables 1 and 2 show the irregular- and regular-wave LCs of the experiment. Detailed comparisons are performed for the regular-wave cases LC 9 and LC 12, and the irregular wave case LC 1. The regular and the irregular cases are then compared with RAOs.

Figure 3 shows comparisons of the wave spectrums in the experiment and the computations. The five-minute runs in the wave tank correspond to 30 minutes in full scale. This results in some differences in wave spectums between different realizations, as seen for LC 1 vs. LC 3. The simulation model was run with superposition of linear Airy waves, corresponding to the characteristics of Table 1, with a simulation length corresponding to 80 minutes in full scale. The differences in excitation between the experiment and model are, to some degree, accounted for when computing RAOs.

MODEL CONSTANTS

The spectral radius for the generalized α-method was set to 0.9. Compared to a spectral radius of 1.0 (corresponding to the

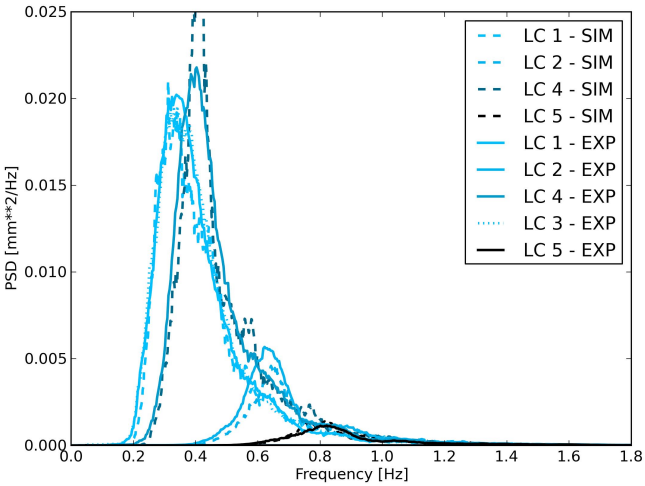

Fig. 3 Wave spectrums from both the simulations (-) and the experimental trials (–)

Newmark method), this gives an algorithmic damping of high-frequency noise, which we found improved the convergence without changing the computed forces. The Rayleigh structural damping model coefficients were chosen to give 1% of critical damping in the floater and tower between 0.3 and 1.3 Hz. The drag and inertia coefficients (C_d and C_m) in the relative form of the Morison equation were chosen as a function of the Keulegan-Carpenter (KC) and oscillatory Reynolds numbers (Re) from experimental data (Sarpkaya and Isaacson, 1981). For LC 9, KC at the still water level (MSL) are 1.6, 1.6, and 19 for TLB S, TLB B, and TLB X3, respectively. The values of Re are 36,000, 37,000, and 3,100. For LC 12, KC at the MSL are 3.8, 3.6, and 43 for TLB S, TLB B, and TLB X3, respectively. Corresponding Re are 73,000, 76,000, and 6,400. The slender cylinders penetrating the surface for TLB X3 have drag coefficients of 1.0 and inertia coefficients of 1.8. The TLB X3 floater body (below the space frame) has coefficients of 1.0 and 2.0 for drag and inertia, respectively, similar to the TLB B and TLB S. The axial drag coefficients for the bottom end caps are set to 2.0. This corresponds to a flat plate at 90-deg angle-of-attack, taking into account the cone for TLB B and the top lid for TLB X3. The value may seem high for TLB S, but the results are inertia-dominated and not sensitive to this parameter. The hysteresis damping force of the mooring line pulleys was determined from the experiment by slowly loading and unloading the mooring lines. There is no tuning involved in the selection of model constants described in this section.

Mooring Lines

The axial stiffness in the mooring lines is shown in Table 3. Table 4 shows the pre-tensions of the mooring lines in the experiment. The variation between mooring lines at the same height is due to the scale models not being vertical and/or not being centered between the anchor points. We do not take this into account in the simulations, where identical pre-tensions for mooring lines at the same height were used, as listed in Table 5. As long as tension is maintained in all mooring lines, the pre-tension level is not important for the taut mooring line stiffness and thereby the motions and force amplitudes.

	1	2	3	4	5	6
TLB B/S	2.899	2.842	2.870	2.341	2.320	2.299
TLB X3	2.494	2.479	2.425	2.312	2.325	2.234

Table 3 Axial stiffness calibration values [N/mm] for the mooring lines (Myhr and Nygaard, 2014)

	Line 1	Line 2	Line 3	Line 4	Line 5	Line 6
TLB B	164.80	164.10	159.70	188.89	184.26	178.66
TLB S	200.73	195.14	197.14	184.79	177.58	179.66
TLB X3	149.51	147.99	142.60	185.55	180.19	173.26

Table 4 Mooring line pre-tension [N] in the experiment (Myhr and Nygaard, 2014)

	Lower (1, 2, and 3)	Upper (3, 4, and 5)
TLB B	170.5 N (0.0160)	184.7 N (0.0177)
TLB S	195.0 N (0.0180)	178.3 N (0.0171)
TLB X3	147.5 N (0.0160)	180.0 N (0.0174)

Table 5 Mooring line pre-tension [N] in the simulations with equivalent pre-strain [mm/mm] shown in parentheses

Preliminary sensitivity studies indicate that small offsets in the initial orientation have limited influence on the computed displacement and line tension amplitudes. Nevertheless, this should be studied further as it may be relevant and important for full-scale prototypes.

Decay Trials and Model Tuning

To replicate the heave decay in the experiment, a small force was applied in the heave direction at the top of the nacelle before being removed. The results are shown in Fig. 4. The computed heave decay was tuned manually by adjusting linear vertical damping applied at one node at the MSL, with final values of 23.0, 25.0, and 23.0 Ns/m for TLB B, TLB S, and TLB X3, respectively.

The heave periods were tuned by adjusting the axial added mass coefficient for the end caps in order to match the heave period in the experiment. This resulted in an axial added mass of 40% of a half-sphere of water on the bottom end cap and the tapered section for TLB B. The corresponding number for the bottom of TLB S is 25% and 55% for TLB X3 (sum of upper and lower end caps).

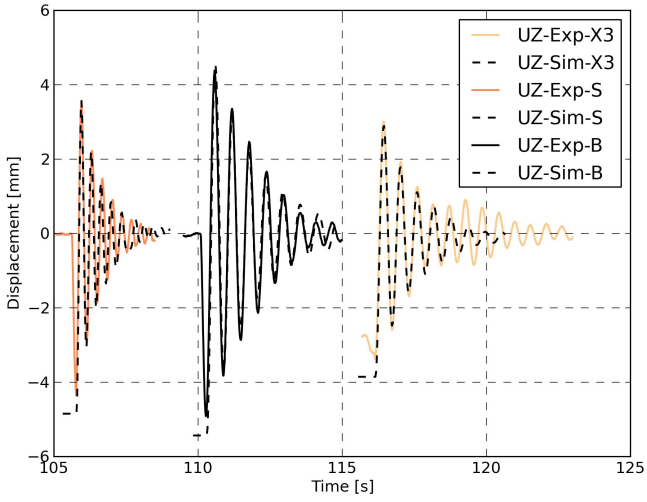

Fig. 4 Experiment heave decay tests for each of the physical models (PMs) compared to computations. The different PM time series are offset to allow presentation in the same figure.

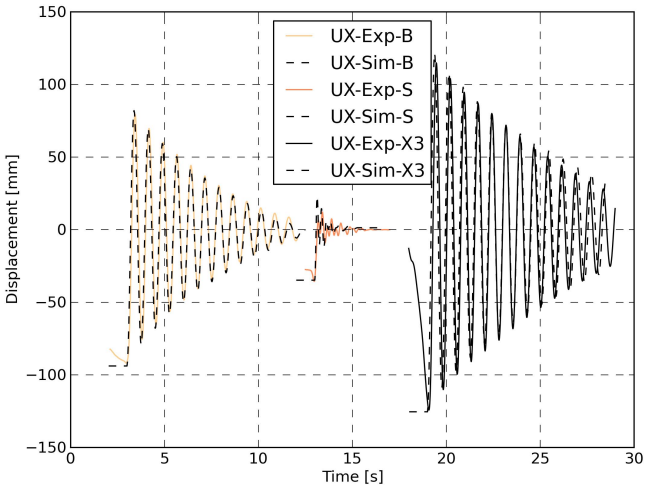

Fig. 5 Comparison of experimental pitch-surge decay data (continuous lines) and computations (dashed lines). The data shown are surge displacements.

The heave period for the experiment and computations, shown in Fig. 4, agree well for the first four cycles, where the amplitude decay is close to linear. In this part, the selected linear damping coefficients give good agreement between the experiment and simulations. The TLB X3 experimental results were disturbed by other modes after about 3 seconds. It was not possible to obtain a perfect heave excitation for X3 in the experiment, but the initial decay nevertheless allowed a tuning of the damping coefficient.

The second decay test was for coupled pitch and surge by exerting a temporary horizontal force on the nacelle. The stiffness-proportional coefficient in the Rayleigh structural damping model for the mooring lines was tuned manually in order to provide the best fit of the pitch/surge decay. The resulting values are 0.0023 s, 0.0050 s, and 0.0005 s for TLB B, TLB S, and TLB X3, respectively. The comparison of experiments and simulations is shown in Fig. 5.

For TLB B and TLB X3, the computed pitch-surge periods are marginally longer than in the experiment. The damping progression agrees well. TLB S, the floater with the lowest mass, has the same mooring system as TLB B, giving significantly shorter eigenperiods, as well as problems in the decay test with small amplitudes and interference from other modes. The period matches well, but the damping in the experiment is hard to interpret due to very small deflections. Overall, the decay tests can be simulated with high accuracy by 3DFloat.

The horizontal wave excitation in the SM is due to the inertia term and drag terms in Morison's equation, scaling with the inertia and drag coefficients, respectively. The heave excitation results from the axial inertia and drag terms in Morison's equation for the end caps, and the dynamic pressure on any surface with a vertical component in the surface normal, such as the bottom end caps, the transition from floater to space frame for TLB X3, and the conical section of TLB B. Due to the taut inclined mooring lines, the stiffness-controlled horizontal and vertical motions interact strongly.

Before embarking on the regular and irregular LCs, we carried out a sensitivity study by varying the Morison coefficients within a range of ±20% in the computations, while comparing the results with the experimental data. We did obtain a slight improvement in match by adjusting the Morison inertial coefficients, but we think the most robust approach is to select Morison coefficients as outlined earlier, tune damping and added mass in the decay tests, and to run the regular- and irregular-wave cases with these coefficients.

REGULAR WAVE TRIALS

The regular wave cases LC 9 and LC 12, shown in Tables 1 and 2, correspond to full-scale wave periods/heights of 10 s/5.2 m, and 11.4 s/12 m, respectively. The wave height to wavelength ratio is 0.03 and 0.06 for LC 9 and LC 12, respectively. The wave height to diameter ratio is above 1 for all floaters and LCs. The maximum diameter to wavelength ratio is 0.08. This means that the waves are non-breaking, small diffraction effects, and important viscous effects. Linear Airy wave theory and Morison's equation should be well suited for these computations. The waves in the simulations are generated by extrapolated Airy theory with a wave height corresponding to the value used as input to the experiment wave-maker. After ramping up the waves over 8 seconds, periodic results are typically obtained after 15 seconds of simulation time.

The periodic experimental results are extracted from the end of the run, due to severe transients when the first waves with large amplitudes hit the scale model. This is a trade-off between waiting out initial transients and growing reflections in the basin. Synchronization of the phases is achieved by an offset of the first wave in the computations.

LC 9: T = 1.58 s and H = 0.13 m (10 s and 5.2 m in full scale)

The simulations were run with regular waves with 2 seconds of initial stabilizing before H was ramped to the desired level over 8 seconds. Typically, few transients are expected for TLB systems, but in order to capture quasi-static, multi-harmonic behavior, ramped loading was found to be helpful. However, this is somewhat contradictory to the experiment where no ramping was used. Past experience was that the first two to three waves typically had a wave height of 120% to 150% of the desired wave height, resulting in a severe impact on the model and causing significant harmonic behavior. The problem of this effect was reduced by the selection of segments at the end of each trial's time domain, though with the compromise of increased reflections in the basin. The compared simulations and experimental results for LC 9 are shown in Figs. 4 to 6.

It is apparent that the heave amplitude and phase were computed quite well for all of the systems, although we experienced some multi-harmonic behavior in the computed heave for TLB S. The hysteresis damping in the pulleys, implemented as a friction hysteresis force applied on the fairlead in the computations, has a

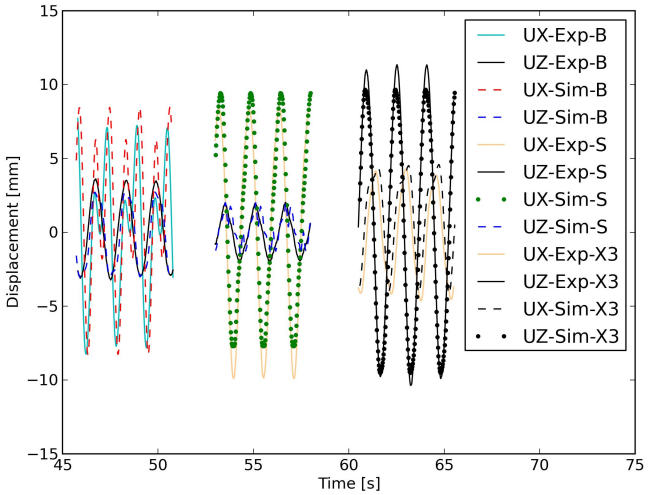

Fig. 6 Top displacement during LC 9 for all systems. Both surge (UX) and heave (UZ) are shown in the plot.

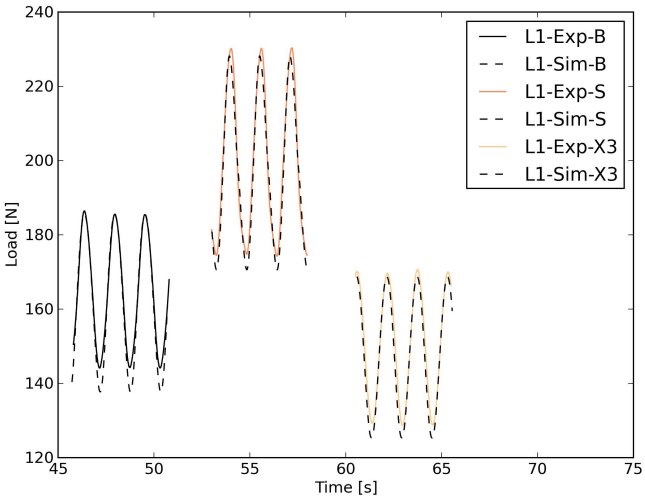

Fig. 7 Force in lower downstream mooring line during LC 9 for all systems

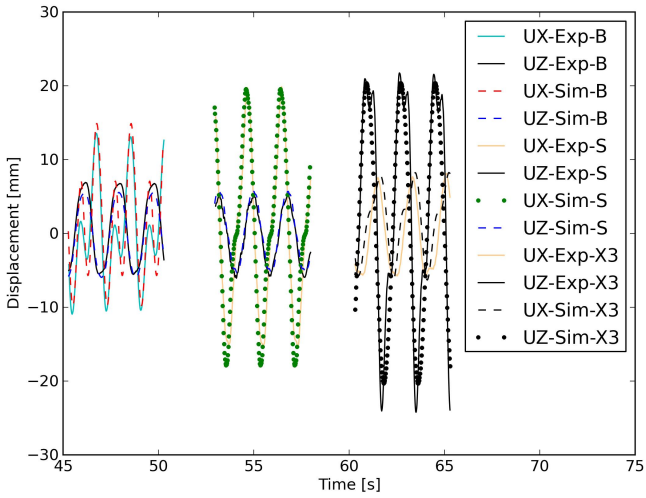

Fig. 9 Top displacement during LC 12 for all systems

significant influence. As the same pulley system was used for all the models, no modification to the hysteresis damping was attempted.

Displacement in pitch-surge is also computed quite well, especially for TLB S and TLB X3, with only minor offsets to the amplitude in the positive and negative directions, respectively. TLB B pitch-surge response is at the wave frequency and at twice the wave frequency (close to pitch-surge eigenfrequency), in both the experiment and the computations. An explanation for the discrepancy is that TLB B, for the regular cases with steep waves, never achieved a quasi-steady-state in the experiment, as one would expect for TLB designs during regular wave excitation. Typically, the pitch-surge eigenfrequency amplitude shifted from almost zero to the extremes, as shown in Fig. 6.

The lower mooring line forces are computed quite accurately for all models. An average discrepancy of less than 5 N, corresponding to less than 8% of the amplitude and less than 3% of the total load, is considered very good. The upper mooring force computations are also similar to the experiment, even with the relatively limited wave load excitations in LC 9. The mean offsets are due to differences in the initial setup in the model and experiment. Amplitudes for all of the models show a good match between the experiment and simulations, but the double frequency in TLB B influences the mooring line response in the computation somewhat more than indicated in the experiment.

The surge (UX) discrepancy for TLB B does not seem to influence the mooring loads significantly. Some discrepancies are observed for all of the PMs, but overall simulations compute results well within 10% of the measured values.

LC 12: T = 1.8 s and H = 0.3 m (11.4 s and 12 m in full scale)

The second regular LC features slight increases in both wave period and wave height. The compared results are shown in Figs. 9, 10, and 11. Slight multi-harmonic behavior is observed for TLB X3 in this case. The effect is present in both the simulation and the experiment. This is likely the result of pressure changes on the upper end cap of the floater. The heave and surge motions are somewhat influenced as a result of the change in added mass and thereby the resulting system inertia, but the experimental data are accurately replicated by the simulations. The surge motion in the experiment for TLB B and TLB S matches the simulations with no significant discrepancies. A slight overestimation of heave for TLB B is observed, while TLB S has an exact match.

The simulated lower mooring line forces are in line with the experiment. Discrepancies of 5% to 10% are observed for the

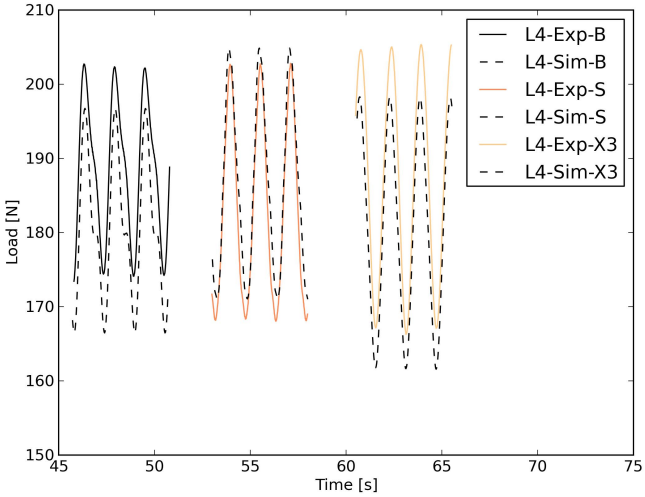

Fig. 8 Force in upper downstream mooring line during LC 9 for all systems

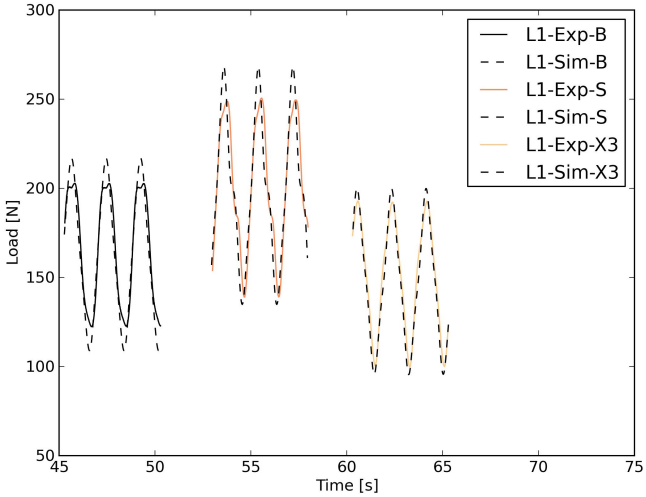

Fig. 10 Force in lower downstream mooring line during LC 12 for all systems

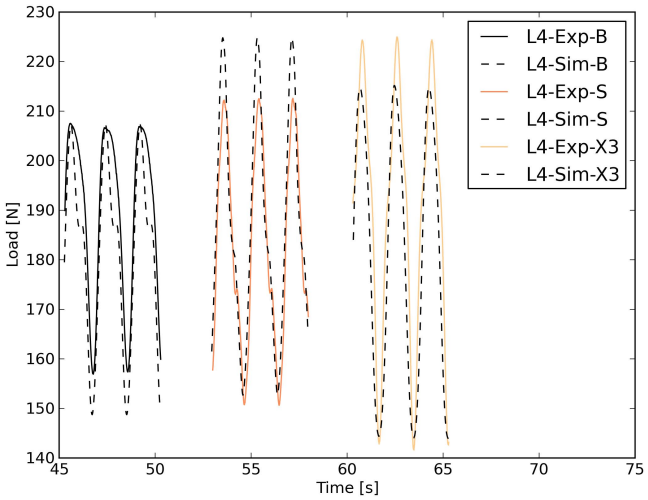

Fig. 11 Force in upper downstream mooring line during LC 12 for all systems

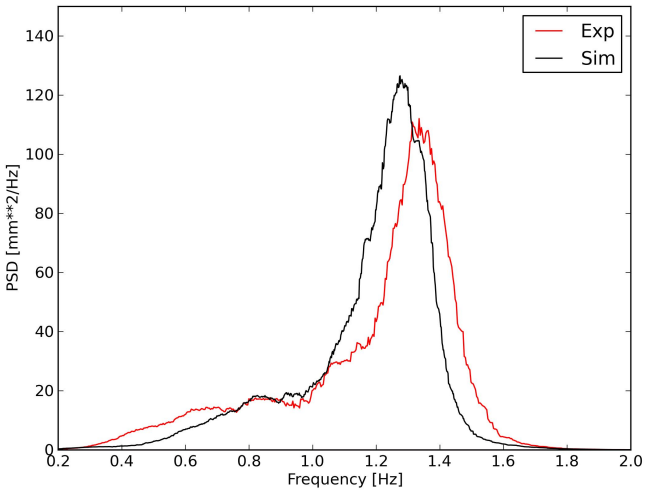

Fig. 12 PSD plot of pitch-surge motion for TLB B in LC 1

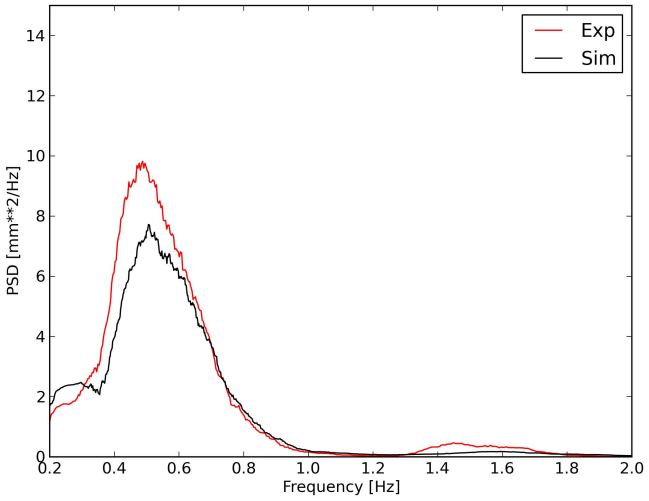

Fig. 13 PSD plot of heave motion for TLB B in LC 1

amplitudes for TLB B and TLB S. This corresponds to about 5% overestimation of the peak line force for TLB S. Nonlinear behavior can be noticed for TLB S. This is likely caused by the nonlinear damping occurring with larger deflections, which is noticed in the decay tests but is also captured by 3DFloat even if the amplitude is slightly off.

The observations of the upper mooring lines for LC 12 are similar to LC 9, but the double frequency is less pronounced in the simulations and is now negligible in the experiment. This is likely to be explained by a small difference in stiffness in the tower part of the model. The amplitudes are fairly in line for TLB B, but simulations overestimate the respective values for TLB S, while the values for TLB X3 are lower. Overall, the amplitudes deviate by $\pm 10\%$, while the total force is off by about $\pm 5\%$.

IRREGULAR WAVE TRIALS

In this section, one case is presented in detail with PSD on linear axes. This gives a visually intuitive interpretation of which frequencies contribute to the fluctuations of the selected response. All results from the regular and irregular LCs are then summarized by RAOs. For linear systems, where the response at one frequency is proportional to the excitation at the same frequency, RAOs are particularly useful. Despite the nonlinearities in this experiment, RAOs offers a first compact overview of the results, and it is interesting to see to what degree the results for one platform design fall on the same line, in order to get a sense of the linearity of the results. The RAO results of higher frequencies more than three times the wave peak frequency should be interpreted with caution. Here, the excitation is essentially zero, and the response is due to nonlinearities. Small absolute differences between the experiment and computations may be presented as large, noisy RAOs. In order to reduce noise for the RAOs, the plotted frequencies are collected from a limited range, depending on the LC. From LC 1 to LC 5, the intervals 0.2–0.8, 0.5–1.7, 0.2–0.8, 0.3–0.8, and 0.6–1.7 Hz are used, respectively.

Figure 12 shows the pitch-surge response for LC1. The differences up to 1 Hz can be partly explained by the differences in wave spectrums seen in Fig. 3. The pitch-surge motion response peak is at the pitch-surge eigenfrequency, despite the low wave excitation at this frequency, as also observed in LC 10 and LC 13. The resonant response is excited by nonlinearities. Figure 13 shows the PSD for the heave motion of TLB B. The wave peak frequency at 0.33 Hz shows up in the computations but not in the experiment. The peak just above 0.4 Hz corresponds roughly to the difference between the heave and pitch-surge eigenfrequencies, which have strong coupling through the mooring lines.

Figure 14 shows the first-order wave excitation and heave/pitch-surge difference frequencies dominating the lower mooring line response. The pitch-surge motion is mainly restricted by the upper mooring lines, as shown in Fig. 15. The upper mooring line response also shows a peak at the pitch-surge eigenfrequency.

It should also be noted that there is a discrepancy between the eigenfrequencies indicated in the simulation and the ones recorded in the experiment. As the decay tests produced very accurate responses, this is likely a result of the desired method of applying the hysteresis damping as friction on the fairleads in the computations. In the experiment, the physical introduction was through friction in the pulleys, corresponding to the full-scale anchor point. Small translations, as expected from high-frequency excitation, will then experience a higher stiffness from the mooring line wires because friction constrains the pulley.

The wave spectrums used in the computations shown in Fig. 3 are the same as the input to the wavemaker, with cut-offs at low frequencies determined by comparison with the measured wave spectrums, and high-frequency cut-offs at three times the wave peak frequencies. The experiment also shows minor wave

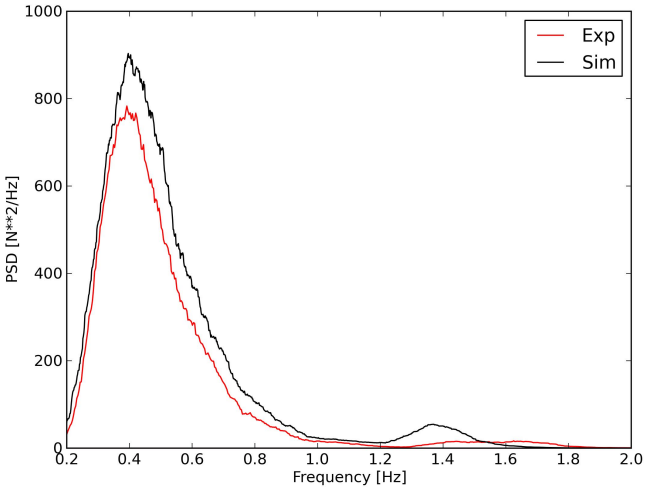

Fig. 14 PSD plot of lower downstream mooring line force for TLB B in LC 1

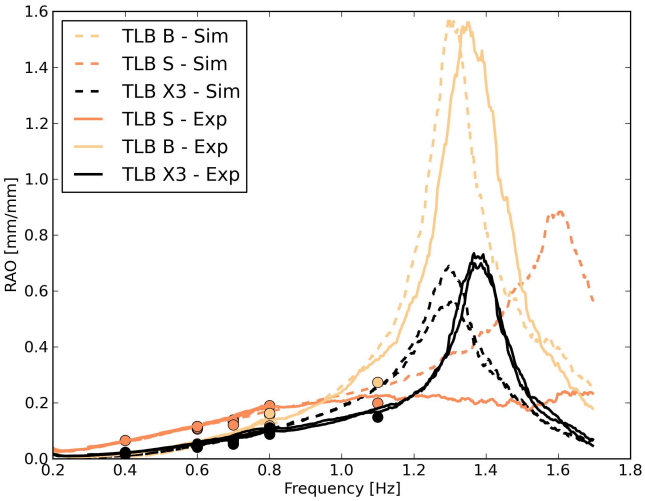

Fig. 16 RAOs for pitch-surge motion for all platforms, with regular cases represented as dots

reflections, from the model and the rig, in multiple directions that are not taken into account in the simulations.

The irregular wave trials were about 300 s each to limit the influence of wave reflections. The corresponding computations are 750 s long. Both the experiment and the simulations are too short to provide realization-independent spectrums. A new functionality in 3DFloat that allows time-accurate computations corresponding to the time-series of the measured waves is currently being implemented. This should reduce the uncertainty due to short wave realizations.

Figures 16 to 19 show RAOs of tower top pitch-surge motion, heave, and two mooring-line tensions for all cases, experiments, and computations. The irregular cases, except for LC 2 and LC 5, are cut off at 0.8 Hz to reduce clutter at high frequencies where the RAOs are less meaningful. For the pitch-surge motion, computations for TLB B produce excellent results both through the wave frequencies and around the pitch-surge eigenfrequency. Both TLB S and TLB X3 achieve good agreement below 1.0 and 0.8 Hz. TLB S deviates significantly at higher frequencies caused by the lack of damping, as discussed for LC 9. During shorter and steeper waves, significant turbulence and vortices are noticed downstream of the floater in addition to run-up due to the relatively large water plane area. This may further introduce nonlinear effects at higher frequencies. Due to the low mass, it is likely that the pitch-surge motion is damped out by effects that are not accounted for in 3DFloat, i.e., radiation damping. In addition, changes in water level and the low draft will influence the eigenfrequencies significantly. Since the results for TLB B, which utilizes the same mooring lines, are accurate, it is not likely that the mooring line stiffness is erroneous.

For TLB X3, the computations follow a smooth exponential curve, but the experimental results have a 0.1 Hz offset in the peak. This is significantly larger than the offset for TLB B. Four effects likely contribute to this result:

(1) The upper end cap in the floater is located close to the still water line. The waves influence the added mass and thereby influence both damping and eigenfrequencies. This is not modeled in the computations. The axial added mass associated with the upper end cap is either fully accounted for, or removed if the end cap comes out of the water.

(2) The stiffness of the mooring system is influenced differently from the pulley friction in the experiment and the computations, as explained earlier. Uncertainties in the measured mooring line stiffness also contribute to the discrepancies.

(3) The bending stiffness of TLB X3, in particular for the transition from end cap to the slim columns, is represented differently in

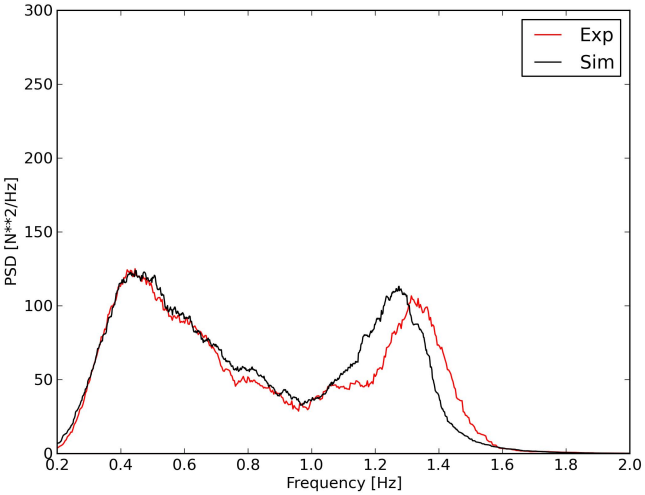

Fig. 15 PSD plot of upper downstream mooring line force for TLB B in LC 1

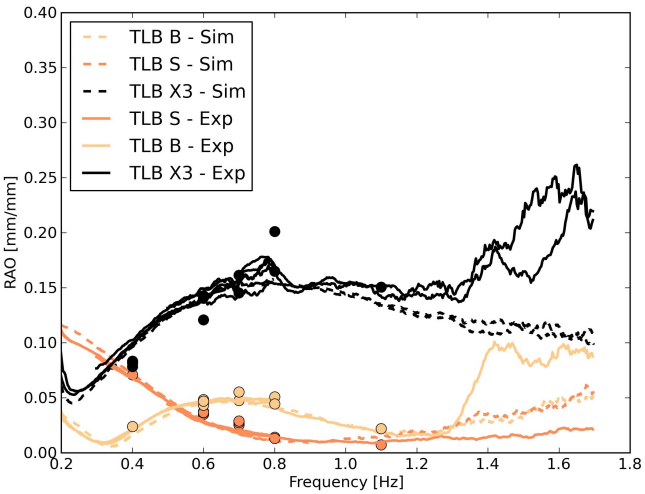

Fig. 17 RAOs in heave direction for all systems, with regular cases represented as dots

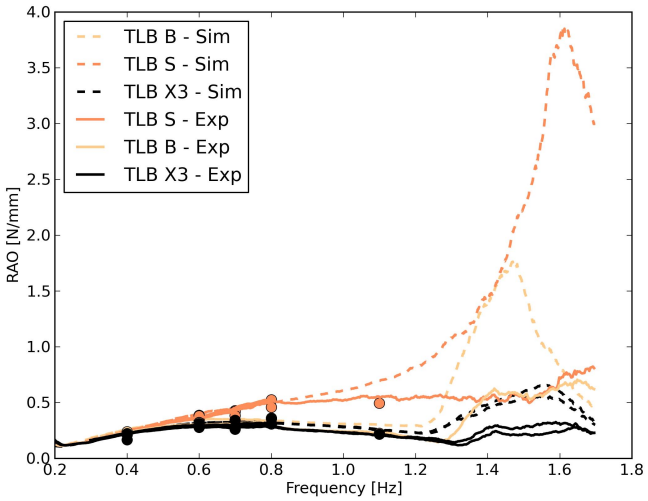

Fig. 18 RAOs for mooring line 1 tension (lower line, downstream direction) for all platforms, with regular cases represented as dots

the experiment scale model and the computations. The flexibility of the end cap is not taken into account in the computations. This may influence the decay tests and thereby the model setup of TLB X3.

(4) At higher frequencies, there will be changes in Re and KC values and thereby possible changes in the C_d and C_m coefficients. The previous sensitivity analyses were run on LC 9 and 12 only and established that a slight change in the coefficients was of less significance. However, the relevance of these, especially for the transition columns, becomes more important with higher frequencies and a corresponding increase in the relative part of the wave action zone affecting these elements. Further sensitivity analysis for the LCs with higher frequencies is therefore suggested.

In the results for heave, the peaks around 0.7 Hz and 1.6 Hz for TLB B and TLB X3 are due to the heave/pitch-surge difference frequency seen in Fig. 12, the pitch-surge eigenfrequency, and the wave spectrum shape seen in Fig. 3. For TLB S, the heave/pitch-surge difference frequency apparently plays less of a role; the RAO peak is around the wave peak frequency. The heave and pitch-surge eigenfrequencies are 2.9 Hz and 2.34 Hz, respectively, well outside the wave excitation frequencies. Overall, good correlation is observed up to about 1.3 Hz for all of the platforms. TLB X3

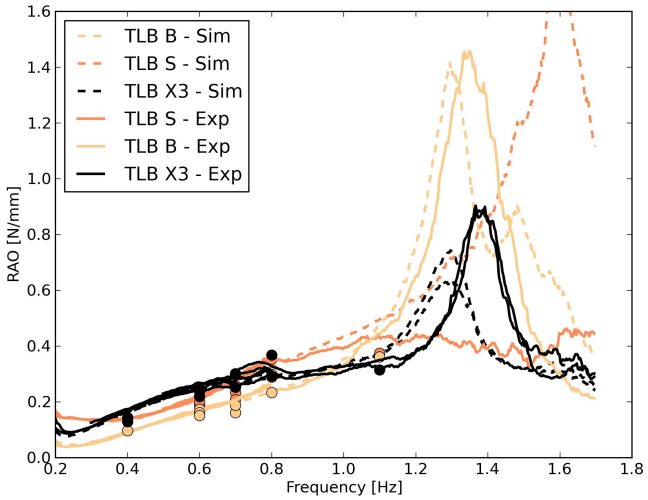

Fig. 19 RAOs for mooring line 4 (upper line, downstream direction) for all systems, with regular cases represented as dots

deviates at slightly higher frequencies than TLB B and TLB S. This is likely in connection with the offset of the peak in pitch-surge, as indicated in Fig. 15, as horizontal translation also implies a vertical component due to the mooring line configuration. The deviation at frequencies above 1.3 Hz is relatively small, as the wave excitation is close to zero. TLB S deviates at 1 Hz and above due to a combination of factors: 1) the wave excitation is low, so the uncertainty increases; 2) lack of radiation damping, which becomes more important at higher frequencies; and 3) a larger water plane area relative to the other concepts. The limited water plane stiffness for TLB X3 is also the reason for the relatively large RAO in heave, as horizontal translations induce a vertical set-down, increasing the heave motion RAO.

Overall, the mooring line forces shown in Fig. 18 and Fig. 19 are computed with high accuracy, although with a slight overestimation of RAO and small offsets on the eigenfrequencies. The exception is TLB S, where the mooring lines deviate severely above 0.8 Hz due to the double frequency response discussed in LC 9. This is consistent with the simulated results for pitch-surge and can largely be explained by the lack of high-frequency damping and the chosen strategy for integration of the hysteresis damping. After passing of waves, we observed turbulence behind TLB S. Computing and comparing accelerations from the experimental data may shed some more light on the responses for TLB S at higher frequencies. Further work is suggested on this topic.

For the upper mooring lines, the simulation provides satisfactory results for TLB S up to about 1.1 Hz, as described earlier. For TLB B and TLB X3, the simulated results are a close match in both RAO and eigenfrequencies with some offsets of the pitch-surge peaks.

CONCLUSIONS

Comparisons between the experiment and computations show overall good agreement. The differences can be explained by the modeling approach and experimental setup. The data should be well suited for further validation of numerical models.

3DFloat is able to capture heave response accurately for all of the concepts. For the pitch-surge motion, 3DFloat computes accurate results for TLB B and TLB X3. Some discrepancies are observed at higher frequencies for TLB S, but these are explained mainly by the lack of radiation damping, which is important for bodies of low mass and high water plane area, and the simplified implementation of the mooring line pulley hysteresis damping.

The upper mooring line forces are computed quite accurately for all concepts. However, the computed response of TLB S results in discrepancies above about 1 Hz. The friction in the mooring system setup likely accounts for some of this discrepancy, especially for the higher frequencies with lower excitation, and should therefore be implemented more accurately in further trials. For lower frequencies and larger excitation shown in regular LCs, 3DFloat produces high quality results, with total mooring forces deviating by less than 5% from the experimental data.

3DFloat performs very well in the area below 1 Hz, and complex multiharmonic behavior is replicated in the simulations only with minor offsets and discrepancies. Morison models are sensitive to high-frequency excitation, and it is common practice to limit excitation above three times the peak frequency for irregular wave computations (Jonkman, 2007). Detailed comparison and evaluation of all of the regular LCs is suggested in order to get a deeper understanding of the accuracy of 3DFloat for different wave conditions.

3DFloat uses generic Jonswap spectrums to compute the waves for the simulations. As the experimental trials were relatively short and therefore may not be a good representation of the spectrums, it

is suggested that simulations are run with wave component tables giving time-accurate representations of the measured wave data.

The TLB systems used in the tests are proven to be robust and predictable, both in the experimental trials and in the simulations. The overall motions are limited, but the mooring line loads and thus the anchoring loads are high. It is important to point out that neither the floaters nor the mooring systems represent full-scale systems. The sub-optimized mooring system makes it difficult to get an indication whether the load-reducing lattice structure of TLB X3 would reduce the overall costs.

ACKNOWLEDGEMENTS

We gratefully acknowledge the funding of the wave tank test and the computations by the MARINET and NOWITECH projects, NMBU, and IFE.

REFERENCES

Anderson, E, et al. (1990). "LAPACK: A Portable Linear Algebra Library for High-Performance Computers," *Proc 1990 ACM/IEEE Conf Supercomput*, New York, NY, USA, IEEE Computer Society Press, 2–11.

Copple, RW, and Capanoglu, C (2012). "Tension Leg Wind Turbine (TLWT) Conceptual Design Suitable for a Wide Range of Water Depths," *Proc 22nd Int Offshore Polar Eng Conf*, Rhodes, Greece, ISOPE, 1, 396–403.

Jonkman, J (2007). *Dynamics Modeling and Loads Analysis of an Offshore Floating Wind Turbine*, Technical Report NREL/TP-500-41958, National Renewable Energy Laboratory, Golden, CO, USA.

Jonkman, J, et al. (2010). "Offshore Code Comparison Collaboration Within IEA Wind Task 23: Phase IV Results Regarding Floating Wind Turbine Modeling," Presented at *Eur Wind Energy Conf (EWEC)*, Warsaw, Poland, NREL/CP-500-47534.

Karimirad, M, and Moan, T (2013). "Stochastic Dynamic Response Analysis of a Tension Leg Spar-Type Offshore Wind Turbine," *Wind Energy*, 16(6), 953–973.

Myhr, A, and Nygaard, TA (2012). "Load Reductions and Optimizations on Tension-Leg-Buoy Offshore Wind Turbine Platforms," *Proc 22nd Int Offshore Polar Eng Conf*, Rhodes, Greece, ISOPE, 1, 232–239.

Myhr, A, and Nygaard, TA (2014). "Experimental Results for Tension-Leg-Buoy Offshore Wind Turbine Platforms," *J Ocean Wind Energy*, ISOPE, 1(4), 217–224.

Popko, W, et al. (2012). "Offshore Code Comparison Collaboration Continuation (OC4), Phase I – Results of Coupled Simulation of Offshore Wind Turbine with Jacket Support Structure," *Proc 22nd Int Offshore Polar Eng Conf*, Rhodes, Greece, ISOPE, 1, 337–346.

Robertson, AN, and Jonkman, JM (2011). "Loads Analysis of Several Offshore Floating Wind Turbine Concepts," *Proc 21st Int Offshore Polar Eng Conf*, Maui, HI, USA, ISOPE, 1, 443–450.

Robertson, A, et al. (2014). "Offshore Code Comparison Collaboration, Continuation Within IEA Wind Task 30: Phase II Results Regarding a Floating Semisubmersible Wind System," *Proc 33rd Int Conf Ocean Offshore Arct Eng*, San Francisco, CA, USA, ASME, 9B, V09BT09A012.

Roddier, D, Cermelli, C, Aubalt, A, and Weinstein, A (2010). "WindFloat: A Floating Foundation for Offshore Wind Turbines," *J Renewable Sustainable Energy*, 2(3), 033104.

Sarpkaya, T, and Isaacson, M (1981). *Mechanics of Wave Forces on Offshore Structures*, Van Nostrand Reinhold Co, 651 pp.

Spæren, A (2013). *Development and Construction of Floating Wind Turbine Models and Test Rig for Wave Tank Test*, Masters Thesis, Norwegian University of Life Sciences, Ås, Norway. Available from http://www.nb.no/idtjeneste/URN:NBN:no-bibsys_brage_43378.

Stewart, GM, Lackner, MA, Robertson, A, Jonkman, J, and Goupee, AJ (2012). "Calibration and Validation of a FAST Floating Wind Turbine Model of the DeepCwind Scaled Tension-Leg Platform," *Proc 22nd Int Offshore Polar Eng Conf*, Rhodes, Greece, ISOPE, 1, 380–387.

Tande, JOG, Merz, K, Paulsen, US, and Svendsen, HG (2014). "Floating Offshore Turbines," *WIREs Energy Environ*, doi: 10.1002/wene.130.

Vorpahl, F, et al. (2013). "Verification of Aero-Elastic Offshore Wind Turbine Design Codes Under IEA Wind Task 23," *Wind Energy*, 17(4), 519-547, doi: 10.1002/we.1588.